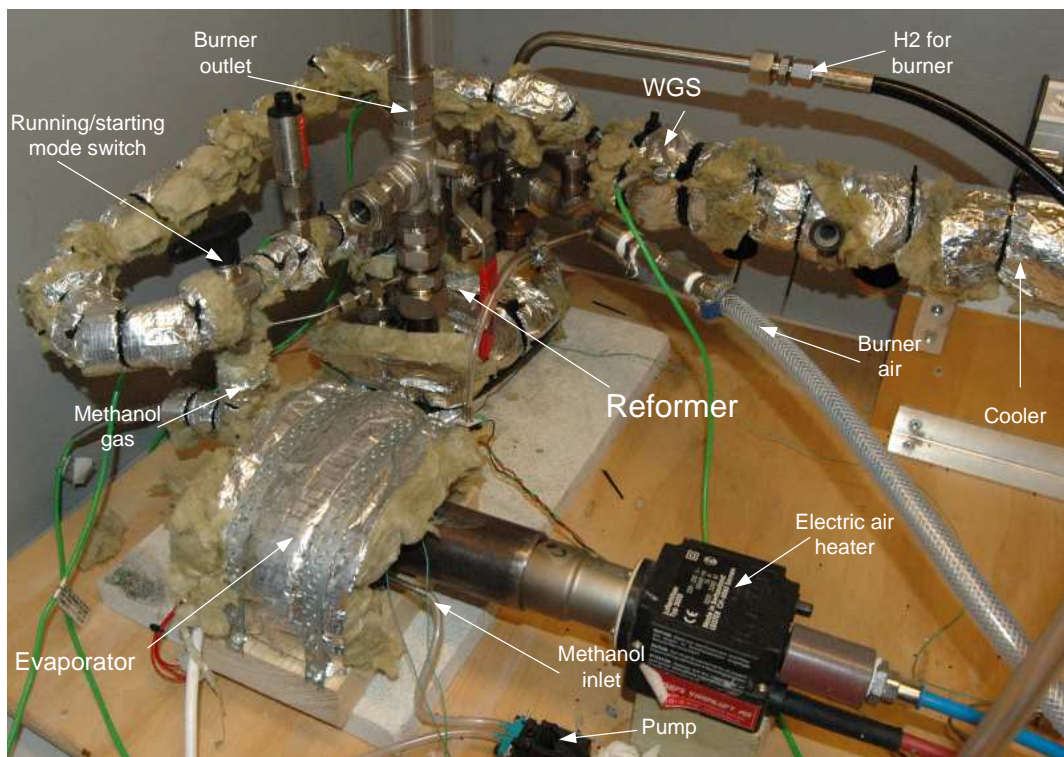

Control of methanol fuelled HTPEM fuel cell system



Title: [Control of methanol fuelled HTPEM fuel cell system]
Semester: [10th]
The period of work: [02-09-08 to 03-05-09]
Supervisor: [Søren Juhl Andreasen]
Group: [EMSD10]
Supplement: [CD]

[Simon Lennart Sahlin]

[Jesper Kjær Sørensen]

SUMMARY:

This project presents a nonlinear model of a methanol fuelled high temperature PEM fuel cell system in a two stage operation. The system contains an evaporator unit, a reformer and burner unit and a fuel cell stack. The nonlinear model simulates a start up and a running mode. The nonlinear model is converted to a linear model and the linear model is used for testing a PI-controller. A fuel estimator is created with the purpose of installing into a running system. The theoretical results showed a reasonable result compared to measured data. The project contains a mathematical parameter search routine for obtaining the controller parameters. The electric efficiency is calculated to about 20% and can be seen in the nonlinear model.

Prints: [6] pcs.
Number of pages: [119] pages
Appendix pages: [121 - 198] pages

Preface

This report is a master thesis for two students attending the 10th semester of Electro Mechanical System Design at the university of Aalborg.

The report contains a CD containing the models, scripts, appendixes and experimental data presented in the report. A PDF version of the report can be found on the CD.

The following notations are used in this report. Citations are encapsulated in [x] where x is a number. The number corresponds to an entry in the bibliography. The bibliography contains the information about the articles and books used in the project.

Equations are encapsulated in (x.y) and numbered by the chapter x and the equation number y, i.e (6.7) corresponds to the 7th equation in the 6th chapter.

Figures marked figure x.y and not encapsulated but numbered by the chapter x and a figure number y, i.e figure 1.2 corresponds to the 2nd figure in the 1st chapter. In some cases the figures are noted with a letter if the figures are placed next to eachother.

Appendices are noted with a capital letter and can be found in the back of the report.

The report requires that the reader has a common knowledge about control strategies, fuel cell systems, and thermodynamics in general.

Contents

1	Introduction	1
1.1	Fuel cell	3
1.2	Types of operation	6
1.3	Components of the system	7
1.4	Project goal	11
1.5	Project scope	11
2	Nonlinear system model	13
2.1	Fuel cell model	13
2.2	Reformer model	28
2.3	Evaporator model	31
2.4	Fuel estimation	34
2.5	System efficiency	35
2.6	Summary	36
3	Linear system model	39
3.1	Linearisation of the temperature models	39
3.2	Summary	46
4	Validation of models	47
4.1	Validation of nonlinear model	47
4.2	Validation of linear model	52
4.3	Summary	57
5	Control strategies	59
5.1	General control systems	59
5.2	Temperature control	66
5.3	Controller design	78
5.4	Summary	85
6	Implementation	87
6.1	Experimental setup	87
6.2	Evaporator	89
6.3	Reformer	92
6.4	Simulated run	105
6.5	Summary	109

CONTENTS

7	Conclusion	111
8	Future work	115
9	Project Summary	117
	References	119
	Appendices	
A	Experiments	121
A.1	Description of system	121
A.2	Experiments with reformer	123
A.3	Experiment with cooler	133
B	Description of model	137
B.1	Constants	137
B.2	Simulink model	138
B.3	Reformer model	142
B.4	Fuel Cell	150
B.5	Evaporator	163
C	Linearisation	171
C.1	Convective loss	171
C.2	Cell voltage	172
C.3	Nonlinear voltage parts	172
C.4	Cathode loss	173
C.5	Anodic loss	175
C.6	Linear voltage approximation	177
C.7	Heat generated	178
D	Labview program	181
D.1	FPGA Program	182
D.2	RT program	183
D.3	Host program	186
D.4	Figures	187
E	Matlab scripts	191
E.1	Fzero coverage	191
E.2	Fzero conservation of mass	193
E.3	Repeating simulation optimizer	195
E.4	Controller parameter search	198

Nomenclature

α_c	Charge transfer coefficient [-]	f	Pump frequency [Hz]
\bar{k}_j	The k'th working point variable for the j'th component	$G(s)$	Transfer function
\dot{n}_j	Molar flow of j'th gas stream [kmol/s]	GDL	Gas diffusion layer
\dot{q}_{air}	Volumetric flow rate[l/min]	h	Enthalpy pr unit [kJ/kmol]
η_{act}	Activation loss [V/cell]	$H(s)$	Feed back transfer function
η_{anode}	Combination of the activation and diffusion loss at the anode	i_o	Exchange current density [A/cm ²]
η_{cath}	Combination of the activation and diffusion loss at the cathode	K_{com}	Constant ration for the mass balance of the reformer
η_{conc}	Concentration loss [V/cell]	K_{ji}	Constant of linearisation of the j'th process with the i'th variable
η_{FC}	Electric efficiency of the system [-]	m_j	Mass of the j'th component [kg]
η_{ohmic}	Ohmic loss[V/cell]	n_{cell}	Number of cells in the stack
λ	Air stoichiometry ratio [-]	R	Universal gas constant [J/(mol · K)]
λ_{H2}	Hydrogen stoichiometry ratio [-]	$R(s)$	System reference signal
ρ_j	Density of the j'th substance [kmol/m ³]	R_{diff}	Diffusion resistance [$\Omega \cdot cm^2$]
$C(s)$	System output signal	T_l	Transport lag time constant [s]
c_j	Specific heat capacity of the j'th component [kJ/kg · K]	T_{cell}	Cell temperature [K]
$D(s)$	Disturbance signal	T_{reform}	Reformer temperature [K]
ESA	Electrochemical surface area	T_{Stack}	The stack temperature [K]
		v_{oc}	Open circuit voltage [V/cell]
		V_{pump}	Stroke volume of the pump [l]
		EES	Engineering Equation Solver
		EMP	Empirical constant [V]
		F	Faradays constant [C/mol]
		s	Complex variable for the laplace transform
		SC	Steam to carbon ratio [-]
		WGS	Water Gas Shift reaction

CONTENTS

Introduction

- 1.1 Fuel cell**
 - 1.1.1 Fuel cell structure
- 1.2 Types of operation**
- 1.3 Components of the system**
 - 1.3.1 Fuel Cell Stack
 - 1.3.2 Evaporator
 - 1.3.3 Reformer and Burner
- 1.4 Project goal**
- 1.5 Project scope**
 - 1.5.1 Project Limitation

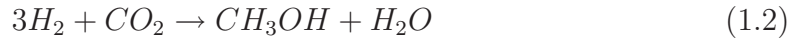
Within the last century, increasing demands for alternative energy sources has emerged. Recent studies suggest that global warming is not all caused by natural means alone, and fossil fuel resources is predicted to deplete in the near future. For this reason research needs to be done on alternative ways of supplying energy to use for transport and general electric demands. Taking a closer look at the fuel cell types, currently being developed, a few possible choices are presented; Solid oxide fuel cell(SOFC), direct methanol fuel cell (DMFC), alkaline fuel cell (AFC) and polymer electrolyte membrane fuel cell (PEMFC). All of these types of fuel cells are still being investigated, because they all have different advantages. The DMFC is fed directly with methanol, while the AFC and PEMFC needs to be fed with hydrogen of a high purity. Using hydrogen gives the fuel cell a good dynamic load resistance and has a non-polluting exhaust. DMFC is often discussed as a good choice for automobiles since no reformer is needed, though performance is rather limited because of lower reaction rate. SOFC's is used in a wide variety of applications, though it is often found in a stationary power generation and with a high power output(300kW - 2MW). To function properly, the SOFC must operated at high temperatures (above 800 °C), which makes the use in automobile applications complicated. The high temperature causes the startup time to be larger, compared to intermediate temperature fuel cells. The cost of components does also have a negative effect on SOFC systems. [11]

Methanol is a low-cost high energy liquid, and based on the current infrastructure for gasoline, implementation can be adapted fairly easy. This project will thereby investigate the use of methanol as fuel in a fuel cell system. Methanol can be produced from almost any hydrocarbon fuel, and with quite high efficiency. A mixture of hydrogen, carbon monoxide, and carbon dioxide is mixed together as seen in (1.1) and (1.2)

1 Introduction



or



These reactions are highly dependent on a suitable catalyst and a fairly high pressure (about 50 bar). In the case of hydrogen generation, the high pressure and catalyst is fortunate, since the reaction do not occur unless the conditions are right. State-of-the-art plants are currently estimated to use about 29 kJ/kg of the supplied fuel. This amount is based on the lower heating value (LHV) of the fuel and is the power used to operate the process. The LHV of methanol is 19.93 kJ/kg and corresponds to an efficiency of about 70%. Although most of the current methanol production is based on natural gas and other fossile fuels, it can also be produced from renewable biomass. The biomass process is estimated to create methanol, in a few years, with an efficiency at about 60% and a cost pr Joule similar to the current refined diesel and gasoline prices, though prices are about a factor of 3 in favour of the gasoline[11].

A fuel cell system can be designed in a lot of ways, though the most common is often in its most basic form, a fuel cell stack, a unit for converting the DC current into AC current, a fan/compressor for supplying the oxidant (Air) and a heat exchanger to extract the heat from the fuel cell exhaust. The complexity of the system is increased if the introduction of another fuel besides pure hydrogen. If a hydrocarbon fuel is used, a reforming unit is needed for some fuel cells. A reforming unit can reform the hydrocarbons into reformat gas containing H_2 , CO , CO_2 and H_2O . Studies show that the composition of the reformatted gas can cause a highly degrading effect on a low temperature PEM fuel cell. By reforming methanol into a high energy reformat gas, the concentration of CO , in the gas, is often up to several percent. This excludes the low temperature PEMFC for now, though studies on high temperature PEM fuel cell (HTPEM) has shown a higher tolerance of CO [10]. HTPEM fuel cells work at about $160\text{-}200^\circ C$ and is suitable for automobile projects. The HTPEM fuel cell does not require any humidification of the cathode and this is why a fairly simple system can be created, as long as the composition of the gas and temperature is under control. This project will investigate the interaction between a reforming unit and a HTPEM fuel cell stack. The system is going to be designed to increase the overall efficiency by utilizing excess heat from the fuel cell stack to evaporate the initial methanol liquid. Excess hydrogen in the fuel cell exhaust gas is used as fuel for the burner part of the reformer. A model will be created to investigate the relation between the different units in the system, and for estimation of controller parameters. Further description of the system can be found in section 1.2.

1.1 Fuel cell

This section describes the basic structure and reactions used in a fuel cell. The reactions are based on a hydrogen based fuel cell.

1.1.1 Fuel cell structure

As seen in figure 1.1, the H_2 rich reformat gas and oxidant O_2 are distributed through the channels in the bipolar plates on both the anode and cathode side respectively. The gas and oxidant is diffused through the gas diffusion layer (GDL) to the catalyst layers, which is placed on both sides of the membrane. The membrane layers are porous carbon layers with dispersed platinum particles. The platinum acts as a catalyst by increasing the surface area, which is key for getting a high reaction rate. This surface area is often called the electrochemical surface area (ESA). When fuel and oxidant are present at the two catalyst layers, an electrical potential difference is created. This potential can be connected to a load and a current can be drawn. The cathode and anode is considered positive and negative respectively.

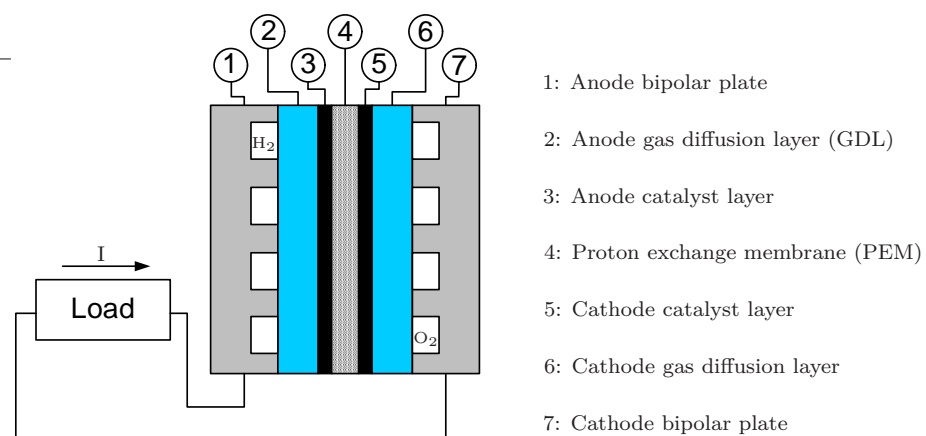


Figure 1.1: *Structure of a single fuel cell unit*

The typical voltage of a single HTPEM fuel cell will not exceed 0.95V at open circuit, though this will drop when a current is drawn. If higher voltages is needed, normally the cells are stacked to create a more applicable potential, see figure 1.2. Assembling cells in a fuel cell stack has the advantage of increasing the potential, but it also complicates matters. Fuel and oxidant need to be distributed evenly to the individual cells. Furthermore, the performance of the cells is very dependent on temperature, which also demands the cells to be cooled evenly in the stack. [8]

When working with fuel cells, hydrogen is the preferred fuel, but it often presents volumetric problems because of the low density. When considering the energy

1 Introduction

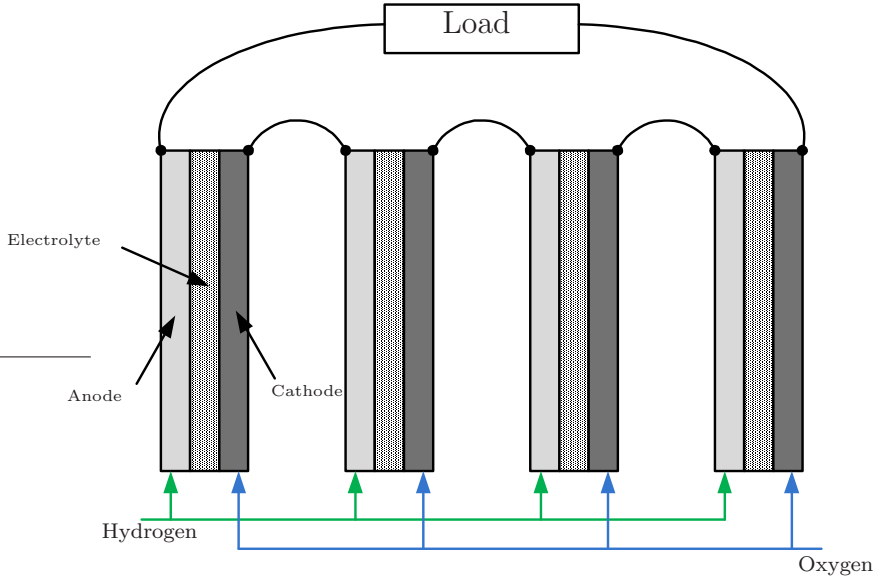


Figure 1.2: Simple edge connection of four cells in series

density in kWh/m^3 , there is about 8 times more energy per volume in methanol compared to hydrogen at 200 bars [2]. By using hydrocarbons as e.g. methanol the volumetric problems are lesser, and can be used directly in a PEM cell (DMFC). This method of using methanol has proven to be with a poor performance and a complicated water management system is needed. This is why a reforming process is more suitable, though with a higher CO concentration in the gas. Since the HTPEM works at temperatures of 160-200 °C, it has a very high tolerance to CO and is therefore an ideal choice when working with reformer systems[7].

The overall reaction in a fuel cell is shown in reaction (1.3)



The reaction (1.3) shows that, hydrogen reacts with oxygen, and the product is water. This reaction can be divided into two reactions. The Hydrogen Oxidation Reaction (HOR) and the Oxygen Reduction Reaction (ORR) as shown in reaction (1.4) and (1.5) respectively.



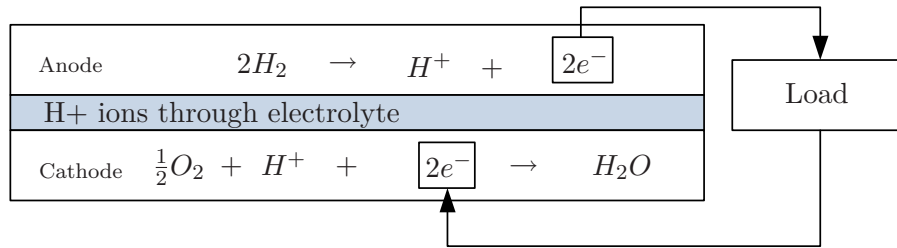


Figure 1.3: *Electron flow in a hydrogen fuel cell*

The HOR reaction occurs at the anode and is often much faster compared to the ORR reaction which happens at the cathode.

A ratio between the amount of methanol and the amount of water in the fuel mixture is called the steam to carbon ratio (SC). The calculation of the portion of methanol in a mixture of methanol and water can be seen from (1.6).

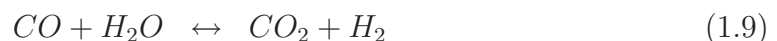
$$\begin{aligned}
 V_{mix} &= V_{MeOH} + V_{H_2O} \\
 &= V_{MeOH} + SC \cdot V_{MeOH} \\
 V_{MeOH} &= \left(\frac{1}{1 + SC} \right) \cdot V_{mix}
 \end{aligned} \tag{1.6}$$

The calculation for the water part is performed by multiplying (1.6) with the steam to carbon ratio. The steam to carbon ratio is an important factor for the steam reforming process. The need for vaporized water to bind with the CO during the reformation process[16]. To further increase the H_2 , and decrease CO , a water gas Shift (WGS) catalyst is utilized. The WGS reaction can be seen from (1.9).

The reformation process is an endothermic reaction that combines a hydrogen rich fuel with steam over a catalyst at high temperatures. The methanol is reformed by a steam reforming process and can be seen in (1.7).



which is the sum of the methanol decomposition and the water gas shift(WGS):



By using a reformation process the storage of hydrogen can be avoided. This opens up for other problems like thermal requirements and more system management, and this leads to a brief introduction of the different components of a reforming system.

1 Introduction

The system consists of a HTPEM fuel cell stack with 65 cells and a blower for the anode convection of the stack. The anode gas inlet line is connected to a cooler which ensures that the anode gas has the right temperature of 180 °C. The cooler is connected to a WGS reactor that removes CO gas from the reformat gas. The WGS-reactor is connected to the gas outlet side of the reformer. The gas inlet side of the reformer is connected to the gas outlet side of the evaporator and the evaporator gas inlet side is connected to a fuel pump. The pump is connected to a fuel tank. The fuel cell stack chathode inlet side is equipped with a blower that supplies air from the surroundings. The exit air from the fuel cell is transported to the evaporator for heating purposes. The anode gas outlet line is connected with the burner gas inlet. The gas is mixed with air and is forced into the burner with the fuel. This can be seen from the schematic in figure 1.4

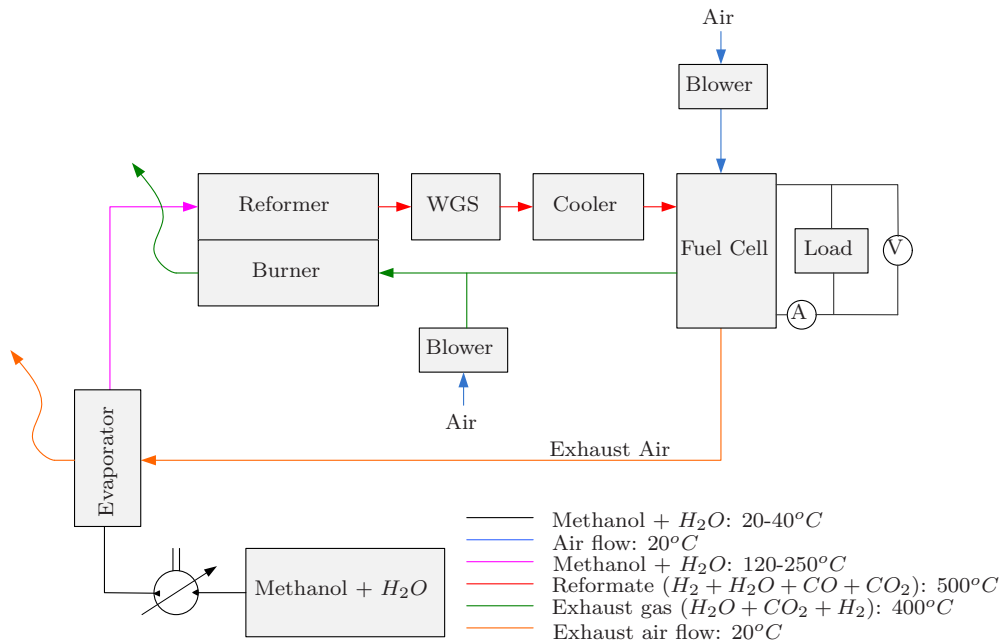


Figure 1.4: Schematic of the system design

The components will be discussed in detail in section 1.3. The system is designed to operate in two modes, startup mode and running mode. This will be described in the next section.

1.2 Types of operation

The system process is divided into 2 phases which contain the startup phase, the running phase. While the system is in the startup phase, the main goal is to raise the temperature of the system components until the different operation temperatures are reached. Initially the evaporator is heated up with electric heaters installed in

the evaporator. The evaporator vaporizes the methanol and this is fed directly into the burner, where the fuel is mixed with air from a blower. This results in a catalytic combustion of the methanol. The exhaust gas from the burner is lead though the fuel cell stack and like in the normal running system and the exhaust air from the fuel cell is passing over the evaporator, and thereby adding heat to the evaporation process. The startup phase of the system can be see in figure 1.5, where the gray lines are not it use.

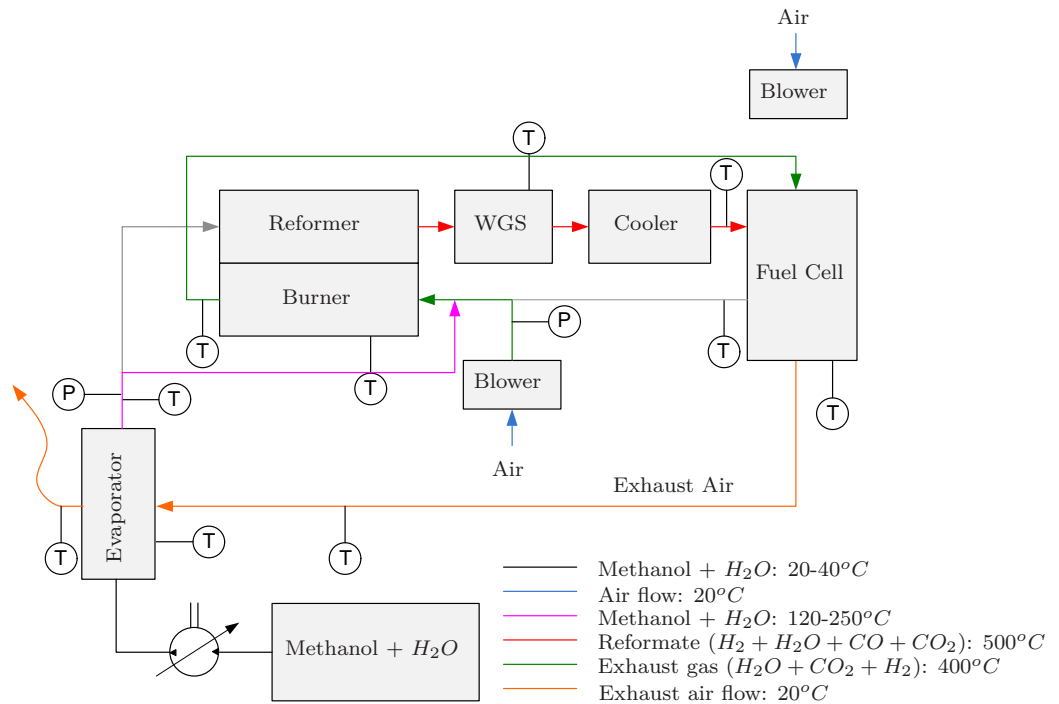


Figure 1.5: Schematic of the system in the startup phase

The system design for a running system is as shown in figure 1.6. The system evaporates and reformats the methanol to H_2, CO and CO_2 , which is let though a WGS, thereby reducing the amount of CO and adding H_2 in the reformat gas for the Fuel Cell. The reformat gas is passed though a condenser to cool down the gas to a proper temperature to avoid damaging the Fuel Cell. The heat of the exhaust air transferred from the fuel cell is directed into the evaporator, and then out of the system. The exit of the anode side of the fuel cell, is led into the burner, because of the excess hydrogen.

1.3 Components of the system

This section has the purpose of describing the different parts of a fuel cell system.

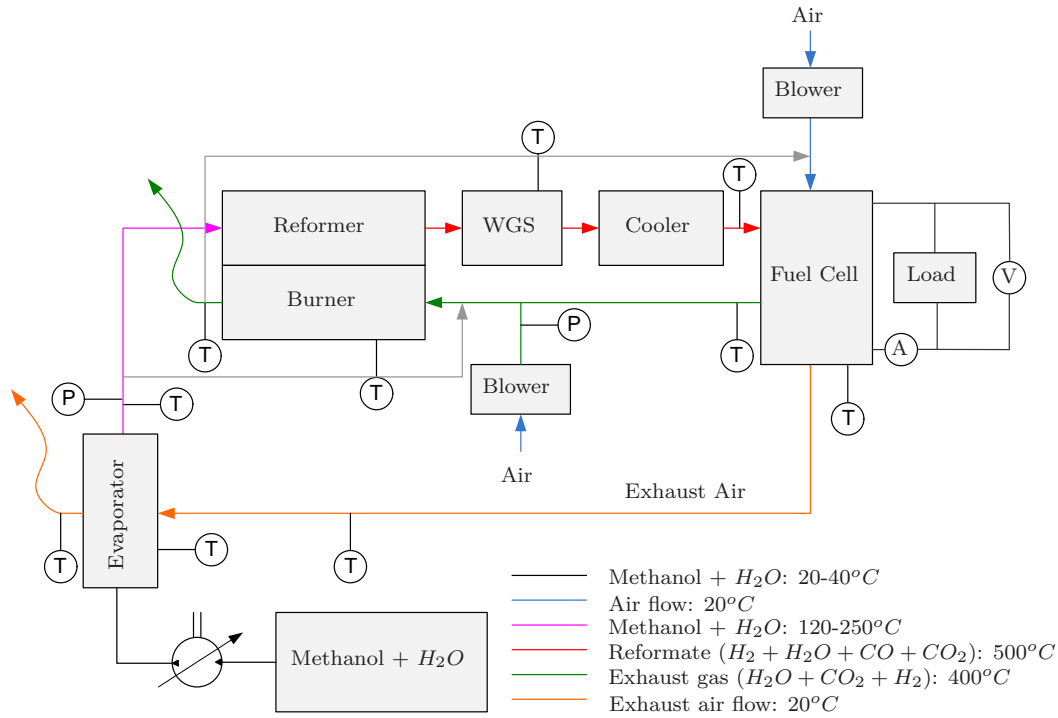


Figure 1.6: Schematic of the system in the running phase

1.3.1 Fuel Cell Stack

The fuel cell stack contains 65 single fuel cells and each cell has a reactive area of 46.16cm^2 . The cells are connected in a serial connection and the fuel cell stack is insulated with a melamine foam layer with a thickness of 0.03m . The operating temperature of the fuel cell stack has an interval between 433 K (160°C) and 473 K (200°C) which is typical for a HTPEM cell. During operation the cells in the stack produce heat and to ensure that the temperature, within the stack, is kept at a given interval. The stack is fed with air at room temperature from an electrical blower. The air is heated inside the stack and transfers the heat out of the stack through the exhaust. A typical HTPEM can be seen from figure 1.7.

Fuel is fed to the fuel cell stack from the reformer and distributed through the gas channels. The stack is initially supplied with 120% of the needed hydrogen in order to have 20% excess hydrogen. The combustion of the excess hydrogen is used to add heat to the endothermic reactions happening in the reformer, where the methanol and watermixture is reformed to be used as fuel for the fuel cell stack.



Figure 1.7: Picture of a HTPEM fuel cell

1.3.2 Evaporator

The evaporator is a heat exchanger made of two aluminum parts, and with a total mass of 0.5kg . The heat exchanger is built into a chamber connected to the exhaust of the fuel cell stack. The installed evaporator can be seen in figure 1.8

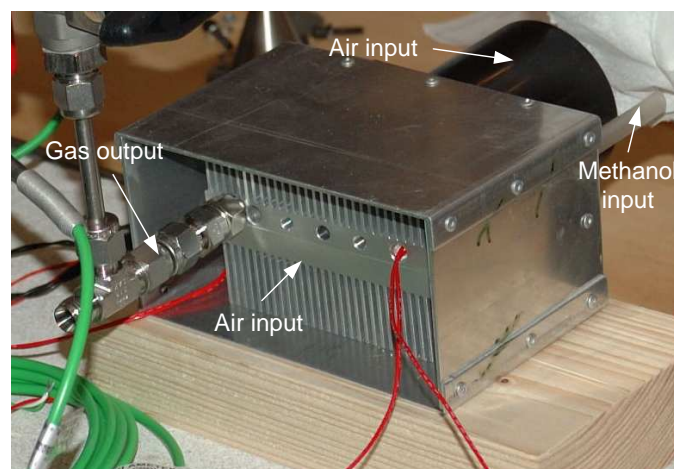


Figure 1.8: Picture of the evaporator without isolation

The two parts of the heat exchanger can be seen from figure 1.9(a) and figure 1.9(b). The heat exchanger has 34 fins on each side and the bottom has two mounting slots for the electrical cartridge heaters, see figure 1.9(b). The bottom of the heat exchanger has flow channels, on the side that is in contact with the top of the heat exchanger, for the methanol flow. In order to avoid leakage a rubber O-ring is inserted in the assembly of the heat exchanger parts.

The methanol enters the flow channels from the pump and is in the fluid phase and at room temperature. Heat is added to the heat exchanger, both from the cartridge heaters and from the passing hot exhaust air. The temperature of the

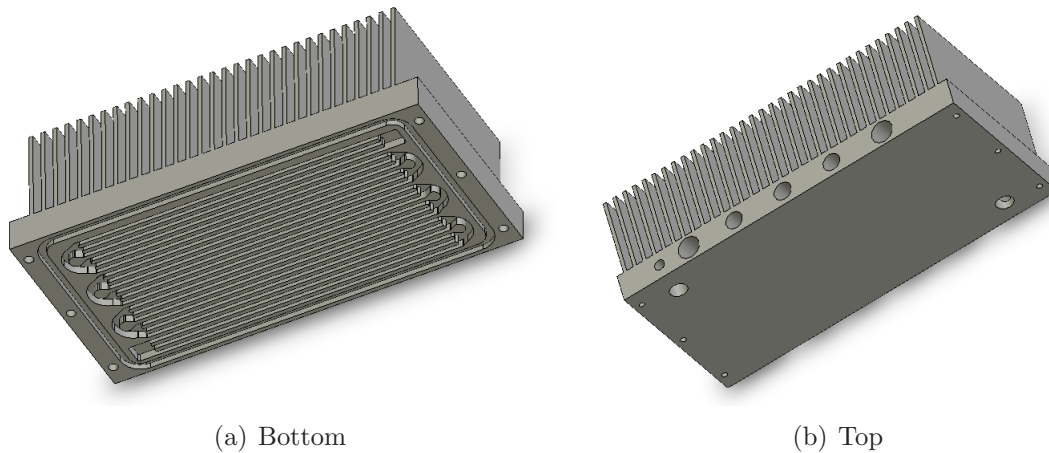


Figure 1.9: *Cad model of the evaporator*

methanol mixture increases until the boiling point is reached and the methanol mixture starts to vaporize. The methanol mixture expands during the vaporization and this expansion moves the vaporized methanol mixture through the evaporator during operation. This step is required by the reformer because the fuel needs to be in gas form for the reformation can happen.

1.3.3 Reformer and Burner

The reformer and burner have the function of changing the gas from the evaporator, into a more useful composition. Steam reforming is the most common way to obtain hydrogen from hydrocarbons in systems. The reformer can be seen from figure 1.10(a), and a view of the reformer installed can be seen from figure 1.10(b).

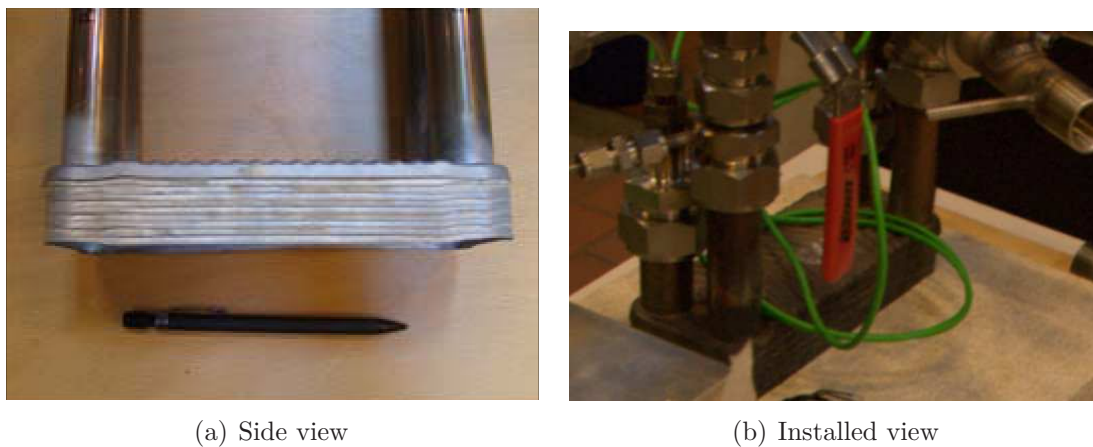


Figure 1.10: *Images of reformer*

The CO tolerance in fuel cells varies from around 20ppm for low temperature PEM fuel cells to around 3% for high temperature PEM fuel cells[6]. In many systems, where Steam Reforming is applied, there is a need for an extra purifier so the amount of CO is minimized. The overall steam reforming reaction, as seen in (1.10), is endothermic and heat must be supplied.



In the reformer a WGS reaction (1.11) is happening at the same time. This WGS reaction is an exothermic process and it releases heat.



In the steam reforming process, steam reacts through a catalyst to produce H_2 and CO_2 . Depending on the operating conditions of the reformer, the reformed gas contains mostly hydrogen, with lesser amounts of carbon dioxide, water, methanol and carbon monoxide. The heat needed in the process varies much on the amount of the number of carbons. If there is a high amount of carbons, the higher amount of heat is needed to evaporate it. Other parameters in the process is temperature, pressure and the molar steam to carbon ratio.

1.4 Project goal

The overall goal of the project is to investigate different control strategies on a HTPEM based fuel cell system. More specifically the focus is to improve the overall power efficiency by investigating control strategies, and the optimization issues in HTPEM fuel cells. This project will investigate the possibility to use the unused hydrogen from the fuel cell as fuel for a burner. To increase the efficiency even further, the use of the exhaust air, from the fuel cell, is used to heat up the evaporator. Within the project scope is the modeling of the system, both nonlinear and linear. The goal of the models should be to test different control strategies. A PI control strategy will be tested and evaluated. An overall model of the system can be seen in figure 1.6.

1.5 Project scope

This report will focus on the following tasks:

1 Introduction

- Creation of a dynamic nonlinear model for the fuel cell system in Matlab Simulink™
- Verification of the fuel cell model by experiments and earlier studies.
- Linearisation of the created nonlinear model.
- Investigation of the connection between the different parts of the system.
- Investigation of the controlling part of the system.

1.5.1 Project Limitation

The project does not contain the following tasks:

- The control systems implemented in this project is limited focusing on the linear continuous control strategies.
- The temperatures of the gas is assumed to be the correct temperature when entering a component of the system.
- The cells of the fuel cell stack are assumed to behave uniformly and the temperature changes between the cells are neglected.
- The temperature of the reformer is equal to the temperature of the burner.
- The internal convection from the gas passing through the reformer is neglected.
- The heat loss of the pipeline connections between the components is neglected.
- The moving air is distributed evenly through the components.

Nonlinear system model

2

- 2.1 Fuel cell model**
 - 2.1.1 The fuel cell voltage
 - 2.1.2 Calculating voltage loss
 - 2.1.3 Fuel cell temperature
- 2.2 Reformer model**
 - 2.2.1 Reformer temperature
 - 2.2.2 Reformation process
- 2.3 Evaporator model**
 - 2.3.1 Evaporator temperature
- 2.4 Fuel estimation**
- 2.5 System efficiency**
- 2.6 Summary**

This chapter contains a presentation of the mathematical model that represents the system components presented in Chapter 1. The models are created in Simulink^(TM) and a description can be seen in Appendix B. The models are solved with an ordinary differential equation solver called "ode15s".

The chapter consists of three sections. The first section represents the mathematical model of the fuel cell stack. The second section is the model of the reformer and the last section contains the model of the evaporator. The system is subjected to a load pattern that can be seen from figure 2.1

The load of the entire system based on the current density. This indicates the power demands from the electrical load, connected to the fuel cell.

2.1 Fuel cell model

The fuel cell model is divided into two parts. The first part calculates the electric potential of the stack and the second part calculates the stack temperature.

2 Nonlinear system model

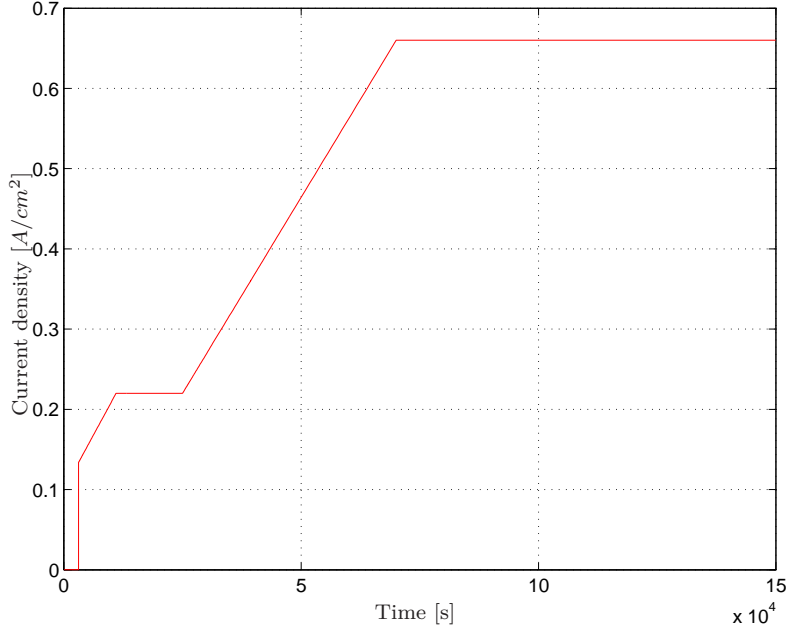


Figure 2.1: *The current density load pattern*

2.1.1 The fuel cell voltage

The fuel cell works almost like a battery delivering a voltage based on an electrochemical reaction between the reactants hydrogen and oxygen. The main difference is that the fuel cell can deliver a voltage for as long as the reactants can be supplied, whereas the battery deteriorates at some point. The voltage equation for the fuel cell is based on a difference between the voltage at thermodynamic equilibrium, where no current is applied, and the loss involved in the increasing of the current. The term reversible voltage v_{rev} is the voltage produced at thermodynamic equilibrium. When current is drawn from the fuel cell, the voltage is decreased in order to keep up the equilibrium. The reversible cell voltage of most feasible fuel cell reactions varies in the range of 0.8V to 1.5V. If a higher voltage is needed from a fuel cell system, several cells are stacked together in series[8]. The voltage of the stack can be represented by (2.1)

$$V_{Stack} = n_{cell} \cdot (v_{rev} - \eta_{act} - \eta_{ohmic} - \eta_{conc}) \quad (2.1)$$

where v_{rev} is the reversible voltage of a single cell, η_{ohmic} is the ohmic loss, η_{act} is the activation loss due to reaction kinetics, η_{conc} is the concentration loss due to mass transport.[8] The characteristics of these losses can be seen in figure 2.2

To calculate the theoretical value of the reversible voltage, the gibbs free energy can be used. The Gibbs free energy is defined as:

$$G = H - T \cdot S \quad (2.2)$$

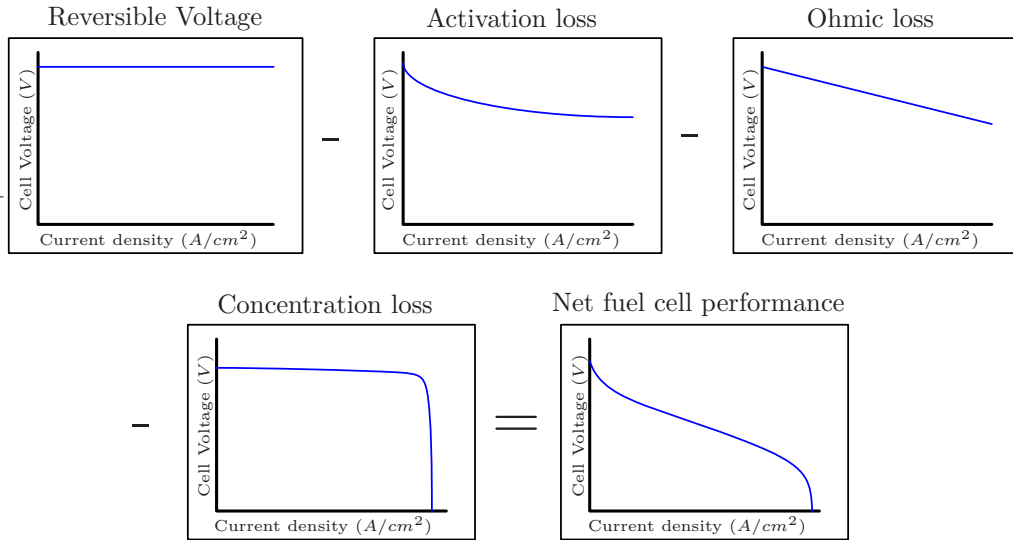


Figure 2.2: Pictorial summary of major factors

where G is the Gibbs free energy, H is enthalpy, T is temperature and S is entropy. The Gibbs free energy is the maximum amount of non-expansion work that can be extracted from a closed system. If a system changes from one initial state to another, the Gibbs free energy ΔG equals the work exchanged by the system with its surroundings, during a reversible transformation from initial state to the final state. When the ΔG is negative it means that the reaction will release energy. In contrast, if ΔG is positive, then work would be to be added to the reacting system to make the reaction go.

When a system reaches equilibrium, at constant pressure and temperature, the Gibbs free energy is at its minimum. The relationship between Gibbs free energy and voltage can be seen in the electrical work done calculated from (2.3)

$$W_{elec} = -\Delta\hat{g}_{rxn} \quad (2.3)$$

The electrical work done by moving a charge Q [C] through an electrical difference E is

$$W_{elec} = EQ \quad (2.4)$$

The charge Q can be related to the number of electrons that can be moved between an electrical difference

$$Q = nF \quad (2.5)$$

2 Nonlinear system model

where n is the number of moles of electrons transferred and F is Faraday's constant. If the reaction is hydrogen based, the number of electrons released is 2. By combining (2.3), (2.4) and (2.3) we get an expression for the reversible voltage at a constant-temperature and constant-pressure process ($dT, dp = 0$).

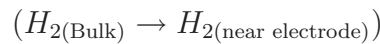
$$\begin{aligned}\Delta\hat{g} &= -nFE \\ E &= -\frac{\Delta\hat{g}}{nF}\end{aligned}\tag{2.6}$$

The theoretical open circuit voltage is calculated to about $1.14V/cell$, when operating at a temperature of $200^\circ C$. However, when the fuel cell is put to use, it is found that the voltage is much less than the theoretical values, due to the activation loss not being zero when the current density is equal to zero. The model uses an open circuit voltage of 0.95 V based on [15]. This is caused by the activation loss is still present at no current density.

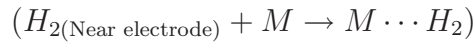
Activation loss

Because of the bonds of the atom and the electrode surfaces, there is an energy barrier. For example, the overall reaction $H_2 \rightleftharpoons 2H^+ + 2e^-$:

1. Mass transport of H_2 gas to the electrode:



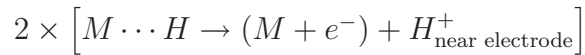
2. Absorption of H_2 onto the electrode surface, where M is the electrode:



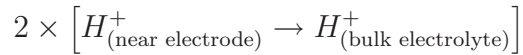
3. Separation of the H_2 molecule into two individually bound hydrogen atoms onto the electrode surface. This is also called chemisorbed.



4. Transfer of electrons from the chemisorbed hydrogen atoms to the electrode, releasing H^+ ions into the electrolyte:



5. Mass transport of the H^+ ions away from the electrode



The overall reaction is limited by the slowest step in the series. As shown in figure 2.3, in order for reactants to be converted into products, it must first make it over the activation hill. The probability for this to happen, determines the rate of which the reaction occurs.

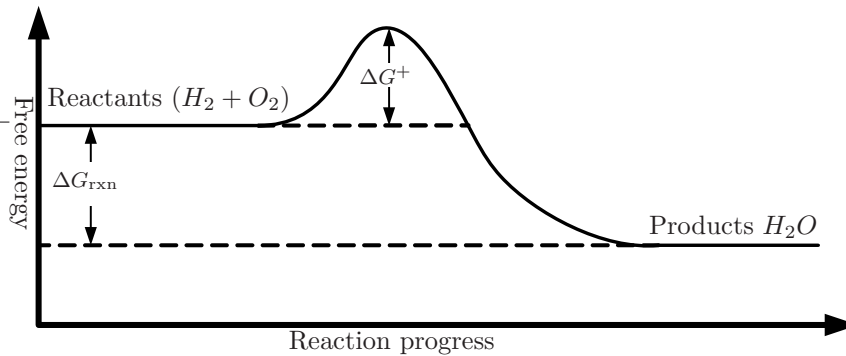


Figure 2.3: Activation barrier (ΔG^\ddagger) which needs to be exceeded to convert reactants to products

The $M \cdots H$ represents a hydrogen atom chemisorbed on the metal surface and the $(M + e^-)$ represents a liberated metal surface site and a free electron in the metal.

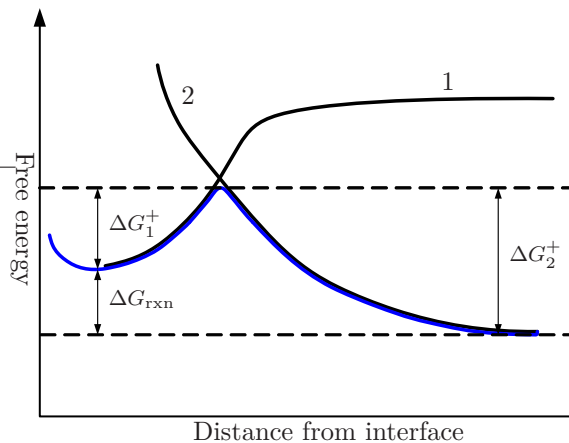


Figure 2.4: Free energy compared to distance from interface

Curve 1 in figure 2.4 depicts the free-energy of the chemisorbed atomic hydrogen, H, which increases with distance from the metal surface. The chemisorption improves the hydrogen stability by partially satisfying the bonding requirements, thus lowering the free energy. Separating the atomic hydrogen from the metal surface destroys this bond, thus increasing the free energy.

Now consider curve 2 which describes the free-energy of a H^+ atom in the electrolyte. It can be noticed that the H^+ ion has the highest free-energy when the ion is close

2 Nonlinear system model

to the metal surface. This means that the “easiest” (minimum) energy path for the conversion of chemisorbed hydrogen to H^+ and $(M + e^-)$ is given by a blue line in figure 2.4. The highest point in the figure describes species in the active state that have overcome the free-energy barrier, and they can be converted into either products or reactants.

Concentration loss

For the fuel cell can produce electricity, a continual supply of fuel and oxidant must be available. At the same time, products must be removed from the fuel cell to avoid “strangling” of the cell. The movement of supplying reactants and removing products is often termed “mass transport”. Reactant depletion or product accumulation at the fuel cell catalyst layer can severely affect the fuel cell performance. The loss in performance is called the “concentration” loss or “mass transport” loss. The concentration loss in a fuel cell often represent the limit of the current density.

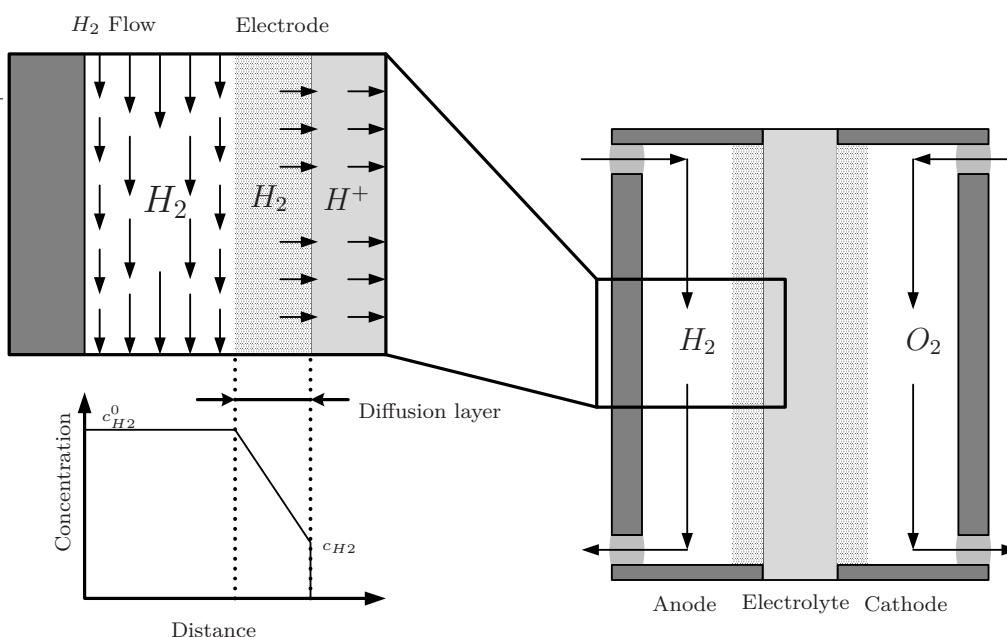


Figure 2.5: *Schematic of diffusion layer*

The schematic shown in figure 2.5 is an illustration on how the diffusion layer influences on the concentration of hydrogen at the electrolyte. Consumption of H_2 gas in the electrode results in a depletion of H_2 . The concentration of H_2 gas falls from its maximum value ($c_{H_2}^0$) to a lower value (c_{H_2}) at the catalyst layer. If the current density is set high, there is a possibility of reactant depletion and product accumulation. If the fuel cell is operated on H_2 and air, only the cathodic overvoltage is important. This is caused by the OOR reaction is slower compared to the HOR reaction, and the fact that the reactant at the cathode is not pure O_2 .

2.1.2 Calculating voltage loss

The voltage loss in the fuel cell is split up in three parts: Ohmic loss, Anode loss and cathode loss. Each of these are discussed below. The cell temperature is assumed to be the same as the stack temperature.

Ohmic loss

Ohmic loss is the resistance in the flow of electrons through the voltage connections, and the resistance of the ions through the membrane. This voltage loss is essentially proportional to current density. This is linear when the temperature is constant and also referred to as resistive loss. Ohmic loss can be calculated using (2.7).

$$\eta_{ohmic} = i \cdot R_{ohmic} \quad (2.7)$$

where i is the current density [A/cm^2] and R_{ohmic} is the equivalent ohmic resistance [$\Omega \cdot cm^2$]. The model for the ohmic resistance is based on the resistance changes with the temperature of the cell and the change can be calculated from (2.8).

$$R_{ohmic}(T_s) = b_1 + a_1 \cdot T_{cell} \quad (2.8)$$

where a_1 and b_1 are fitting parameters and presented in Appendix B. T_{cell} is the stack temperature. The linear nature of the function (2.8) is verified by [10].

Anode loss

The anode voltage loss is primarily based on the presence of CO in the syngas for the fuel cell. Assuming Butler-Volmer kinetics applies to the system, and assuming a symmetry factor of $\alpha = 0.5$, the anode loss equation is simplified to (2.9). The forward and backward rate terms are calculated by the inverse hyperbolic sinus function.

$$\eta_{anode} = \frac{R \cdot T_{cell}}{\alpha_a \cdot F} \cdot \sinh^{-1} \left(\frac{i}{2 \cdot k_{eh} \cdot \theta_{H_2}} \right) \quad (2.9)$$

where T_{cell} is the cell temperature, α_a is the anode charge transfer coefficient, θ_{H_2} expresses the surface coverage of hydrogen and k_{eh} is the H_2 electro oxidation rate. The equations for both the coverage of H_2 and CO can be seen in Appendix B.4.2. The modeling approach is solving the equations for the coverage at equilibrium, using a numerical solver in MATLAB and return the value for the H_2 coverage to the Simulink model.

2 Nonlinear system model

Cathode loss

Because of the continual backward and forward flow of electrons from and to the electrolyte, there is a need to specify a term that indicates the transfer rate at equilibrium. This is referred to as the “exchange current density”, and is often indicated by i_0 . When the “exchange current density” is high, the surface of the electrode is more ‘active’ and a current in one particular direction is more likely to flow. This “exchange current density” i_0 is one of the main elements in performance of a fuel cell electrode. This means that the exchange current density value must be as high as possible. In the modeling of the cathode loss certain changes were made to comply with the HTPEM fuel cell used in the project. A modeling strategy for the exchange current density i_0 from [15] was implemented in the model and the exchange current density increases as a function of the cell temperature T_{cell} , see (2.10). The exchange current density compared to temperature can be seen from figure 2.6.

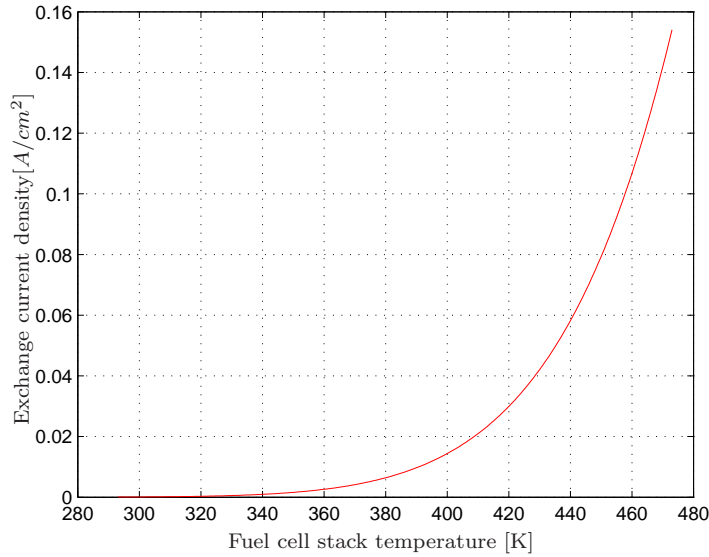


Figure 2.6: *Exchange Current Density vs. Stack temperature*

$$i_0(T_s) = a_2 \cdot e^{-b_2 \left(\frac{1}{T_s} - \frac{1}{T_{limit}} \right)} \quad (2.10)$$

where T_{limit} is 433K(160°C) and the lower limit of the HTPEM’s temperature operating range. The constants a_2 and b_2 are fitting parameters, found in earlier experiments[15], and they can be seen from appendix Appendix B.1. These constants shape the exchange current density with the change in temperature.

The cathode loss is a summation of the activation loss and the concentration loss. The activation loss η_{act} is the voltage required to drive the chemical reactions at

the electrodes of the fuel cell. This loss is nonlinear and have a large impact at low current densities. Activation loss is caused by the slowness of the reactions taking place on the surface of the electrodes. The activation loss can be calculated as shown in (2.11).

$$\eta_{act} = \frac{R \cdot T_{cell}}{2 \cdot \alpha \cdot F} \ln \left(\frac{i}{i_0} \right) \quad (2.11)$$

The constant α is called the “charge transfer coefficient” and is held constant, which is commonly used in thermal fuel cell models. For most electrochemical reactions, α ranges from about 0.2 to 0.5.

Diffusion loss is commonly known as concentration loss and result from a decrease of the available reactant over the length of the fuel cell membrane[11]. The concentration losses can be calculated by (2.12).

$$\eta_{conc} = \frac{R \cdot T_{cell}}{4 \cdot \alpha_c \cdot F} \cdot \ln \left(\frac{i + i_o}{i_o} \right) \quad (2.12)$$

The overall cathode loss can be calculated with (2.13)

$$\eta_{cathode} = \frac{R \cdot T_{cell}}{4 \cdot \alpha_c \cdot F} \cdot \ln \left(\frac{i + i_o}{i_o} \right) + \frac{R_{diff} \cdot i}{\lambda - 1} \quad (2.13)$$

where R is the universal gas constant [$J/(mol \cdot K)$], T_{cell} is the cell temperature [K], α_c is the charge transfer coefficient $[-]$, F is Faradays constant [C/mol], R_{diff} is the diffusion resistance [$\Omega \cdot cm^2$], i_o is the exchange current density [A/cm^2] and λ is the air stoichiometry ratio $[-]$. The stoichiometry is a measure for the amount of reactant present for a given process. A stoichiometric ratio of 1 means that the amount of reactant is precisely enough for the reaction to occur, and a stoichiometric ratio higher than 1 results in an excess of reactants after the process has occurred.

The modeling of the cathode loss is performed almost like the model mentioned in (2.13) but with the exchange current density of (2.10). It is assumed that the air stoichiometry is large enough to avoid concentration loss. The last term of (2.13) is substituted by an empirical constant.

$$EMP(T_s) = a_{30} \cdot e^{-b_{30}(T_s - T_{limit})} \quad (2.14)$$

2 Nonlinear system model

This constant EMP account for various deviations between the experiments and the model. The reason for the empirical constant is the loss is not linear at higher temperatures and the empirical factor is added[15]. The constants a_{30} and b_{30} are the fitting parameters and they are presented in Appendix B.1. These parameters have been obtained from simulation of the polarisation curve of the fuel cell, see section 4. Adding the changes from (2.10) and (2.14) respectively, results in an equation for the cathodic voltage loss.

$$\eta_{cathode}(T_s, i) = \frac{R \cdot T_s}{4 \cdot \alpha_c(T_s) \cdot F} \cdot \ln\left(\frac{i}{i_0}\right) + EMP(T_s) \quad (2.15)$$

The charge transfer coefficient $\alpha_c(T_s)$ can be seen in Appendix B. The change of the cathode voltage with the temperature held constant at 453K(180 °C) and the current density changing, can be seen from figure 2.7

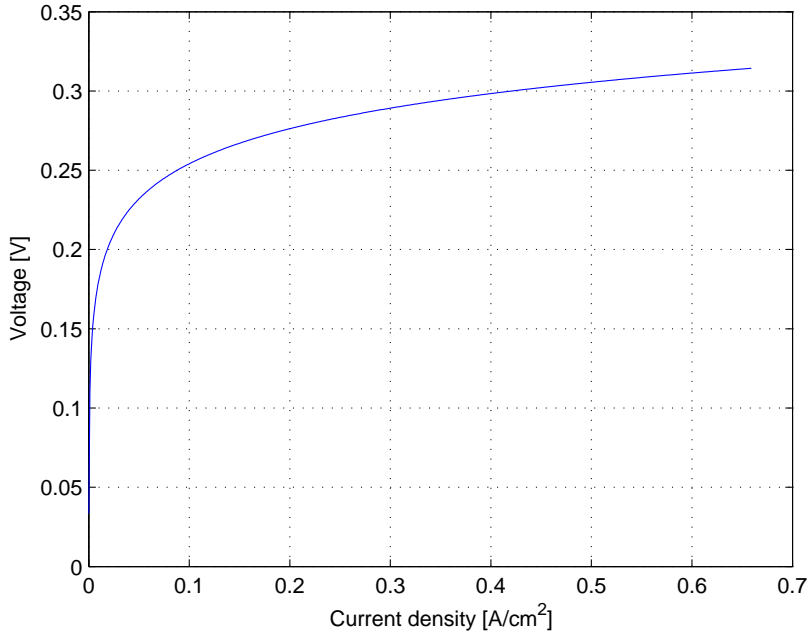


Figure 2.7: Cathode voltage loss compared to current density at 180 °C

As the three voltage losses is described a stack voltage based on current density can be calculated.

Stack voltage

The governing stack voltage equation is shown in (2.1) and is rewritten to include the cathode and anode loss instead of activation and concentration loss, see (2.16).

$$V_{stack} = n_{cell} \cdot (v_{oc} - \eta_{ohmic} - \eta_{cath} - \eta_{anode}) \quad (2.16)$$

where V_{oc} is the open circuit voltage, η_{ohmic} is the ohmic loss. η_{cath} represents the combination of the activation and diffusion loss at the cathode and η_{anode} represents the activation and diffusion loss at the anode. N_{cell} represents the number of cells in the stack. The model for calculating the voltage of the stack has been presented and it can be seen that most of the losses are directly affected by a change in the stack temperature. This

2.1.3 Fuel cell temperature

The temperature of the fuel cell stack is used in all of the equations for the voltage and it is a crucial part in modeling the fuel cell. It is assumed that the temperature of the stack is uniform and that all entrance and exhaust effects are neglected. A schematic of the thermal model is depicted in figure 2.8.

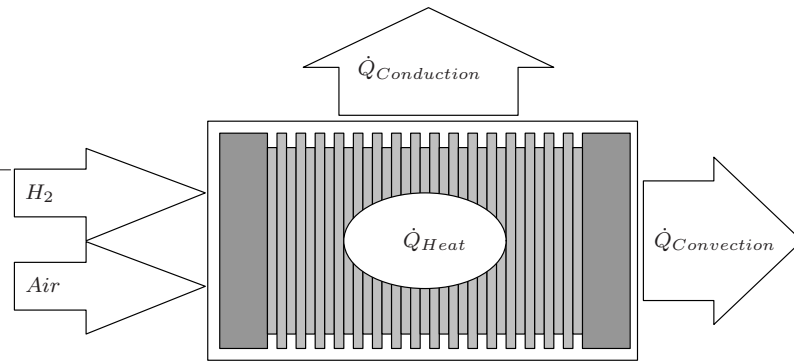


Figure 2.8: *Thermal model of the Fuel Cell stack*

where \dot{Q}_{Heat} is the heat generated inside the fuel cell stack, $\dot{Q}_{Conduction}$ is the heat lost from the fuel cell stack by conduction, and $\dot{Q}_{Convection}$ is the energy transported away from the stack by forced convection.

Heat generated inside the fuel cell stack

In the model the fuel cell produces heat when in operation and the heat is calculated from (2.17). The heat is based on the difference of the reversible voltage v_{ocv} and the voltage drawn from the cell v_{cell} . The voltage of the cell is the electric potential that is usable for running electric appliances.

2 Nonlinear system model

$$\dot{Q}_{Heat} = i \cdot (v_{ocv} - v_{cell}) \cdot n_{cell} \cdot A_{cell} [W] \quad (2.17)$$

where i is the current density and v_{ocv} is the open circuit voltage of the cell, (2.6) and v_{cell} is the cell voltage from (2.16). n_{cell} is the number of cells used to convert the cell voltage to stack voltage and A_{cell} is the area of a single cell. When the fuel cell is operating this is the only function in the stack that transfers energy into the system. The reason for the heat being generated is the voltage loss from (2.16) are converted to heat as the chemical reactions happen.

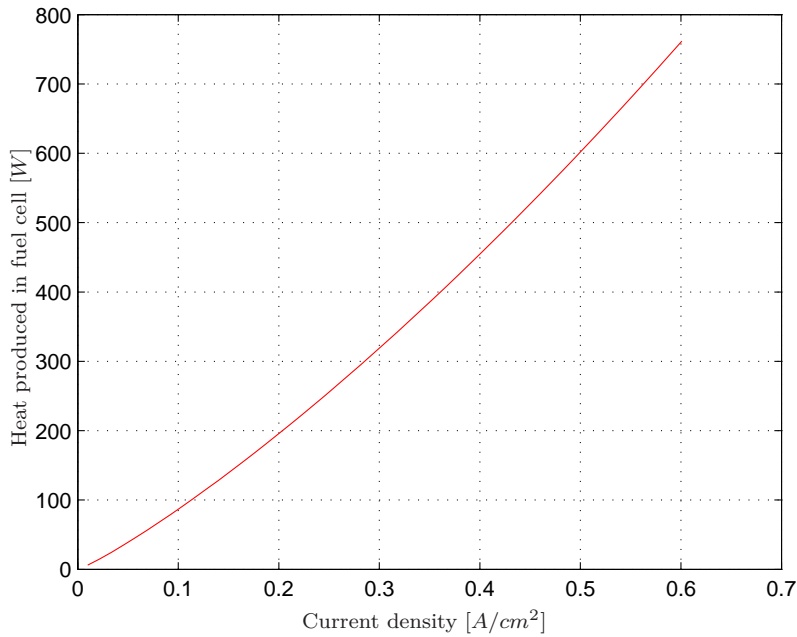


Figure 2.9: Heat generated compared to the current density at constant temperature (180°C)

The heat produced inside the fuel can be seen from figure 2.9 for a constant temperature of 453K (180 °C). The heat must be transferred away by conduction and convection to keep a steady temperature in the fuel cell.

Heat transfer due to conduction from the fuel cell stack

From figure 2.8 it can be seen the loss of heat from the fuel cell stack to the surroundings is modeled as conduction. As mentioned earlier it is assumed that the stack has uniform temperature and the conduction model can be seen from (2.18)

$$\dot{Q}_{conduction} = -k \cdot A_{surface} \cdot \frac{(T_s - T_{ambient})}{x} [W] \quad (2.18)$$

where k is the thermal conductivity factor [$W/m \cdot K$], $A_{surface}$ is the surface areal, T_s is the stack temperature, $T_{ambient}$ is the ambien temperature. To prevent a high heat transfer by conduction, from the fuel cell stack, a layer of insulation is applied. The thickness of the insulation is represented by the x in (2.18) and k is a coefficient of heat transfer based on the type of the insulation applied to the stack. The insulation is melamine foam and it is assumed that the conduction is linear with the temperature, which can be seen from figure 2.10.

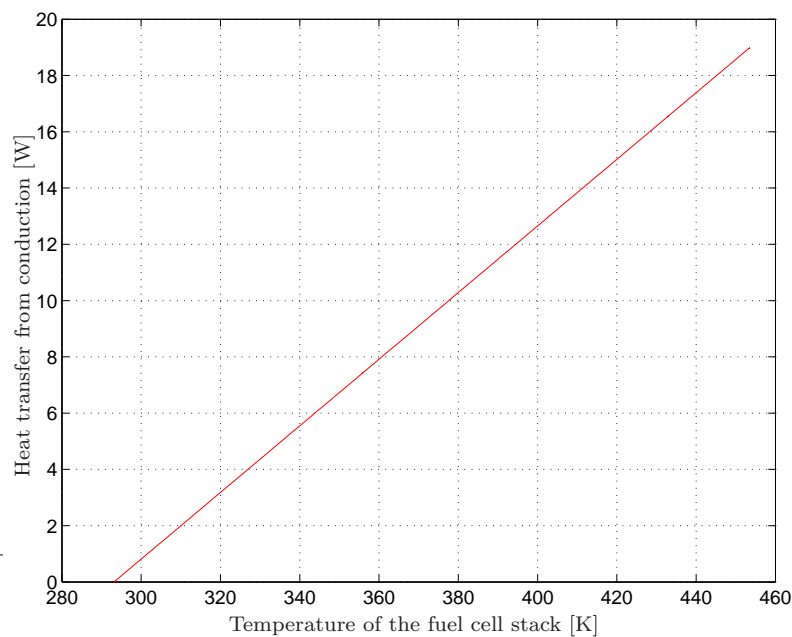


Figure 2.10: Heat transferred from the stack based on conduction

For the reactions from (2.15) to occur oxygen must be supplied from ambient air and this involves the heat transfer by convection.

Heat transfer due to convection in the fuel cell stack

Since the fuel cell stack needs oxygen to produce a voltage and since it can produce enough heat to create a high stack temperature, convection must be applied by an external blower forcing air through the fuel cell stack. The mathematical model calculates the change in enthalpy of the air between the inlet temperature and the exhaust temperature. It is assumed that the exhaust temperature is equal to the stack temperature. The enthalpy is based on regressions for the enthalpy of air, from the program Engineering Equation Solver (EES). The enthalpy is multiplied with the molar flow of air resulting in a heat transfer rate, see (2.19).

2 Nonlinear system model

$$\dot{Q}_{convection} = \dot{n}_{air} \cdot (h(T_{exhaust}) - h(T_{inlet})) \quad [W] \quad (2.19)$$

where $h(T)$ is a regression for the enthalpy in kJ/mol of air as a function of temperature and \dot{n}_{air} is molar flow of air in mol/s .

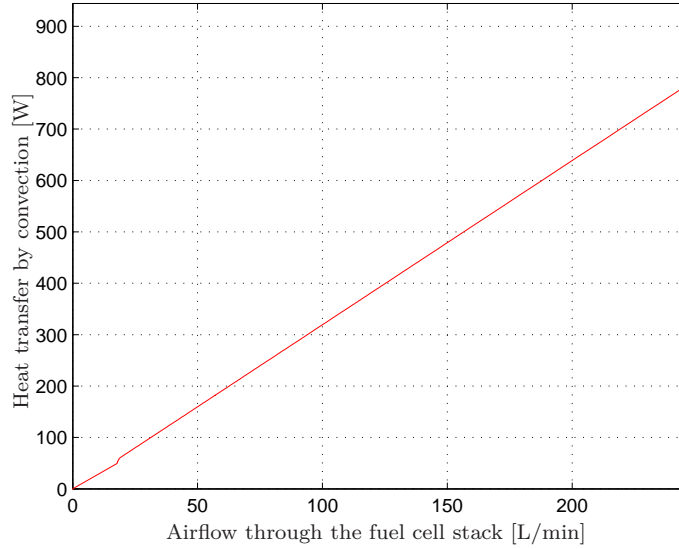


Figure 2.11: Convection plotted against airflow at constant temperature ($180^{\circ}C$)

Plotting the convection against the airflow of the stack gives a view of the convection heat transfer. The change in convection when the airflow increases has linear characteristics if the temperature of the stack is 453 K ($180^{\circ}C$). The heat production and heat transfers, used in the model, have been described and the temperature can be calculated in the following section.

The temperature of the stack

When calculating the temperature of the fuel cell stack the heat transfers. The heat transfers (2.17), (2.18), and (2.19) are summed up in (2.20). The sign notation is positive for heat being created by the system and negative for heat being transported out of the system.

$$\dot{Q}_{stack} = \dot{Q}_{Heat} - \dot{Q}_{Conduction} - \dot{Q}_{Convection} \quad (2.20)$$

The difference in the heat lost and heat generated will result in the power applied to or subtracted from the system, depending on the sign of the sum \dot{Q}_{stack} and this will result in a change in temperature. The powers involved in the fuel cell stack thermal model can be seen from figure 2.12

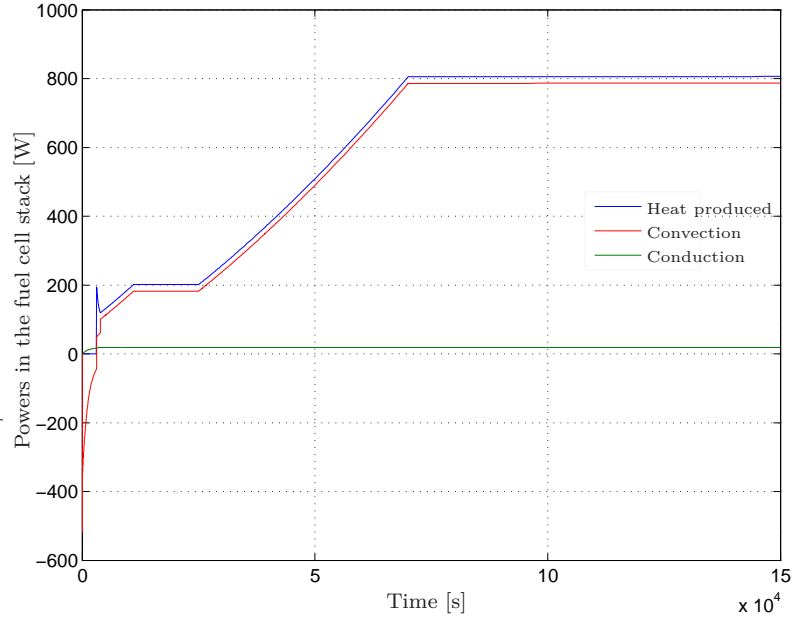


Figure 2.12: Heat transfers in the fuel cell stack

The heat transfers is summed up to represent the heat transfers of the system \dot{Q}_{stack} . The power generated inside the fuel cell stack is added to the fuel cell and the power from the convection and conduction is subtracted. From figure 2.12 it is shown that the convection has the same characteristics as the energy produced inside the fuel cell. The convection balances (2.20) so the temperature calculated in (2.21) is kept constant.

$$T_s = \frac{1}{m_{stack} \cdot c_{stack}} \cdot \int_0^t \dot{Q}_{stack} dt \quad (2.21)$$

where T_s is the stack temperature, m_{stack} is the mass of the fuel cell stack, c_{stack} is the specific heat capacity, and \dot{Q}_{stack} is the power transferred to or from the system. The temperature of the fuel cell stack is modeled from (2.21). The calculation integrates over the power and changes the temperature as the time changes from 0 to a given time t [17].

The interconnection between the thermal model and the voltage model can be seen in Appendix B. It may be noted that since the temperature has a direct influence on the electrochemical loss of the fuel cell stack voltage, it is important to keep the temperature at a steady state.

This concludes the presentation of the nonlinear fuel cell stack model and a presentation of the nonlinear modeling of the reformer can begin.

2.2 Reformer model

The reformer model is divided into two parts. The first part calculates of the temperature of the reformer and the second part calculates of the molar fractions of the reformat gas.

2.2.1 Reformer temperature

Since the burner and reformer in the laboratory are integrated into one component the model of the reformer temperature receives the power from the burning of the H_2 or CH_3OH depending on the respective mode of the system. The modeling of the temperature for the reformer is based on a summation of the heat transfers. The sign notation is positive when transferring energies into the reformer system and negative, when the energies are consumed in the reformer. A diagram of the energies taken into considerations can be seen from figure 2.13.

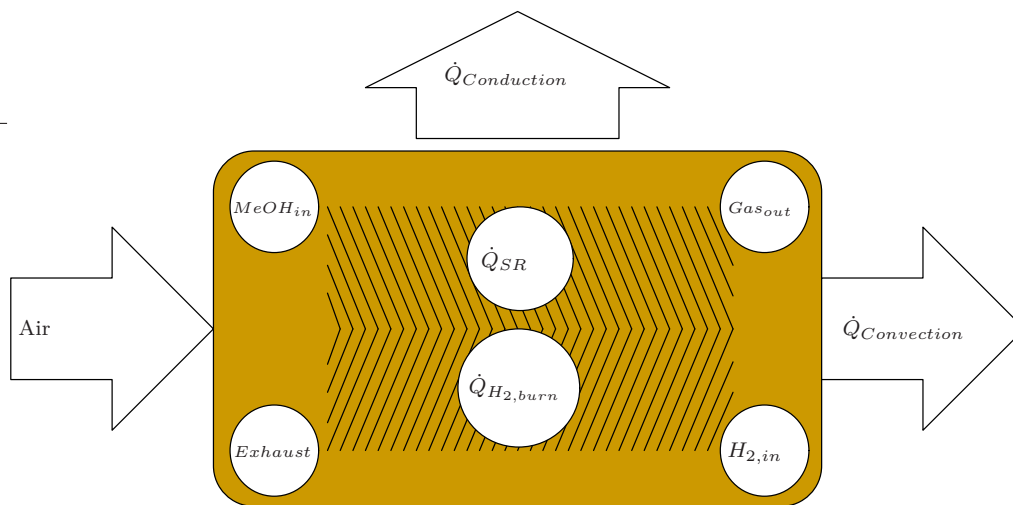


Figure 2.13: *Thermal model of the reformer.*

From figure 2.13 depicting the energy transfers considered in the thermal model of the reformer. The reformer temperature is controlled by forced convection from a blower, where air at room temperature is blown into the burner and leaves at the reformer temperature. The modeling of the convection is performed analog to the convection of the fuel cell stack, see (2.19). The model neglects the convection by the reformat gas because the burner convection, and the loss from the reformation process, is assumed to dominate the temperature. The heat loss from conduction is taken into account and the conductive power is modeled from (2.18). The reformer is heated by burning the remaining H_2 in the cathode exhaust gas stream. The respective reactions happening in the reformer are divided into two types of reaction. The steam reforming reaction can be seen from (1.7) and the enthalpy required to

make the reaction happen is $49.4kJ/mol$. This reaction breaks up the methanol into the respective gas components. The molar flow of the fuel from the evaporator is multiplied with the enthalpy of the steam reforming process to model the power needed to reform the fuel. It is assumed that the steam reforming process only needs to break up the methanol part of the incoming fuel. The energies are summed up to balance the energy in the reformer system. see (2.22)

$$\dot{Q}_{reformer} = \left(\dot{Q}_{burn} - \left(\dot{Q}_{Convection} + \dot{Q}_{SR} + \dot{Q}_{conduction} \right) \right) \quad (2.22)$$

The temperature can be calculated by integration of the sum of the energy transfers, see (2.23)

$$T_{reformer} = \frac{1}{m_{reformer} \cdot c_{reformer}} \int_0^t \dot{Q}_{reformer} dt \quad (2.23)$$

2.2.2 Reformation process

The governing reactions have been presented earlier, see (1.7), and regressions have been made based on minimizing the Gibbs free energy and obtaining an equilibrium in the gas. These regressions are based on the steam to carbon ratio and the temperature of the reformer at which the reformation occurs[1]. The regressions are all linear regressions from EES, and of the 6th order. In the model of the reformer it is assumed that the steam to carbon ratio is a constant of 1.5. The change of the fractions compared to the temperature can be seen from figure 2.14.

The fraction of the hydrogen in the gas decrease with higher temperature and the fraction of CO increase with increasing temperature. The fractions are calculated in the reformer model and sent to the WGS. The model of the reformer is bound by the law of conservation of mass and therefor a mass balance must be presented. The mass of the fuel fed to the reformer must be the same as the mass of the reformat gas leaving the reformer. The mass balance can be seen from (2.24)

$$\begin{aligned} \dot{n}_{MeOH} \cdot M_{MeOH} + \dot{n}_{H_2O} \cdot M_{H_2O} &= x_{MeOH} \cdot M_{MeOH} \cdot \dot{n}_{gas} \\ &+ x_{CO} \cdot M_{CO} \cdot \dot{n}_{gas} + x_{CO_2} \cdot M_{CO_2} \cdot \dot{n}_{gas} + \\ &x_{H_2} \cdot M_{H_2} \cdot \dot{n}_{gas} + x_{H_2O} \cdot M_{H_2O} \cdot \dot{n}_{gas} \end{aligned} \quad (2.24)$$

when solving (2.24) with respect to the gas flow out of the reformer \dot{n}_{gas} a ratio between the fuel gas and the reformat gas can be calculated. This ratio is assumed constant with respect to the reformer temperature.

This change from fuel gas to reformat gas is used later in the fuel calculation for the system. The change in gas flow is applied with a constant K_{com} , since the

2 Nonlinear system model

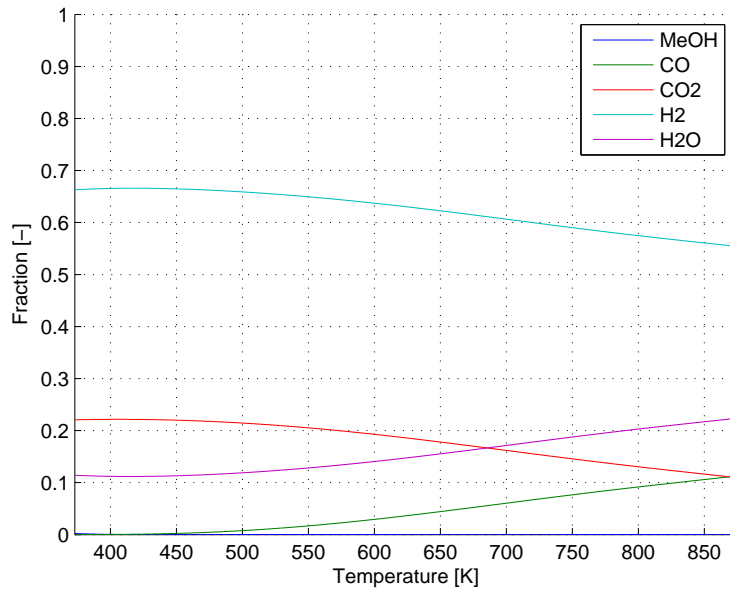


Figure 2.14: Gascomposition with constant SC-ratio of 1.5 and a change in temperature from 373K to 873K

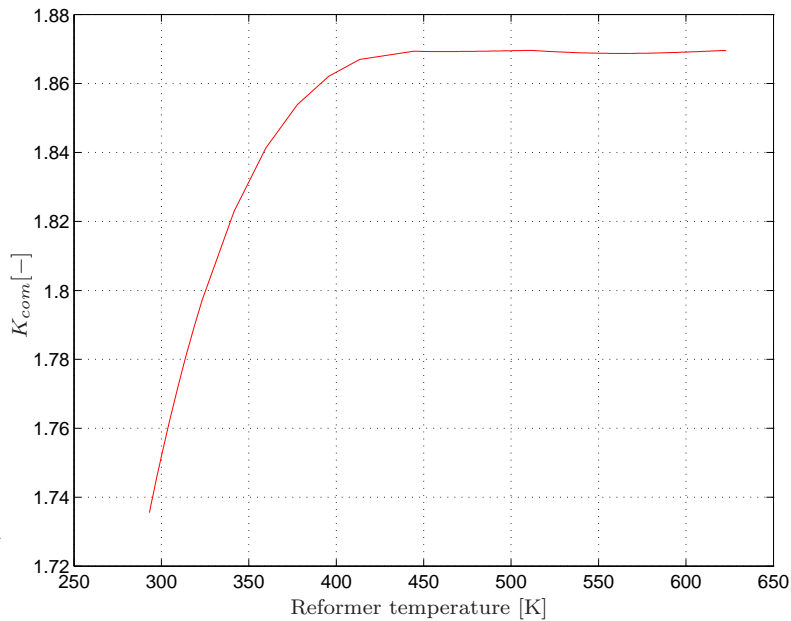


Figure 2.15: Plot of the change in the ratio between \dot{n}_{gas} and \dot{n}_{mix} with respect to reformer temperature. The steam to carbon ratio is 1.5

steam to carbon ratio is assumed to be constant. The change of K_{com} is 0.12 over a temperature range of 200K, and is caused by the change in H_2 fraction. The change is neglected and a constant of 1.86 is used in the model.

The reformer in different operating modes

During the startup mode of the system the reformer receives no vapor flow, since this is redirected to the burner and combusted. The burner releases heat from the combustion and heat is transferred from the burner to the fuel cell stack. The hot air heats up the fuel cell stack and when the temperature of the stack reaches 383K(110°C) the running mode can begin. The temperature of the reformer is held constant at 433K(160°C) since the heating of the fuel cell stack is supposed to be none destructive to the stack membranes. The degradation and possibly destruction of the membranes would be more likely at temperature above the 473K(200°C) which is the top of the HTPEM operation temperature. As the required gas into the reformer needs to be at a specific temperature the evaporator is modeled and is shown in the next section.

2.3 Evaporator model

The evaporator is a heat exchanger that has the purpose of heating the methanol-water mixture to the point of boiling and then super heating the vapors to a temperature of 393 K (120°C). The model of the power needed to evaporate the mixture is divided into two parts. The first part calculates the power needed to evaporate the flow of methanol. The second part is the power needed to evaporate the flow of water.

At the startup operating mode, the evaporator only evaporates a fuel of pure methanol. This requires the fuel tank to be split into two separate containers, one with methanol and one with distilled water. When in startup mode the evaporator will primarily be heated by the electric heaters incorporated into the evaporator. The air from the stack will have a temperature of 293K(20°C) and rising. As the stack is warming up the electric heaters will primarily be heating up the fuel.

2.3.1 Evaporator temperature

The temperature of the evaporator is calculated like the temperature of the reformer and the fuel cell stack. A summation of the energies applied to the evaporator and the calculation of the temperature by integration of the summation. The temperature is critical for the calculation of the power needed to evaporate the mixture and the assumption of uniform temperature applies. The summation of the power and temperature can be seen from (2.26).

2 Nonlinear system model

$$\dot{Q}_{Evap} = \dot{Q}_{Air} + \dot{Q}_{Electric} - \dot{Q}_{vaporize} \quad (2.25)$$

$$T_{Evap} = \frac{1}{m_{Evap} \cdot c_{Evap}} \cdot \int_0^t \dot{Q}_{Evap} dt \quad (2.26)$$

Data for the powers that are summed up in (2.25) can be seen from figure 2.16. The powers are based on the system load, see figure 2.1.

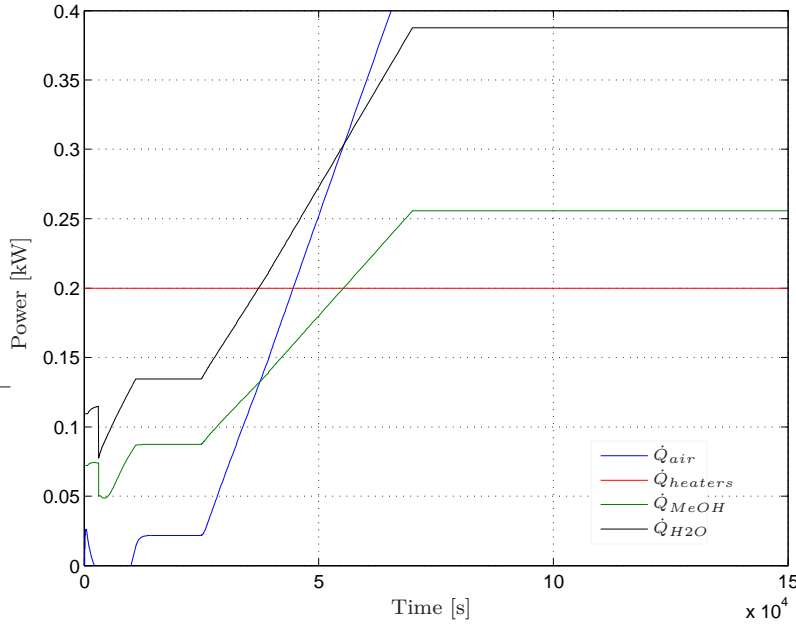


Figure 2.16: Comparison of difference energies in the evaporator

The temperature of the air, exiting the evaporator, is assumed to be the same as the evaporator. The enthalpy is calculated at the input and output of the air flow, and this difference in enthalpy is multiplied with the airflow. This is assumed to be the heat added to the evaporator from the fuel cell exhaust. The other contribution to the evaporator is two 100W electric heaters.

Modeling the vaporization power

The model of the power needed to vaporize the fuel, is based on the first law of thermodynamics. The model represents the three stages that both methanol and water is in during the vaporization process.

The first stage is the preheating of the fluid, where the fluid is heated from ambient temperature of 293K(20°C) to the evaporation temperature. The boiling temperature is calculated with regressions made by [12]. The boiling temperature is based on the steam to carbon ratio of the fuel, see figure 2.17

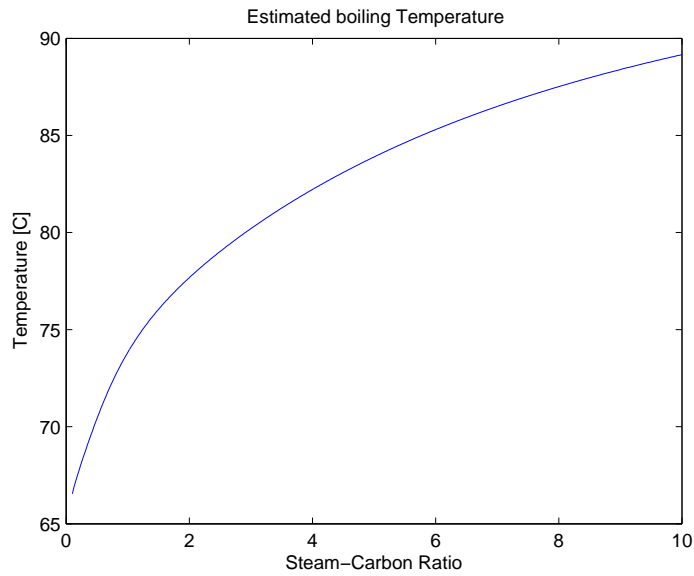


Figure 2.17: The boiling temperature in Celcius

Methanol has a boiling point of 64.5°C and water boils at 100°C. The model of preheating the methanol is made by calculating the enthalpy when the temperature changes from ambient to the boiling temperature. The second stage of the vaporization is the phase change of the fluid. The model assumes that the phase changes instantaneously and that all the fluid is vaporized. The required enthalpy for the phase change is the enthalpy of vaporization for the methanol and a regression has been made from the data in EES. The last stage of the vaporization is the super heating of the methanol vapors. A T-s diagram of the process can be seen from figure 2.18 where the three phases are marked.

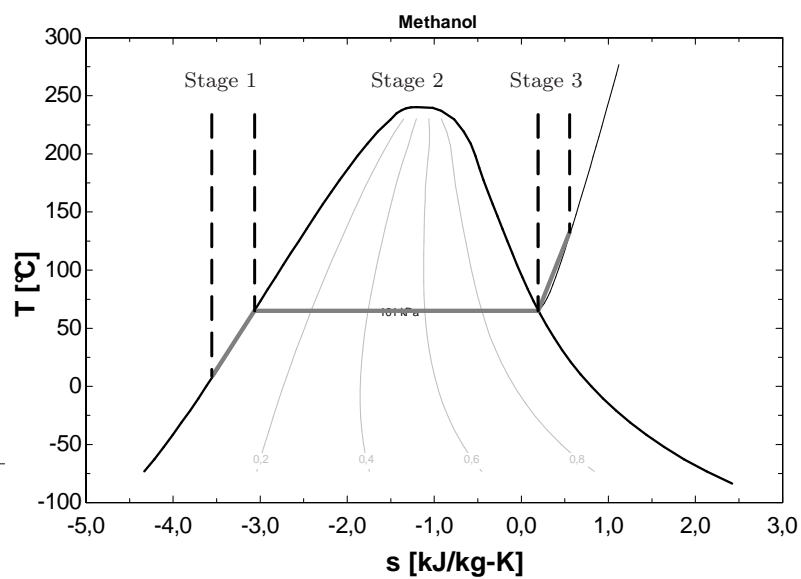


Figure 2.18: T-s Diagram of the process

2 Nonlinear system model

The process is the same for the water in the mixture and regressions for the enthalpy in the three stages is based on data from EES. The calculation of the power needed to evaporate the mixture is calculated from the product of the enthalpy at a given stage and the molar flow of the respective fluid. The powers of the three stages are summed up to represent the power needed to preheat, vaporize and superheat the given fluid.

Since the model is assuming the instantaneous change of phase for the given fluid, some logics has been implemented in the model. The temperature of the evaporator is compared to the boiling temperature of the fuel. When the evaporator temperature is above the boiling point, the power consumption for super heating the fluid is applied to the sum the powers, otherwise the super heating power is neglected.

2.4 Fuel estimation

The reason for developing an estimator is to control the energy supplied to the fuel cell and to achieve a constant hydrogen stoichiometry. The estimator should be able to be run online in the system, which means that the hydrogen fraction and mass conversion, K_{com} , is estimated. During the operation of the fuel cell, the needed amount of fuel can be calculated based on the current drawn from the fuel cell stack, see (2.27). Equation (2.27) only describes the usage of the hydrogen and is only applicable for estimation of fuel for a system running on pure hydrogen. Since this system is running on methanol it is necessary to make a number of modifications for the estimation to apply.

$$\dot{n}_{H_2} = \frac{A_{cell} \cdot i \cdot n_{cell}}{2 \cdot F} \left[\frac{mol}{s} \right] \quad (2.27)$$

where n_{cell} is the number of cells, i is the current density, A_{cell} is the areal of the cell, and F is Faraday's constant. Assuming that (2.27) can be utilized to calculate the needed fuel based on the current density, an estimator can be derived. The fuel delivered to the fuel cell equals the flow of methanol delivered by the pump and the fraction of hydrogen that the flow is reformed into. Since only a fraction of the methanol is reformed into hydrogen, the hydrogen fraction $x_{hydrogen}(T_r)$ is also an important factor of the fuel estimation, see (2.28). The composition of the gas changes when the temperature of the reformer changes.

$$\dot{n}_{estimated} = \frac{A_{cell} \cdot i \cdot n_{cell} \cdot \lambda_{hydrogen}}{2 \cdot F \cdot x_{hydrogen}(T_r)} \left[\frac{mol}{s} \right] \quad (2.28)$$

When the fraction of hydrogen is decreasing, more fuel is needed and when the fraction is increasing the fuel supplied must decrease. Since the project uses the exhaust gas of the fuel cell stack cathode a control factor for the amount of hydrogen in the exhaust gas is needed. $\lambda_{hydrogen}$ is the stoichiometric factor for the excess of hydrogen. This excess hydrogen is also used in fuel cells working on pure hydrogen, though this is to avoid starvation. The increasing and decreasing of the hydrogen in the reformat gas is coupled with the temperature of which the reforming process is taking place. The estimator controls the frequency of the fuel pump. The estimator must take into account the changes happening to the fuel, when the fuel travels from the pump to the fuel cell stack. The pump is a fixed volume pump and the volume of the pump stroke V_{pump} must be applied in the estimator.

$$f_{pump,est} = \frac{A_{cell} \cdot i \cdot n_{cell} \cdot \lambda_{hydrogen}}{2 \cdot F \cdot x_{hydrogen} \cdot \rho_{MeOH} \cdot K_{com}(T_r) \cdot V_{pump}} [Hz] \quad (2.29)$$

The estimator, from (2.27), calculate the amount of hydrogen needed in mol/s , but the pump delivers the flow in liters and therefore the estimator must use the density of the methanol in $kmol/m^3$ to convert between these two units. The estimator also needs to account for the steam reforming action since the law of conservation of mass applies to the steam reforming. The amount of gas that enters the reformer is lower compared to the amount of gas leaving the reformer, but both amounts are of the same mass. This is accounted for by the factor K_{com} which is the ratio between the flow in and out of the reformer. This is independent of the temperature as can be seen in figure 2.15.

2.5 System efficiency

Efficiency is a great tool for comparing energy conversion devices. The concepts when talking about efficiency is the “ideal” efficiency and “real” efficiency, where the ideal is the reversible and the real is the practical efficiency. The efficiency is the ratio between the energy converted and the energy supplied. The electric efficiency can be calculated by (2.30).

$$\eta_{FC} = \frac{U \cdot I - P_{blower} - P_{Evaporator}}{\dot{m} \cdot HHV_{MEOH}} \quad (2.30)$$

where U is the electric voltage of the fuel cell stack, I is the current drawn from the stack, P_{blower} is the power needed to drive blowers for the convection of the fuel stack and reformer respectively. $P_{evaporator}$ is the power consumed in the evaporator for the electric heaters. When calculating the electric efficiency of the fuel cell stack, the power supplied to the stack is the methanol fuel supplied during running operation. The efficiency is based on the higher heating value(HHV) of the methanol due to

2 Nonlinear system model

the methanol entering the system in fluid phase and the higher heating value is the highest amount of energy that can be converted. The efficiency is based on the load pattern applied to the system figure 2.1, and the efficiency can be seen in figure 2.19.

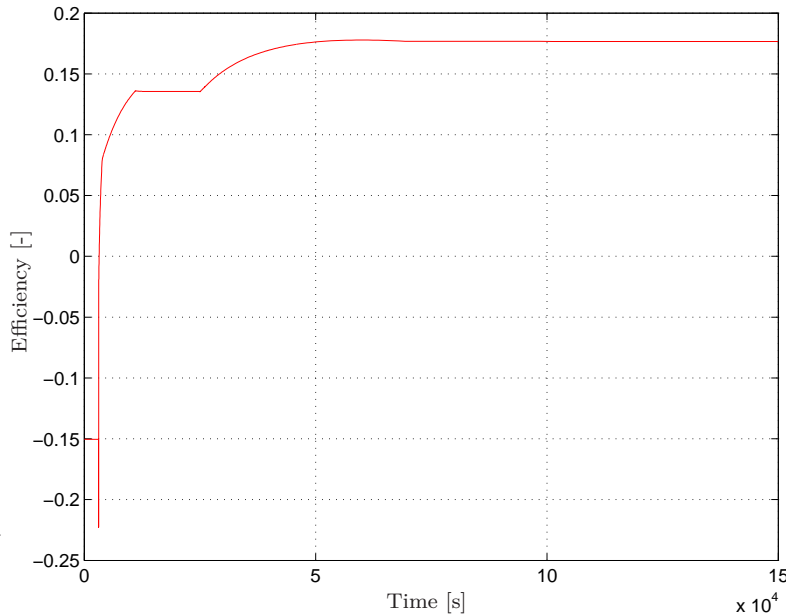


Figure 2.19: *Plot of the modelled efficiency.*

It can be seen from figure 2.19 that the efficiency is negative while the fuel cell stack produces less electric power than the electric heaters provide. The efficiency for the system is approximately 17% based on the higher heating value. The model of the entire system has been presented and must be validated against experiments and data from articles. The efficiency of the system is affected directly by the amount of the methanol needed for driving the system. The temperature affects the voltage of the stack and changes in temperature is mapped into the voltage of the stack. The power needed for the evaporator $P_{evaporator}$ is also a major factor for the efficiency. Minimizing the need for electric heaters is positive for the efficiency of the entire system. The negative part of the efficiency presented in figure 2.19 is based directly on the electric heaters in the evaporator. The model of the system must be validated against data from experiments and data from articles.

The calculated efficiency can be seen in figure 2.19, and is calculated to be a little below 20%.

2.6 Summary

The nonlinear model is based on calculating the voltage and temperature. The available voltage of the fuel cell is based on an open circuit voltage, anode and

cathode losses. The temperature for the fuel cell, reformer and evaporator is calculated. The fuel cell is heated by the loss of current in the fuel cell, and is controlled by forced convection from a blower. The conduction of the fuel cell is included and are based on the difference between the fuel cell stack and ambient temperature. The temperature of the reformer is based on a catalytic burn of excess hydrogen from the fuel cell. The temperature is controlled by forced convection through the burner side. The conduction of the reformer is based on the temperature of the reformer compared to ambient temperature. The evaporator is heated by the exhaust air from the fuel cell, and assumes the temperature of the outlet air is the same as the evaporator temperature. By using the change in enthalpy of the inlet and outlet air, the heat transferred to the fuel can be calculated. The estimation of required fuel is based on used hydrogen in the fuel cell and an excess hydrogen factor λ_{H_2} . The mass conversion factor is assumed constant, and the hydrogen fraction in the gas is estimated on the reformer temperature. The efficiency of the system is calculated to approximately 18% at a current density of 0.66 based on the higher heating value.

Linear system model

3.1 Linearisation of the temperature models

3.1.1 The Stack Temperature

3.1.2 Reformer temperature

3.2 Summary

This chapter focus on the linearisation of the fuel cell stack temperature and reformer temperature. The chapter documents the linear models for which the control of the respective temperatures can be applied. The chapter also presents a transient model of the respective temperatures, from which the controller parameters can be calculated. The linearisation of the temperature models presented in Chapter 2 is performed with a first order Taylor series, see (3.1).

$$f(x_1, x_2) = f(\bar{x}_1, \bar{x}_2) + \left(\frac{df}{dx_1}(x_1 - \bar{x}_1) + \frac{df}{dx_2}(x_2 - \bar{x}_2) \right) \quad (3.1)$$

where the partial derivatives are evaluated at $x_1 = \bar{x}_1$ and $x_2 = \bar{x}_2$. The higher order terms of the Taylor series, are neglected, when considering small deviations from the operating point (\bar{x}_1, \bar{x}_2) [13]

3.1 Linearisation of the temperature models

This section presents the linearized temperature of the stack and the presentation of the linearized reformer temperature is performed after the stack temperature.

3.1.1 The Stack Temperature

The temperature of the stack is based on an energy balance in the dynamic model of the entire system. The model applies conduction, convection and heat produced inside the fuel cells and balance this to calculate the temperature, see (3.2).

$$m_{stack} \cdot c_{stack} \frac{dT_s}{dt} = -\dot{Q}_{conduction}(T_s) - \dot{Q}_{convection}(T_s, \dot{n}_{air}) + \dot{Q}_{electric}(i, v(T_s, i)) \quad (3.2)$$

3 Linear system model

The conductive term is based on the temperature of the stack and the ambient temperature and the constant of convection, which is a linear approximation of the losses due to conduction. The convective term of the power balance is a nonlinear approximation that calculates the energy transported away from the system, based on the enthalpy difference of the air at the inlet and outlet of the stack. The convective term is used for the control of the temperature based on controlling the airflow into the stack. The electric term is the heat generated from the cells in the stack and this is dependent on both the current density and the voltage of the cells. The voltage of the cells is dependent of both current density and the temperature of the stack. These individual terms needs to be linearized.

Conduction

The conductive term is based on the difference between the stack temperature and the ambient temperature multiplied with a constant, which is a linear approach to the approximation, see (3.3).

$$\dot{Q}_{cond} = \frac{k \cdot A_{stack}}{x} \cdot (T_s - T_a) \quad (3.3)$$

where k is the thermal conductivity of the insulating material in $J/(m \cdot K)$, A_{stack} is the conductive area of the stack in m^2 and x is the thickness of the insulation material in m, and T_a is the ambient temperature in K.

Convection

The convective term is based on the difference in the enthalpy of the air at the inlet and outlet of the fuel cell stack. The enthalpy is approximated from a linear first order regression of enthalpy data from EES see (3.4).

$$\dot{Q}_{conv}(T_s, \dot{n}_{air}) = \dot{n}_{air} \cdot (h(T_s) - h(T_a)) \quad (3.4)$$

where h is the enthalpy pr mol of air in $J/kmol$ and \dot{n}_{air} is the molar flow of air in $kmol/s$. By rewriting the molar airflow \dot{n}_{air} to a volumetric airflow \dot{q}_{air} multiplied with a constant results in a more comprehensible equation. The enthalpy regression accounts for the changes of the enthalpy of the air with respect to temperature. The rewriting and linearisation can be found in Appendix C and the resulting equation

can be seen from (3.5).

$$\dot{Q}_{conv,lin} = \overbrace{\dot{Q}_{conv}(\bar{T}_s, \bar{q}_{air})}^{K_{conv_{wp}}} + \overbrace{\left. \frac{\partial \dot{Q}_{conv}}{\partial \dot{q}_{air}} \right|_{\bar{T}_s, \bar{q}}}^{K_{conv_q}} \cdot (\dot{q}_{air} - \bar{q}_{air}) + \overbrace{\left. \frac{\partial \dot{Q}_{conv}}{\partial T_s} \right|_{\bar{T}_s, \bar{q}}}^{K_{conv_{T_s}}} \cdot (T_s - \bar{T}_s) \quad (3.5)$$

Since the derivatives from (3.5) is evaluated in the working point they can be expressed at constants, see (3.6). The equations for the derivatives can be seen from (C.2) and (C.3) respectively.

$$\dot{Q}_{conv,lin} = K_{conv_{wp}} + K_{conv_q} \cdot (\dot{q} - \bar{q}) + K_{conv_{T_s}} \cdot (T_s - \bar{T}_s) \quad (3.6)$$

The linearisation of the convection is now complete. This convection is used to control the temperature of the stack and remove some of the heat that is generated inside the stack.

Heat generated i fuel cell

The fuel cell generates heat when current is drawn from the stack and the heat can be expressed from (3.7). This expression is nonlinear and needs to be linearized.

$$\dot{Q}_{heat} = (v_{rev} - v_{cell}(T_s, i)) \cdot i \cdot n_{cell} \cdot A_{cell} \quad (3.7)$$

The linearization can be seen in Appendix C and the result can be seen from (3.8)

$$\dot{Q}_{heat,linear} = \overbrace{\dot{Q}_{heat}(\bar{T}_s, \bar{i})}^{K_{heat_{wp}}} + \overbrace{\left. \frac{\partial \dot{Q}_{heat}}{\partial T_s} \right|_{\bar{T}_s, \bar{i}}}^{K_{heat_{T_s}}} \cdot (T_s - \bar{T}_s) + \overbrace{\left. \frac{\partial \dot{Q}_{heat}}{\partial i} \right|_{\bar{T}_s, \bar{i}}}^{K_{heat_i}} \cdot (i - \bar{i}) \quad (3.8)$$

Evaluating the partial derivatives and the working point, represented in (3.8), as constants results in (3.9).

$$\dot{Q}_{heat,linear} = K_{heat_{wp}} + K_{heat_{T_s}} \cdot (T_s - \bar{T}_s) + K_{heat_i} \cdot (i - \bar{i}) \quad (3.9)$$

3 Linear system model

The linearized fuel cell stack temperature

Now the three parts of the stack temperature model has been linearized. The governing equation of the stack temperature can be expanded by inserting (3.3), (3.6) and (3.9) in (3.2). This gives (3.11).

$$\begin{aligned}
 m_{stack} \cdot c_{stack} \frac{dT_s}{dt} &= - \left(\frac{k \cdot A_{stack}}{x} \cdot (T_s - T_a) \right) \\
 &- \left(K_{conv_{wp}} + K_{conv_{T_s}} \cdot (T_s - \bar{T}_s) \right) + K_{conv_q} \cdot (\dot{q}_{air} - \bar{q}_{air}) \\
 &+ K_{heat_{wp}} + K_{heat_{T_s}} \cdot (T_s - \bar{T}_s) + K_{heat_i} \cdot (i - \bar{i}) \quad (3.10)
 \end{aligned}$$

Separation and factorization of the variables can be performed in order to ease the Laplace transformation of the temperature model, see (3.11).

$$\begin{aligned}
 m_{stack} \cdot c_{stack} \frac{dT_s}{dt} + T_s \cdot \left(\frac{k \cdot A_{stack}}{x} + K_{conv_{T_s}} - K_{heat_{T_s}} \right) &= \\
 \frac{k \cdot A_{stack}}{x} \cdot T_{amb} - K_{conv_{wp}} - K_{conv_q} \cdot (\dot{q}_{air} - \bar{q}_{air}) & \\
 + K_{heat_{wp}} + K_{heat_i} \cdot (i - \bar{i}) + (K_{conv_{T_s}} - K_{heat_{T_s}}) \cdot \bar{T}_s & \quad (3.11)
 \end{aligned}$$

Applying the Laplace transformation of (3.11) and summing up the constant parts in one constant results in (3.12).

$$\begin{aligned}
 \left(m_{stack} \cdot c_{stack} \cdot s + \left(\frac{k \cdot A_{stack}}{x} + K_{conv_{T_s}} - K_{heat_{T_s}} \right) \right) \cdot T_s(s) &= \\
 \frac{k \cdot A_{stack}}{x} \cdot T_{amb} - K_{conv_{wp}} + K_{heat_{wp}} - K_{conv_q} \cdot (\dot{q}_{air}(s) - \bar{q}_{air}) & \\
 + K_{heat_i} \cdot (i(s) - \bar{i}) + (K_{conv_{T_s}} - K_{heat_{T_s}}) \cdot \bar{T}_s & \quad (3.12)
 \end{aligned}$$

A linear model the stack temperature represented in SimulinkTM can be seen from figure 3.1.

For the purpose of control the investigation of the transients of the linear model is in order. The linear temperature model is turned into a transient model by neglecting the stationary contributions. This changes the output of the model to only provide

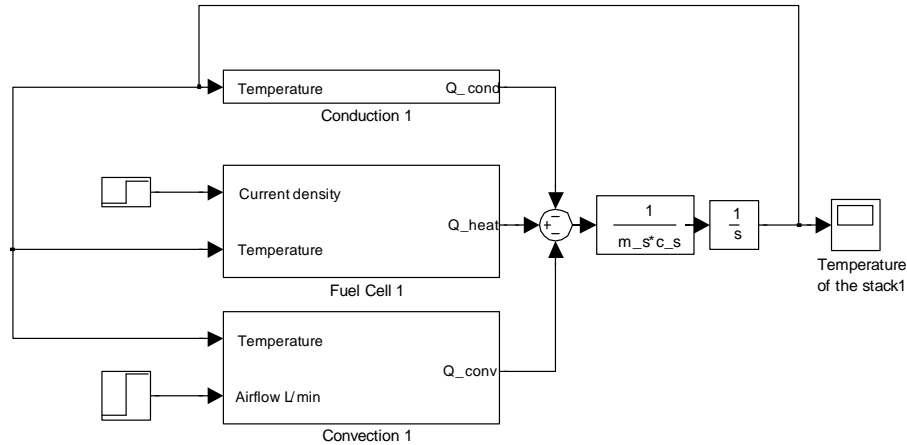


Figure 3.1: *Linear Model of the stack temperature*

an amplitude of the change instead of a value for the temperature. For a reduction of (3.12) to a transient model, see (3.13).

$$\left(m_{stack} \cdot c_{stack} \cdot s + \left(\frac{K_{conds}}{k \cdot A_{stack}} + K_{conv_{T_s}} - K_{heat_{T_s}} \right) \right) \cdot T_s(s) = -K_{conv_q} \cdot \dot{q}_{air}(s) + K_{heat_i} \cdot i(s) \quad (3.13)$$

The model for the transients of the fuel cell model has been presented. The model is linear and the model can be used for the control of the fuel cell. The model is linearized in a working point and the constants are calculated based on the working point parameters. From (3.13) it can be seen that the temperature of the stack is dependent of the current density to add heat to the system and the airflow to remove heat from the system, shown by the sign convention.

3.1.2 Reformer temperature

The reformer temperature is governed by a balance of heat transfers, see (3.14).

$$m_r \cdot c_r \cdot \frac{dT_r}{dt} = \dot{Q}_{H2burn}(T_r, i) - \dot{Q}_{SR}(T_r, i) - \dot{Q}_{conv}(T_r, \dot{q}) - \dot{Q}_{cond}(T_r) \quad (3.14)$$

where \dot{Q}_{H2burn} is the heat transfer from the burner in kW , \dot{Q}_{SR} is the heat transferred for the endothermic reformation process in kW , \dot{Q}_{conv} and \dot{Q}_{cond} are

3 Linear system model

the heat transfers from convection and conduction respectively. The applications of convection and conduction in (3.14) are modeled by (3.3) and (3.6) respectively. The heat supplied by burning the hydrogen \dot{Q}_{H2burn} is calculated from the current density of the fuel cell stack and the temperature of the reformer, see (3.15). The energy lost to the steam reforming process is also based on both the current density and the temperature of the reformer, see (3.16).

$$\dot{Q}_{H2burn} = (f_{pump}(i, T_r) \cdot K_{system} - FC_{usage}(i)) \cdot HHV_{hydrogen} \quad (3.15)$$

$$\dot{Q}_{SR} = f_{pump}(i, T_r) \cdot K_{pump} \cdot K_{evaporator} \cdot H_{SR} \cdot 1000 \quad (3.16)$$

where the constants K_{system} is the changes made to the fuel from being pumped into the system and until the burning process. K_{pump} and $K_{evaporator}$ represents the changes happening to the fuel when it enters the pump and is evaporated. $HHV_{hydrogen}$ is the higher heating value for the hydrogen being burned. H_{SR} is the enthalpy required for the steam reforming process. The fuel cell uses some of the hydrogen in the gas during operation and this is modeled with (2.27). A mathematical relation between the fuel pump frequency and the current density was proposed in (2.29). This estimator is nonlinear since it depends on the temperature and the current density. In order to simplify the estimation for the calculation and implementation, the values from (2.29) for the fraction of the hydrogen in the reformat gas is assumed constant. The change of the molar flow inside the reformer due to the reformation process is assumed constant as well, and the equation for the estimation can be seen from (3.17).

$$f_{pump,lin} = \frac{n_{cell} \cdot A_{cell}}{2 \cdot F} \cdot \overbrace{\frac{\lambda_{H_2}}{x_{H_2} \cdot \rho_{MeOH} \cdot K_{com} \cdot V_{pump}}}^{K_{estimator}} \cdot i \quad (3.17)$$

The change in pump frequency has a linear relationship with the current density and can be summed up into one constant and by inserting both (3.17) and (2.28) into (3.15) and (3.16) respectively. Rewriting of the respective equations for the reformation and burning processes results in (3.18) and (3.19).

$$\dot{Q}_{H2burn} = \overbrace{\left(K_{estimator} \cdot K_{system} - \frac{n_{cell} \cdot A_{cell}}{2 \cdot F} \right)}^{K_{H2burn}} \cdot HHV_{hydrogen} \cdot i \quad (3.18)$$

$$\dot{Q}_{SR} = \underbrace{K_{estimator} \cdot K_{pump} \cdot K_{evaporator} \cdot H_{SR} \cdot 1000}_{K_{SR}} \cdot i \quad (3.19)$$

Inserting (3.18) and (3.19) into (3.14) results in a linear equation with the dynamics of the temperature for the reformer, see (3.20). This represents the linearized temperature of the reformer with the given variables from the reformer.

$$\begin{aligned}
 m_r \cdot c_r \cdot \frac{dT_r}{dt} &= K_{H2burn} \cdot i - K_{SR} \cdot i \\
 &- K_{conv_{wp}} K_{conv_{T_r}} \cdot (T_r - \bar{T}_r) - K_{conv_q} \cdot (\dot{q} - \bar{q}) - \\
 &- \underbrace{\frac{k_{reformer} \cdot A_{reformer}}{x_{reformer}}}_{K_{cond_r}} (T_r - T_a)
 \end{aligned} \tag{3.20}$$

The linearized model is presented in Simulink™ and the model can be seen from figure 3.2.

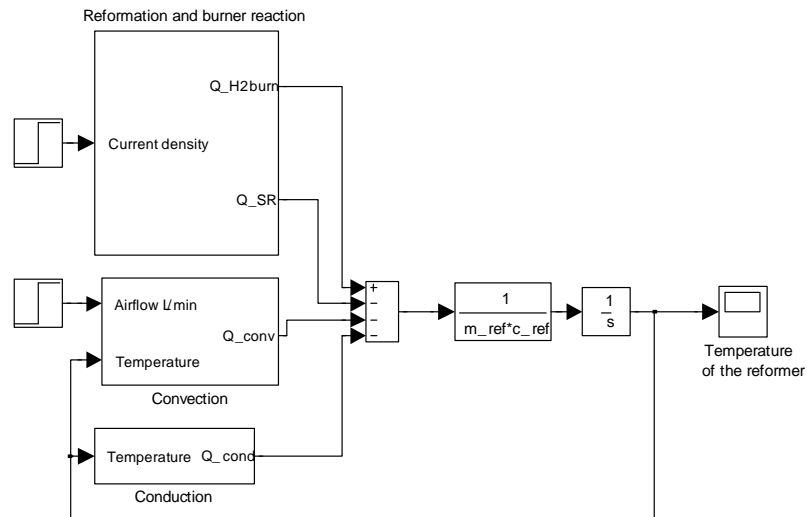


Figure 3.2: Linear model of the reformer temperature from Simulink™

In order to be able to study the transient responses from the reformer temperature, based on changes in the variables, the constant terms, e.g. terms involving \bar{T}_r , are neglected. The model is transformed into a transient model based only the changing variables using Laplace transform. The various factors are collected with respect to their given variables, see (3.21).

$$(m_r \cdot c_r \cdot s + K_{conv_{T_r}} + K_{cond_r}) \cdot T_r = (K_{H2burn} - K_{SR}) \cdot i - K_{conv_q} \cdot q \tag{3.21}$$

The transient model of the reformer temperature has been presented and it is a linear model. This model is the base for the calculation of the controller parameters for

3 Linear system model

the reformer. The model shows that the temperature is dependent of two variables, the current density and the airflow. The current density adds heat to the reformer and the airflow removes heat from the reformer as was expected.

3.2 Summary

The models from Chapter 2 have been linearized and the respective temperatures have been presented with the variables that affect the temperature. The models have all been approximated with a first order Taylor series and this approximation will result in deviations from the nonlinear temperatures. The deviations from the respective linearized parts of the model are dependent of the deviation from the operating point. These models are to be validated against the nonlinear model to see if the linear model is a good approximation.

Validation of models

4.1 Validation of nonlinear model

4.1.1 Polarisation curve

4.1.2 Reformer conduction model

4.1.3 Convection

4.2 Validation of linear model

4.2.1 Fuel cell stack

4.2.2 Reformer temperature

4.3 Summary

This chapter contains the validation of the models presented in Chapter 2. The models are validated against data from various experiments.

4.1 Validation of nonlinear model

4.1.1 Polarisation curve

The polarisation curves in the model is validated against experiments in [9]. The empirical value used in (2.14) is fitted by two parameters, a_{30} and b_{30} . A script is made in MatlabTM and can be seen in Appendix E.3. The range for $a_{30} \in [0.3, 0.6]$ and $b_{30} \in [0.026, 0.028]$ is searched for the best set of fitting parameters.

The script routine is changing the coefficients a_{30} and b_{30} from chosen intervals. These intervals are spread out over an repeating number, and the repeating number is set to 10. First a loop changes a_{30} to the starting number and the whole interval of b_{30} is run. This can be seen in figure 4.1 and it can be seen that for every change of a_{30} there is 10 changes in b_{30} .

At every change of b_{30} the model is processed with a changing current density from 0.01 to 0.66 A/cm^2 . The values of a_{30} and b_{30} can be seen in B.1. The temperature is held constant at 180 $[^{\circ}C]$ and CO is at set at 1000 ppm. This is evaluated against experimental data and a difference at every timestep is calculated. The absolute value of all the time steps are added together and is saved with the parameters a_{30} and b_{30} . This gives a total of 100 simulations and it is evaluated at which index the score is the lowest. This can also be seen from figure 4.1 as the score is compared to the simulated run number.

4 Validation of models

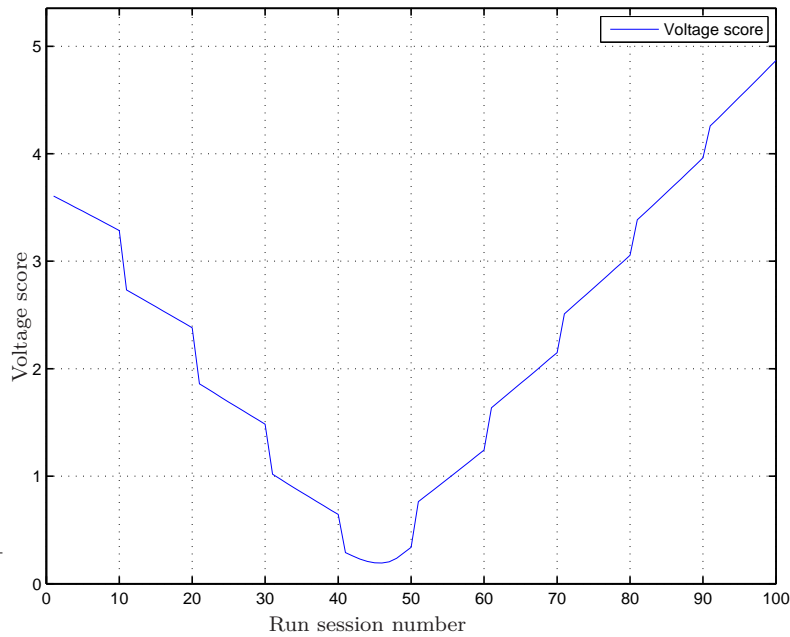


Figure 4.1: *Simulated run sessions*

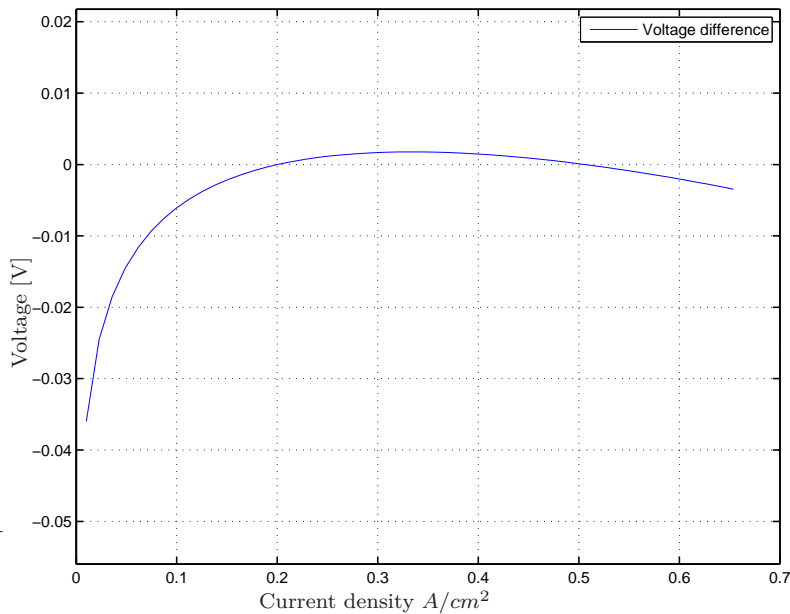


Figure 4.2: *Difference in voltage from experimental data compared to simulated*

The lowest score is found at run 46 and got the score 0.1924. The difference in voltage for this operating point can be seen in figure 4.2 and it shows that the largest difference is present at low current densities. The two polarization curves are compared in figure 4.3.

It is considered precise enough for the simulation to run, though if other constants needs to be evaluated it is possible to change the a_{30} and b_{30} to other constants. The

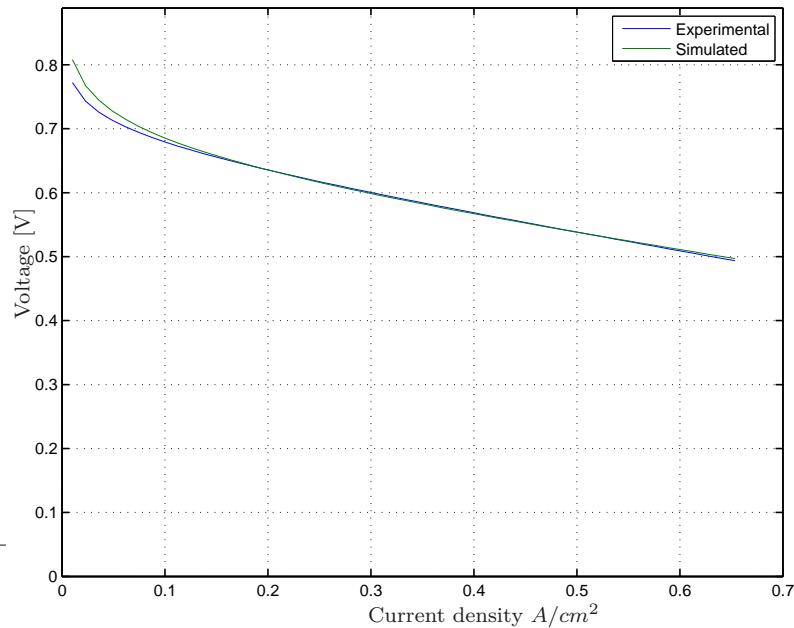


Figure 4.3: Polarization curves of the simulated parameters plotted against the experimental data from [9]

simulations shows that the deviations from the polarization curve has the largest value at current densities lower than $0.1 A/cm^2$, see figure 4.3. This might be caused by the used mass flow controllers, and their lacking ability to deliver flows at very low current densities. The measurements for the experiments in [9] and the measurements at current densities lower than $0.1 A/cm^2$ shows very few data points and therefore the uncertainties in this region will be larger. The model of the fuel cell stack is assumed correct for the purpose of control.

4.1.2 Reformer conduction model

To validate the model for the heat transfer by conduction for the reformer an experiment is performed. The reformer is heated up until a temperature of $350 ^\circ C$ is reached. The reformer is heated with hydrogen and the feed of hydrogen is cut off, and convection is stopped. The temperature of the reformer were logged by Labview™ software developed for the project. The change in temperature can be seen from figure 4.4.

It can be seen from figure 4.4 that the convection applied in the model of the system does not return the same drop in temperature as the experiments. This may be caused by differences between the model and the experiment. In the experiment the reformer were insulated with a 1 cm thick layer of insulation around the main of the reformer where the temperature is measured, but the pipes of the reformer is not insulated. This may add to the change in the reformer temperature from the

4 Validation of models

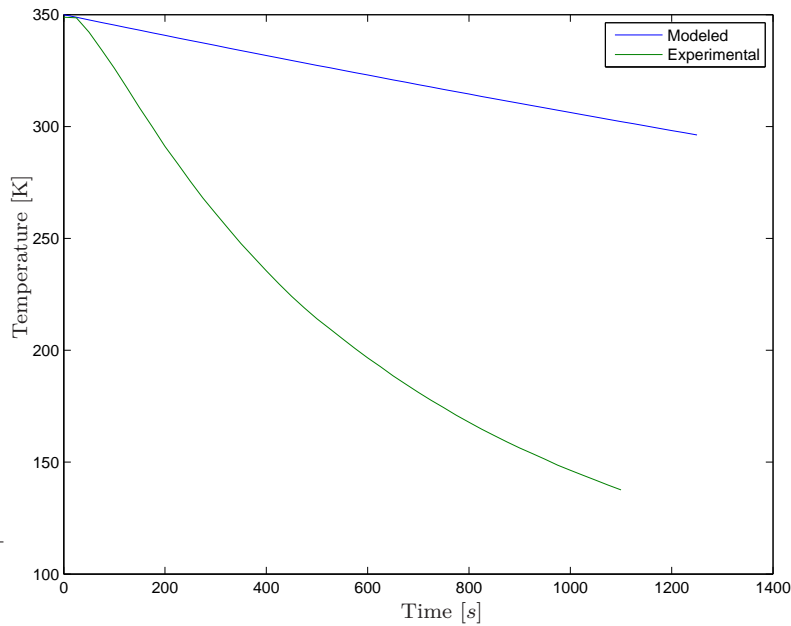


Figure 4.4: *Temperature plot of conduction in model compared to experimental conduction*

experiment. The reformer had earlier been used for the steam reforming process and it is uncertain if the reformer lost heat due to the endothermic reformation process. The conduction from the model represented by the blue line is only based on the area perpendicular to the surfaces. The area of which conduction is calculated from may be estimated wrong, and a factor of 6.5 for the correction is added to the conduction model. The corrected convection can be seen from figure 4.5.

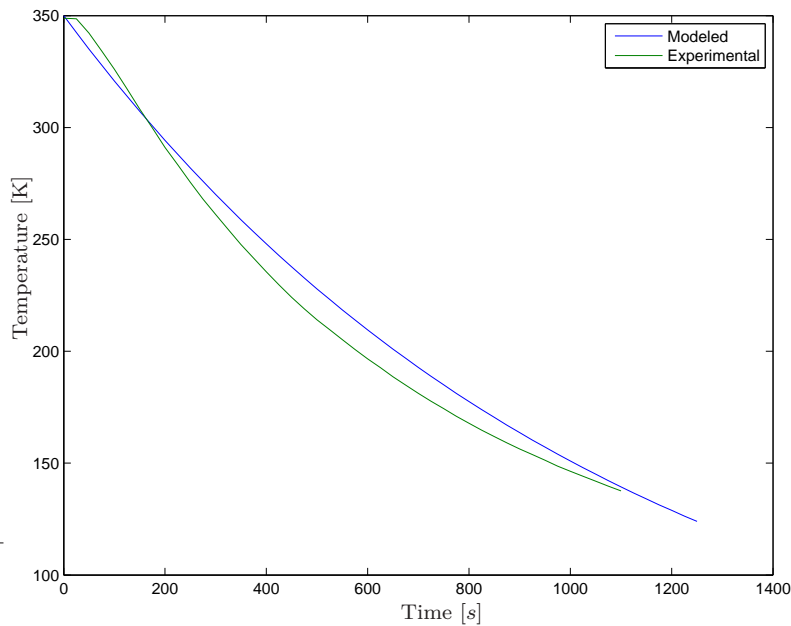


Figure 4.5: *Plot of the corrected conduction compared to experimental conduction*

The tendency of the two temperatures are alike and the constant for the convection model is considered correct. Since the conduction and convection is only based on two experiments, more extensive experiments must be conducted.

4.1.3 Convection

An experiment is performed in order to calculate the temperature control of the reformer by convection. In the experiment the stack is heated to a temperature of 308°C and the feed of the hydrogen used in the burner is stopped. The airflow is set to a fixed rate of 50 l/min and the temperature is logged. The model is build to calculate the temperature based on both the convection of the reformer and the conduction from the reformer. It would be impossible to neglect the temperature drop due to the conduction in the experiment and the model must account for the change in temperature due to conduction. The model output is plotted against the temperature logged in the experiment figure 4.6

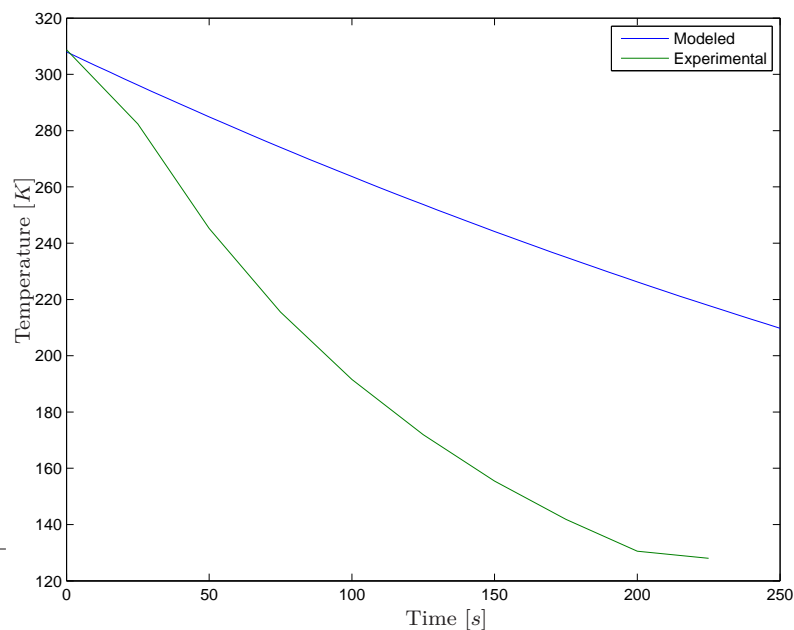


Figure 4.6: *Temperature plot of refoermer due to convection compared to experimental convection*

The convection from the model shows a lesser decrease in temperature than the experimental data presented. The uncertainties regarding the convection is difficult to predict, but the temperature is measured close to the entrance of the fuel into the reformer and the rapid decrease may partially be caused by the measuring point. Multiplying the modeled convection with a constant for the correction is in order. Choosing a constant value of 4 presents good coherence with the data from the experiment and the model output can be seen from the figure 4.7

4 Validation of models

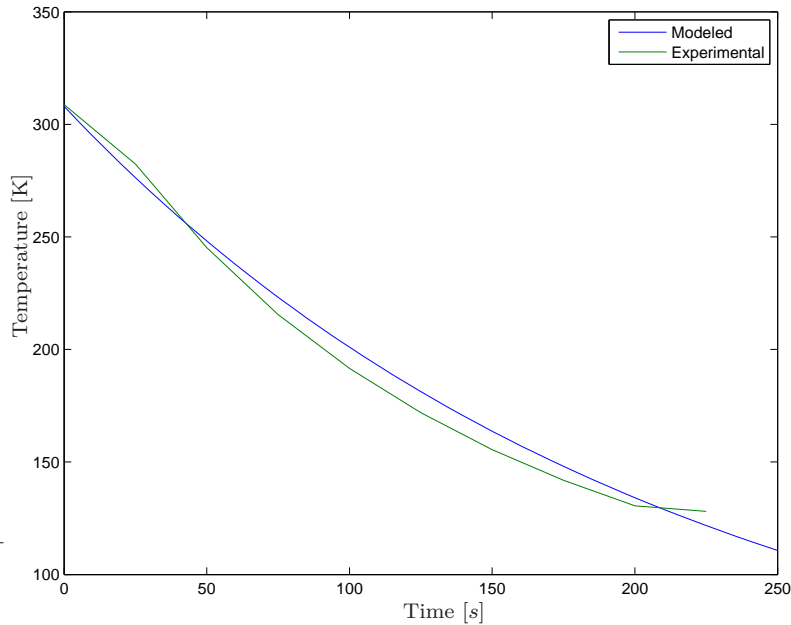


Figure 4.7: *Plot of the corrected convection compared to experimental convection*

The change in temperature in the experiment and the model of the convective changes in temperature exhibits the same tendencies and the amplitude of the changes is approximately the same, thus the convection is assumed correct.

4.2 Validation of linear model

The nonlinear and linear model needs to be compared to see how the linearisation influences the equations. Both models are subjected to the same parameters and the results of each model is plotted to show the differences. The linear temperature models is linearized in a working point and the parameters for the working point is presented in table 4.1.

Variable	Value
Current density i	0.3 A/cm^2
Stack temperature T_s	450 K
Reformer temperature T_r	600 K
Stack airflow $\dot{q}_{air,s}$	10 l/min
Reformer airflow $\dot{q}_{air,r}$	8 l/min

Table 4.1: *Working point parameters for the respective linear models*

4.2.1 Fuel cell stack

The model of the fuel cell stack temperature, that is linearized in section 3, only models the temperature changes. The model calculates the convection, conduction and heat generated inside the fuel cell stack. Only the convection and generated heat will be compared because the conduction equation is already linear.

Convection

Both models are subjected to a change in airflow from 0 to 100 l/min and the temperature is held constant at 453K(180°C). The result can be seen from figure 4.8.

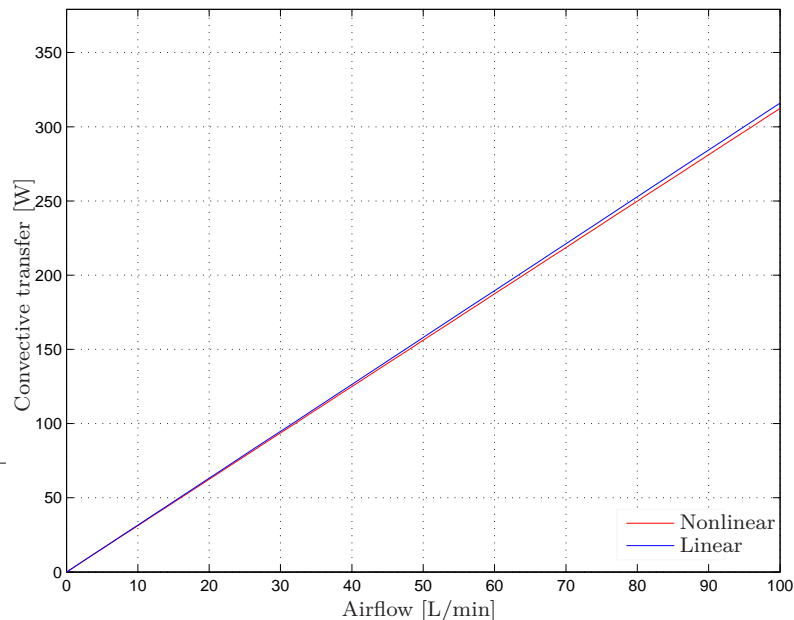


Figure 4.8: Convection plotted with a ramp change in airflow from 0 to 100 l/min

From figure 4.8 it can be seen that the coherence between the linear and nonlinear convection is acceptable. The slope of the convections are approximately the same and they both start in the origin. The linear model has a higher convective power at higher airflows, though is assumed negligible.

Changing the calculation of the convective term to model a variation in temperature from 433K(160°C) to 453K(180°C) at a constant airflow, shows the deviations for the linear convection model, see figure 4.9.

The difference in the linear and nonlinear based on the temperature is very small, see figure 4.9. The slope of the lines are the same and they are both in the same region. This concludes the validation on the convection in the linear model and the heat generated inside the fuel cell stack will be covered.

4 Validation of models

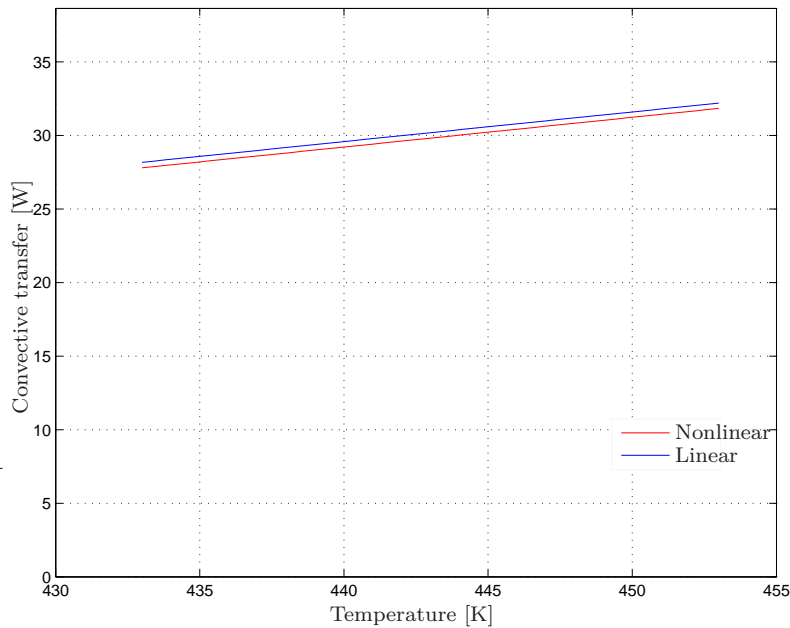


Figure 4.9: Changes in convection with constant airflow (8l/min) and change in temperature

Heat generated

The heat produced inside the fuel cell stack, at a given current density and stack temperature, must be validated. First the changes of the heat generated, based on changes in temperature, is investigated. The current density is kept constant at 0.3 A/cm^2 and the temperature is varied from 433K to 473K. The temperature changes the voltage and thereby affects the heat generated inside the fuel cell stack.

It can be seen, from figure 4.10, that there is a presence of an offset in the linear model. The nonlinear model is subjected to a fixed value for the coverage of the cells, which may cause the offset. The linear model shows the linear change of the heat generated as expected. The offset may be neglected, since the Taylor expansions of the nonlinear equations will result in a loss of precision. The linear model changes more than the nonlinear model, but the change is in the same magnitude, and the higher heat production in the linear model will result in a higher air flow in the linear model. Plotting the change in the heat produced when changing the current density, from 0.01 to 0.6 A/cm^2 , and keeping a constant temperature of 450K. This can be seen from figure 4.11.

From figure 4.11 it can be seen that the model of the heat generated changes sign at very low current densities, which is undesirable. This is most likely caused by the deviation from the operating current density, of which the heat generation is linearized. The linear model changes the heat production faster compared to the nonlinear model and this might be caused by the linearisation process thus leading

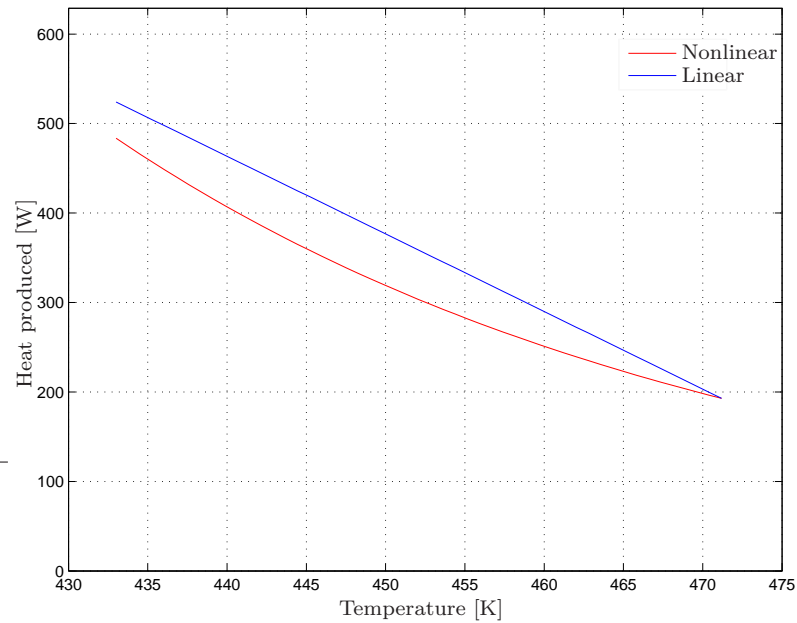


Figure 4.10: *Change in the heat generated based on a change in temperature*

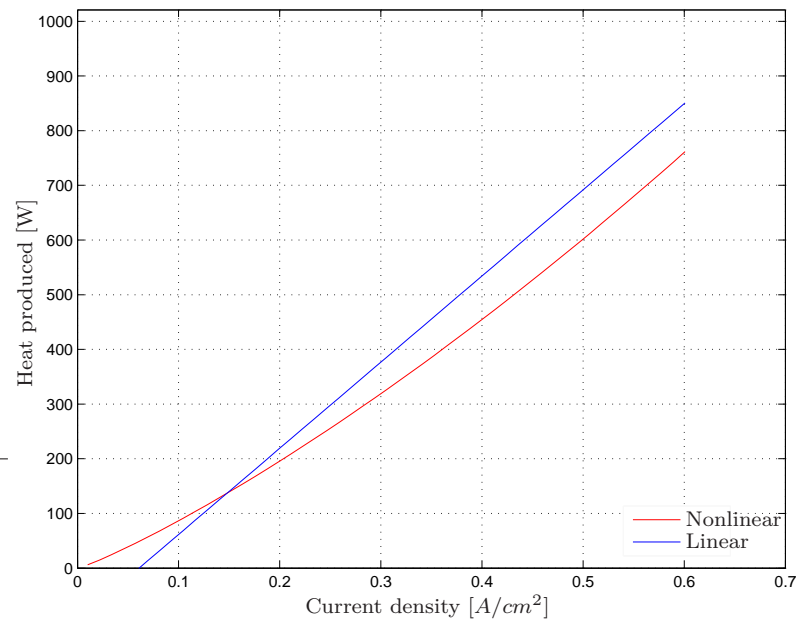


Figure 4.11: *Change in heat based on current density and at constant temperature at 180°C*

to some degree of uncertainty. The characteristics of the heat generation at high current densities are approximately the same though with a small offset in the favor of the linear model. The higher heat production will cause the linear model to apply a higher airflow to control the temperature. The offset is present in the heat generation, based on both the temperature and current density. This is neglected

4 Validation of models

neglected in the transient model. The linear model is assumed valid for the change in heat based on temperature and current density.

4.2.2 Reformer temperature

The thermal linear model for the reformer must be validated to fit with the parameters from the nonlinear model. As in the fuel cell validation, the conduction is linear and will not need any linearisation.

Convection

Plotting the convective heat transfer for the reformer is done at a constant airflow of 30 l/min and the temperature changes from 500 to 700K , see figure 4.12.

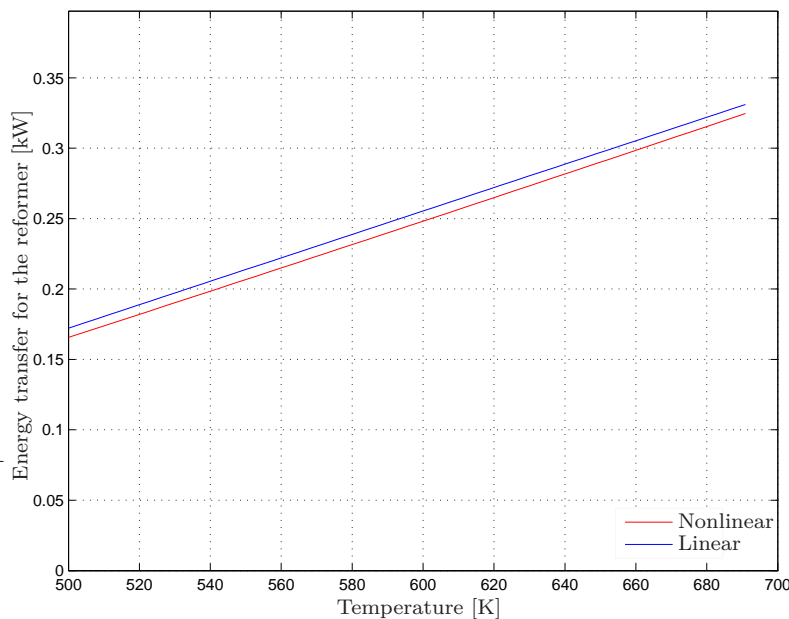


Figure 4.12: *Change in convection at constant airflow and change in temperature*

The change in the nonlinear heat transfer is higher compared to the change in the linear model. This is based on the enthalpy regression, as was the case with the fuel cell stack convection. The operation point for the convection, with respect to temperature, is 600K and the temperature in this validation is varied from 500 to 700K . The change of the heat transfer, with the higher temperature, is lower for the linear model as expected. Investigating the change in the convection is done by keeping a steady temperature at 600K and changing the airflow from 0.1 to 100 l/min . This can be seen from figure 4.13.

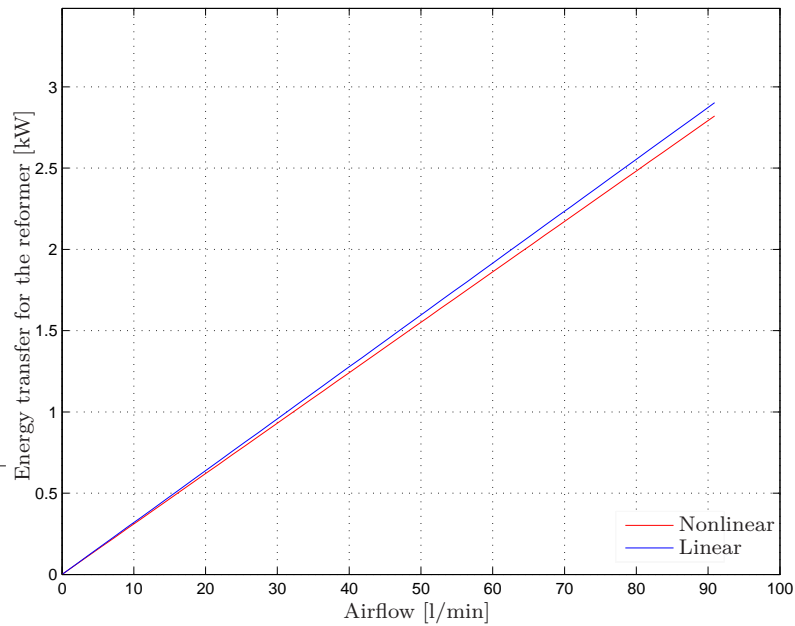


Figure 4.13: *Change in convection at changing airflow*

The convective heat transfer for the linear thermal reformer model is based on the operation point. The chosen operation point shows that the convective powers of the reformer is higher compared to the convective part of the nonlinear model. The differences is evaluated to be small enough to be neglected.

4.3 Summary

The linear model of the stack temperature and reformer temperature both shows good coherence with the nonlinear models, with respect to the convection. The heat generation of the linear fuel cell temperature model shows a constant deviation from the nonlinear model. The current density based heat generation does not start from origin, but the slope of the linear model is equal to the slope of the nonlinear model at higher current densities. The change in temperature for the linear model is higher compared to the nonlinear model, though the change has the same magnitude. The linear model has an approximate constant difference from the nonlinear model. The results is evaluated to be valid and the linear models can still be used for control strategies. As the constants, in the transient model, is neglected control strategies will be valid.

Control strategies

- 5.1 General control systems**
 - 5.1.1 Transport lag
 - 5.1.2 The feed forward approach
 - 5.1.3 Antiwindup
 - 5.1.4 Model overview
 - 5.1.5 Controller demands
- 5.2 Temperature control**
 - 5.2.1 Reformer
 - 5.2.2 Fuel cell stack
- 5.3 Controller design**
 - 5.3.1 Reformer temperature controller
 - 5.3.2 Fuel cell stack temperature controller
- 5.4 Summary**

This chapter is divided into three parts. The first part presents the general control of systems and the control approach for the project. The second part presents the models to be controlled and the responses of the models. The third part of the chapter contains the controller design and the responses for the controllers.

5.1 General control systems

Any system can be broken down into an input $R(s)$ and an output $C(s)$ and through measurement the output is fed back and subtracted from the input to represent the error $E(s)$. The system can be seen from figure 5.1. The relation between $E(s)$ and $C(s)$ is the open loop transfer function transfer function $G(s)$. The measurement may be converted by the feedback transfer function $H(s)$.

Most open loop transfer functions are stable but may destabilize when the output is fed back and subtracted from the input. To investigate the stability of the system the feedback loop must be closed. The function is called the closed loop transfer function, see (5.1).

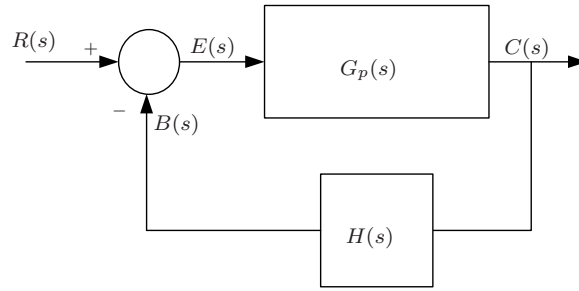


Figure 5.1: *The common closed loop configuration*

$$\begin{aligned}
 C(s) &= G_p(s) \cdot E(s) \\
 E(s) &= R(s) - B(s) \\
 &= R(s) - H(s) \cdot C(s) \\
 C(s) &= G_p(s)[R(s) - H(s) \cdot C(s)] \\
 C(s) + G_p(s) \cdot H(s) \cdot C(s) &= G_p(s) \cdot R(s) \\
 \frac{C(s)}{R(s)} &= \frac{G_p(s)}{1 + G_p(s) \cdot H(s)} \tag{5.1}
 \end{aligned}$$

The closed loop transfer function must be stabilized and the root locus method is a method for analyzing the stability. The poles and zeros of $G(s)$ is obtained and plotted in the imaginary s-plane. The purpose of the root locus method is to investigate the closed loop poles for the plant. The s-plane is defined so the closed loop poles in the negative left half plane are in the stable region and the poles and zeros in the positive right half plane are in the unstable region. The general open loop transfer function (5.2) has m poles and n zeros respectively. The order of m must be higher than n in order to have a realizable system.

$$G_p(s) = \frac{(s + z_n)(s + z_{n-1}) \dots \cdot (s + z_1)(s + z_0)}{(s + p_m)(s + p_{m-1}) \dots \cdot (s + p_1)(s + p_0)} \tag{5.2}$$

The root locus starts from the poles and travels towards the zeros of the open loop transfer function as the gain K is varied from zero to infinity. The gain is a measure for the amplification that a controller can apply to the controlled variable. The gain is limited by the physical system being investigated and the gain can not amplify the error signal more than is allowed by the boundaries for the controlled variable. The root locus is symmetric about the real axis. The presence of a complex pole, or zero, will also force the presence of the complex conjugate pole, or zero. A zero can cancel out a pole and vice versa. The reason for using root locus plots for control purposes is that the knowledge of the open loop poles and zeros gives a good knowledge about the placement of the closed loop poles. The closed loop pole(s)

closest to the imaginary axis is called the dominant closed loop pole(s) and are the most important pole to investigate, since it dominates the response of the system. Changing the input from one value to another value instantly with a step function results in a system response. This response can be shaped and this is the goal of the control strategies. The cancellation of one of the dominant poles by adding a zero and placing another pole will alter the response of a system and this method is called pole/zero placement. The cancellation and addition of poles and zeros are summed up in a transfer function, which commonly is called a controller or compensator. A compensator is multiplied with the open loop transfer function and the result is an altered system with the response wanted. The controller is most commonly a piece of software or an analog circuit board which receives the feedback signal and alters the control signal in order to make a faster response. The compensator may induce an overshoot or oscillations in the response of the system, which may unwanted, depending on the systems working environment. A system that cannot become unstable has all the poles and zeros placed in the left half plane of the s-plane. This is called a minimum phase system. When a pole or zero is placed in the right half plane, the system is called a non-minimum phase systems. The non-minimum phase systems will become unstable if the closed loop poles are placed in the right half plane. Caution must be exercised when changing the gain K a non-minimum phase system since closed loop poles of the non-minimum phase system moves towards the right half plane. The placement of a closed loop pole in the right half plane will make the error increase and thereby the output increase beyond the possible boundaries of the system. When the poles of the system is placed in the left half plane of the s-plane the error decreases and the response settles on the input. If the dominant closed loop pole is placed on the imaginary axis the system will be oscillatory and the error will never decay nor increase. After a short introduction to control strategies the explanation of the two degree freedom systems follows.

Two-degree-of-freedom systems

The system presented in figure 5.1 is a system with one input and one output. This type of system can be used to represent many systems and are the most common configuration for control systems. The system considers only the direct relation between a reference and an output. This may not always be the case since the system may be dependent of two variables, see figure 5.2.

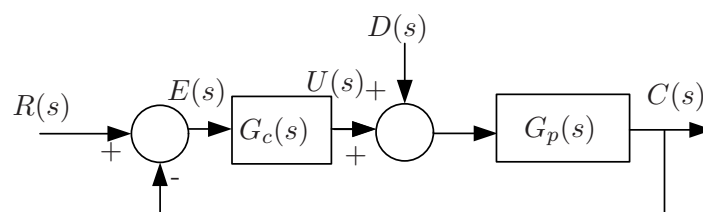


Figure 5.2: A two-degree freedom system in general

5 Control strategies

The two-degree-of-freedom system is dependent of the reference $R(s)$ and a disturbance $D(s)$. The output must be investigated for both the inputs and the system must be stable against disturbances. The control transfer function $G_c(s)$ only changes the controlled variable $U(s)$ based on the error and the controller must be stable against the disturbances. After a short introduction to root loci and control systems the discussion of transport lag will continue.

5.1.1 Transport lag

For some reason there may be a delay in a system of some sort. This delay can occur i. e. due to a slow reacting transducer or a chemical reaction happening. The transport lag must be dealt with in the control strategy. When modeling the lag a transfer function in the continuous control with the (5.3)

$$G_{lag}(s) = e^{-T_l \cdot s} \quad (5.3)$$

Where the lag time constant T_l is the time in seconds and s is the complex variable for the Laplace transfer. This presents an infinite amount of zeros in the right half plane of the s -plane. This creates an instability of the system based on the amount of gain that can be applied. Since the lag is dominated by the poles closest to the imaginary axis the lag can be approximated with the Pade approximation. The general approach of the approximation is presented in (5.4).

$$e^{-T_l \cdot s} = \frac{1 - \frac{T_l \cdot s}{2} + \frac{(T_l \cdot s)^2}{8} - \frac{(T_l \cdot s)^3}{48} + \dots}{1 + \frac{T_l \cdot s}{2} + \frac{(T_l \cdot s)^2}{8} + \frac{(T_l \cdot s)^3}{48} + \dots} \quad (5.4)$$

The approximations creates per definition zeros in the right half plane which can be seen from a first order approximation of a 30 second lag, see (5.5). The 30 second lag time constant is empirical.

$$G_{lag}(s) = \frac{-s + \frac{1}{30 \cdot 2}}{s + \frac{1}{30 \cdot 2}} \quad (5.5)$$

Plotting the root loci for (5.5) can be seen from figure 5.3.

The lag from figure 5.3 presents a zero in the right half plane. The lag transfer function closed loop poles moves from the pole in the left half plane towards negative infinity and from the positive infinity towards the zero in the right half plane. This causes no problem since the lag transfer function always is multiplied onto the transfer function that is lagged. The transport lag has been presented and the presentation of the feed forward approach follows.

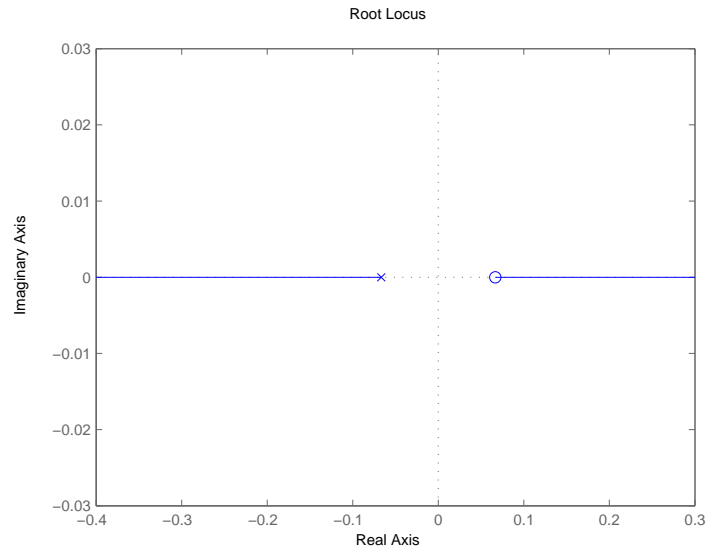


Figure 5.3: *Root locus for a lag of 30 seconds*

5.1.2 The feed forward approach

The reason for using the feed forward technique for thermal chemical systems is the chemical reactions. These reactions must be fed with the right amount of reactants for the reaction to occur. The feed forward in the systems investigated in this project are based on the reactions in the burner and the fuel cell stack respectively. The burner part of reformer burns the excess hydrogen from the fuel cell and oxygen is needed for the combustion. From experiments, see section 6.3.1, the air to hydrogen ratio must be at least 5-8 times higher in order to avoid a pyrolytical burn of the hydrogen. The fuel cell cathode reaction requires a correct amount of oxygen to occur. The feed forward functions supply the needed reactant based on the current density. The feed forward is a part of the controllers for the respective temperatures. The feed forward transfer function must supply the air for the burner and the controller keeps the temperature at the reference.

5.1.3 Antiwindup

A common thing when using the PI-controller is that integral part tend to dominate the calculation. The integral part of the calculation must be limited and this is called integrator anti-windup. This is applied since the controller has an upper limit to the voltage that the controller can supply. The approach for the anti-windup applied in the linear model of the reformer, can be seen from figure 5.4.

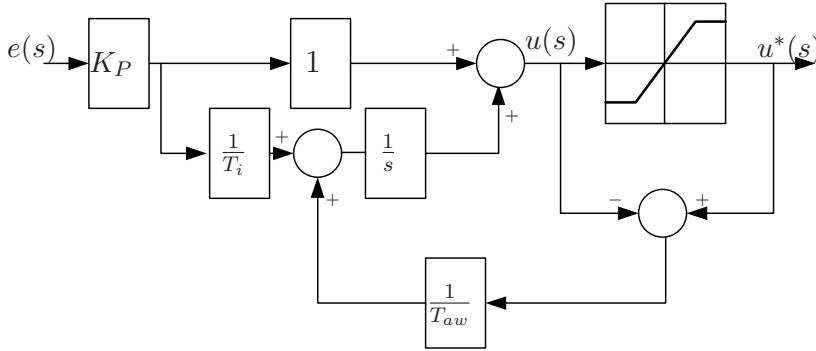


Figure 5.4: *Anti-windup scheme for the controller of the air blown into the reformer burner side.*

The saturated variable $u^*(s)$ is the output from the controller which complies with the controller limits. When the controller reaches the limits for the output and the controller calculates a value higher than the top limit of the output, the sum under the saturation on figure 5.4 changes sign. This results in a subtraction for the input for the integral part of the controller. When no saturation appears the anti-windup is neglected. The rule for the anti-windup constant T_{aw} is that it must be lower than the integral constant T_i , see (5.6).

$$T_{aw} \leq T_i \quad (5.6)$$

This antiwindup must be implemented in the controller for the model.

5.1.4 Model overview

The models of both the reformer and fuel cell stack temperature has been presented and the control of these temperatures can be performed. The temperatures are controlled by convection from a blower and the blower must be controlled by a control algorithm from a digital controller. The control algorithm is presented in this section. The general control of the two temperatures can be seen from figure 5.2 and adding the feed forward controller based on the disturbance to the system results in figure 5.5.

The control approach assumes that the temperature can be controlled by controlling the one variable, marked $u(s)$, and expecting the other variable to be a disturbance, marked $d(s)$. The disturbance has a feed forward function, marked $G_{ff}(s)$ which change the controlled variable according to the disturbance. The controller of the system, marked $G_c(s)$, calculates the needed change of the controlled variable based on the error, marked $e(s)$. The output of the controller is usually a voltage and drives an actuator. The actuator in the system investigated is a blower and the voltage

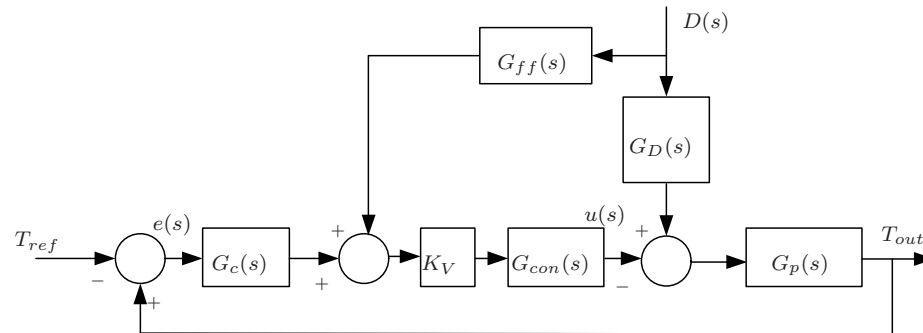


Figure 5.5: A general control approach

is converted to an airflow. The disturbance $d(s)$ is the input of the disturbance transfer function $G_D(s)$ and the input to the plant $G_P(s)$ is the difference between the controlled variable and the disturbance transfer function output. The output of the plant is the temperature gradient and this is integrated in order to obtain the temperature of the system T_{out} and this is fed back to the error calculation. This is the general approach to the control of the temperature. It is perhaps more common to change the sign on the error calculation, so the error equals the reference minus the measured value. But since the controller only needs to be active when the reference temperature is reached the controller must be deactivated when the error is negative. The controlled variable is the airflow through the stack and the reformer for the respective model. The controller can only send air into the model for cooling purposes and not be active when the controller error is negative. The disturbance of the system is for the reformer system the change in flow based on the estimator. When the current density changes the flow of the fuel changes. The disturbance in the linear fuel cell model is the change in heat produced by the fuel cell stack based on a change in the current density.

5.1.5 Controller demands

When defining what a good controller is, a set of parameters are needed. These parameters are dependent of the given system and must be realizable. A realizable controller is compatible with the limits of the system, e.g. the controller cannot require a larger amount of air than the blower can deliver. The parameters also include the amount of error allowed by the controller and the "sluggishness" of the controller. The parameters for the reformer are the following

- The overshoot must be within 0 to 2% of the reference temperature.
- The lag of the controller must be minimal.
- The controller must only react when the temperature is above the reference temperature.

The overshoot restriction of the reformer temperature is a restriction on the controller parameters. Overshoot is the allowed temperature difference above the reference temperature and the controller parameters must be adjusted accordingly. The controller is faster than the system it controls and the controller must be quick to react. Oscillations in the temperature is unwanted since these may have unwanted effects on the output of the system, especially on the stack temperature since the characteristics of the voltage resemble those of the temperature.

5.2 Temperature control

The control strategy for the respective temperature models is presented in this chapter. The open loop transfer functions are calculated in order to investigate the placement and behavior of the closed loop poles. The closed loop transfer functions are calculated in order to obtain the step response. This is done for both the reformer and the fuel cell stack models.

5.2.1 Reformer

The transient model of the reformer was presented in (3.21) and the transient model presents only the dynamic of the model and not the changes in actual value of the temperature. The transient model can be seen from figure 5.6.

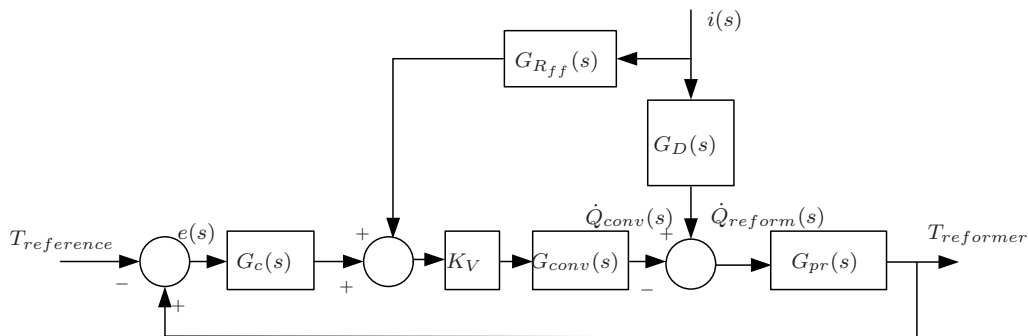


Figure 5.6: *The transient model of the reformer*

The transfer functions that converts a variable to an power balance input can be represented in a Laplace transform. To start with the most important one the transfer function for the plant can be seen from (5.7). The transfer function transfers the result of the balance of the respective heat transfers into the temperature of the reformer. This transformation is based on the left hand side of (3.21) which controls the dynamics of the temperature. This transfer function is assumed to be inalterable and the response of the temperature must be shaped by using controllers.

$$G_{pr}(s) = \frac{1}{m_r \cdot c_r \cdot s + K_{convTr} + K_{cond_r}} \quad (5.7)$$

The transfer function $G_{conv}(s)$ is the transfer function between the airflow $\dot{q}(s)$ and controlled variable \dot{Q}_{conv} . There is no dynamics involved in the transfer function and the function is only a constant, which can be seen from (5.8). The convection transfer function is calculated from (3.21) and contains the factors in front of the variable \dot{q}_{air}

$$G_{conv}(s) = K_{conv_q} \quad (5.8)$$

The feed forward transfer function $G_{R_{ff}}(s)$ has earlier been mentioned to be the function supplying the air to the reaction. In order to be able to plot the root loci of the transient model and thereby the reformer, the contribution of convection added by the feed forward transfer function must be included in the disturbance transfer function. The transfer function $G_{R_{ff}}(s)$ for the reformer feed forward controller is based on the estimated amount of excess hydrogen from the fuel cell, in l/min , and this is multiplied with the air stoichiometry for the burner λ_{H2Burn} , see (5.9).

$$G_{R_{ff}} = \frac{\left(K_{estimator} \cdot K_{system} - \frac{n_{cell} \cdot A_{cell}}{2 \cdot F} \right) \cdot 1000 \cdot 60 \cdot \lambda_{H2Burn}}{\underbrace{1000 \cdot \rho_{H2} \cdot K_V}_{K_{r_{ff}}}} \cdot i \quad (5.9)$$

where K_V is the conversion factor from the blower voltage to the airflow in $[l/min]$. The conversion between the molar flow of the volumetric flow is the density of the hydrogen. The disturbance transfer function $G_D(s)$ transforms the current density into the heat provided from burning the hydrogen and the power needed for the steam reforming process, see (5.10).

$$G_D(s) = K_{H2} - K_{SR} \quad (5.10)$$

Looking at figure 5.6 there are two components dependent of the current density. These can be written in one function which represents the change of the system based on the change in the current density. Summing up the changes based on the current density, can be seen from (5.11).

$$\begin{aligned} G_{Di}(s) &= \left(G_D(s) - G_{R_{ff}} \cdot K_V \cdot G_{conv} \right) \\ &= \left(K_{H2} - K_{SR} - K_{r_{ff}} \cdot K_V \cdot K_{conv_q} \right) \end{aligned} \quad (5.11)$$

5 Control strategies

Since the reformer experiments, from section 6.3.1, presented a lag in the change of the reformer temperature, when the frequency of the pump changed, a transport lag must be implemented in the transient model of the disturbance. This transport lag is multiplied to the entire disturbance transfer function $G_{Di}(s)$. The transport lag is approximated with a first order pade approximation from MATLAB, see (5.5). The lag of the function must be multiplied with the entire disturbance transfer function, see (5.12).

$$\begin{aligned} G_{Di_{lag}} &= G_{Di}(s) \cdot G_{lag}(s) \\ &= \frac{(K_{H2} - K_{SR} - K_{r_{ff}} \cdot K_V \cdot K_{conv_q}) \cdot \left(-s + \frac{1}{T_l \cdot 2}\right)}{s + \frac{1}{T_l \cdot 2}} \end{aligned} \quad (5.12)$$

The controller transfer function $G_c(s)$ is neglected for now and assumed to be a gain of unity. This is done since the controller is to be derived from the control strategies later on. Plotting the root loci of the system requires the open loop functions. Starting with the open loop function for the temperature reference signal the open loop transfer function can be seen from (5.13).

$$\begin{aligned} \frac{T_{reformer}(s)}{T_{reference}(s)} &= G_c(s) \cdot K_V \cdot G_{con} \cdot G_P(s) \\ &= \frac{1 \cdot K_V \cdot K_{conv_q} \cdot 1}{m_r \cdot c_r \cdot s + K_{conv_{Tr}} + K_{cond}} \end{aligned} \quad (5.13)$$

The open loop transfer function for the disturbance signal, assuming the controller is unity and that the temperature reference signal is neglected, can be seen from (5.14).

$$\begin{aligned} \frac{T_{reformer}(s)}{i(s)} &= G_{Di_{lag}} \cdot G_P(s) \\ &= \frac{(K_{H2} - K_{SR} - K_{r_{ff}} \cdot K_V \cdot K_{conv_q}) \cdot \left(-s + \frac{1}{T_l \cdot 2}\right) \cdot 1}{\left(s + \frac{1}{T_l \cdot 2}\right) \cdot (m_r \cdot c_r \cdot s + K_{conv_{Tr}} + K_{cond_r})} \end{aligned} \quad (5.14)$$

With the given transfer functions presented the control of the system can be initiated.

Root loci of the reformer system.

Plotting the root locus requires the knowledge of the poles and zeros of a the given function. The poles for the transfer function of open loop convection. It can be seen from (5.13) that the transfer function only has one pole and no zeroes due to the presence of an s in the denominator of the transfer function. Therefore the root locus must only consist of one pole, which can be seen from figure 5.7.

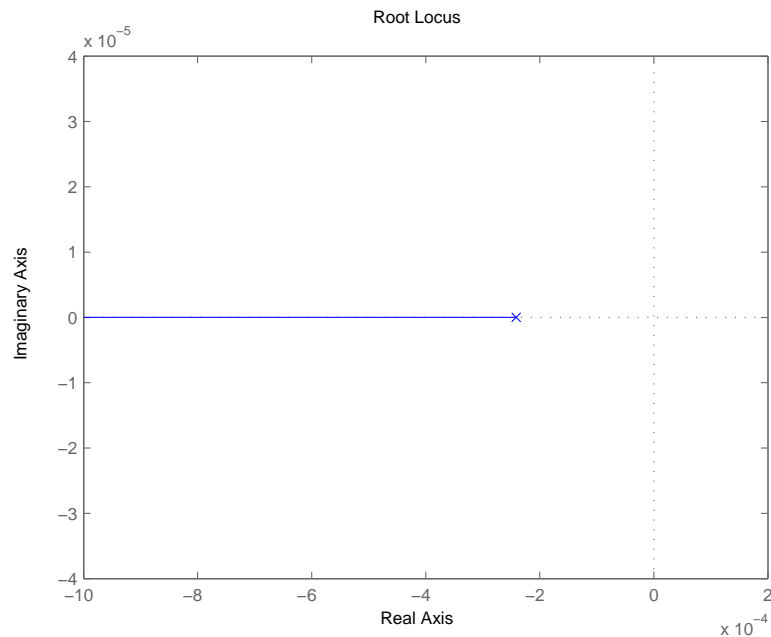


Figure 5.7: Root locus plot of the convection part with unity control

From figure 5.7 it can be seen that the root locus moves away from the imaginary axis as the gain increases towards infinity. This can be changed by adding a more dynamic controller than unity. Looking at the open loop transfer function for the disturbance signal, see (5.14), it can be seen that the root loci should have a zero and two poles. This is caused by the s present in the numerator of (5.14). Furthermore it can be seen that the zero is placed in the positive right half plane of the s -plane, due to the negative sign in the numerator of (5.14).

From figure 5.8 it can be seen that the root locus moves towards the right half plane as the gain increases. The reason for the zero in the right half plane is the lag implemented in the modeling. (5.5) presents a zero and a pole which is multiplied with the disturbance function and this sets a limit to the amount of gain that can be applied. To obtain the response of the system the loop must be closed.

5 Control strategies

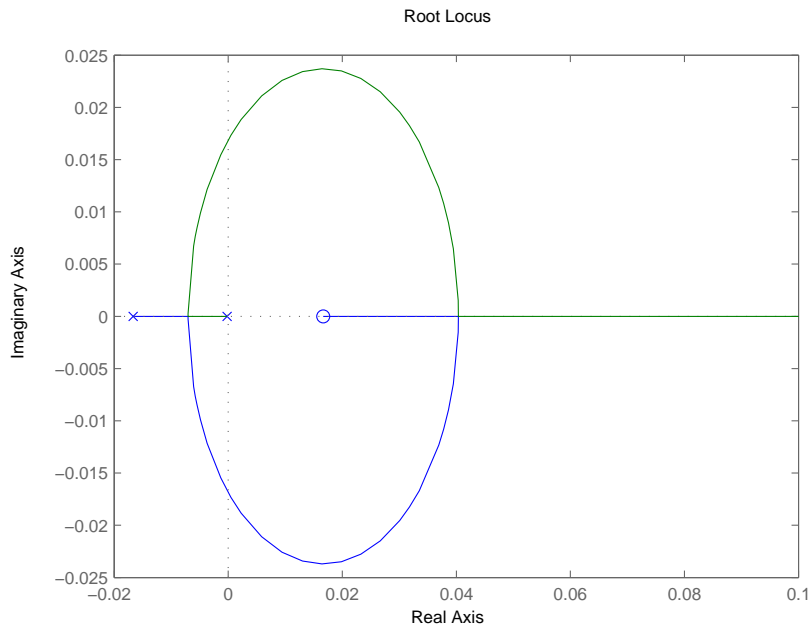


Figure 5.8: Root locus plot of the open loop transfer function between the reformer temperature and the current density.

Closed loop of the reformer system

To close the loop of the reformer the closed loop transfer function for the disturbance and the reference respectively must be calculated. Since the controllers only may function when the temperature is above the reference some changes to the general closed loop must be applied. The reference is negative and the measured temperature is fed back with a positive feedback, see figure 5.9.

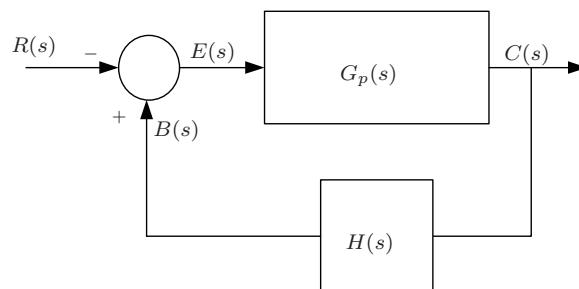


Figure 5.9: A negative reference system with positive feedback

Recalculating the closed loop transfer function from (5.1) and solving the relationship between $C(s)$ and $C(s)$ gives a new transfer function, see (5.15).

$$\begin{aligned}
 C(s) &= G_p(s) \cdot E(s) \\
 E(s) &= B(s) - R(s) \\
 &= H(s) \cdot C(s) - R(s) \\
 C(s) &= G_p(s)[H(s) \cdot C(s) - R(s)] \\
 C(s) - G_p(s) \cdot H(s) \cdot C(s) &= -G_p(s) \cdot R(s) \\
 \frac{C(s)}{R(s)} &= \frac{-G_p(s)}{1 - G_p(s) \cdot H(s)} \tag{5.15}
 \end{aligned}$$

The negative signs present in both the numerator and the denominator of the closed loop transfer function. Closing the loop of the temperature reference and applying (5.15). When figure 5.6 is analyzed with no disturbance the model can be rearranged to figure 5.10.

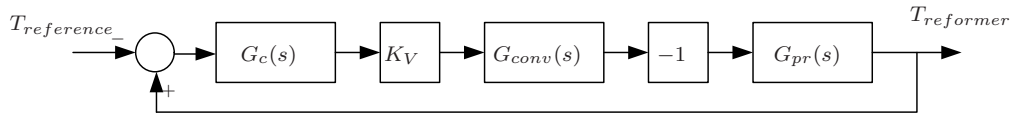


Figure 5.10: The altered system approach for the closing of the feedback loop of the system.

Solving the closed loop transfer function of figure 5.10 using (5.15), gives (5.16).

$$\frac{T_{reformer}(s)}{T_{reference}(s)} = \frac{-G_c(s) \cdot K_V \cdot G_{con}(s) \cdot (-1) \cdot G_{pr}(s)}{1 - G_c(s) \cdot K_V \cdot G_{con}(s) \cdot (-1) \cdot G_{pr}(s)} \tag{5.16}$$

Inserting the respective systems from (5.7) and (5.8) into (5.16) and assuming the controller transfer function $G_c(s)$ is a unity gain, gives (5.17).

$$\frac{T_{reformer}(s)}{T_{reference}(s)} = \frac{K_V \cdot K_{conv_q}}{m_r \cdot c_r \cdot s + K_V \cdot K_{conv_q} + K_{conv_{Tr}} + K_{cond_r}} \tag{5.17}$$

With the closed loop transfer function calculated, the step response of the reformer can be achieved.

To calculate the closed loop transfer function for the disturbance is based on the open loop transfer function, presented in (5.14). The reference temperature input of the reformer is neglected and the reformer model can be rearranged, see figure 5.12.

Looking at figure 5.12 the transient model can be recognized as a normal control system with a negative feed back and a feedback function. This results in an application of (5.1) and the closed loop transferfunction can be derived, see (5.18).

5 Control strategies

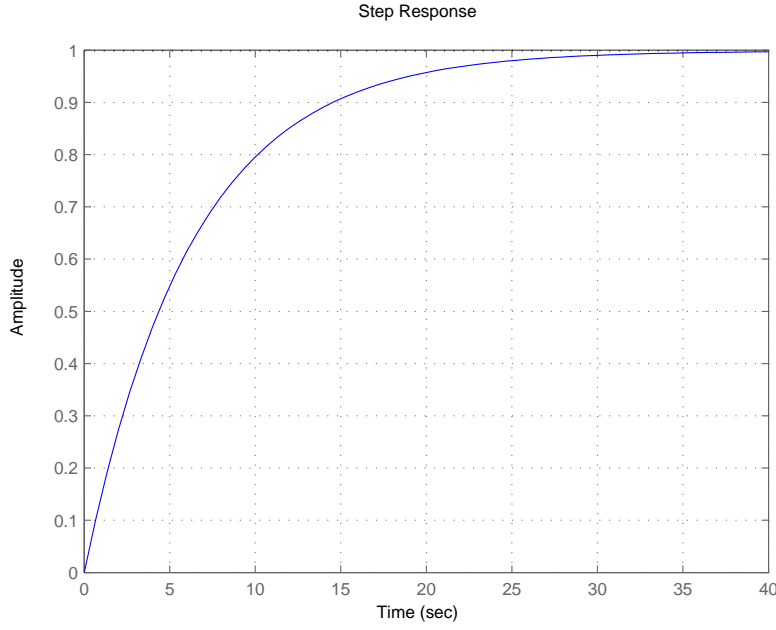


Figure 5.11: Step response of the reference with resulting change in reference temperature.

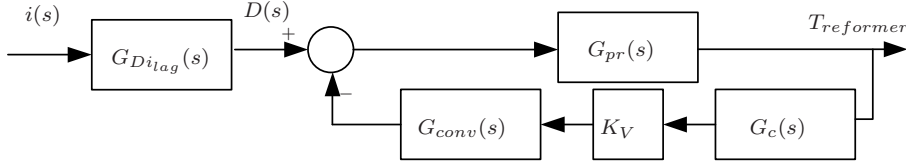


Figure 5.12: The rearranged transient model

$$\frac{T_{reformer}(s)}{i(s)} = G_{Diag}(s) \cdot \frac{G_{pr}(s)}{1 + G_c(s) \cdot K_V \cdot G_{conv}(s) \cdot G_{pr}(s)} \quad (5.18)$$

Inserting (5.7), (5.8) and (5.12) in (5.14) and assuming the controller is unity gives (5.19).

$$\frac{T_{reformer}(s)}{i(s)} = \frac{\left(K_{H2} - K_{SR} - K_{rff} \cdot K_V \cdot K_{conv_q}\right) \cdot \left(-s + \frac{1}{T_l \cdot 2}\right)}{\left(s + \frac{1}{T_l \cdot 2}\right)} \cdot \frac{1}{m_r \cdot c_r \cdot s + K_V \cdot K_{conv_q} + K_{conv_{Tr}} + K_{cond_r}} \quad (5.19)$$

5.2.2 Fuel cell stack

Building the transient model and investigating the control issues of the fuel cell stack temperature is also needed in order to control the entire system. Like the modeling of (3.21) as a block diagram, the same approach is applied with (3.13), see figure 5.13.

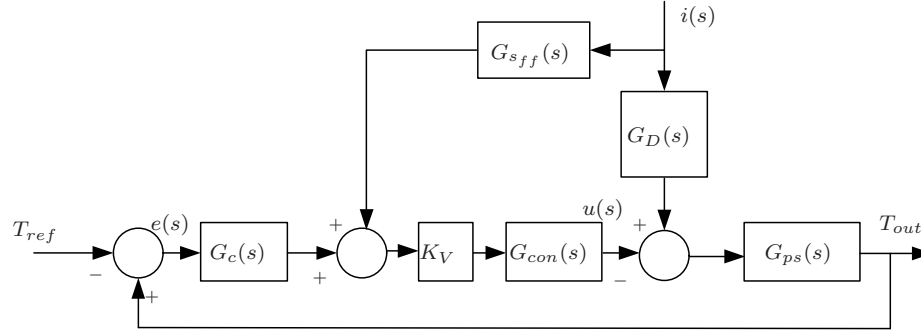


Figure 5.13: The setup for the control of the stack temperature

The transfer function for the stack temperature $G_{ps}(s)$, or the plant, is based on the left hand side of (3.13), which can be seen from (5.20).

$$G_{ps}(s) = \frac{1}{m_s \cdot c_s \cdot s + K_{cond_s} + K_{conv_{T_s}} - K_{heat_{T_s}}} \quad (5.20)$$

The transfer function for the convection is a constant that changes the convection contribute from the airflow. The transfer function can be derived from (3.13), and the transfer function is presented in (5.21).

$$G_{conv}(s) = K_{conv_q} \quad (5.21)$$

The feed forward transfer function can be determined from the amount of air that is needed for the reaction happening inside the fuel cell stack. The amount of air sent into the fuel cell can be calculated from (5.22) and the air blown into the stack is at room temperature T_a .

$$G_{sff} = \underbrace{\frac{n_{cell} \cdot A_{cell}}{4 \cdot F \cdot x_{O_2}} \cdot \frac{60}{\rho_{air}(T_a)}}_{K_{ff_s}} \cdot \frac{1}{K_V} \quad (5.22)$$

The disturbance transfer function is a constant that relates the current density with the power balance of the stack, see (5.23).

5 Control strategies

$$G_D(s) = K_{heat_i} \quad (5.23)$$

From figure 5.13 it can be seen that the feed forward air controller (5.22) can be summed up with the disturbance transfer function, from (5.23), since both the respective functions are constants multiplied onto the current density. The feed forward function $G_{ff_s}(s)$ is multiplied with the convection transfer function from (5.21) and the voltage constant K_V , resulting in (5.24).

$$\begin{aligned} G_{D_i}(s) &= G_D(s) - G_{s_{ff}}(s) \cdot K_V \cdot G_{con}(s) \\ &= K_{heat_i} - K_{ff_i} \cdot K_V \cdot K_{conv_q} \end{aligned} \quad (5.24)$$

One of the things necessary for a change in current density is the presence of a given amount of hydrogen, and from (5.14) a lag was presented, due to the transport time from the pump to the reformer exit. This must also be implemented in the fuel cell stack temperature control. The approach is to lag the current density and force the system to wait for the right amount of hydrogen. Since the transport lag time constant for the hydrogen moving through the WGS-reactor and the cooler is undetermined, this is left for future studies. The lag, from (5.5), is applied, see (5.25).

$$\begin{aligned} G_{D_{lag}}(s) &= G_{lag} \cdot G_{D_i} \\ &= \frac{-s + \frac{1}{T_l \cdot 2}}{s + \frac{1}{T_l \cdot 2}} \cdot \left(K_{heat_i} - K_{ff_i} \cdot K_V \cdot K_{conv_q} \right) \end{aligned} \quad (5.25)$$

Since the transfer functions for the respective parts of the fuel cell stack model has been presented and the respective open loop functions for inputs of the system. The open loop transfer function for the reference temperature, neglecting the input from the current density, can be seen from (5.26).

$$\begin{aligned} \frac{T_s(s)}{T_{ref}(s)} &= G_c(s) \cdot K_V \cdot G_{conv}(s) \cdot G_{ps}(s) \\ &= \frac{-1 \cdot \left(G_c(s) \cdot K_V \cdot K_{conv_q} \right) \cdot 1}{m_s \cdot c_s \cdot s + K_{conv_{T_s}} + K_{cond_s} - K_{heat_{T_s}}} \end{aligned} \quad (5.26)$$

The open loop transfer function for the input from the current density can be seen from (5.27).

$$\begin{aligned} \frac{T_s(s)}{i(s)} &= G_{D_{lag}}(s) \cdot G_{ps}(s) \\ &= \frac{\left(K_{heat_i} - K_{ff_i} \cdot K_V \cdot K_{conv_q}\right) \cdot \left(-s + \frac{1}{T_{i,2}}\right)}{\left(m_s \cdot c_s \cdot s + K_{conv_{Tr}} + K_{cond_s} - K_{heat_{Tr}}\right) \cdot \left(s + \frac{1}{T_{i,2}}\right)} \end{aligned} \quad (5.27)$$

With the open loop transfer functions calculated the respective root loci can be plotted.

Root loci for the fuel cell stack

Plotting the root loci for the open loop transfer function presents a problem. The negative sign, in (5.26), is neglected since closing the loop also presents negative signs in both the numerator and the denominator. The root locus can be seen from figure 5.14.

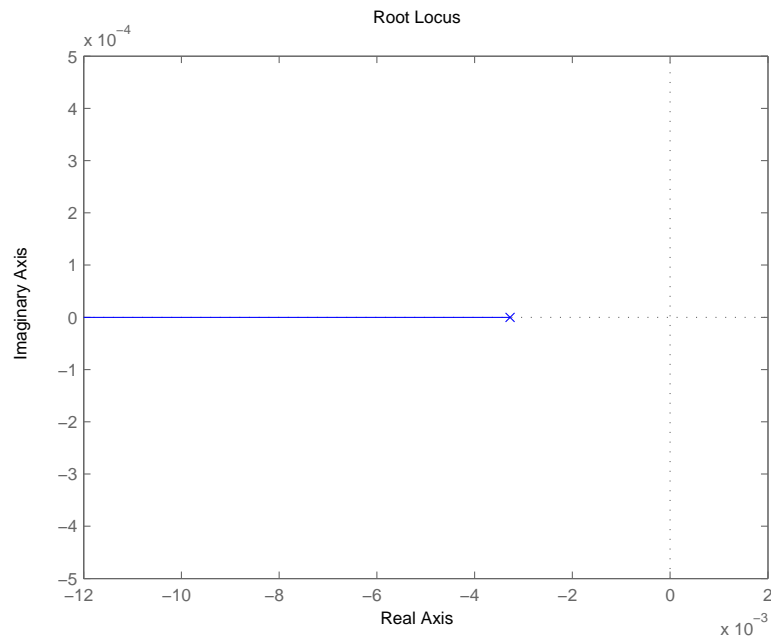


Figure 5.14: Root locus for the reference open loop transfer function

From this it can be seen that the closed loop poles moves towards negative infinity as the gain increases towards infinity. The root locus is plotted with a gain of unity in the controller. The change of the temperature based on the current density from the open loop transfer function, presented in (5.27) can be presented, see figure 5.15.

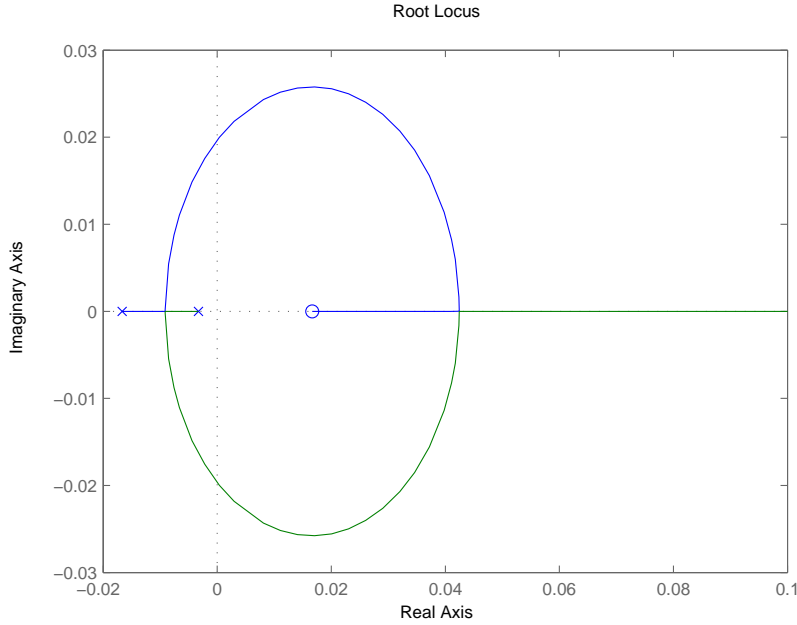


Figure 5.15: Root locus plot of the disturbance open loop function

The lag presents the zero in the right half plane as with the reformer disturbance plot. With the root loci presented for the linear stack model.

Closed loop for the stack temperature

Closing the feedback loops for the respective open loop transfer functions are completely analog to the method in the reformer. The relation between the reference temperature T_{ref} and the stack temperature T_{stack} is a negative reference system with positive unity feedback. This can be calculated from (5.15). The closed loop transfer function can be seen from (5.28).

$$\frac{T_{stack}}{T_{reference}} = \frac{-G_c \cdot K_V \cdot G_{conv} \cdot (-1) \cdot G_{ps}(s)}{1 - G_c \cdot K_V \cdot G_{conv} \cdot (-1) \cdot G_{ps}(s)} \quad (5.28)$$

When inserting the expressions from (5.20), (5.21) and (5.25) into (5.28) and assuming that the controller is a gain of unity results in (5.29).

$$\frac{T_{stack}(s)}{T_{ref}(s)} = \frac{K_V \cdot K_{conv_q}}{m_s \cdot c_s \cdot s + K_{cond_s} + K_{conv_{T_s}} - K_{heat_{T_s}} + K_V \cdot K_{conv_q}} \quad (5.29)$$

The step response of the stack is the response to a rapid change in the input which is the temperature reference T_{ref} . The step response can be seen from figure 5.16.

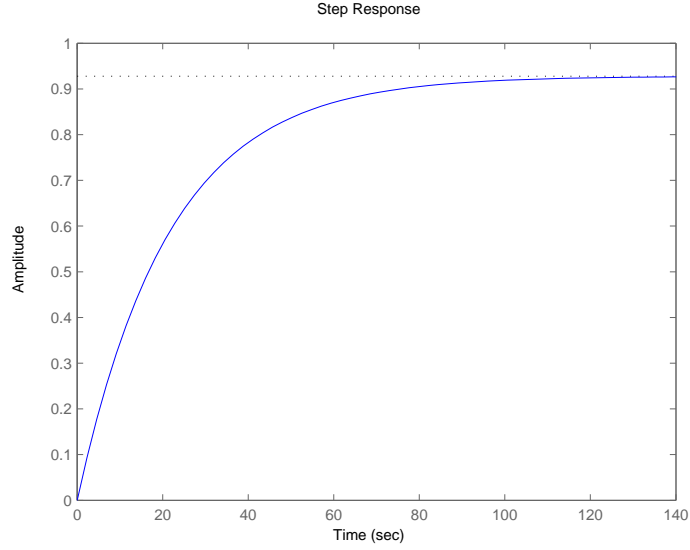


Figure 5.16: Stepresponse of the stack temperature closed loop system

When the step response of the reference has been presented, the loop for (5.27) must be closed. The system is analyzed with the disturbance being positive and the feedback branch contains the convective parts of the model, which is analog to figure 5.12. The transfer function can be seen from (5.30).

$$\frac{T_{stack}(s)}{i(s)} = G_{lag} \cdot \frac{G_{ps}(s)}{1 + G_{ps}(s) \cdot G_c(s) \cdot K_v \cdot G_{con}(s)} \quad (5.30)$$

Inserting the respective expressions for the systems referred to in (5.30), from (5.20),(5.21) and (5.25) results in (5.31).

$$\begin{aligned} \frac{T_{stack}(s)}{i(s)} &= \frac{\left(K_{heat_i} - K_{ff} \cdot K_V \cdot K_{conv_q}\right) \cdot \left(-s + \frac{1}{T_i \cdot 2}\right)}{\left(s + \frac{1}{T_i \cdot 2}\right)} \\ &\cdot \frac{1}{m_s \cdot c_s \cdot s + K_{cond_s} + K_{conv_{T_s}} - K_{heat_{T_s}} + K_V \cdot K_{conv_q}} \end{aligned} \quad (5.31)$$

Plotting the step response of the stack temperature based on a step change in the current density is presented in figure 5.17

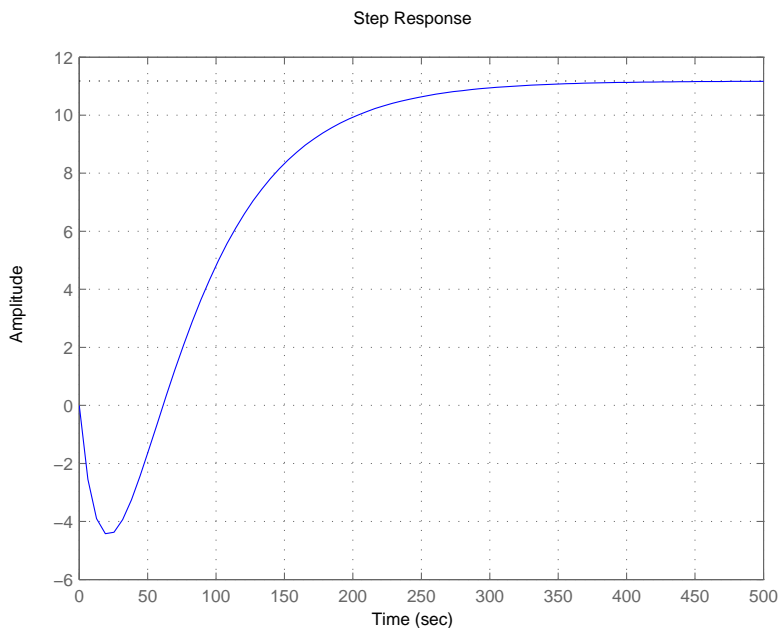


Figure 5.17: *Step response of the temperature at a current density step*

The change in the temperature decreased due to the presence of the lag. The lag temperature loses heat to conduction and the change results in a decrease of the temperature.

5.3 Controller design

The closed loop responses of the system has been presented and the controllers have been assumed to have a gain of unity. Changing the controller transfer function $G_c(s)$ for the respective reference changes the dynamics of the system. The changes are applied to the open loop transfer function of the respective models. The reason for changing the dynamic is to get a faster response of the system when a change in the disturbance is applied. The most common linear controller is the PID-controller and this is analyzed along with the effects of adding the PI-controller to the system. The differential part of the controller reacts on small changes of the error and noise will trigger a control. To avoid the problem of the noise in signals the PI controller is chosen, but the PID controller can also be applied. The method for applying the PI-controller is presented in this section but the application of the PID-controller is completely analog. Controllers in real time digital control systems are discrete controllers and the controllers are to be discretized, in a way so that they are based on the current error and the error from the run before this one. The transformation from the continuous s-plane to the discrete z-plane is called z-transformation. This transformation is neglected in this project.

5.3.1 Reformer temperature controller

The PI-controller is also known as a proportional(P) and integral(I) controller. The controller is usually a piece for software in a digital control system, or it can be made from operational amplifiers. In both cases the controller makes changes to a voltage of an actuator that tries to correct the error of the system. The PI-controller can be seen from (5.32). The proportional part of the controller ensures a fast response and the integral part ensures that the steady state error is removed.

$$G_c(s) = K_p \left(1 + \frac{1}{T_i \cdot s} \right) \quad (5.32)$$

Where K_p is the proportional constant and T_i is the integral constant. These constants changes the poles for controller and shapes the root locus for the system. It is assumed that the controller only has positive constants. otherwise the controller would add poles and zeros in the right half plane and that would increase the instability of the system. Rearranging the controller to better apply for the root locus, can be seen from (5.33).

$$G_c(s) = K_P \cdot \frac{\left(s + \frac{1}{T_i} \right)}{s} \quad (5.33)$$

It can be seen from the rearranged controller that it adds a zero to the root locus. The controller is multiplied with the open loop transfer function of the reformer, from (5.13), and result in (5.34).

$$\frac{T_{reformer}(s)}{T_{reference}(s)} = K_p \cdot \frac{s + \frac{1}{T_i}}{s} \cdot \frac{K_V \cdot K_{conv_q}}{m_r \cdot c_r \cdot s + K_V \cdot K_{conv_q} + K_{conv_{Tr}} + K_{cond_r}} \quad (5.34)$$

Plotting the root locus for the reformer transfer function with the controller and neglecting the negative sign in the numerator of the open loop transfer function can be seen from figure 5.18, and the integral constant T_i is set to 0.06.

Now the closed loop poles can be plotted closer to the imaginary axis of the s-plane. The root locus changes when the zero moves towards the poles by changing the integral constant. The step response must be generated for the open loop transfer function and therefore the loop must be closed, using (5.1), see (5.35).

$$\frac{T_{reformer}}{T_{reference}} = \frac{K_P \left(s + \frac{1}{T_i} \right) K_V K_{conv_q}}{m_r c_r s^2 + \left(K_{conv_{Tr}} + K_{cond_r} + K_P K_V K_{conv_q} \right) s + \frac{1}{T_i} K_P K_V K_{conv_q}} \quad (5.35)$$

5 Control strategies

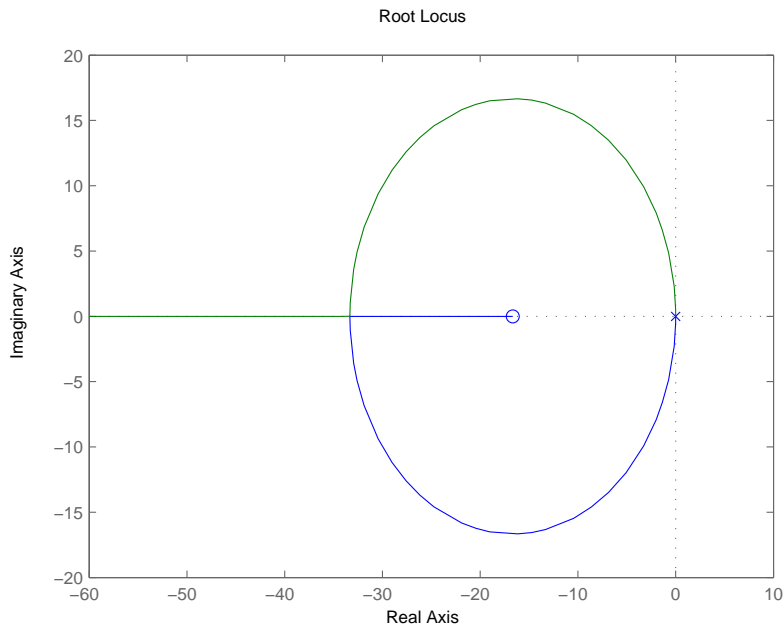


Figure 5.18: Root Locus plot of the reformer with a PI-controller with a $T_i=0.06$

Calculating the parameters for the controller is dependent of the demands, for the controller that were presented in section 5.1.5. A mathematical search method was created to locate for a good set of parameters for the controller. The step response of the reformer with the controller is basis for the script. The method set a value for T_i and then runs through the gain K_P and tests all the step responses. The overshoot is calculated for the response and is used as a search parameter. The overshoot was restricted to 2%.

K_P	T_i	Overshoot[%]
100	5.8	1
116	5	1
84	6.9	1

Table 5.1: Sets of variables from the parameter search

If the overshoot of the step response fit inside the restriction, the gain K_P and integration constant T_i was saved along with the overshoot. The table was afterwards sorted in ascending order with regards to the overshoot. The best approximation was the one with the lowest overshoot. Three sets of variables from the search can be seen from table 5.1 and the step response of the variables can be seen from figure 5.19.

The temperature is assumed to have reached the reference temperature when the temperature output is within 2% and all the sets of parameters have an allowable overshoot. The temperature controller has an influence on the disturbance closed

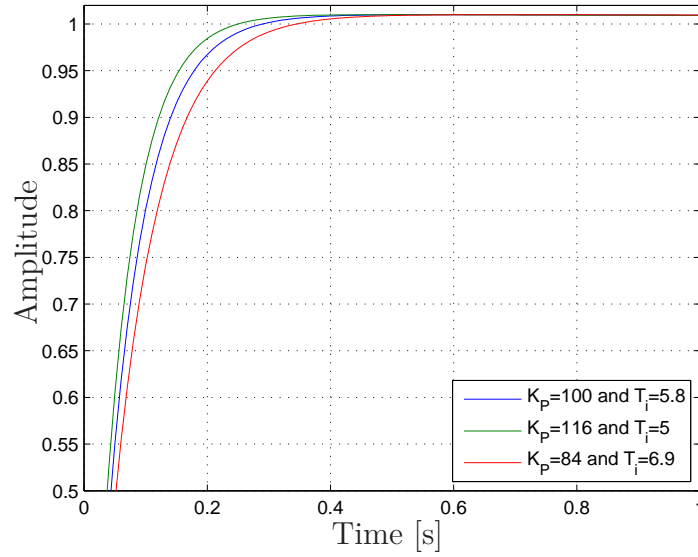


Figure 5.19: Step response with a change in temperature using a PI controller.

loop transfer function, which can be seen from (5.18), and inserting (5.33) instead of $G_c(s)$ results in (5.36).

$$G_{c_i}(s) = \frac{\left(-s + \frac{1}{T_i \cdot 2}\right) \cdot \left(K_{H2} - K_{SR} - K_{rff} \cdot K_V \cdot K_{convq}\right)}{\frac{\left(s + \frac{1}{T_i \cdot 2}\right)}{s}} \cdot \frac{1}{m_r C_r s^2 + \left(K_{convTr} + K_{cond_r} + K_p K_V K_{convq}\right) s + \frac{1}{T_i} K_p K_V K_{convq}} \quad (5.36)$$

The system must be stable with regards to a step response for both the reference and the current density and the controller parameters from table 5.1 must be inserted in the transfer function and the step response must be obtained. The step response for the tree sets can be seen from figure 5.20.

From figure 5.20 it can be seen that the parameters with $K_P = 116$ and $T_i = 5$ have the fastest response and lowest overshoot when a change in current density occurs. These parameters are used in the linear model for the temperature of the reformer. Implementing the controller in the linear model of the reformer temperature and obtaining the temperature response from the change in input from both the temperature reference and the disturbance can be seen from figure 5.21. The reference changes from 400K (125°C) to 550K (277°C) at $T = 3000$ s and the current density changes from 0.3 to 0.66 at $T = 5000$.

As it can be seen from the figure that the reformer temperature does not cross the reference of the of the controller and thereby the controller makes no changes. The

5 Control strategies

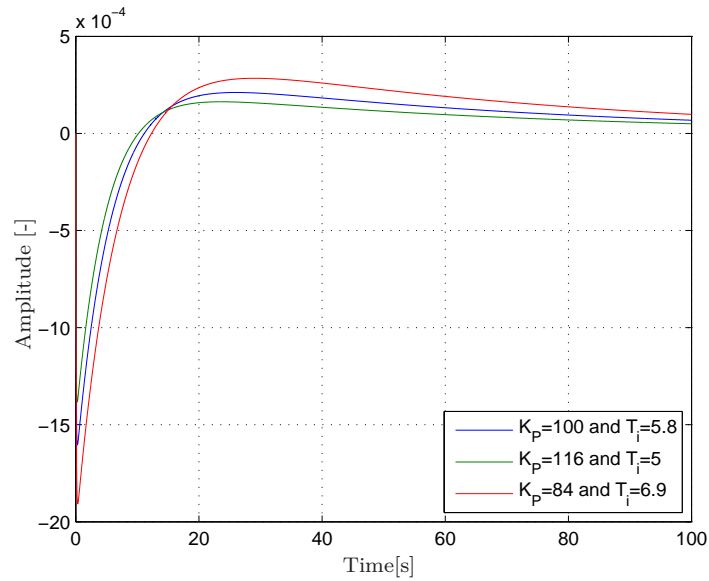


Figure 5.20: Step response for the temperature with the parameters from table 5.1

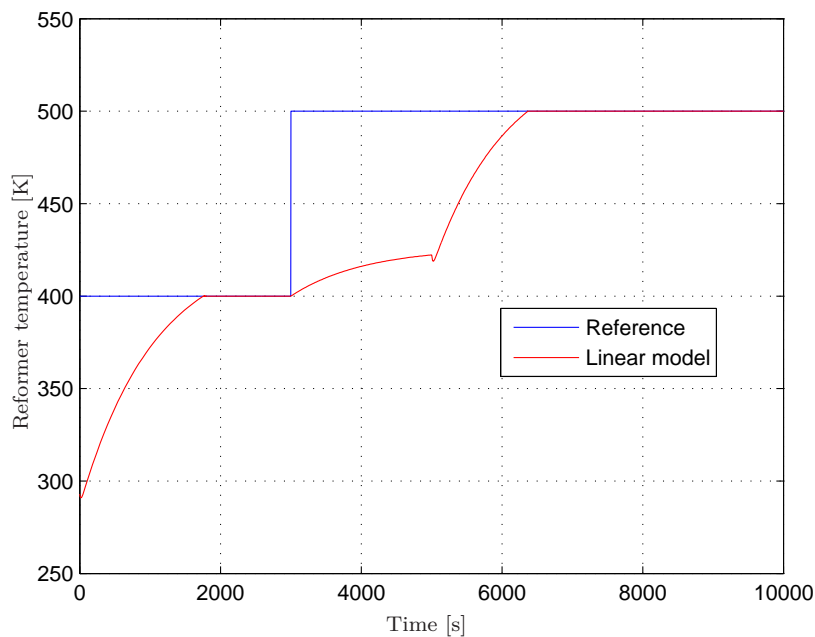


Figure 5.21: PI-controlled reformer temperature using λ_{H_2} at 1.6 and λ_{H_2burn} of 5

reason for the temperature not following the reference is that the heat input from the current density is too low. The plot in figure 5.21 was performed with a hydrogen stoichiometry λ_{H_2} of 1.6, which shows to be too low for the reformer.

5.3.2 Fuel cell stack temperature controller

The controller presented in (5.33) can also be added to the temperature controller for the fuel cell stack and this changes the closed loop transfer functions from (5.29) to (5.37).

$$G(s) = \frac{K_P K_V K_{conv_q} s + \frac{1}{T_i} K_P K_V K_{conv_q}}{m_s c_s s^2 + (K_{cond} + K_{conv_{T_s}} - K_{heat_{T_s}} + K_P K_V K_{conv_q}) s + \frac{K_P K_V K_{conv_q}}{T_i}} \quad (5.37)$$

The search method for the controller parameters is extended for the stack controller and the result can be seen from table 5.2. The search for the parameters for the proportional gain K_P was varied from 2 to 250 in the search algorithm and the search parameters for the integral constant T_i was varied from 2 to 14.5 and the three best sets of results are shown in table 5.2.

K_P	T_i	Overshoot[%]
150	13.6	1
228	9.1	1
156	13.1	1

Table 5.2: Sets of variables from the parameter search

In order to select the best parameters, from the three given sets in table 5.2, the step response is plotted for all the parameters to see the response of the system with the given parameters. The step response can be seen from figure 5.22.

The step response from figure 5.22 of the PI-controller parameter search, shows that the second set of parameters results in the fastest response but has a higher overshoot than the first set of parameter, but the difference is negligible. The controller has an impact on the disturbance since the PI-controller is placed in the feed back path of the closed loop transfer function. If the closed loop transfer function for the disturbance is recalculated from (5.30) and (5.33), (5.21) and (5.20) is inserted the closed loop transfer function for the disturbance results in (5.38).

$$G_d(s) = \frac{\left(K_{heat_i} - K_{ff} \cdot K_V \cdot K_{conv_q} \right) \left(-s + \frac{1}{T_i \cdot 2} \right)}{s \left(s + \frac{1}{T_i \cdot 2} \right)} \cdot \frac{1}{m_s c_s s^2 + (K_{cond} + K_{conv_{T_s}} - K_{heat_{T_s}} + K_P K_V K_{conv_q}) s + \frac{K_P K_V K_{conv_q}}{T_i}} \quad (5.38)$$

5 Control strategies

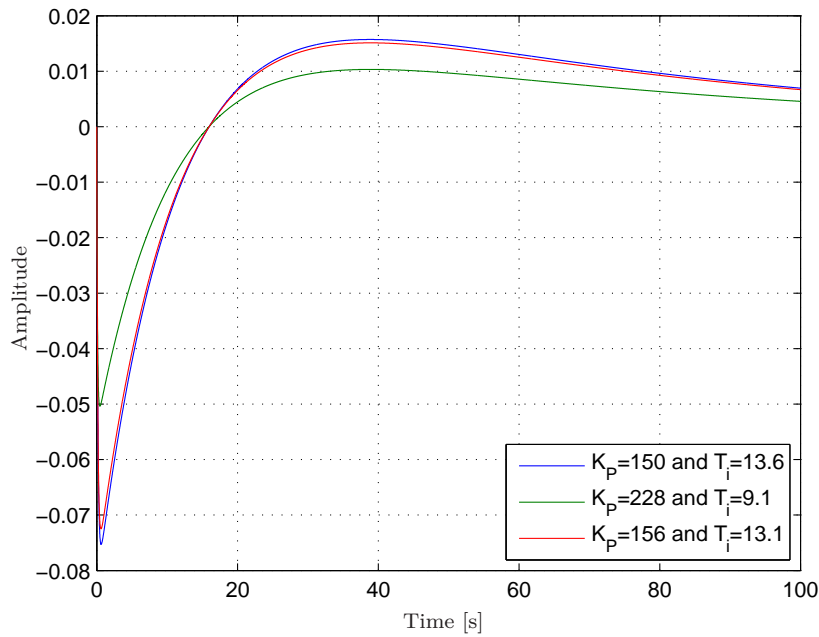


Figure 5.22: Step response with a change in temperature

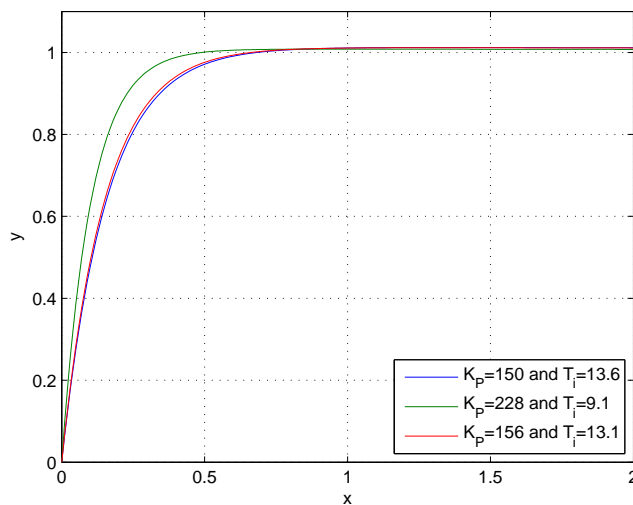


Figure 5.23: Step response of the disturbance with the PI controller, using parameters from table 5.2

Plotting the step response for the closed loop transfer function can be seen from figure 5.23.

It can be seen that the set of parameters where $K_P = 228$ and $T_i = 9.1$ again has the fastest response with a change in the disturbance. Inserting the controller parameters in the linear model for the stack temperature gives the response for the

temperature. The temperature is held at 433K (160°C) until the time reaches 2000 seconds then the temperature is stepped up to 453K (180°C). The current density is held at 0.15 and then the current density is stepped up to 0.4 when the time reaches 4000 seconds. The response from the model can be seen from figure 5.24

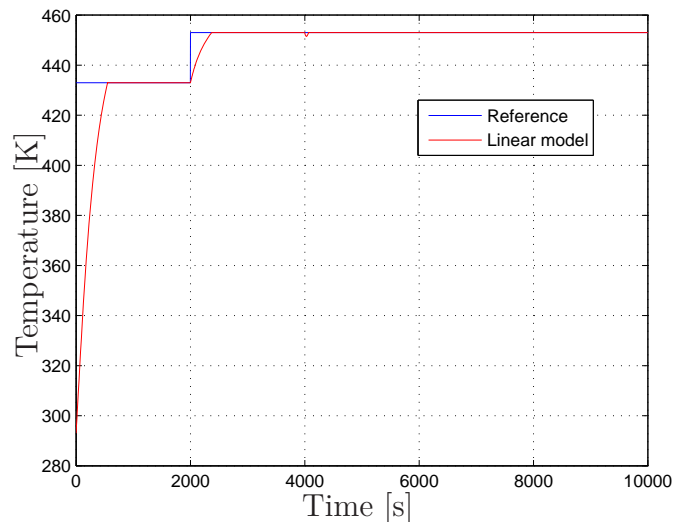


Figure 5.24: Temperature response for the linear model of the stack temperature with $K_P = 228$ and $T_i = 9.1$

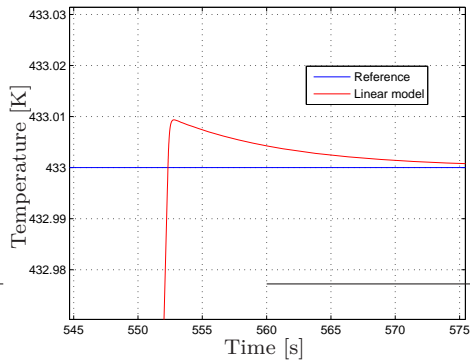
The temperature responds to the changes in both the reference and the disturbance. Taking a closer look at the temperature when the reference is changed shows a small overshoot in the temperature which was expected from table 5.2. The first temperature change is where the temperature is held at 433 and the temperature response can be seen from figure 5.25(a).

The overshoot was expected to be 1% and the model shows that it is lower than expected. The change of the temperature at 2000 seconds of the simulation shows the same overshoot. When the current density changes from 0.15 to 0.4 A/cm^2 and the changes in temperature can be seen from figure 5.25(b).

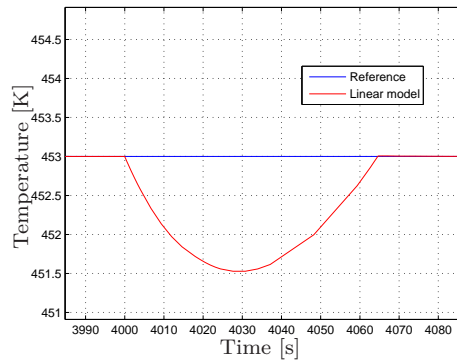
5.4 Summary

This chapter has shown that it is possible to control the system with a PI-controller and that the parameters for the controllers can be determined from a parameter search in MatlabTM. The model includes the lag from the reformation process and the system response did not change much from the reference. The overshoot of 1% does not comply with the thermal system since the change in the temperature is less than 0.01K from simulations. The reformer temperature model showed that the

5 Control strategies



(a) Zoom of the overshoot at the temperature of 433K



(b) Zoom of the step change in current density at $T=4000$

amount of hydrogen in the exhaust gas was too low for the temperature to reach the reference during a step up in reference.

Implementation

- 6.1 Experimental setup**
- 6.2 Evaporator**
- 6.3 Reformer**
 - 6.3.1 Temperature experiments
 - 6.3.2 Gas flow in the system
 - 6.3.3 Dry gas composition
- 6.4 Simulated run**
- 6.5 Summary**

This chapter investigates the physical system and evaluates on the first estimated system parameters. More plots of the experiments can be seen from Appendix A. The program, used to control the system, is described in Appendix D

6.1 Experimental setup

Before a fuel cell is attached to the reformer system, the need for a measurement of the available H_2 and CO is required. As mentioned before, the fuel cell is able to sustain an CO amount of 2-3%. A mass spectrometer is used, as shown in figure 6.1, to measure the molar fractions in the reformer gas. At the first experiments the WGS is empty and this requires the mass spectrometer to be able to read up to 5-8% CO . All experiments are made with a SC ratio of 1.5.

Pure H_2 is used to fuel the burner and is manually controlled by the labview program. The amount of H_2 is initially set to around 2 l/min and the flow of air into the burner is set to about 10 times the H_2 flow. The flow of H_2 is measured from the MFC. This airflow is applied to avoid flashback in the burner. A flashback would be noticed by a high temperature rise at the burner inlet. This flashback is quite damaging to the burner, firstly because the metal cant withstand the temperatures, and the catalyst in the burner would sinter.

The fuel pump mentioned in this system, is a fixed displacement pump. By applying an PWM signal to the pump at 24 V , the pump will transfer 30ml of methanol mix to the evaporator. The maximum frequency for the pump is 20 Hz, though by the mathematical model, shown in Chapter 2, the frequency will not exceed approximately 14 Hz at a current density of 0.66. Some plots in this chapter will show the frequency of the pump, for comparison of the model and the system.

6 Implementation

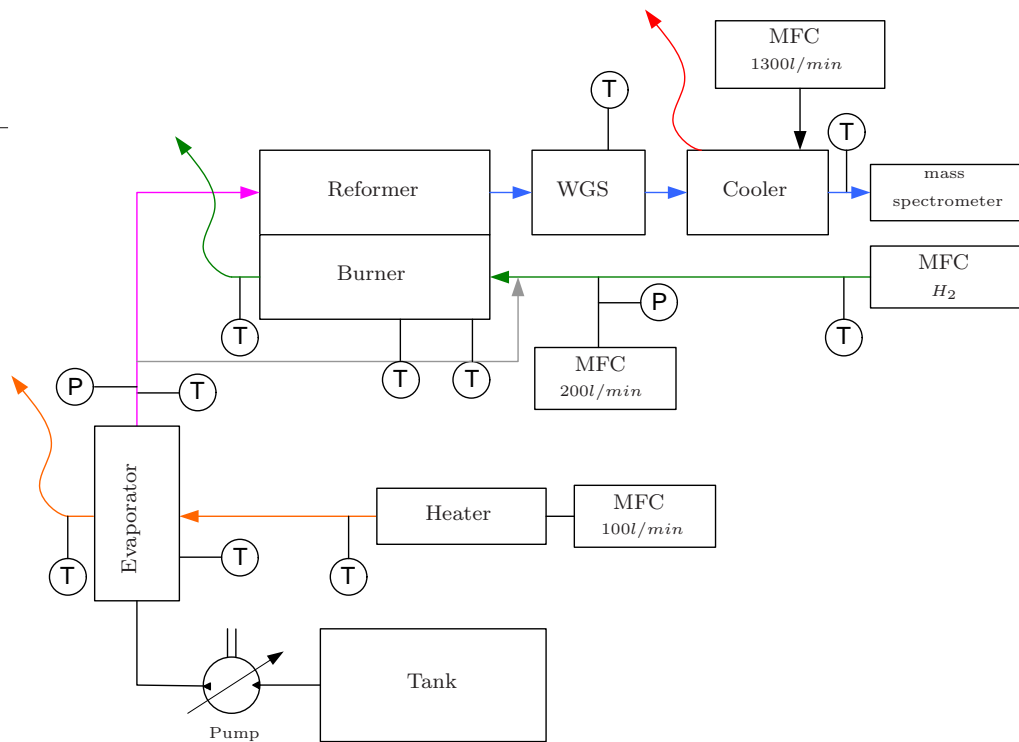


Figure 6.1: *Running system without a fuel cell*

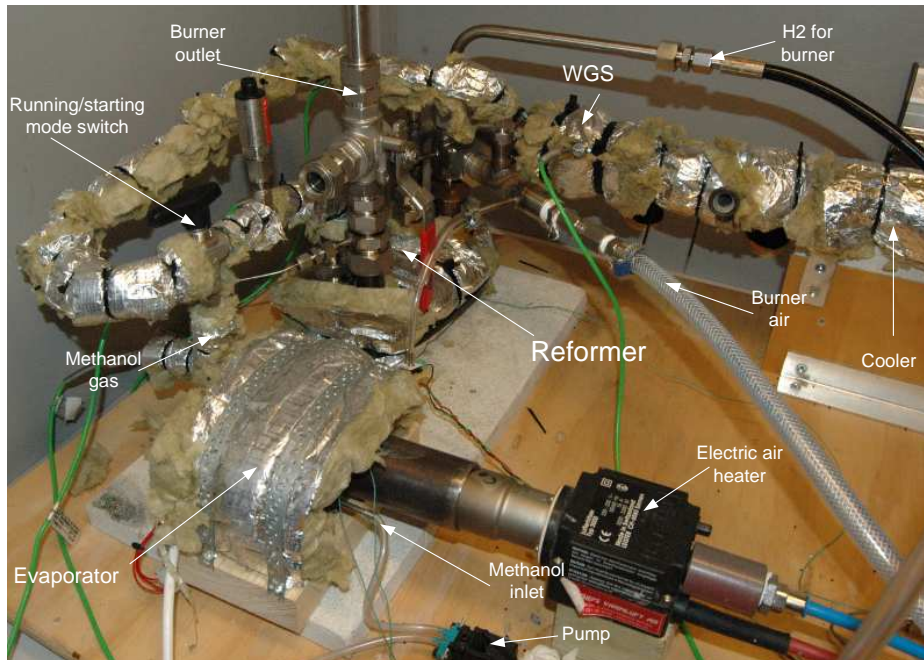


Figure 6.2: *System overview*

The mass flow controller (MFC) is used to drive the airflow for the burner, evaporator and the cooler. The input for the MFC's are 0-10V, and the maximum available flow is 100 l/min, 200 l/min and 1300 l/min. The 100 l/min is installed on the burner

input, the 200 l/min is installed on the evaporator, and the 1300 l/min is installed on the cooler. The delivered flow is measured from the MFC's as a feedback, and converted in the program. The MFC's has a rated settling time of $< 500ms$, though overshoot on the delivered flow is common.

As shown in figure 6.2 and figure 6.1, the first component in the gas flow is the evaporator and is described below.

6.2 Evaporator

As shown in section 1.3 the evaporator contains 34 fins and have a mass of about 0.5kg. The mixture is led into the evaporator as shown at figure 6.2, where the methanol is vaporized. The evaporator is heated by an electric air heater, which simulates the exhaust of the fuel cell, see figure 6.2. The airflow is varied throughout the experiments, and the temperature is initially set to about $160^{\circ}C$.

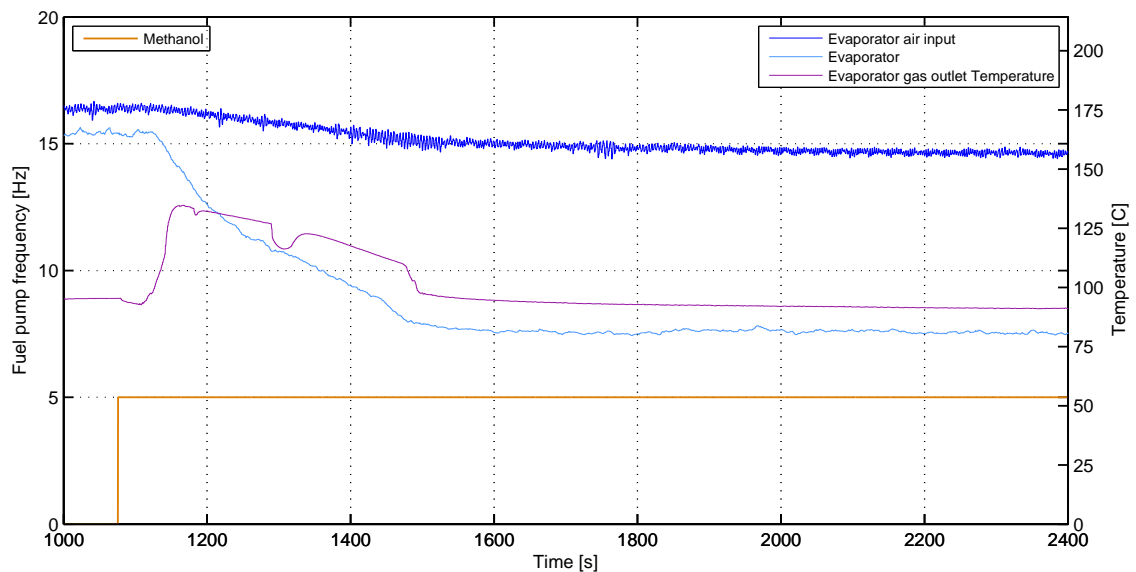


Figure 6.3: *Evaporator temperature with 5 Hz methanol flow. Airflow at 60 l/min*

As shown in figure 6.3 the evaporator falls in temperature when there is a flow of 5Hz on the methanol pump. This temperature is decreasing until it reaches the condensing temperature of the fuel mix. As mentioned before, the temperature of the evaporator should be above $120^{\circ}C$, to ensure the mix is evaporated.

The evaporator should be able to evaporate a 5Hz flow from the pump as shown in figure 6.3, though some problems is shown in the setup of the system.

A thermal image is taken from the evaporator casing and it can be noticed that the evaporator is quite revealed to the outside air. There is no isolation at the front side

6 Implementation

of the evaporator, so loss of heat due to conduction is higher in this area. This can be seen in figure 6.4(c) and figure 6.4(d).

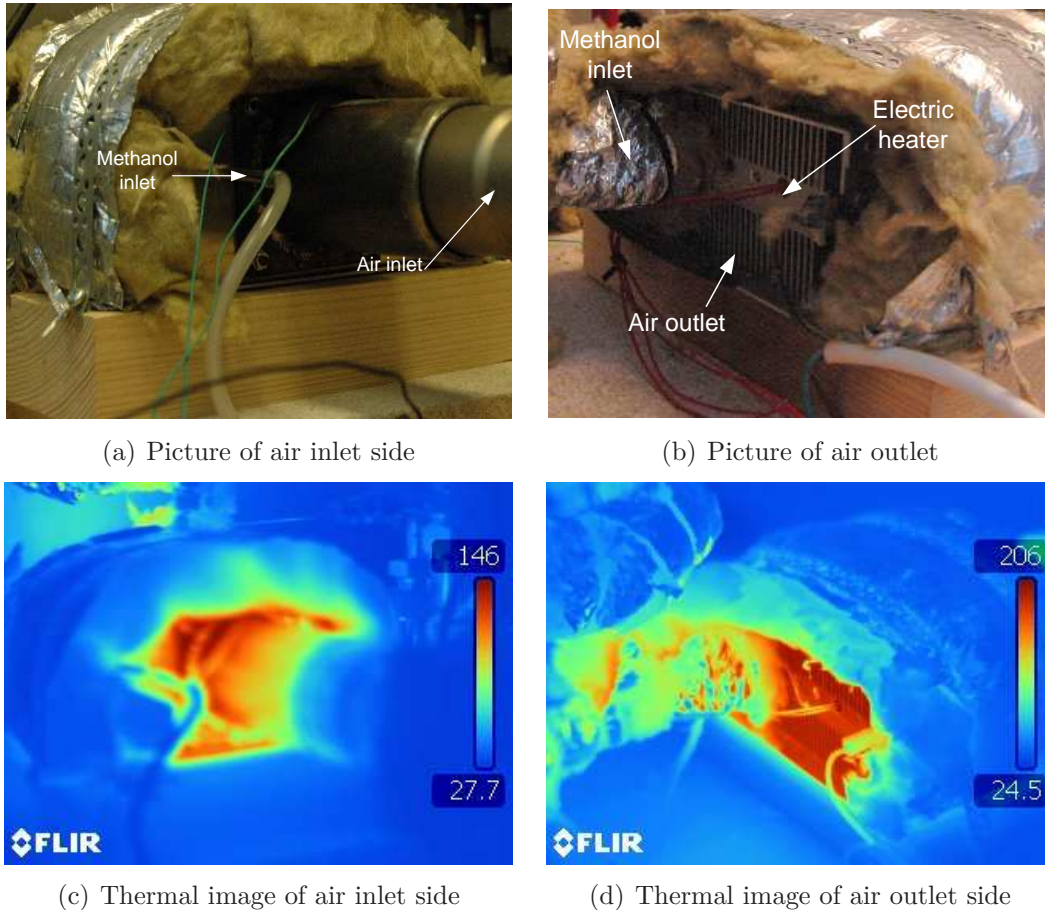


Figure 6.4: *Images of evaporator*

Considering the airflow through the evaporator, the model is based on the fact that the output temperature is the same as the evaporator temperature. Because of physical setup, a measurement of the output temperature is not available, though it is estimated that the temperature is higher compared to the evaporator temperature.

The redesign should be done with more attention to the way the fuel is passed through the evaporator. As the output air, from the fuel cell, is in a pipe with a diameter of about 50 mm, the evaporator width would be about the same. With the same amount of material as the current evaporator the length would be increased. As described in [17] the most effective heatexchanger should be designed with a counterflow, because the difference in temperature would be the largest compared to the inlet air and the methanol mix. This means that the flow of fuel and the flow of air would be in each direction towards each other. As the nonlinear model describes, the heat transfer is calculated by

$$\dot{Q} = \dot{n} (h_{out} - h_{in}) \quad (6.1)$$

The model assumes the enthalpy of the output air is only dependent on the evaporator temperature. If a regression on the output temperature and the airflow, a more precise calculation on how much heat is transferred to the methanol.

The model assumes no loss of heat due to conduction, though the evaporator is only covered partly with a layer of isolation. At the start of the experiment, a pump frequency of 5 Hz caused the evaporator to reduce its temperature to the condensing temperature of the fuel mix. If the mixed methanol and water is not in a vapor phase, this might cause the gas composition to change rapidly and this is not desirable.

As the evaporator is not able to keep up at the given variables, the electric air heater is turned up. When a flow of methanol is started, the temperature of the evaporator is monitored and if the gas outlet temperature falls below $100^{\circ}C$, the methanol pump is stopped. This ensures the flow of methanol is evaporated when it enters the reformer. This increased temperature of the air inlet is used in the rest of the experiments.

The next step in the gas flow is the input into the reformer, and the reformer is described below.

6.3 Reformer

The reformer is designed with a burner on the one side and a reformer on the other. The advantages of this design is, good heat transfer, compact design and a low thermal mass. The volume of the reformer is 0.4l and the weight is around 1kg. This can be seen from figure 6.5, the burner inlet and outlet can be seen. The reformer is located on the far side of the picture, and can be seen with a reformer inlet and outlet.

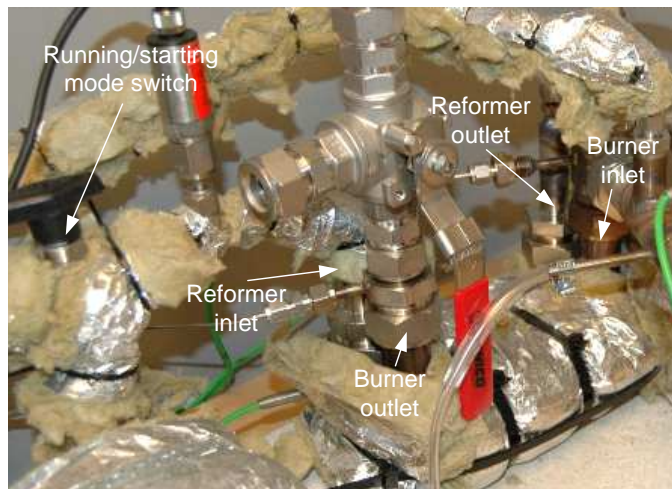


Figure 6.5: *Reformer image*

Initially the reformer was covered in the middle with a layer of Rockwool, to decrease the thermal gradient through the reformer. Experiments based on [16] show that the temperature difference can be up to 150 °C. A thermal picture was taken and can be seen in figure 6.7(a) and figure 6.7(b). The thermal loss due to conduction was a concern, so some improvements was made to reduce the thermal conductivity. This is done by adding Rockwool at the ends of the reformer, and this can be seen from figure 6.5.

6.3.1 Temperature experiments

The placement of the different temperatures sensors can be seen in figure 6.6. “Burner Temperature 1” is shown as “T1”, “Burner Temperature 2” is “T2”, “Reformer outlet temperature” is “T3” and “Burner gas outlet temperature” is “T4”. The temperature sensors used is a K type sensor, and is attached with a high temperature resistant glue. As shown in [16] the temperature on the length is as high as 150°C, though on the width of the reformer the temperature difference is about 50°C. As the temperature on the reformer side is about the same as the burner side, the reference temperature is set at the burner side.

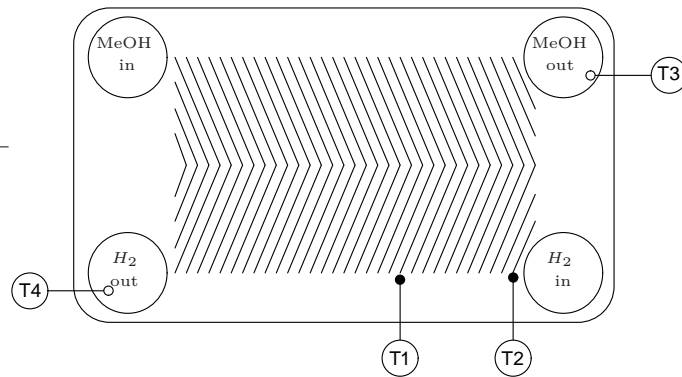


Figure 6.6: *Placement of temperature sensors*

The next experiment is conducted to see how much hydrogen and air that is needed for the reformer to reach the desired temperature. The experiment is shown in figure 6.8. Two temperature sensors is applied to the burner. One at the gas inlet of the burner side (Burner temperature 2) and another about 2 cm down the burner areal (Burner temperature 1). “Burner temperature 1” is chosen as reference temperature, because of a faster feedback of the temperature is possible.

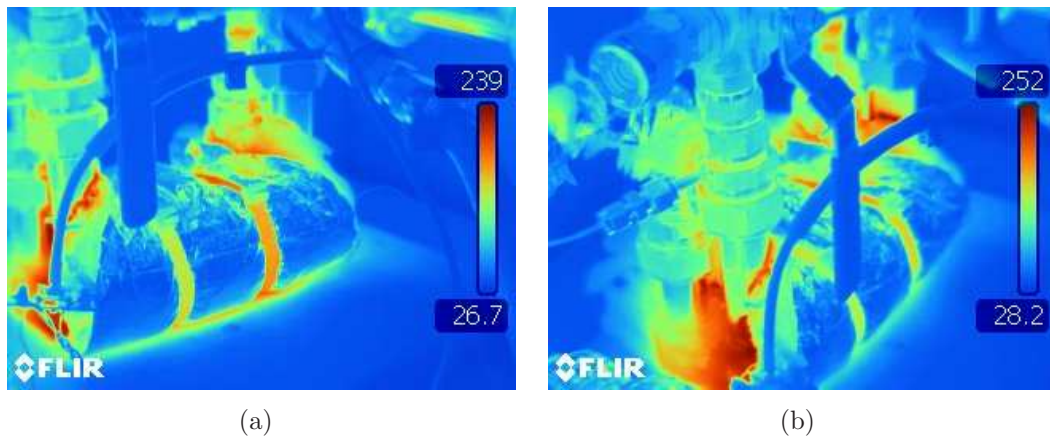


Figure 6.7: *Thermal images of reformer without end isolation*

The desired temperature of the reformer is about $350\text{ }^{\circ}\text{C}$, though different temperatures is read throughout the reformer length[16]. The difference between “Burner temperature 1” and “Burner temperature 2” is about $50\text{-}100\text{ }^{\circ}\text{C}$, thus the reference temperature for “Burner temperature 1” is $350\text{ }^{\circ}\text{C}$.

In figure 6.8 there is no flow of methanol through the reformer part. This means that the loss of temperature in the reformer only depends on the conduction and convection from the airflow. The airflow is set to 10 times the flow of the hydrogen and is based on experiments in [3]. At about 250s, the feed forward is changed to deliver 9 times the hydrogen flow and at 280s the feed forward is changed to 8. If there is any indication on flashback in the burner, the temperature would change rapidly. This does not seem to happen, since the temperature in the outlet gas is

6 Implementation

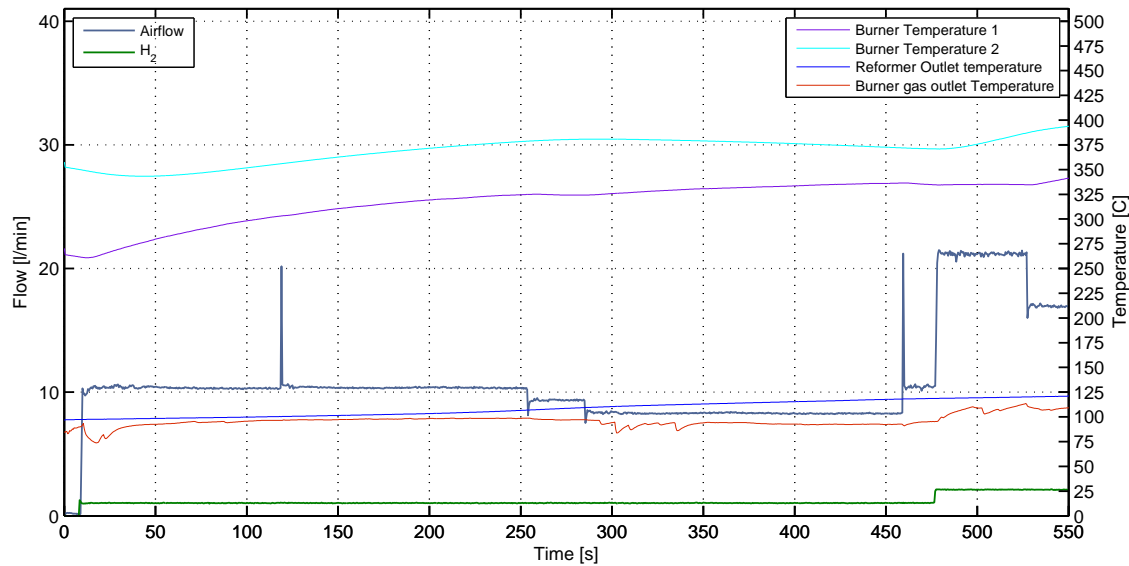


Figure 6.8: *Airflow compared to hydrogen flow in burner*

almost constant. At about 460s the feed forward gain is changed back to 10 and the hydrogen flow is changed to $2\text{l}/\text{min}$. The temperature of the reformer is tested in the same way, and it is concluded that a gain of 5 is enough for the temperature to be stable.

The same experiment is shown later in figure 6.9 where a PI regulator is applied. The reference set point is 350°C and the gain of the regulator is set at a low level ($K_p = 0.001, T_i = 0.01$). The oscillating change in temperature is not desirable, and will be covered later in this chapter. As for the finished system, a change in hydrogen can happen, and this could look something like the effect the slow PI regulator is doing. So by leaving the PI regulator at a low regulation, the effects of changing temperatures can be seen in the composition. As mentioned before, the difference in the two temperature measuring points is about $50\text{-}100^{\circ}\text{C}$ and the temperature at “Burner temperature 1” is changing faster compared to “Burner temperature 2”.

An experiment was carried out to test a starting sequence to see how long it takes to change the temperature from 150 to 350°C . This is shown in figure 6.10 and it takes about 350s. At 800s the reference temperature reaches 350°C and the temperature is kept relatively constant.

The experiment continues in figure 6.11 where the methanol pump frequency is set to 5Hz.

The temperature of “Burner gas outlet temperature” is decreasing throughout the experiment, though this is leveling out at about 125°C . Fittings and tubes at the exit temperature is not isolated in any significant way, and this might suggest that a larger mass of the reformer should be used.

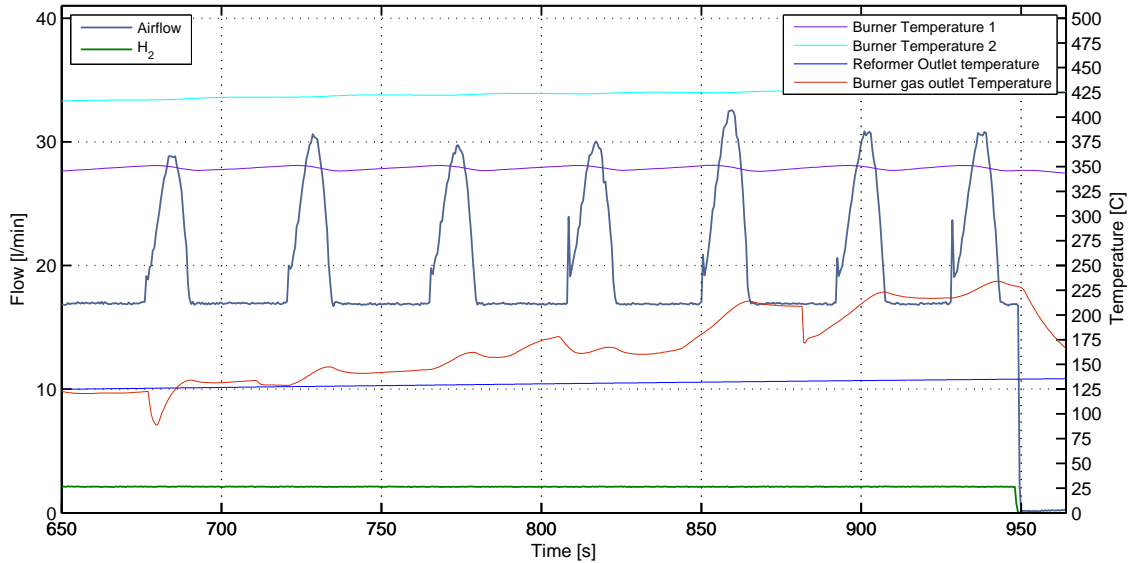


Figure 6.9: *Controlling temperature of reformer with a low gain controller*

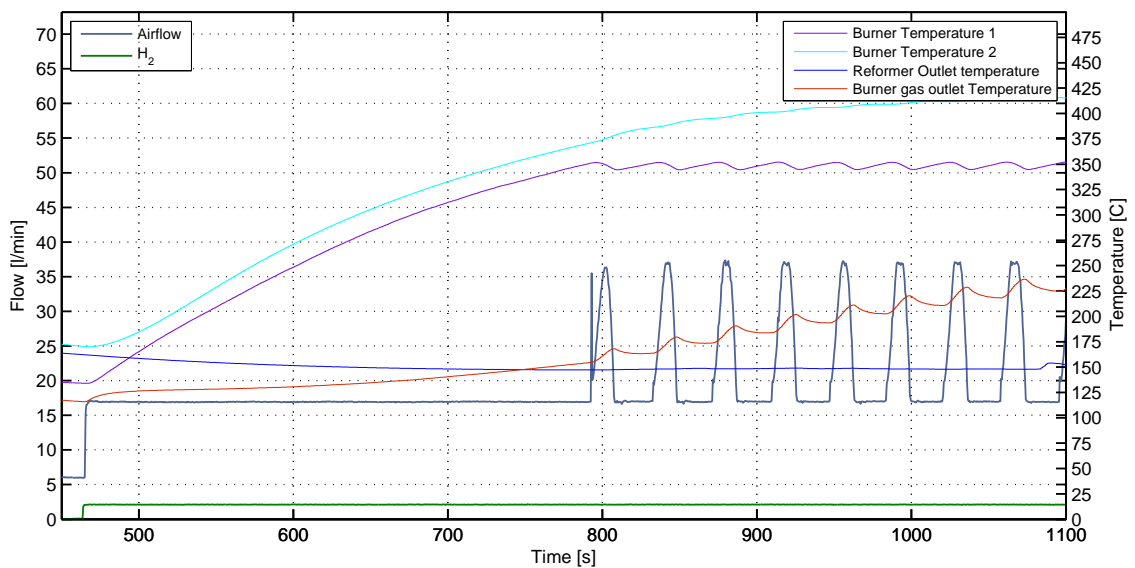


Figure 6.10: *Startup from 150°C with 2l/min and 8 times the airflow in feed forward gain*

6.11 was also conducted to see the temperature is in the reformed gas. The next step in the system is to direct the gas through the WGS (as shown in figure 6.1). This WGS catalyst is designed to withstand a temperature at around 300°C. The temperature is measured at about the halfway between the reformer gas outlet and the WGS inlet. The temperature in the end of the WGS container is measured, and is much below the 300°C first estimated. The temperature measured at the WGS can be seen in figure 6.11 and is a little below 100°C. As the

6 Implementation

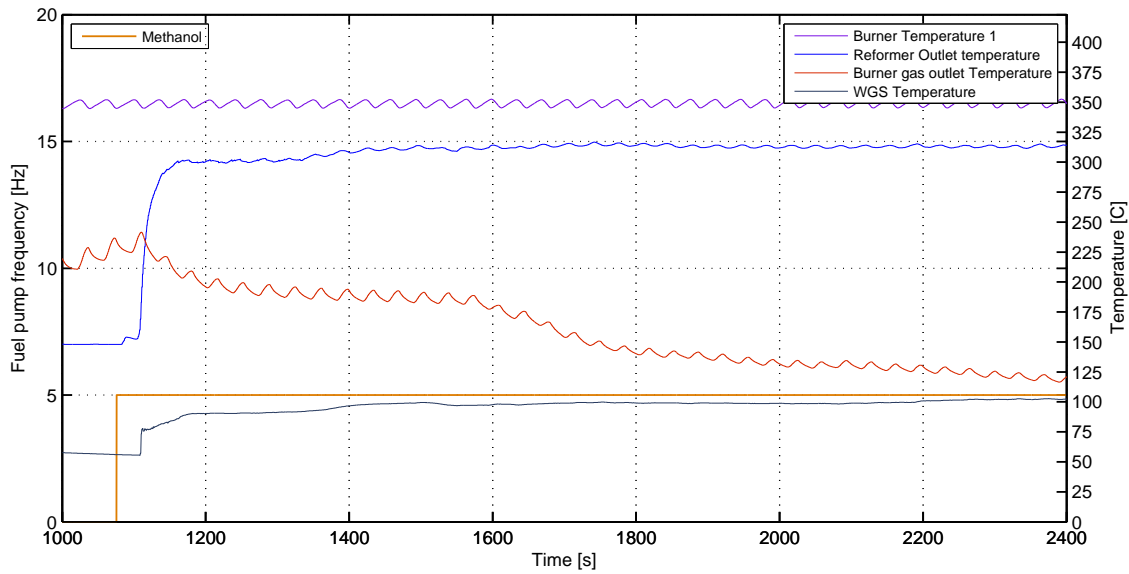


Figure 6.11: *Change in methanol flow from 0 to 5 Hz*

Temperatures is compared in figure 6.12 between the reformer outlet temperature, WGS temperature and Cooler temperature. The temperature of the fuel cell is about $160\text{-}180^{\circ}\text{C}$ and the input temperature of the gas flow is measured to around 80°C at the cooler outlet.

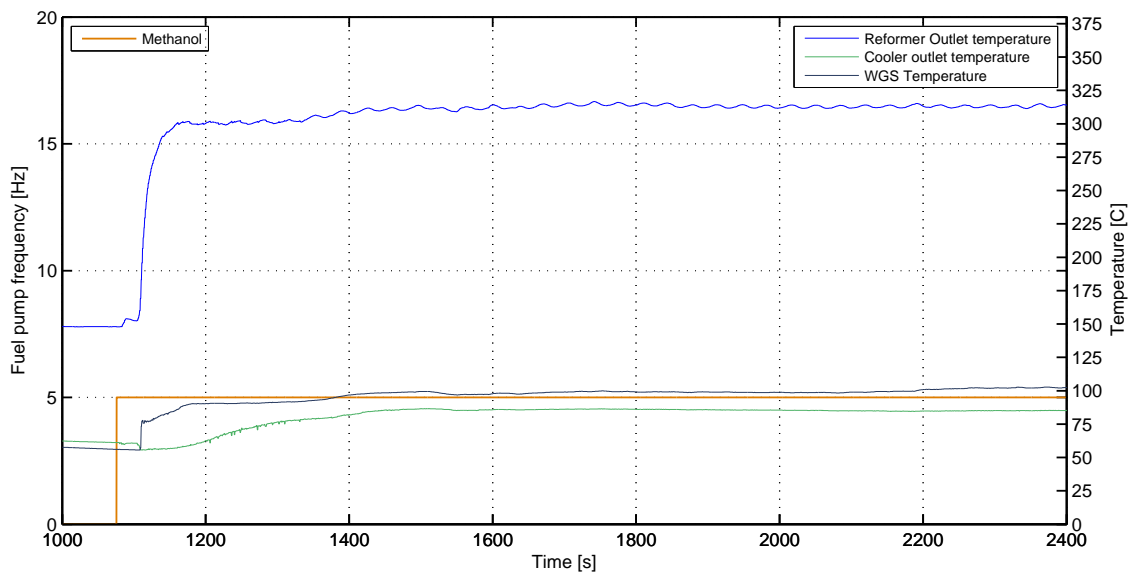


Figure 6.12: *Temperatures measured after the reformer with a methanol flow of 5Hz*

As the ripple on the burner is undesirable, some changes in the PID parameters was conducted. The change can be seen in figure 6.13 where the parameters from table 6.1 is changed. The PID regulator in the program can be seen from Appendix D.2.

Seconds	P	I	D
Start	0.001	0.01	0
540s	0.01	0.01	0
815s	0.1	0.01	0
900s	1	0.01	10

Table 6.1: *PI parameters change in figure 6.13*

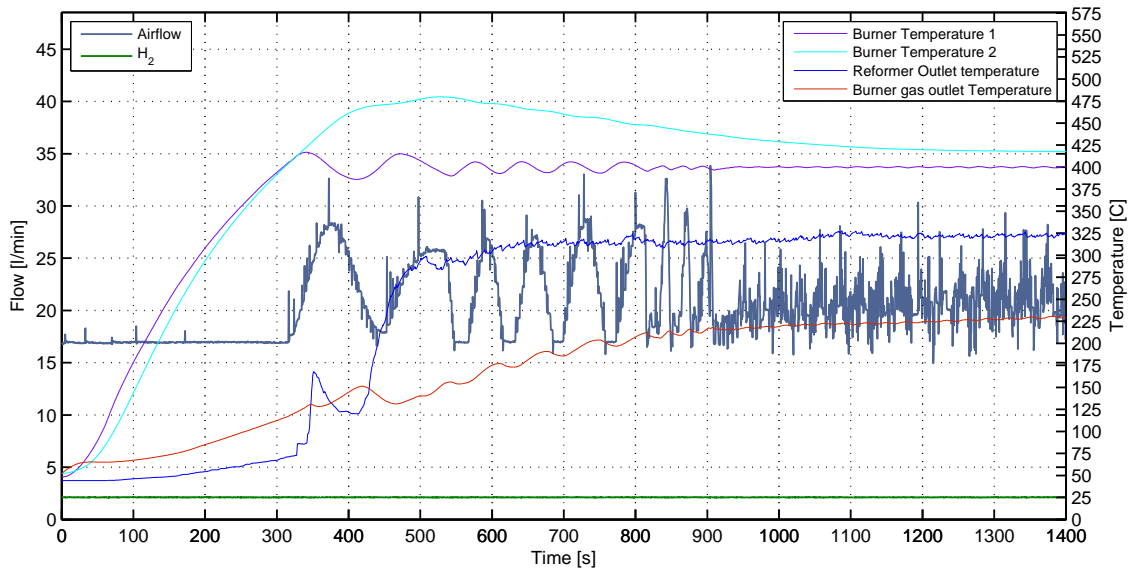


Figure 6.13: *Changing the controlling variables*

To avoid temperature fluctuations, a differential part is added to the regulator. Differential regulators are known to add stability to the system, but if there is noise in the reference signal, the differentiator can reduce stability.

There is some times a need to combine a PI and a lead-compensator in a regulating system. Such a combination is often called a PID regulator, though the theoretical PID regulator is not physical installable. The theoretical PID regulator can be seen in (6.2).

$$G_c(s) = K_p \left(1 + \frac{1}{\tau_i s} + \tau_d s \right) \quad (6.2)$$

This theoretical PID-system has two zeros and one pole, and this it cannot be realized. If we modify the differentiator to only being effective under a certain frequency, you can get a controlling system like (6.3).

$$G_c(s) = K_p \left(1 + \frac{1}{T_i s} + \frac{T_d s}{\alpha T_d s + 1} \right) \quad (6.3)$$

6 Implementation

where $\alpha < 1$. This is a transfer function with two zeros and two poles. This system is able to be realized, at least at certain frequency areas.

The influence of the MFC's in the system is not included in any way, and this might cause some variations compared to the theoretical model. If the MFC's are used in future work, the need of identifying the transfer function for the MFC is required. As mentioned before the overshoot of the MFC's is high and because of this the use of MFC's in this system is not desirable.

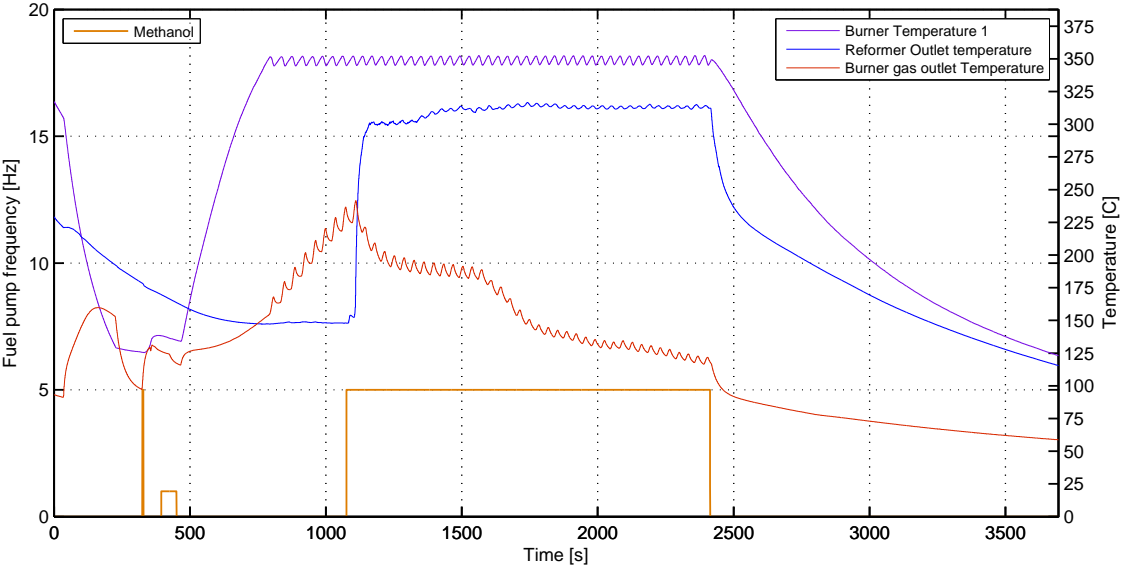
6.3.2 Gas flow in the system

When doing these experiments, a lag is measured between the input flow of methanol and the reformed gas. During the experiments a few indications were seen on how long this gap is.

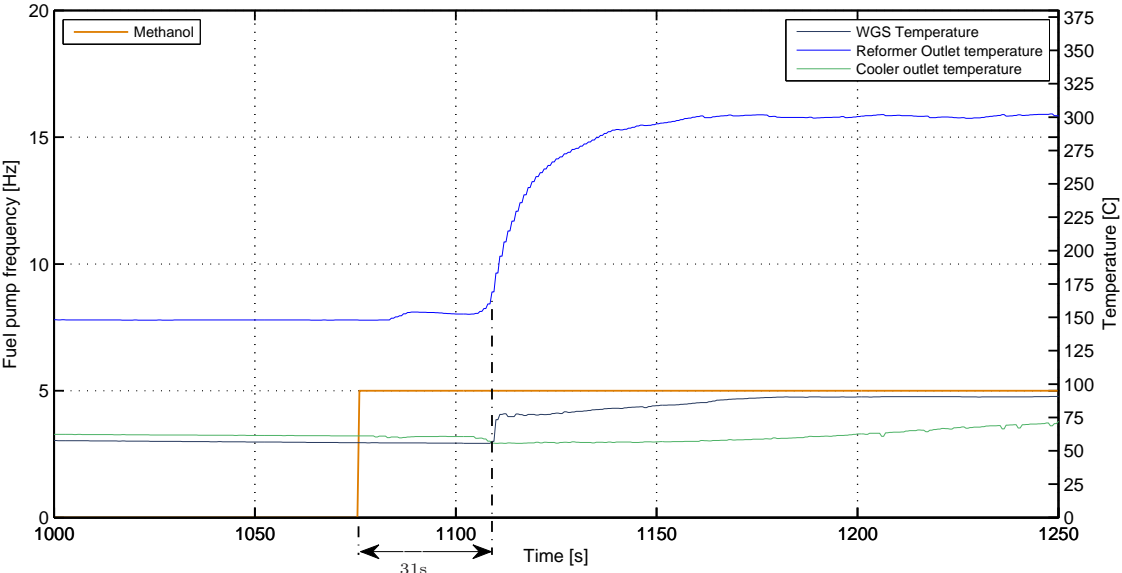
Since there are no flow measurements on the system, another way to see how long the lag is, is to look at the temperature change when the methanol flow is turned on. A noticeable change of temperature in the reformed gas can be seen at about 1100s into the measurement figure 6.14(a).

The change in methanol is zoomed in at the frequency change, so an estimation of the lag can be seen in figure 6.14(b). When the flow of methanol is started, there is a lag of about 31s before the temperature change is noticed. This temperature change can be noticed in the reformer gas outlet and also in the WGS container. This container is empty in this experiment, so this only validates the transport lag time. This transport lag is considered to be the same as the flow lag through the reformer and evaporator, though an experiment with a flow measurement should be conducted to verify the temperature and flow correlation.

Another experiment was conducted at 1 Hz flow instead and this can be seen in Appendix A.2.4. This experiment concludes the same, though there is not the same noticeable change in temperature.



(a) Temperatures compared to methanol flow



(b) Zoomed in at the frequency change from 1000s to 1250s

Figure 6.14: Influence in temperature at the reformer gas exhaust when the pump frequency changes from 0 to 5 Hz

6.3.3 Dry gas composition

The molar fractions is made with a Pfeiffer Omnistar mass spectrometer, calibrated to measure H_2 , CO_2 , CO , and CH_4 . This mass spectrometer measures the dry gas composition of the gas placed as shown in figure 6.1. On the reformer gas outlet, a switch valve is installed between outside air and the reformatted gas. This can be seen from figure 6.15.

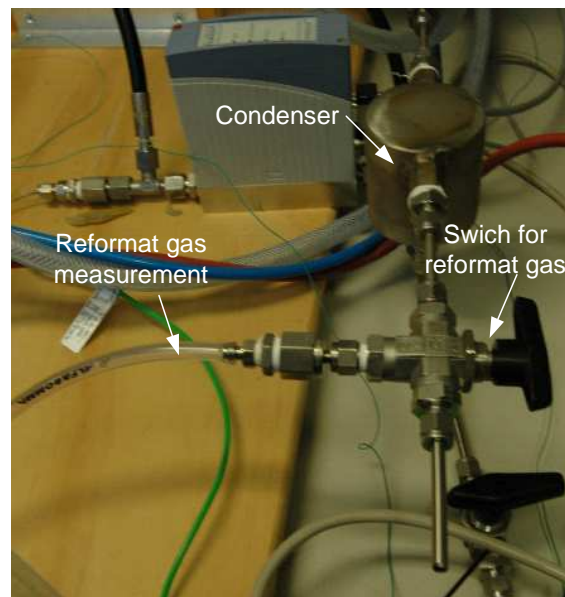


Figure 6.15: *Condenser before the mass spectrometer*

Switching from air to reformat gas can be seen in almost all the experiments, at the change in gas composition. The spectrometer is very sensitive to condensed water which requires the water and methanol is extracted by a condenser before gas is measured. As the methanol and water is extracted from the gas, the measurement of the gas is the dry gas composition. This can be calculated by (6.4)

$$x_{drygas} = \frac{x_{gas}}{1 - (x_{h_2o} + x_{ch_3oh})} \quad (6.4)$$

The molar fraction in (6.4) describes the relationship between the drygas fraction compared to the real gas composition. First measurements was done without any WGS catalyst and at a low methanol flow (1 Hz). The results can be seen in figure 6.16 and shows how the composition changes over time. The measurement is started at about 50 seconds after the methanol pump is started, and the switch valve is changed to the gas flow at 80 seconds. The measurement ends up at about 6% CO, 16% CO₂ and 75% H₂.

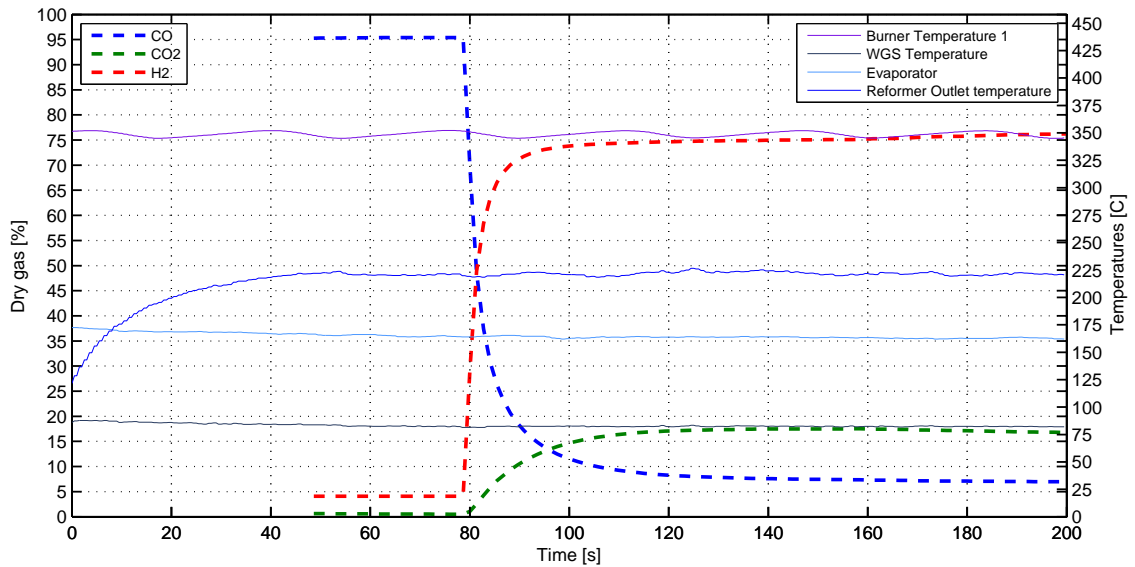


Figure 6.16: Sample measurement from mass spectrometer. Measurement is without a WGS catalyst and 1 Hz methanol pump frequency

The container is filled with a WGS catalyst BASF SP-68, and the temperature is monitored in the next experiments. The rated operating temperature is about 200 - 300 °C, though typical operating temperatures are in the range of 230 - 260 °C. Temperatures above 280 °C should be avoided, though peaks can be tolerated up to 320 °C [4]. The catalyst is installed in a 8 cm long cylindric container with a diameter at about 3 cm.

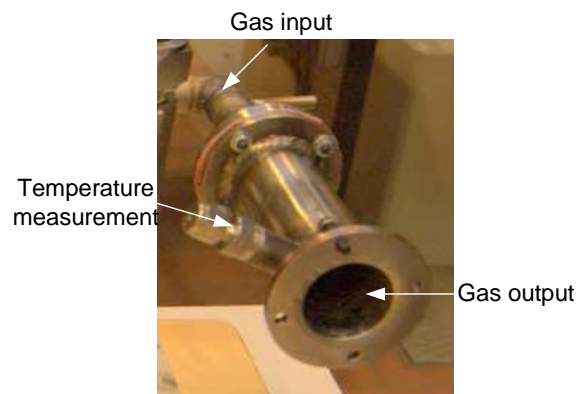


Figure 6.17: WGS container

The container is placed in a horizontal position, though it is considered a vertical position is better. As the catalyst is installed in 1.5x1.5 mm pellets, the room for installing the catalyst is limited. The rising WGS temperature is compared to the dry gas fraction and shown in figure 6.18.

Isolation is installed on the WGS container, and figure 6.18 shows the center temperature of the catalyst to from about 120 to 200 °C. This is a bit under

6 Implementation

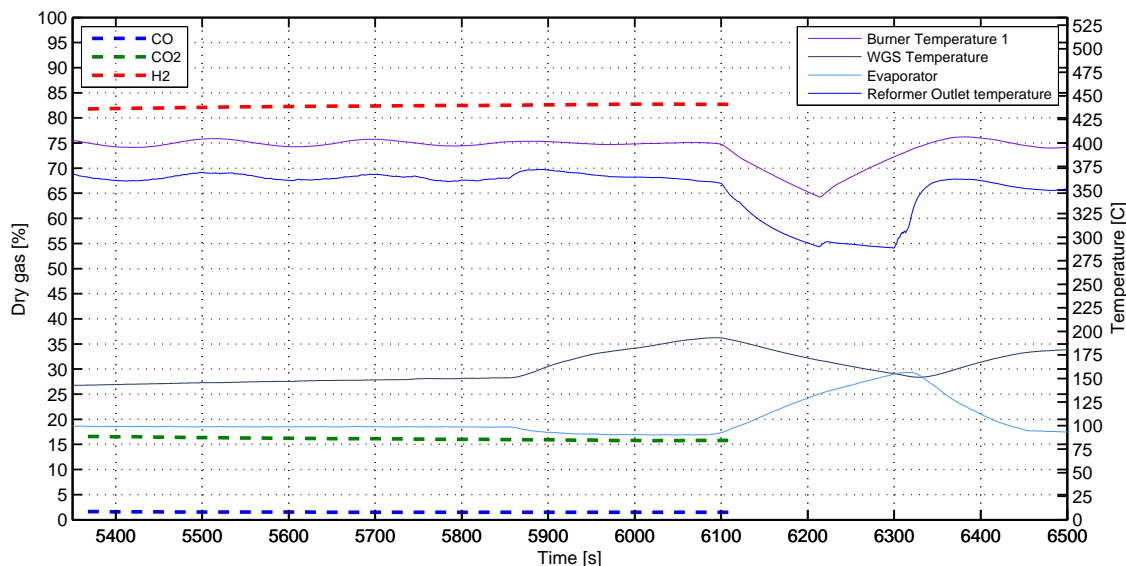


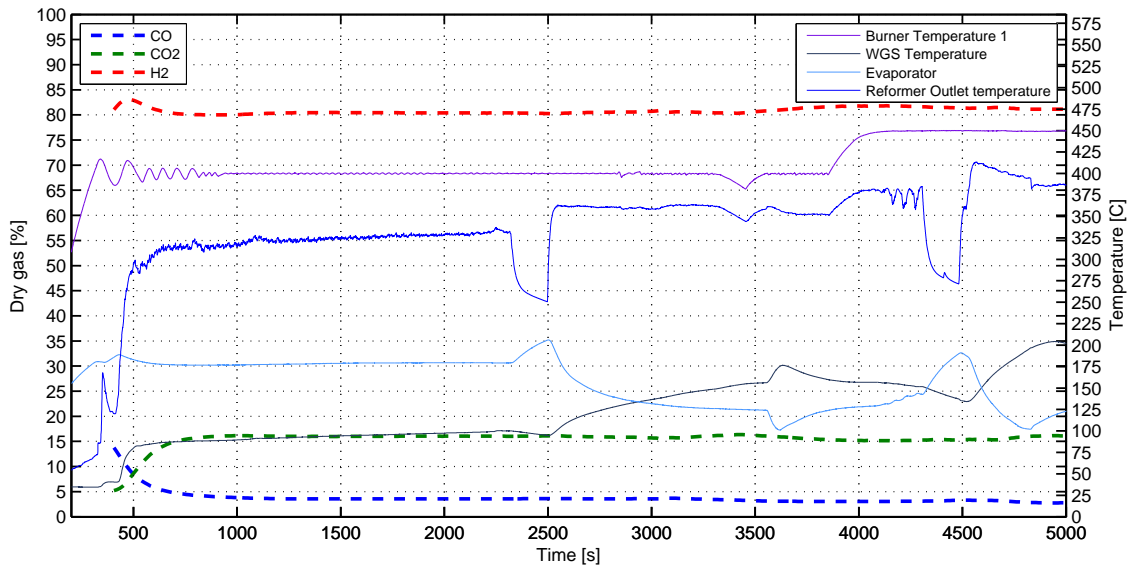
Figure 6.18: Sample measurement from mass spectrometer. Measurement with WGS SP-06 catalyst and the container with the catalyst has been isolated. The pump is set at 5Hz

the rated temperature, though before more isolation is installed, more investigation on the gas inlet temperature is necessary. In the dry gas concentrations, it can be noticed that the CO concentrations are greatly reduced. This measurement is taken about 5400 seconds (about 1:30 hours) and it can be seen that the CO concentrations are stable about 2% CO.

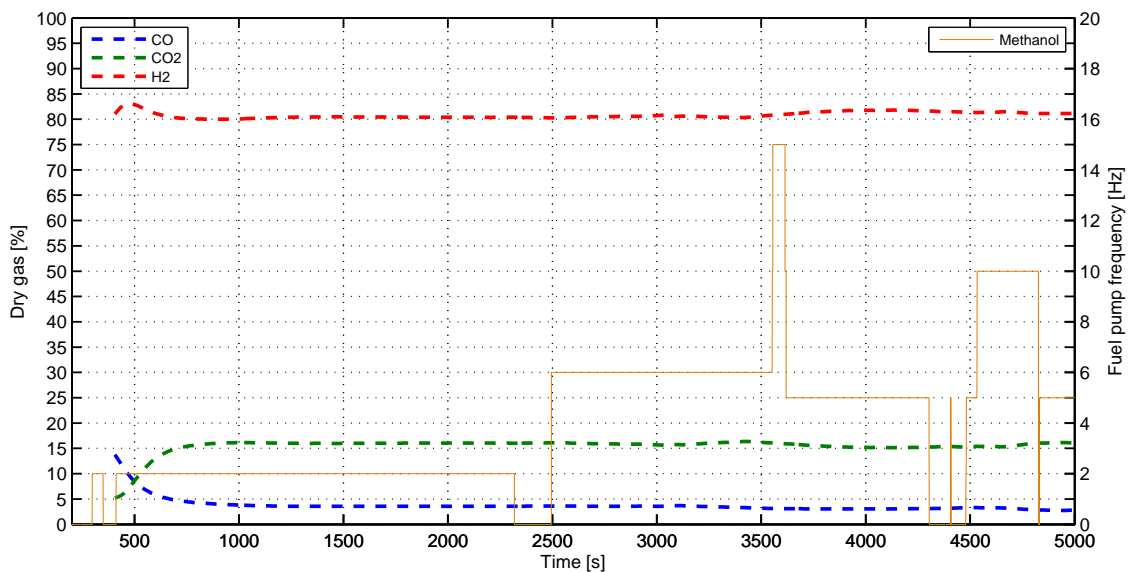
The experiment shown in figure 6.19 shows the dry fraction compared to the methanol flow and the temperature of the system. The temperature of the WGS catalyst changes by the rate of the flow from the reformer. This temperature changes from 100°C to about 200°C. The flow is manually changed so the temperature of the evaporator is always higher compared to the boiling point of the mixed fuel. Molar fractions compared to temperature can be seen in figure 6.19(a) and methanol flow in figure 6.19(b).

At about 4000 seconds into the experiment the reference temperature of the reformer is changed to 400°C. At about 3500s into the experiment, a change in methanol flow is made to 15 Hz. This change does inflict on the temperature of the WGS and the evaporator. The evaporator temperature decreases rapidly and the WGS temperature changes about the same though in the opposite direction. As the temperature is changed to 400°C, the CO₂ concentrations are rising and the CO concentrations are falling. This can indicate that the reaction rates on the WGS reaction are increasing, though more research into this catalyst has to be made.

The mass spectrometer is recalibrated, and new measurements are taken. In the next experiment, measurements are taken with changing flow of methanol. As shown in



(a) Measurement of WGS temperature and varying methanol pump frequency



(b) Pump frequency compared to dry gas fractions

Figure 6.19: *Measurement from mass spectrometer*

figure 6.20 the different temperatures are compared to the methanol flow. It can be noticed how the temperature at “burner temperature 2” is changing compared to the regulated “burner temperature 1”. The startup of the reformer with no methanol flow, the “burner temperature 2” is higher, though after the methanol flow is started, the temperature drops much below the regulated temperature. As the maximum temperature of the heat exchanger is about 500 degrees, the temperature of the reformer might be higher and might damage the heat exchanger. This temperature difference in the reformer can also have an influence in the gas composition. The dry gas composition can be seen from figure 6.21(a) and figure 6.21(b).

6 Implementation

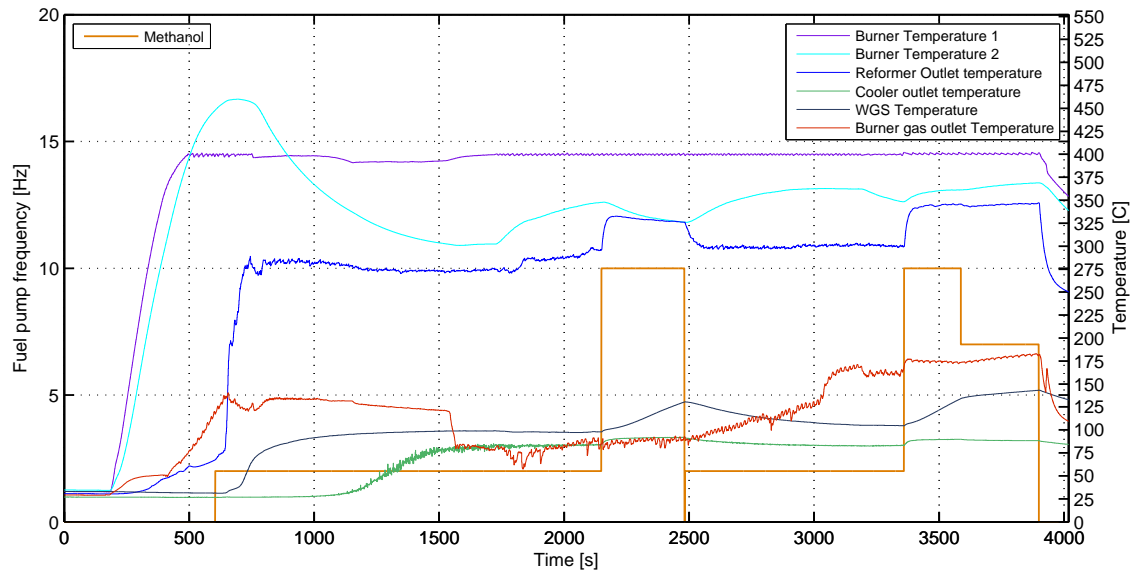
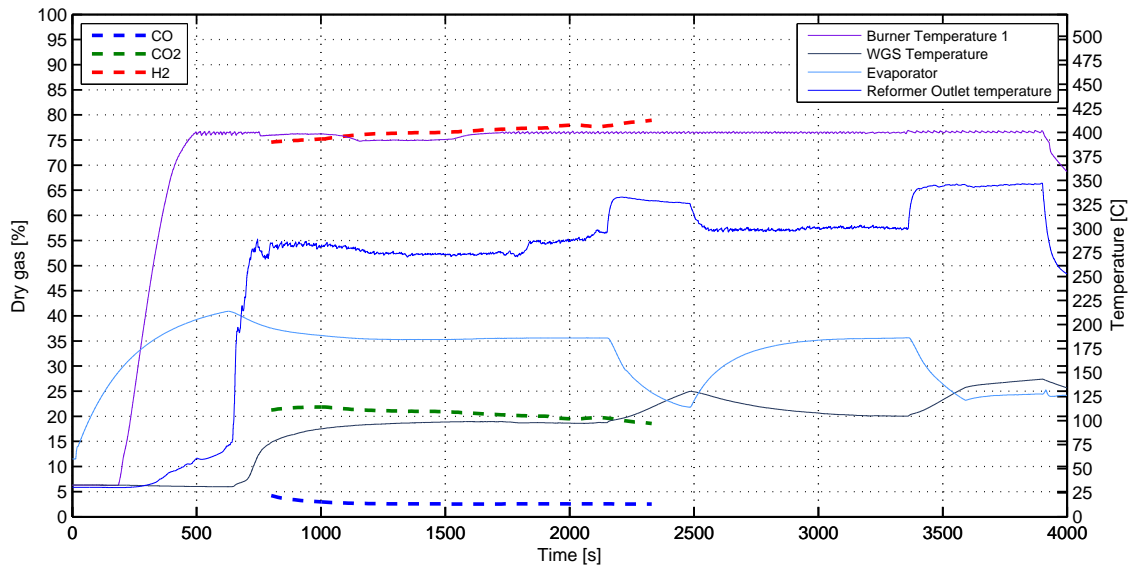


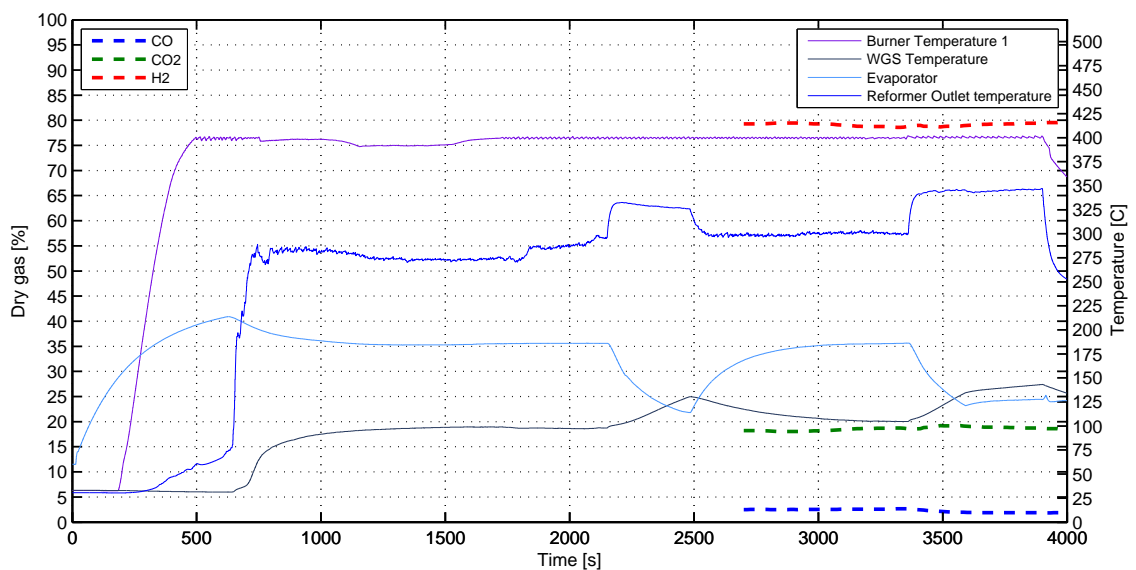
Figure 6.20: *Temperatures compared to methanol flow. Same experiment is compared to dry gas fraction in figure 6.21*

It can be noticed that the temperature of the WGS is changing from 100 to about 140°C, and it is seen that the concentration of CO is decreasing. The output gas from the reformer (300°C) is not needed to be lowered by any external equipment, because it is estimated that the temperature is lowered enough by the unisolated tubes between the reformer and WGS. The measured gas composition in figure 6.21 is about 3% CO, 19% CO₂ and 80% H₂ at a setpoint of 400°C at the burner.

The output gas temperature of the WGS is, at its highest, at 200 °C. This could indicate that the heat lost in the unisolated tubes between the reformer and WGS is lowering the temperature too much. The cooler installed is thereby unnecessary large and the loss in the tubing is estimated to be enough for the gas to enter the fuel cell. A temperature sensor is placed on the surface side of the reformer, to test the difference between the burner temperature and the reformer surface temperature. The temperature sensor is not attached to the reformer, and is thereby not comparable to the experiments done in [4]. The next section investigates the needed amount of hydrogen added to the burner.



(a) Measurement with mass spectrometer from 700s to 2400s



(b) Measurement with mass spectrometer from 2600s to 4000s

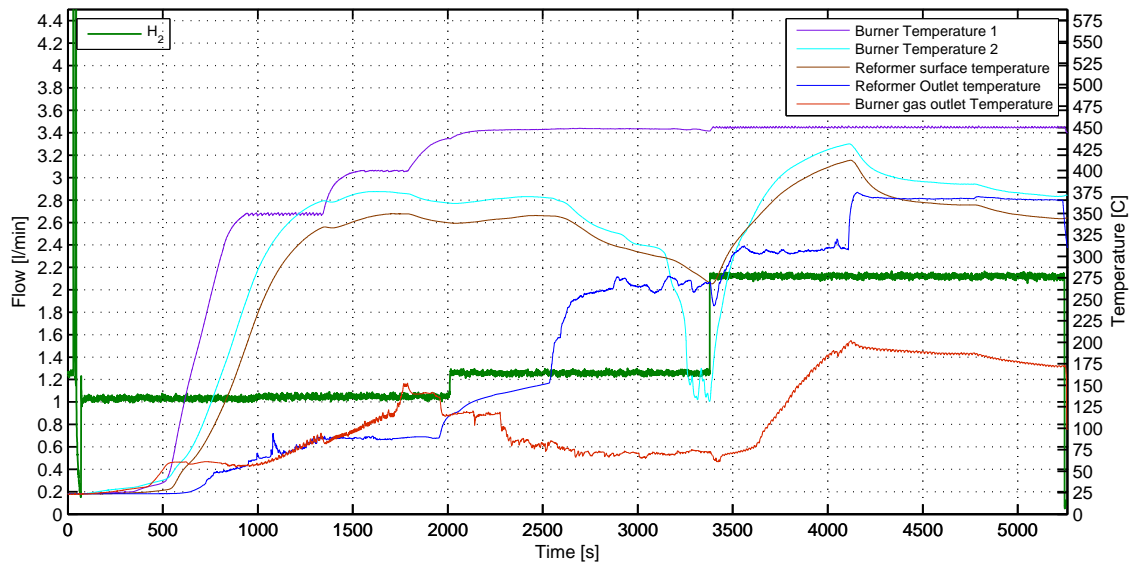
Figure 6.21: Measurements with mass spectrometer with changing methanol flow. The methanol flow can be seen from figure 6.20

6.4 Simulated run

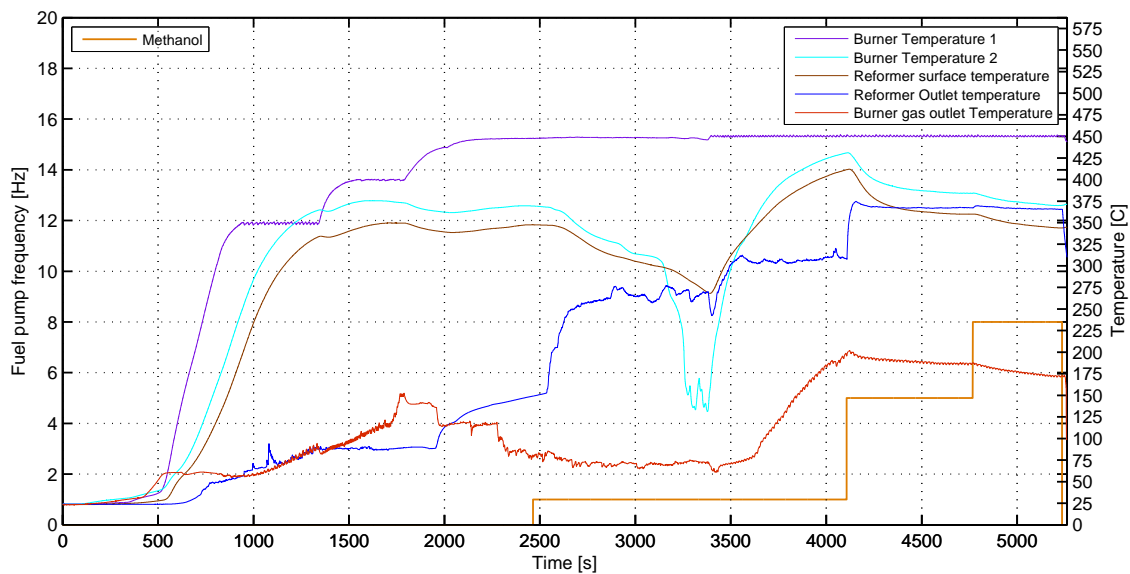
To determine the needed excess hydrogen for the burner, a series of experiments was conducted. The temperature of the reformer was logged and compared to the methanol flow in the reformer. The required temperature of the reformer is 350°C and is measured in the exit gas of the reformer. Temperatures on the surface of the reformer and burner was also logged. As the temperature in the evaporator is not

6 Implementation

able to be held at a acceptable level, at the given flow rates from the model, the temperature of the electric heater is increased.



(a) Temperature compared to hydrogen flow



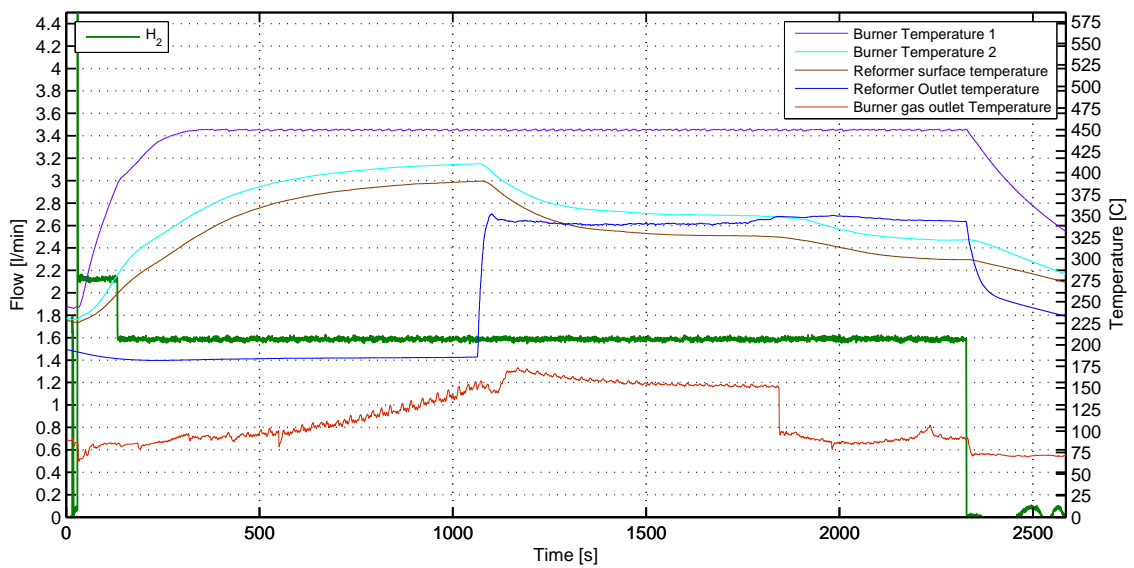
(b) Temperature compared to methanol flow

Figure 6.22: First simulated experiment - Temperature of reformer and burner compared to methanol flow

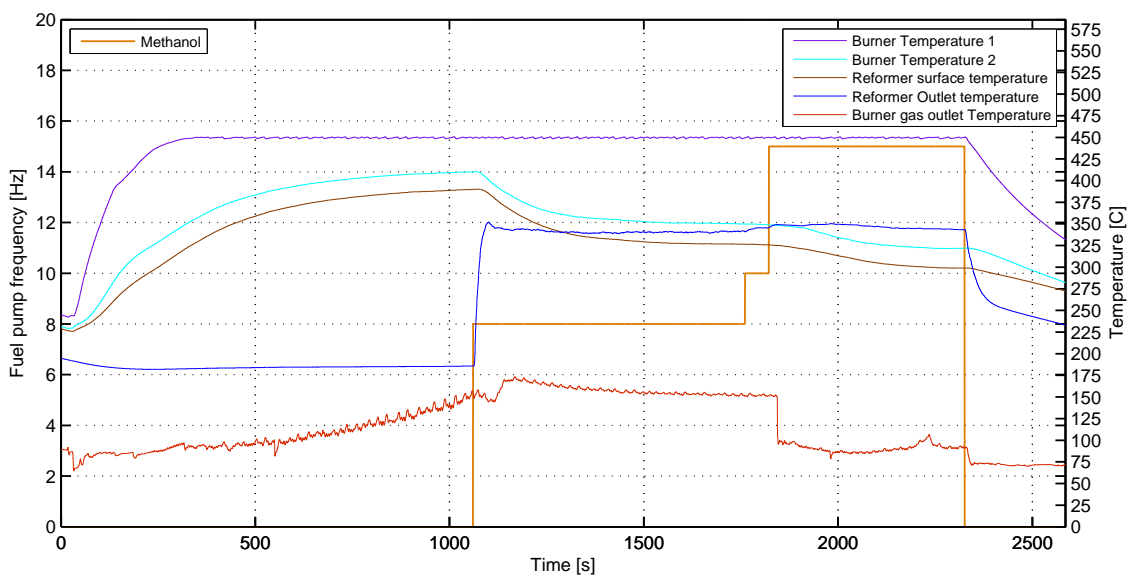
The temperature of the reformer outlet gas is monitored as the flow of hydrogen and methanol is changed, and this can be seen in figure 6.22(a) and figure 6.22(b). Before the methanol flow is started, the reformer is heated to about 400°C with 1 l/min hydrogen. The feed forward is set to a gain of 5 times the airflow, and by this ratio the temperature of 300°C is reached in about 500 seconds. As the

temperature at the reformer is lower compared to the 350°C goal temperature, the reference temperature is changed to 400°C and then 450°C .

As the temperature drops at the burner and reformer, the hydrogen flow is changed to 2 l/min at about 3400s . This increases the temperature of the reformer again and the flow of methanol is changed to 8 Hz at about 4700s . The temperature of the reformatted gas is stable at about 360°C and a second experiment was conducted with these data in mind.



(a) Temperature compared to hydrogen flow

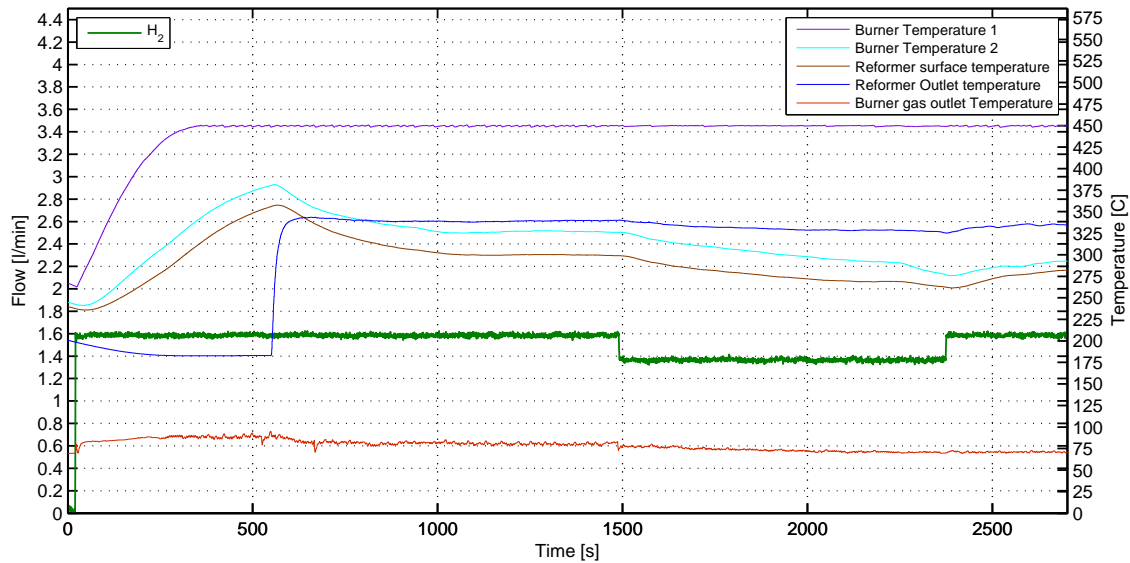


(b) Temperature compared to methanol flow

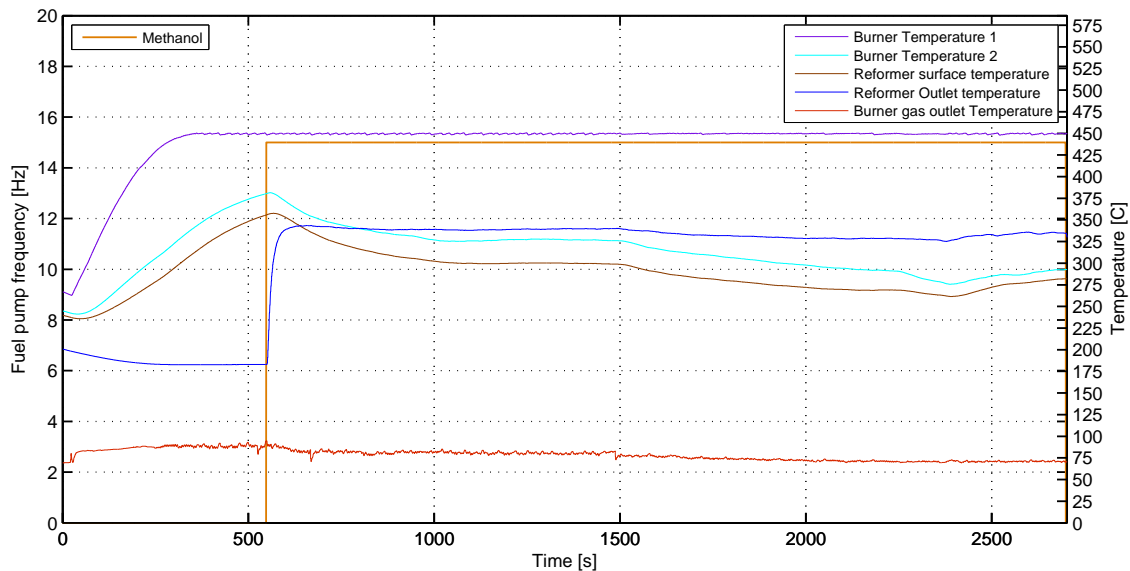
Figure 6.23: *Second simulation experiment - Temperature of reformer and burner compared to methanol flow*

6 Implementation

The second experiment was done with the burner reference temperature of 400°C and the flow of hydrogen was changed to 1.6 l/min . This can be seen from figure 6.23(a) and figure 6.23(b). The methanol flow was changed to 8 Hz and the temperature was monitored. This flow was kept for 800s and the temperature of the reformatted gas was stable at about 350°C . The methanol flow was changed to 15 Hz, and the temperature was stable for another 500 seconds.



(a) Temperature compared to hydrogen flow



(b) Temperature compared to methanol flow

Figure 6.24: *Third simulated experiment - Temperature of reformer and burner compared to methanol flow*

In the third experiment the flow was set to 1.6 l/min and the methanol flow was set to 15 Hz at about 550s. The temperature of the reformer outlet gas is seen stable at

about 340°C and this is kept for about 1000s. At 1500s the hydrogen flow is changed to 1.4 l/min and the temperature of the gas is decreasing. At about 2400s the flow of hydrogen is changed back to 1.6 l/min and it is concluded that the burner flow at 15Hz methanol flow is about 1.5 l/min .

The 15Hz methanol flow is set after a calculation made in the model, where the fuel cell is at its maximum capacity. As the temperature is held constant at a hydrogen flow of 1.5 l/min and the calculated hydrogen usage in the fuel cell is 2 l/min . The estimated λ_{h_2} is calculated to 1.75, which means that 175% excess power from the fuel is required.

6.5 Summary

The feed forward gain on the burner side is estimated to be around 5 times the hydrogen flow. This gain must be high enough for the hydrogen is catalytic burned. The evaporator is estimated to be too small for the system with the parameters from the model. Too much power is lost due to conduction and the assumption on the output air, being the same as the evaporator, is questionable. The gas compositions measured does imply that the WGS reaction is temperature dependent, because at higher temperatures, the CO concentrations is lowered. The measured CO concentrations is about 3% CO, 19% CO₂ and 80% H₂ with a setpoint of 400°C at the burner. The change in methanol does not seem to have a large impact on the composition of gas, though since the measured gas is made with a mass spectrometer, alternative measurements could be adviceable. The temperature of the burner seems fairly easy to control, though a specific blower might reduce the small deviations from the specified setpoint. Experiments were made with the intent of identifying the needed amount of H₂ for the burner, so the temperature of the reformer does not fall in temperature at maximum rated methanol flow. This was estimated to be around 1.5 l/min hydrogen with airflow feed forwarded with a gain of 5. The needed λ_{h_2} is estimated to be about 1.75.

Conclusion

The model is evaluated as being fast and reliable enough for controllers to be tested. The model has a low simulation time and simulates the system in two modes; Start up and running mode. From a control point of view, the model describes the bottlenecks in the system. The model can be used to evaluate a lot of issues with the system, i.e. fuel needs for the fuel cell and reformer, heating demands for the vaporation, or the reformatted gas composition at different temperatures. As these parameters can be changed, the model calculates electric efficiency of the system and effects of the changes can be viewed quickly.

The nonlinear model has been linearized and acts as the base for the controller parameters calculation. The feedforward function is part of the controllers for the reformer and fuel cell stack models. The reformer feedforward transfer function shows a high convective heat transfer, which may be based on the burner stoichiometry. The approach of using the feed forward airflow controller is good for the system, since the feed forward function is used to avoid the flashback from the burning of the hydrogen. The difference in controller parameters, compared to the implemented system, is assumed to be caused by the mass flow controllers. The mass flow controllers are known to cause large overshoots at step changes, and is highly tuned. Before implementing the parameters from the controlling chapter, ordinary blowers should be used.

The linear models are all created with a changeable working point. This means that the equations can be changed quickly according to different operating points. The model assumes a constant steam to carbon ratio. Changing this ratio will require the user to recalculate the variables for the hydrogen coverage of the cell. The model does not apply changes to the hydrogen fraction, though this is assumed valid, since the change of the hydrogen fraction is small compared to the temperature. The parameter search scripts are based on the linear model of the system. Changes in the linear model will also change the output controller parameters from the script.

The responses of the system components are assumed to have reached the reference temperature when the output is within 2%. All the controller parameters showed a 1% overshoot and a fast response. The response from the linear model, of the fuel cell stack, shows that the controllers in theory are faster than the thermal systems that they are controlling. The model for the fuel cell stack had no problem changing the reference temperature. A problem was found in the reformer model as the reformer had trouble reaching the reference temperature. This is explained with a combination of low λ_{h_2} of 1.5, and the loss from convection and conduction. From experiments the hydrogen stoichiometry was found to be 1.75 and this will

7 Conclusion

supply more hydrogen as fuel for the burner. This would increase the temperature and decrease the efficiency based on the extra fuel needed.

The approach for lagging the current density shows usable results. Lagging the current density showed that a step change of the current density was possible within 30 seconds. The reformer linear model did not reach the temperature specified, but the characteristics for the reformer temperature showed that a fast change in the current density was possible. The air for the feed forward controller is also lagged since it is based on the amount of hydrogen at the reformer. Changing the current density from a higher current density to a lower current density without a lag, could force a flashback inside the reformer. This is caused by the feedforward controller would react too fast and would decrease the air below the allowable limit.

The estimator is designed with an implementation in mind. In the nonlinear model the estimator uses the hydrogen fraction from the reformer gas composition regressions. The linear model uses a constant for the hydrogen fraction, though this may be calculated from a linear regression based on the reformer temperature. The reformer temperature is controlled and if the reformer temperature is constant, the hydrogen fraction may also be assumed constant. Both the linear model and the nonlinear model estimator uses a constant mass conversion factor in the reformer, with a value at about 1.86, though deviation at changing temperatures and SC ratio is required to be included. The calculation that involves the hydrogen consumption, in the fuel cell, can also be lower compared to the experimental amount. The estimator is inserted into the nonlinear model, and it is seen that the inserted λ_{H_2} is the same as the measured hydrogen input for the burner. If this estimator is implemented in a real system, the hydrogen fraction must be known, and the conversion factor K_{com} has to be tested.

The model assumes no loss in tubes, and this might cause some deviations from the model to the physical system. The heat transferred from the fuel cell is set to the same temperature as the heat inserted in the evaporator, though it is not the case. The temperature of the output air from the fuel cell might also be lower compared to the fuel cell temperature. If the airflow from the fuel cell is increased, the temperature of the air might decrease, and this should be investigated. For the model to apply in this area, experiments has to be conducted where the airflow compared to the temperature is plotted.

The evaporator has a problem concerning the available heat transferred from the fuel cell. If the assumption, that the temperature of the outlet is the same as the evaporated temperature, then the available energy transferred from the fuel cell should be sufficient. Even though the assumption is correct, the electric heaters, used in the evaporator, would still be required. In the current system, 200W is used from the electric power generated at the fuel cell.

The amount of excess fuel λ_{H_2} , used in the burner, was estimated to be around 120% in the initial phase. The nonlinear model estimated that this was too low for the reformer to keep its temperature, and λ_{H_2} was changed to about 1.5 which was sufficient. The experiments and the linear model showed that the estimated λ_{H_2} of 1.5 was too low, and the experiment worked only with a λ_{H_2} above 1.75. This experiment was done on a catalyst that had been used in other experiments as [16], and the temperature in those experiments was above the limit of the reformer. This might have caused λ_{H_2} in the experiment to be higher compared to a newer heat exchanger. A newer reformer should be installed and the experiment should be conducted again.

The efficiency of the system is calculated by comparing the input from the fuel to the electrical output. The electrical usage for the blowers and evaporator is subtracted from the fuel cell electrical output. The electric heaters, in the evaporator, is assumed to be about 25% of the electrical output from the fuel cell. A significant way to increase the overall efficiency would be to utilize the excess heat from the burner, and thereby reducing the need for electrical heaters in the evaporator. The calculated efficiency from the model is approximately 18%.

The input fuel, based on the estimator, is one of the main factors when talking about efficiency. As the input fuel for the system is based on the estimator, a good approximation on the hydrogen usage and the reformation hydrogen fraction is crucial. Even though the parameters of the estimator is known, the need for excess fuel might still be necessary, because if the reformer lacks hydrogen, the reformer might decrease in temperature. If the fuel estimator delivers a higher amount of fuel, compared to the necessary amount, the input hydrogen for the burner would increase, and thereby increasing the fan connected to the burner. The system is currently not designed to utilize the excess burner gas, though if the evaporator could utilize the excess heat, the need of electric heaters would be lowered. By removing the electric heaters in the evaporator, would directly inflict on the efficiency, since the heaters is run on electricity from the fuel cell. This is why efficiency is highly dependent on the electric heaters in the evaporator, methanol flow estimation, and temperature of the reformer.

7 Conclusion

Future work

The project presents a good base for control strategies, though some of the work presented in this report must be investigated in the future.

The evaporator shows a dropping temperature when experiments with high fuel flows are performed. Investigations on how much the heat is transferred to the evaporator from the fuel cell exhaust air. If the need for electric heaters in the evaporator is reduced, the use of more controlling applications is needed.

The flow of methanol enters at the side of the evaporator, where the air from the fuel cell has the highest temperature. If the entry of the liquid methanol was presented at the colder side, the methanol vapor would maybe exit the evaporator at a higher temperature.

Some considerations for the reconstruction of the system may be needed, as the need for the cooler was lesser or none. The fittings used in the system also presents large volumes for the flows and this may reduce the amount of heat for fluid passing through the phases.

The startup mode for the system assumes that the system can be heated from burning pure methanol in the burner and the convection can transfer the heat from the burner to the fuel cell stack. This has only been modeled, and a physical experiment needs to be performed. For the methanol can be inserted directly in the burner, the need of two pumps needs to be implemented. One with methanol and one with water.

The control strategies applied to the system was based on a PI-regulator and changing the control strategies might reveal better response. Implementing faster and more reliable blowers for the system might improve the reduce the reformer temperature gradients. Stable temperatures in the reformer might cause the reformat gas to be with higher hydrogen concentrations, though this has to be tested.

Investigations for the estimator in a real system should be applied, since the estimator is only presented in the model. To validate the estimation of the fuel, data for the gas composition and the hydrogen usage in the fuel cell stack must be investigated.

Project Summary

This project investigates the efficiency of a methanol fuelled high temperature PEM fuel cell system. The system is created to run in two operation modes; startup mode and running mode. The purpose of the project is also to investigate a general control approach for the system, using a feedforward approach. The system contains an evaporator unit, a reformer and burner unit and a fuel cell stack. The system is modeled with the start up and a running stage. The start up stage uses pure methanol for the burner and convection is used for heating up the respective components of the system. The nonlinear model simulates the start up and the running stage. In the running stage the reformer unit is heated by burning the excess hydrogen from the fuel cell stack exhaust gas. The system reformer unit uses the endothermic steam reforming process and is heated directly by the burner. To obtain a constant stoichiometry for the hydrogen, in the exhaust gas, an estimator is presented. The estimator shows good theoretical results but has not been tested on a physical system. The feedforward approach is used in the system to feed the reactions happening in both the reformer and fuel cell stack. The electric efficiency for the system is calculated to approximately 18% based on the higher heating value of methanol.

The nonlinear model is converted to a linear model and is used for testing a PI-controller. The investigation of a fuel estimator, based on the current density, has been presented. To obtain a good set of controller parameters, a mathematical parameter search routine is presented in MatLabTM.

Experimental work is presented to obtain knowledge about the hydrogen stoichiometry. The experiments are performed by simulating the fuel cell exhaust using a mass flow controller. The hydrogen needed, for keeping a constant reformer temperature, is found by varying the flow of hydrogen in the burner. The hydrogen stoichiometry is varied, in the nonlinear model, until the model has the same amount of excess hydrogen as shown in the experiments.

Bibliography

- [1] Søren J. Andreasen, Søren K. Kær, and Mads P. Nielsen. Experimental evaluation of a pt-based heat exchanger methanol reformer for a htpem fuel cell stack. *ECS Transactions*, 12(1):571–578, 2008.
- [2] Søren Juhl Andreasen and Søren Knudsen Kær. 400 w high temperature pem fuel cell stack test. *ECS Transactions*, 5(1):197–207, 2007.
- [3] Søren Juhl Andreasen and Søren Knudsen Kær. Modelling and evaluation of heating strategies for high temperature polymer electrolyte membrane fuel cell stacks. *International Journal of Hydrogen Energy*, 33(17):4655 – 4664, 2008.
- [4] BASF. Basf catalyst selectra sp - 60, 2008. Found on CD, “Selectra SP 60, Product Bulletin - Mar 08-2.pdf”.
- [5] CRCnetBASE. *Handbook of Chemistry & Physics*. Taylor and Francis Group, LLC, 89th edition, 2009. ISBN:142006679X.
- [6] Inc. EG&G Services Parsons. *Fuel Cell Handbook*. Science Applications International Corporation, 5th edition, 2000.
- [7] Chao Pan et al. Integration of high temperature pem fuel cells with a methanol reformer. *Journal of Power Sources*, pages 392–398, 2005.
- [8] Ryan O’Hayre et al. *Fuel Cell Fundamentals*. John Wiley and Sons, Inc, 2005. ISBN: 0-471-74148-5.
- [9] Anders R. Korsgaard and Mads Pagh Nielsen, December 2005. Found on CD, PBI_FUEL_CELL_MODEL.EES, Data are fitted to a PEMEAS MEA operated from 160 to 180 [°C].
- [10] Anders R. Korsgaard, Rasmus Refshauge, Mads P. Nielsen, Mads Bang, and Søren K. Kær. Experimental characterization and modeling of commercial polybenzimidazole-based mea performance. *Journal of Power Sources*, 162(1):239 – 245, 2006.
- [11] James Larminie and Andrew Dicks. *Fuel Cell System Explained*. John Wiley and Sons, Inc, 2003. ISBN-13: 978-0-470-84857-9.
- [12] Mads Pagh Nielsen. Regressions for boiling temperatures of mixed fuel based on [5] and [14]. Research based on [5] and [14].
- [13] K. Ogata. *Modern Control Engineering*. Prentice Hall, 4. edition, 2001. ISBN: 0-13-043245-8.
- [14] R.H. Perry and D.W. (Editors) Green. *Perry’s Chemical Engineers’ Handbook*. McGraw-Hill, 2007. ISBN:0-07-142294-3.

- [15] P. L. Rasmussen. *Investigation of Lifetime Issues in HTPEM Fuel Cell Based CHP Systems: Stack Level Degradation*. AAU, 1. edition, 2008. HyTec 10th semester Master Thesis.
- [16] Søren J. Andreasen, Søren K. Kær, and Mads P. Nielsen. Experimental evaluation of a pt-based heat exchanger methanol reformer for a htpem fuel cell stack. *ECS Transactions*, 12(1):571–578, 2008.
- [17] R. H. Turner Y. A. Cengel. *Fundamentals of thermal-fluid science*. McGraw Hill, 2 edition, 2005. ISBN: 007-123926-x.

Experiments

A

A.1 Description of system

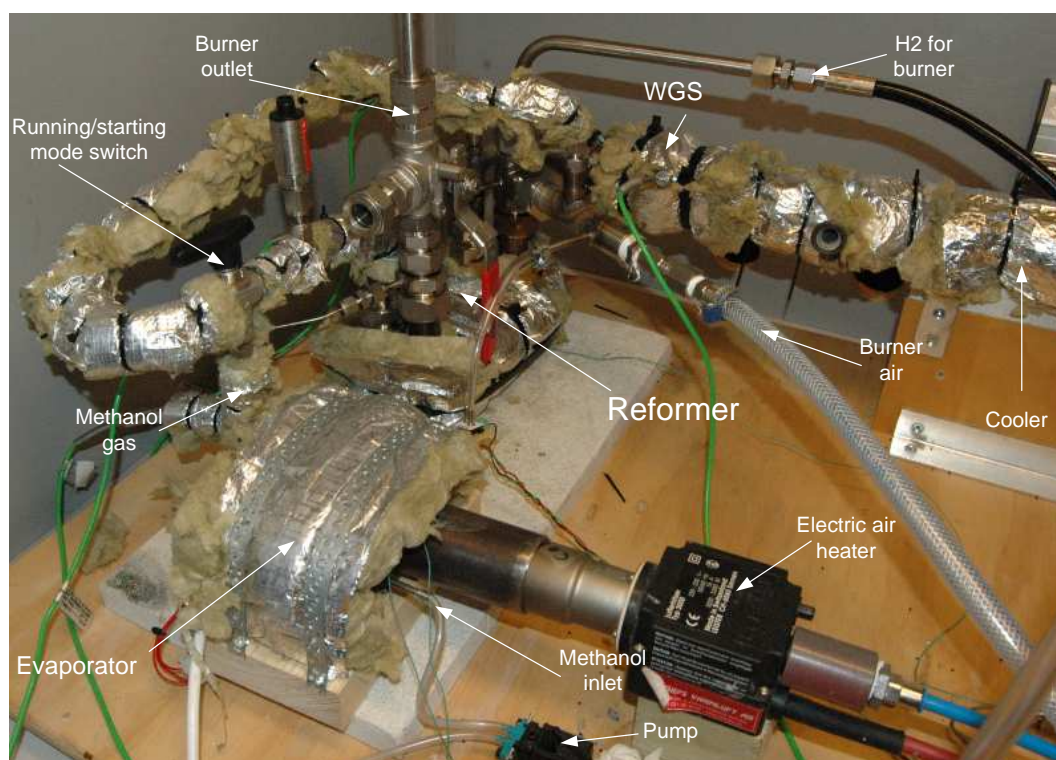


Figure A.1: *System overview*

Figure A.1 is a general overview of the system. From below, a mixture of methanol and water is pumped into the evaporator. The exit gas is sent either into the reformer, or into the burner. This is done by changing the state of the running/startup switch. The outlet of the reformer can be noticed on the far side of the reformer, where the reformatted gas is directed into the WGS container.

The MFC is of the type Bürkert 8626 and has an analog input reference at 0-10V. The installed MFC's in the system is a 100 l/min , 200 l/min and a 1300 l/min , where the burner, evaporator and cooler is installed respectively.

As shown in figure A.1 the WGS is isolated. Before isolation a thermal image was taken of the WGS. This can be seen from figure A.2(a) and figure A.2(b).

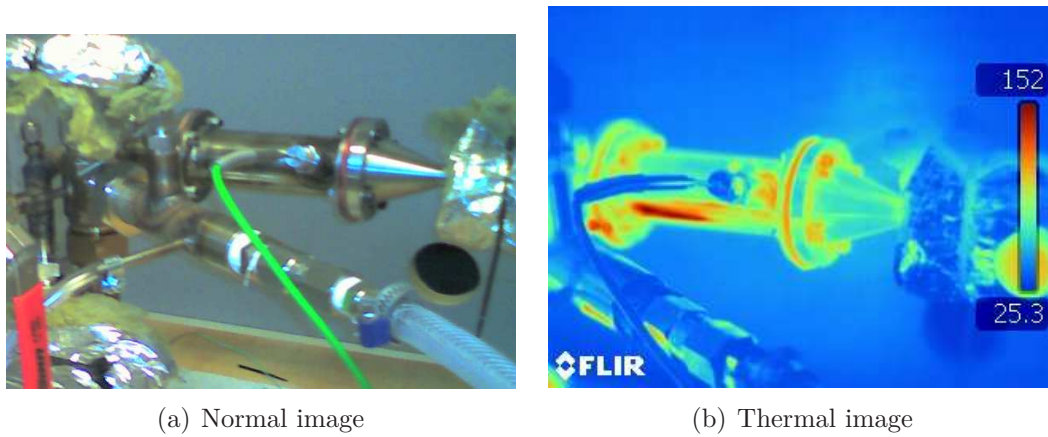


Figure A.2: *WGS container*

Temperatures are measured to about 150 °C at the inlet.

A thermal image was taken of the reformer and this can be seen from figure A.3(b).

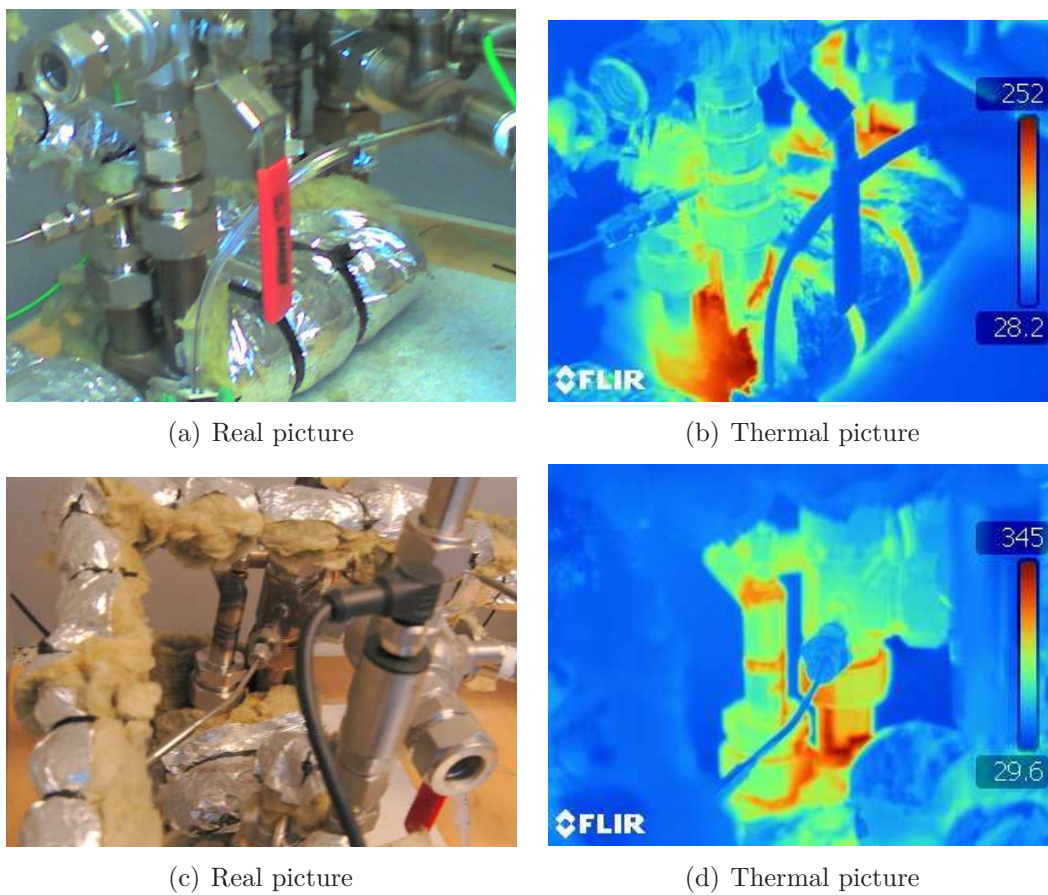


Figure A.3: *Reformer images*

As shown in figure A.1 there is added isolation at the ends of the reformer.

A.2 Experiments with reformer

A.2.1 Experimental setup

Figure A.4 is a drawing of the Reformer burner seen from above.

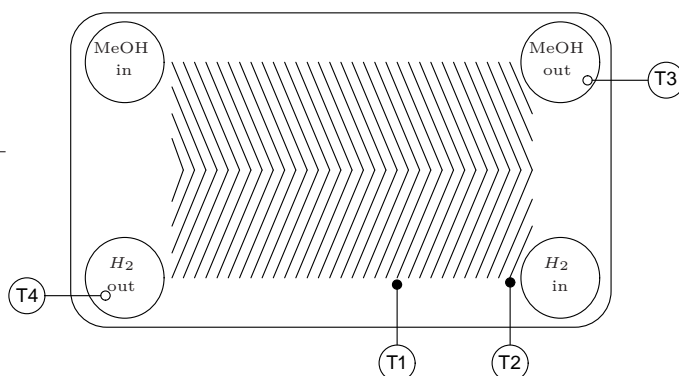


Figure A.4: Placement of temperature sensors “Burner Temperature 1” and “Burner Temperature 2”

In figure A.4 the placement of the different temperatures sensors can be seen. The temperature sensors used is a K type sensor, and is attached with a high temperature resistant glue. “Burner Temperature 1” is shown as “T1”, “Burner Temperature 2” is “T2”, “Reformer outlet temperature” is “T3” and “Burner gas outlet temperature” is “T4”.

A.2.2 Startup and shutdown of reformer

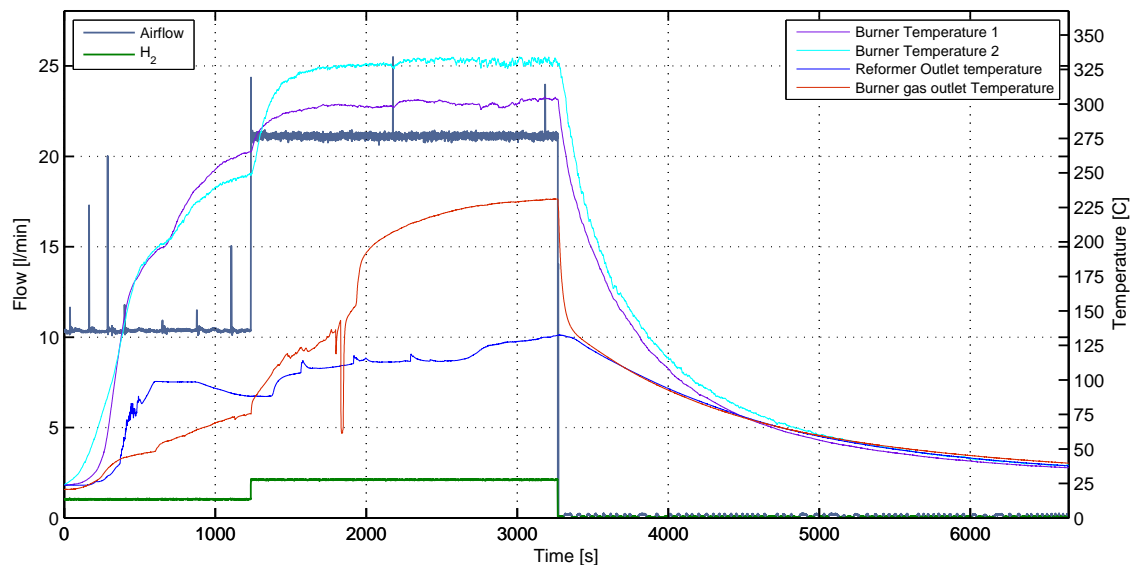


Figure A.5: Startup and shutdown of reformer. Starting up with 1 l/min H_2 and a airflow of 10 times the H_2 flow. This experiment is without an isolating cover hence the lower temperatures of the burner

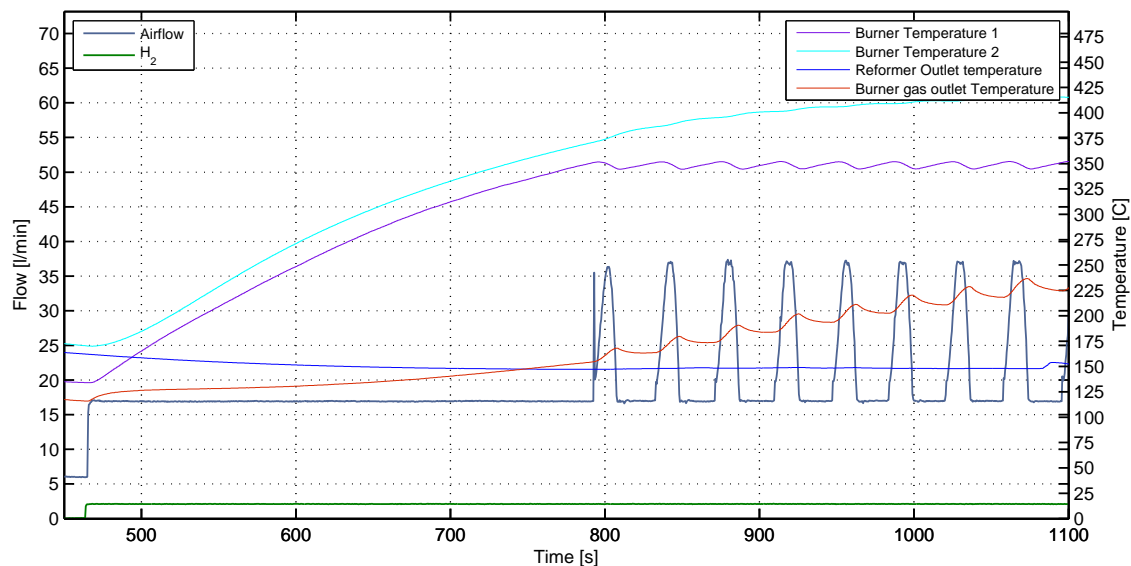


Figure A.6: Startup from $150^{\circ}C$

A.2.3 Controlling temperature of reformer

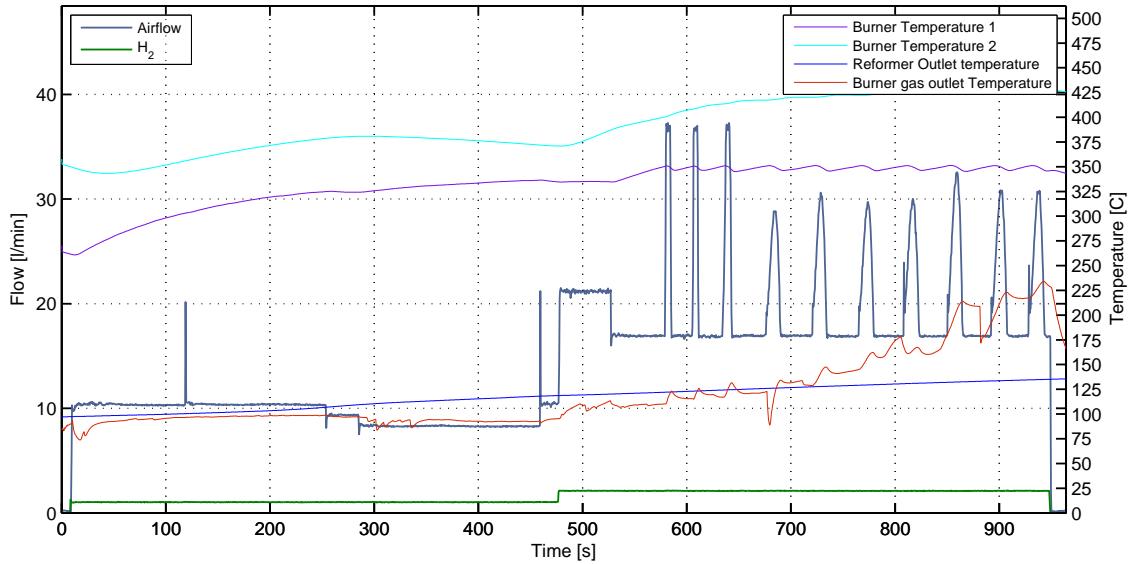
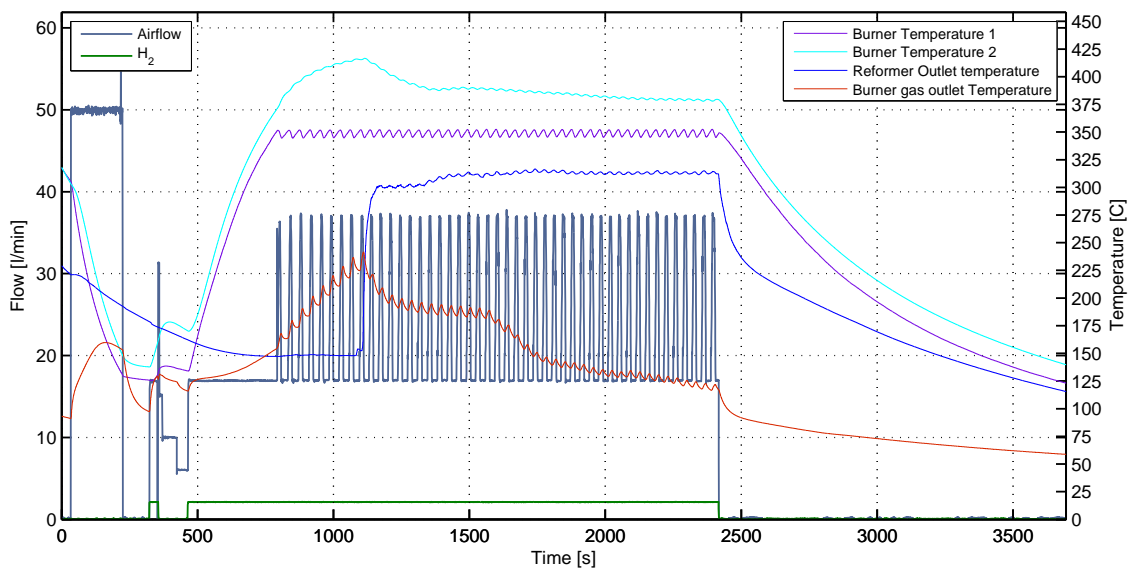


Figure A.7: Controlling temperature with a feed forward and PI regulator



A.2.4 Experiment with a change in methanol flow to determine the lag

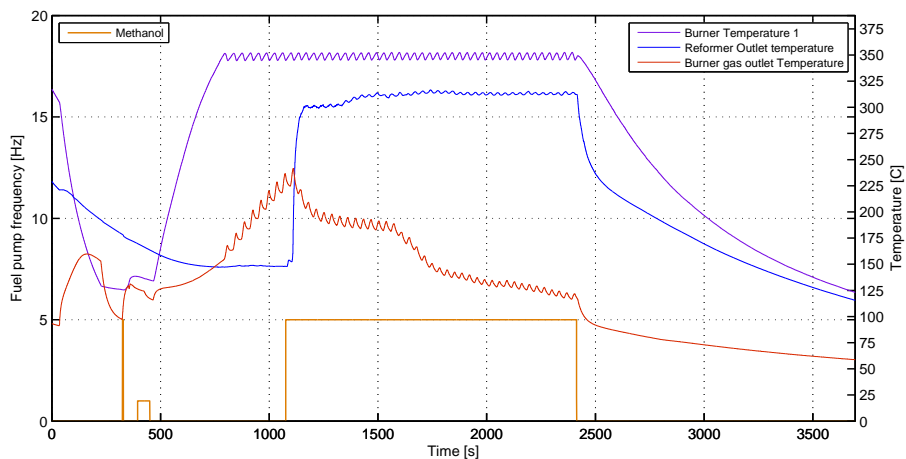


Figure A.8: Phase lag experiment 1

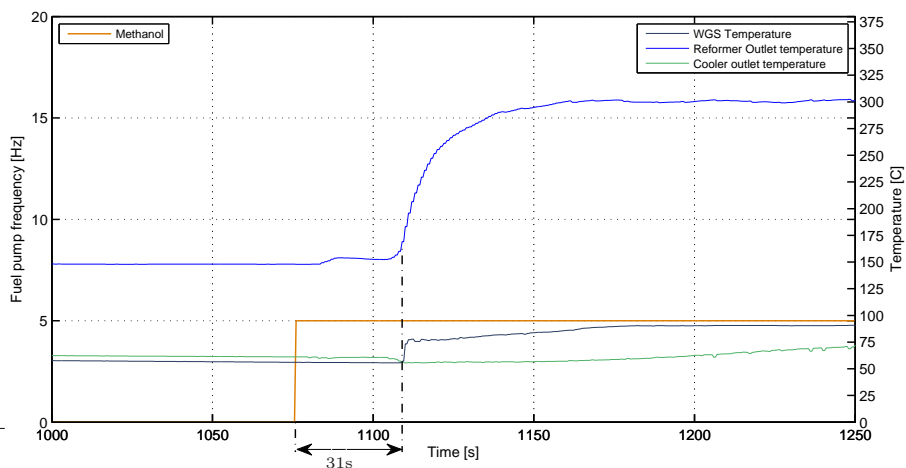


Figure A.9: Influence in temperature at the reformer gas exhaust when the pump frequency changes from 0 to 10 Hz. Zoomed in at the frequency change from 1000s to 1250s (see figure A.8)

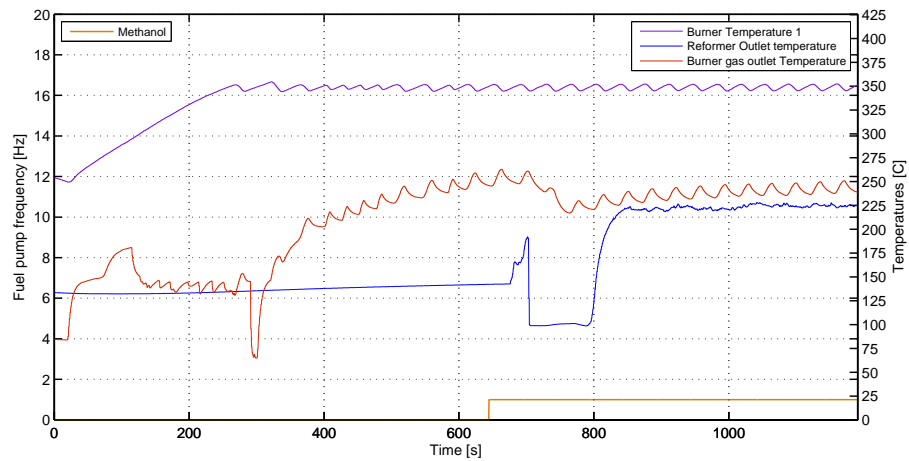


Figure A.10: Phase lag experiment 2

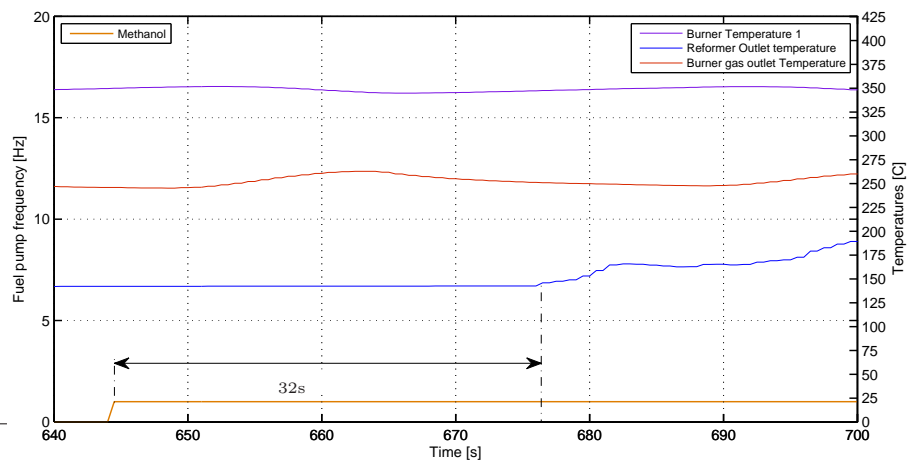


Figure A.11: Influence in temperature at the reformer gas exhaust when the pump frequency changes from 0 to 1 Hz. Zoomed in at the frequency change from 640s to 700s (see figure A.10)

A.2.5 Determine the lowest amount of hydrogen needed at maximum pump frequency

First experiment

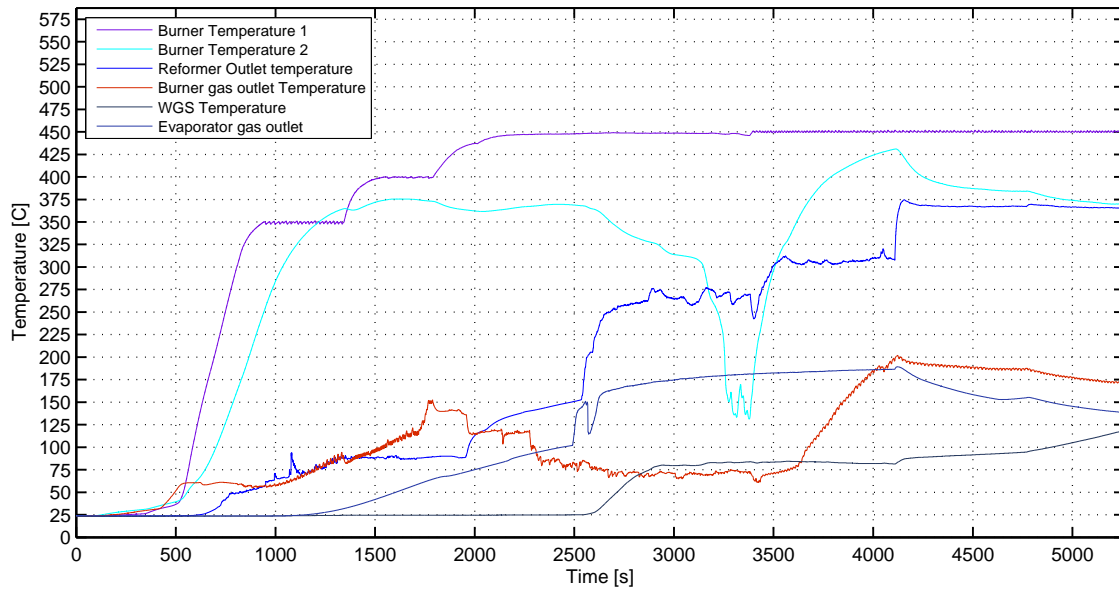


Figure A.12: *First experiment*

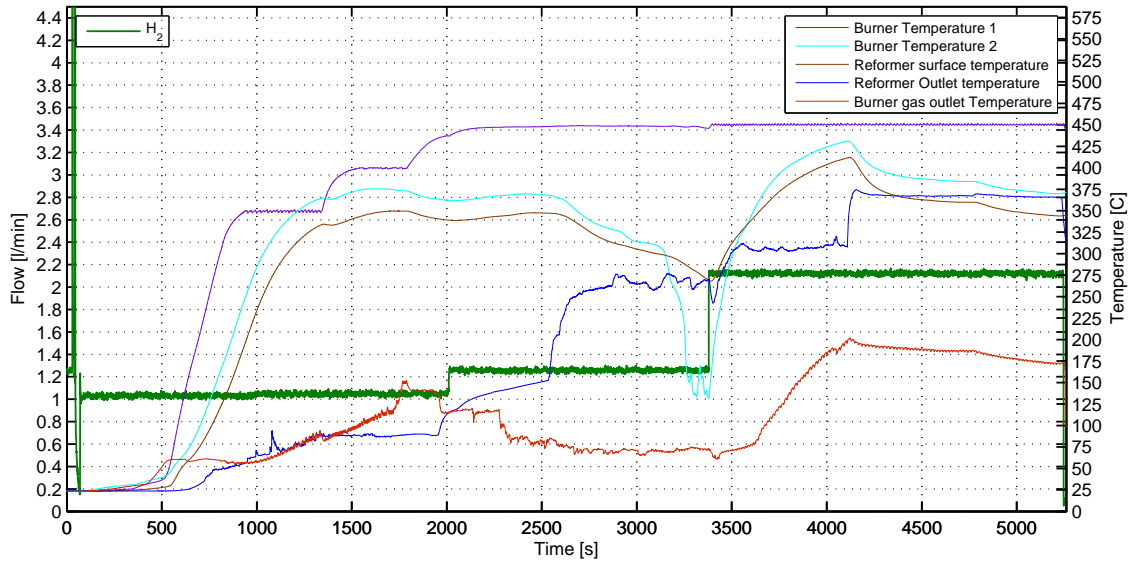


Figure A.13: First experiment

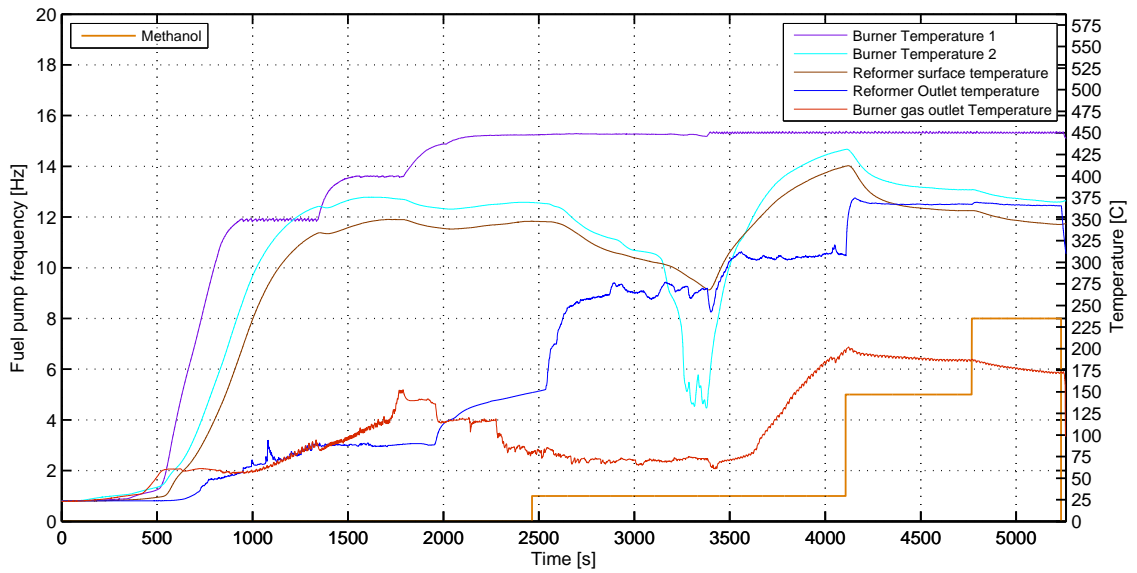


Figure A.14: First experiment

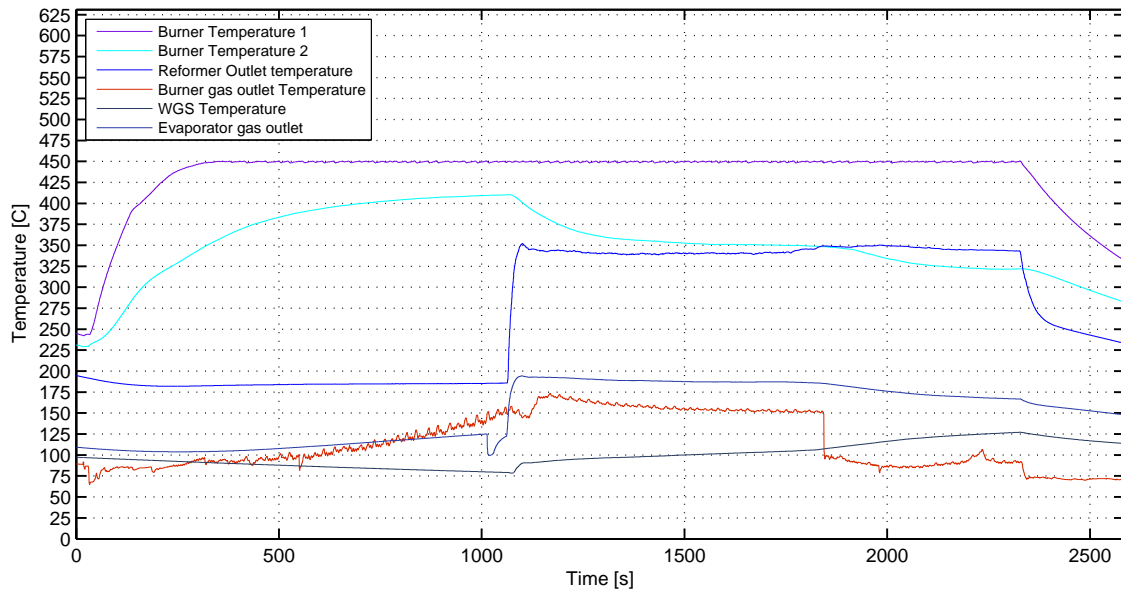


Figure A.15: *Second experiment*

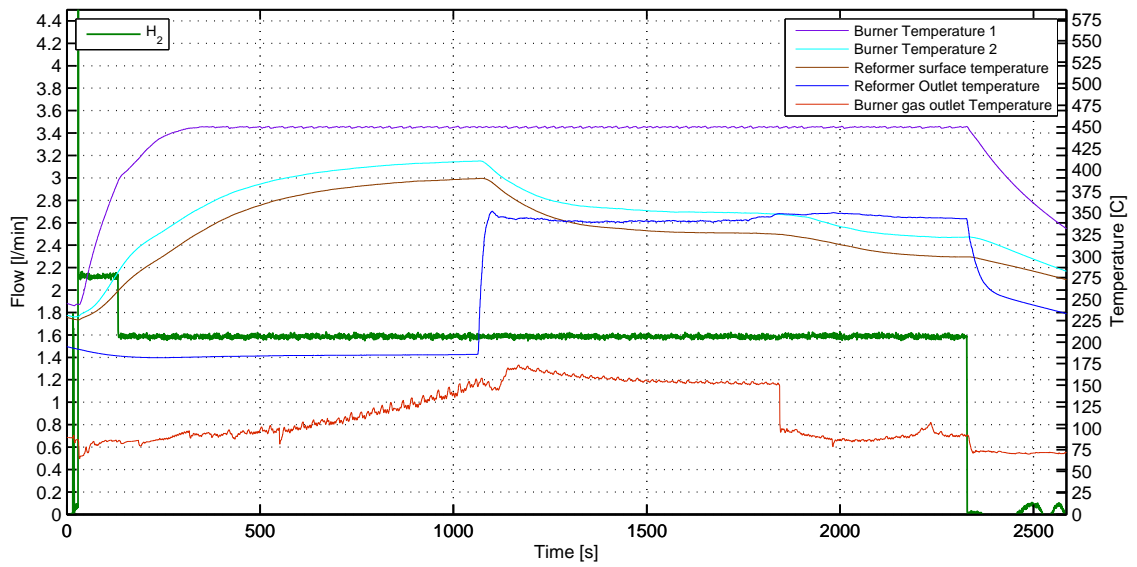


Figure A.16: *Second experiment*

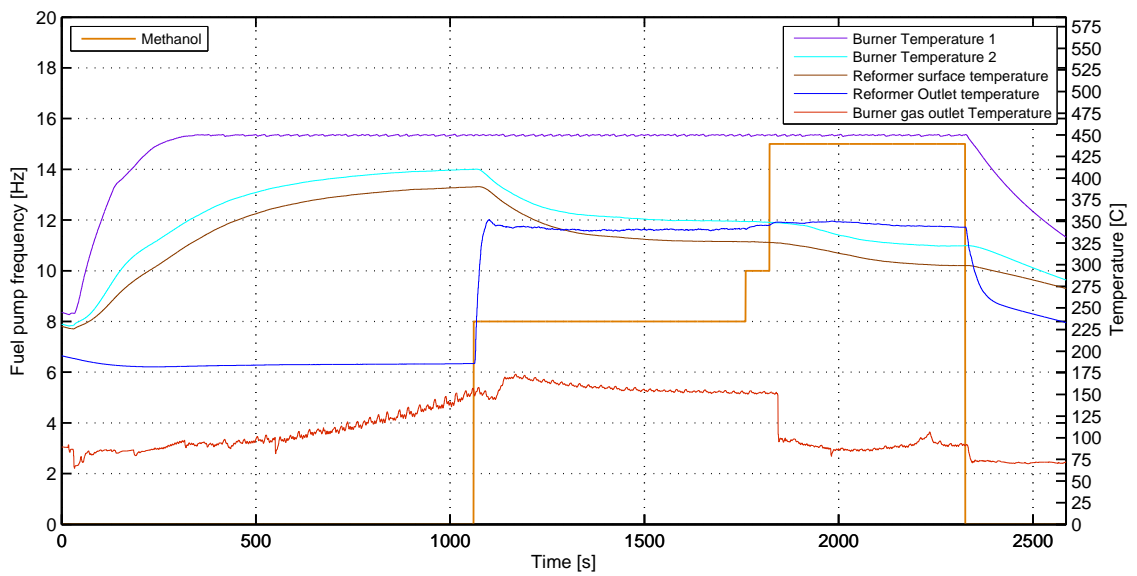


Figure A.17: *Second experiment*

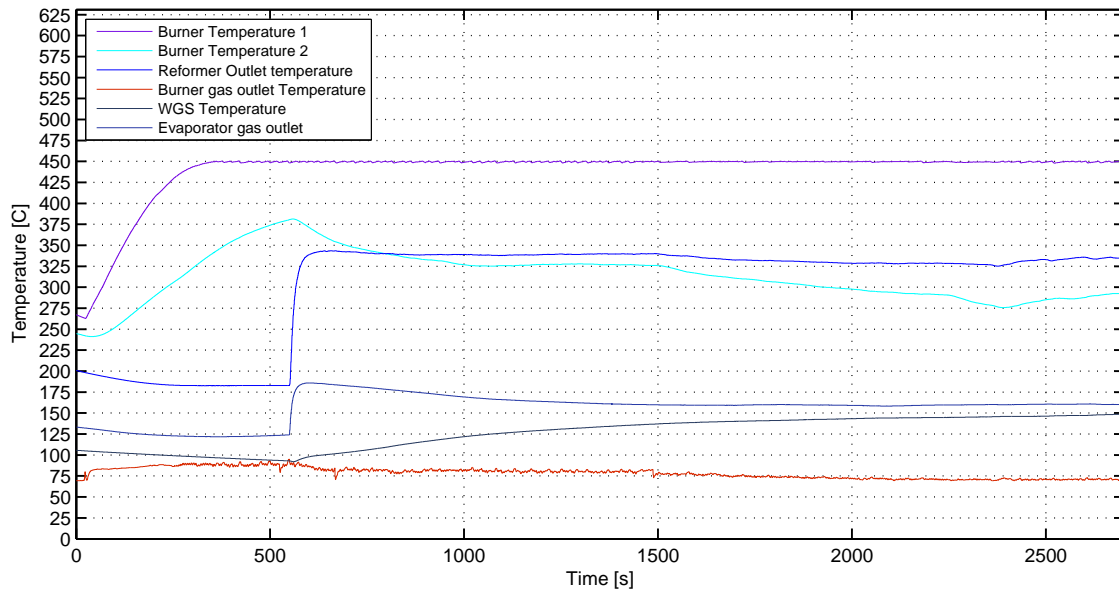


Figure A.18: *Third experiment*

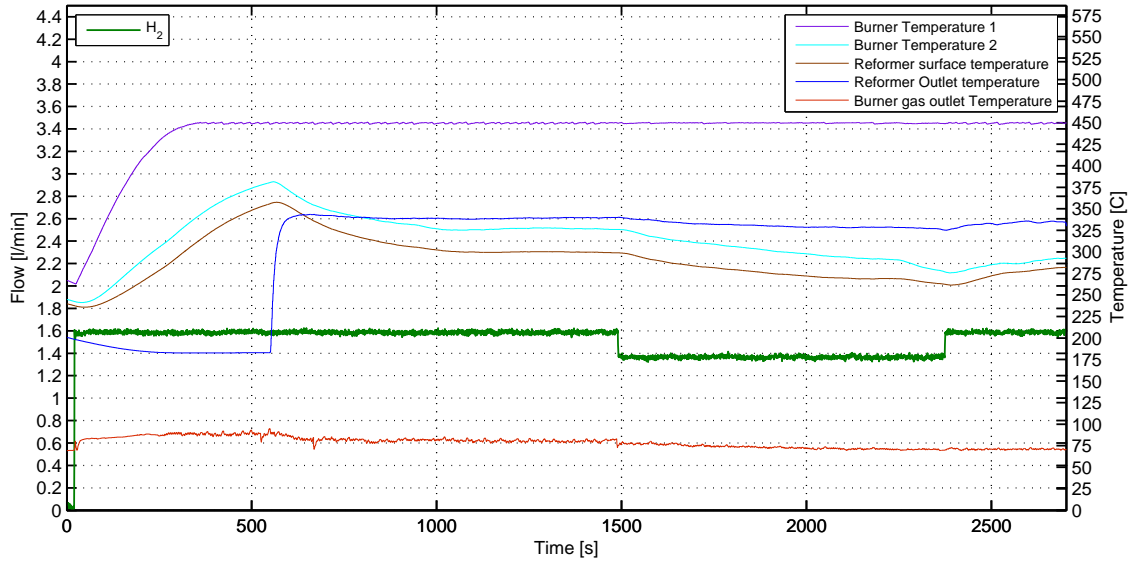


Figure A.19: *Third experiment*

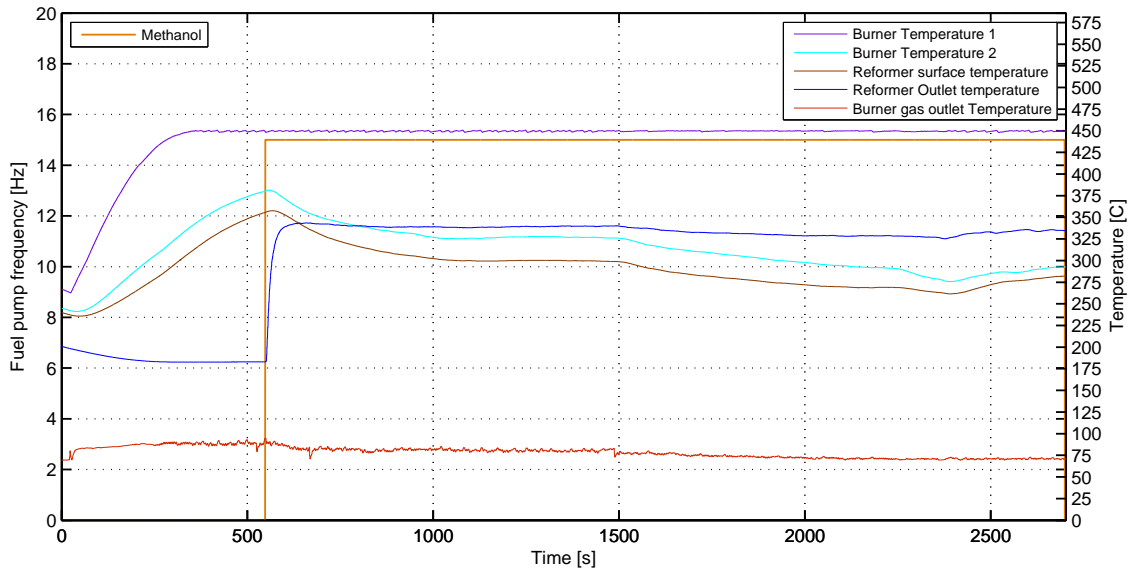


Figure A.20: *Third experiment*

A.3 Experiment with cooler

This experiment shows the characteristics of the heatexchange which is used as cooler in the overall system. The experimental setup can be seen in figure A.21

The purpose of the heatexchanger is to be able to cool the H_2 at $300\text{ }^\circ\text{C}$ to about $180\text{ }^\circ\text{C}$. This is done by a counterflow of air at about $20\text{ }^\circ\text{C}$ with a flow from 0 to 400 l/min . This can be seen in figure A.22.



Figure A.21: *The setup of the cooler test*

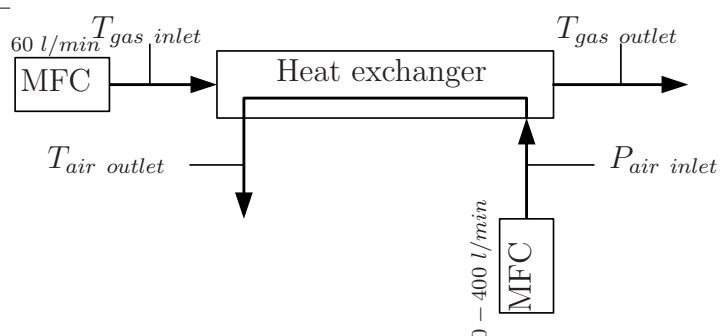


Figure A.22: *Drawing of heatexchanger*

The size of the cooler is highly over dimensioned, though the main goal of the cooler is to ensure the safety of the fuel cell, so a temperature above the fuel cell can be avoided. A blower can be installed by comparing the pressure at a given flow. This can be seen in figure A.23

The temperature of the heat exchanger is fully able to keep a stable temperature at 180 [°C] at about 80 [l/min], though a more suitable cooler should be found because of the high conduction of this heat exchanger.

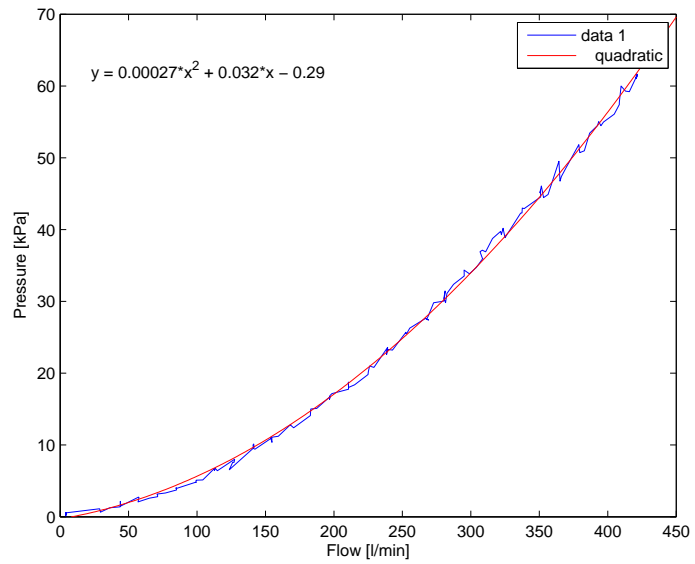


Figure A.23: *Pressure - Flow Characteristic*

Description of model

B

B.1 Constants

The constants of the ulinear Simulink Model has been presented here.

$C_{cells} = 65$	$E_{bfh} = 47904$
$C_{cell_{area}} = 45.16 [cm^2]$	$E_{kec} = 196829$
$Electric_{power} = 1000 [W]$	$E_{keh} = 34777$
$U_{rev} = 1.2 [V]$	$E_{kfc} = 19045$
$u_{ocv} = 0.95 [V]$	$E_{kfh} = 1.899e5$
$Lambda_{air} = 2.5 [-]$	$k_{cond} = 0.03$
$T_{amb} = 293.15 [K]$	$A_1 = 0.0035$
$T_{limit} = 433.15 [K]$	$A_2 = 0.0027$
$T_{start} = 293.15 [K]$	$A_3 = 0.0099$
$p_{amb} = 1.013 [bar]$	$A_4 = 0.0036$
$SC_{ratio} = 1.5 [-]$	$A_5 = 0.0134$
$D_{hyd} = 0.001$	$A_{stack} = 0.023$
$k_{channel} = 0.003343$	$x_1 = 0.02$
$m_s = 2.8$	$x_2 = 0.03$
$c_s = 970 \left[\frac{J}{kg \cdot K} \right]$	$k_{reactor} = 0.000043$
$R = 8.314 \left[\frac{kJ}{kmol \cdot K} \right]$	$A_{reactor,total} = 0.04467$
$F = 96485$	$H_{wgs} = -41.1$
$alfa_{anod} = 0.5 [-]$	$H_{sr} = 49.4$
$k_{ha1} = 2.3$	$m_{reformer} = 1.5$
$k_{ha2} = 2.2571e - 2$	$c_{reformer} = 0.9$
$k_{ha3} = -1.4286e - 5$	$m_{heater} = 0.5$
$k_{ny1} = -1 * (0.000004079)$	$cp_{alu} = 0.9458$
$k_{ny2} = 3.9763e - 8$	$a_1 = -0.000166667$
$k_{ny3} = 9.0515e - 11$	$b_1 = 0.228858333$
Desorption	$a_2 = 4.641e - 2$
$b_{fc} = 8.817e12$	$b_2 = 6.143e3$
$b_{fh} = 2.038e6$	$a_3 = 0.000820312455$
Electro Oxidation	$b_3 = 0.430604326$
$k_{ec} = 3.267e18$	$a_{30} = 4.3e - 1$
$k_{eh} = 25607$	$b_{30} = 2.72e - 2$
Adsorption	$k1_{reg} = 40.08912844923$
$k_{fc} = 94.08$	$k2_{reg} = 2.5706646294883$
$k_{fh} = 2.743e24$	$k3_{reg} = 18.357126208929$
$E_{bfc} = 127513$	$k4_{reg} = 4.2845217013023$

B.2 Simulink model

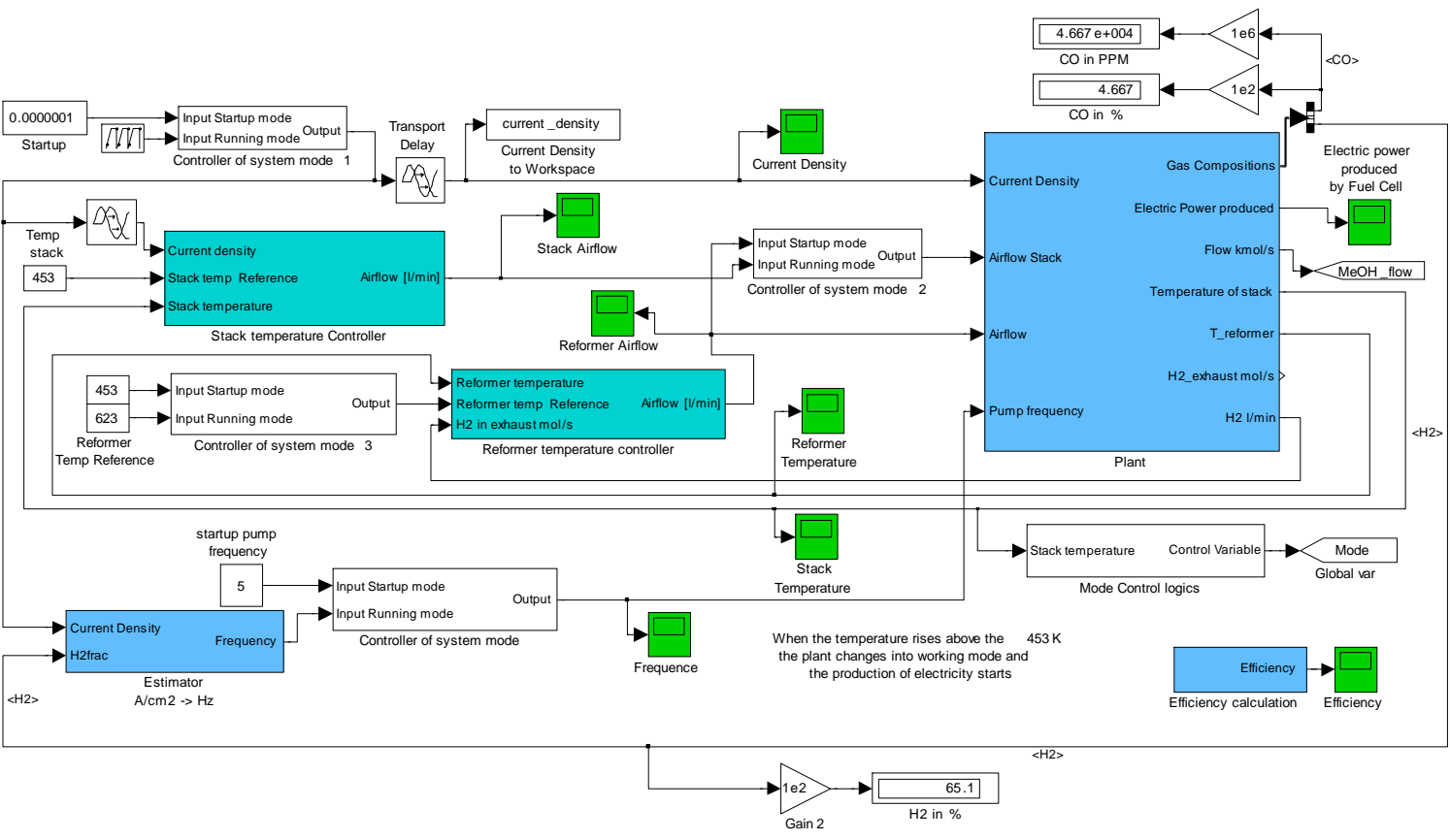


Figure B.1: Fuel Cell Model system

The main part of the model is presented in figure B.1. It consists of controllers and a plant. The input is the current density and is varying over time. This can be seen in figure B.2(a).

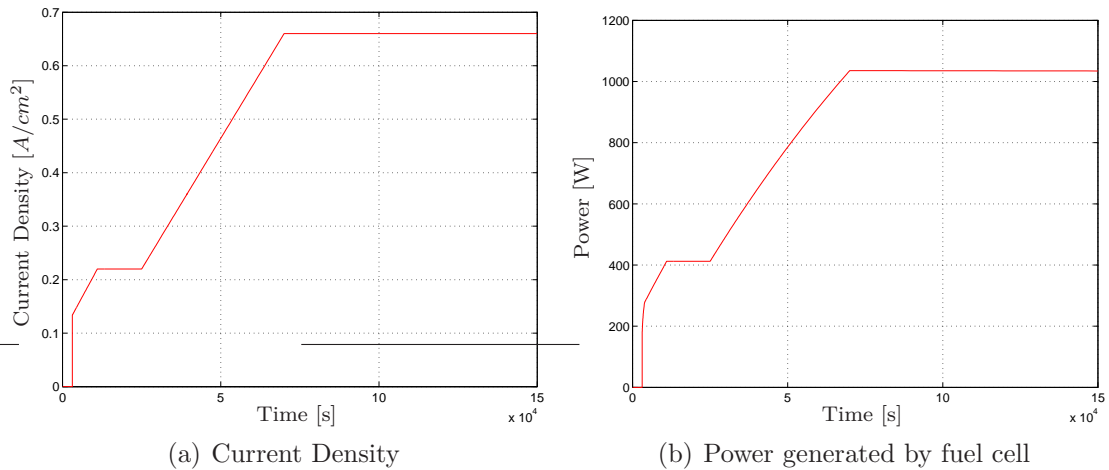


Figure B.2: *Current density and Power generated by fuel cell*

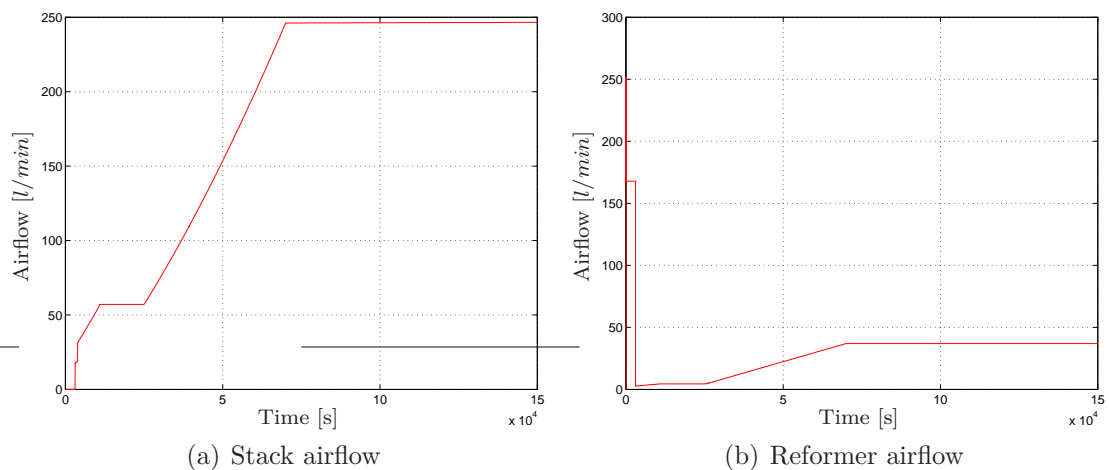


Figure B.3: *Airflow for stack and reformer respectively*

The current density is input for the plant, temperature controller and the estimator. The current density is delayed by 30 seconds for the inputs for the fuel cell and controller because of the delay there is between the flow change in the pump and the gas reaches the fuel cell. The estimated power output from the cell can be seen in figure B.2(b)

The airflow created from the input from the controllers can be seen in figure B.3(a) and figure B.3(b).

The temperature of the reformer and fuel cell stack can be seen in figure B.4(a) and figure B.4(b). The frequency of the fuel pump can be seen in section figure B.5(a) and the electric efficiency of the system can be seen in figure B.5(b).

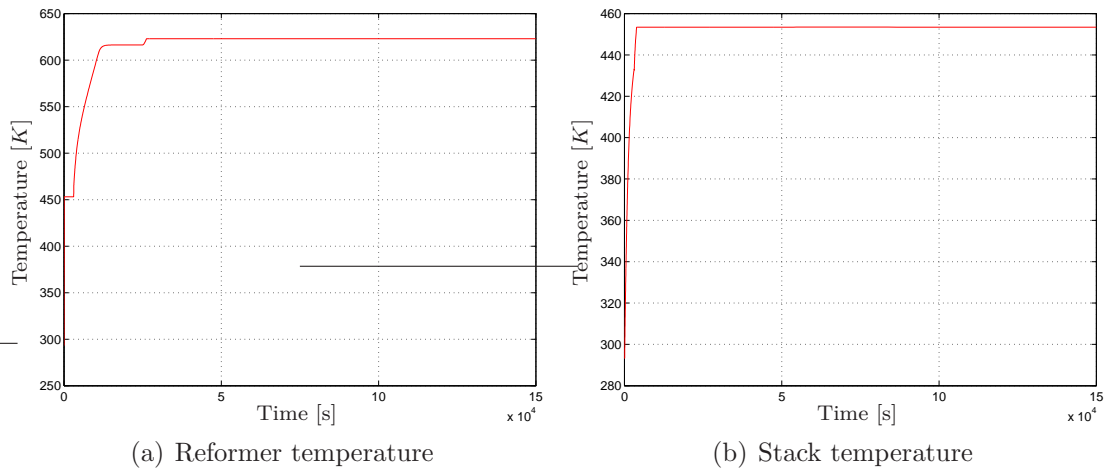


Figure B.4: *Temperature of the controlled parts of the system*

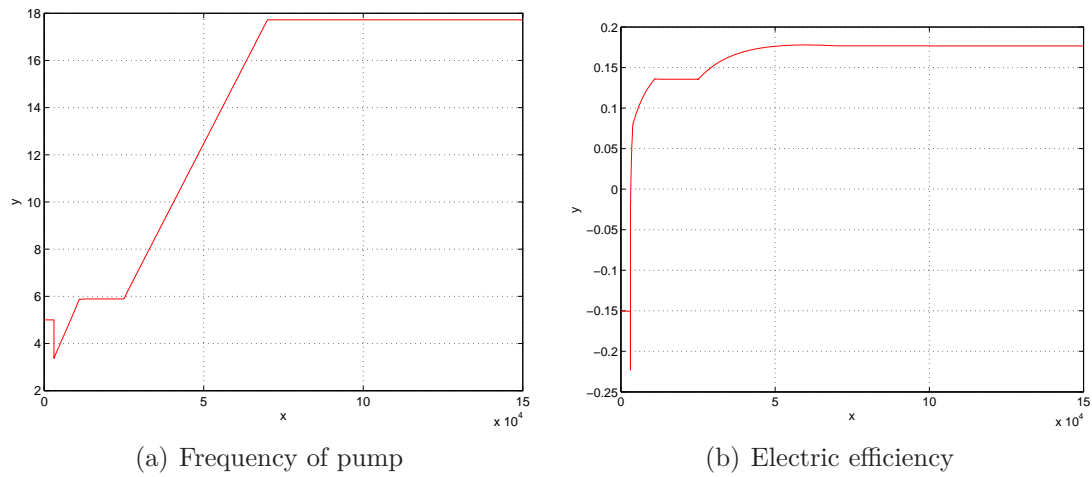


Figure B.5: *Electric efficiency and fuel pump frequency*

The plant in the model consists of a reformer/burner, evaporator and fuel cell as shown in figure B.6. The reformer is explained in more detail in B.3.

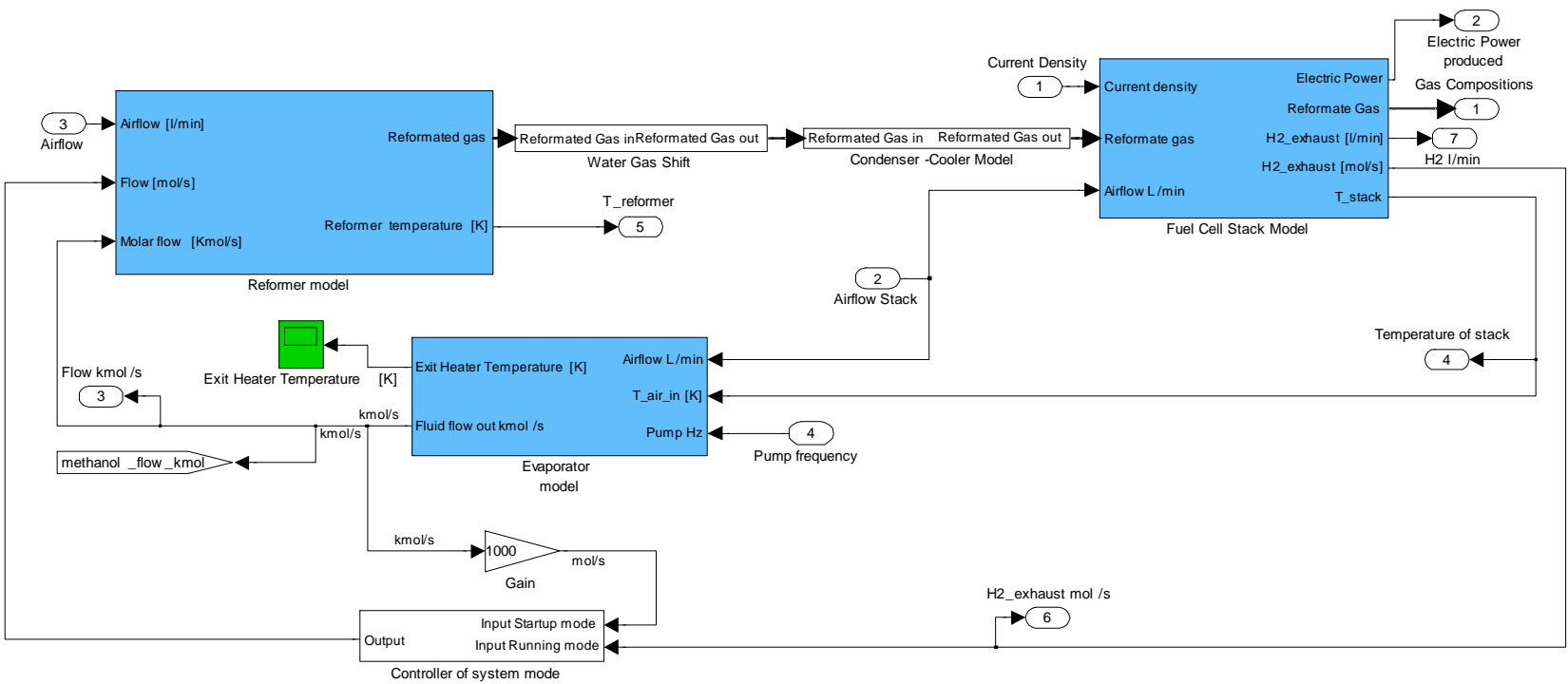


Figure B.6: Fuel Cell Model

B.3 Reformer model

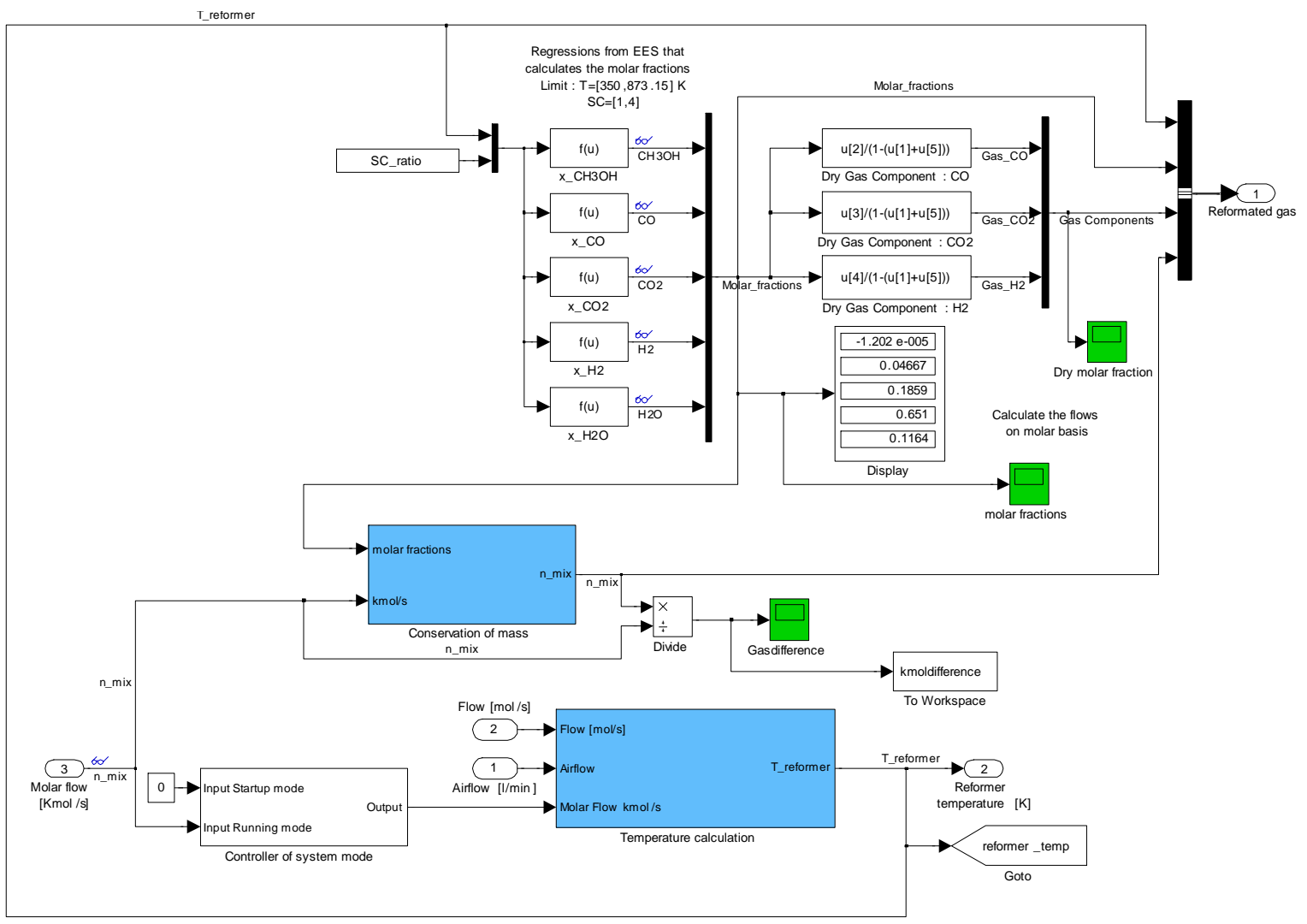


Figure B.7: Reformer Model

The reformer model consists of two parts. The first part calculates the reformatted gas fractions, and the second part calculates the temperature of the reformer. As the molar flow of the methanol and the reformatted gas is not the same, the model calculates the reformatted gas by applying the rules of conservation of mass. This can be seen in more detail in figure B.10

B.3.1 Calculation of molar fractions

Regressions are calculated by EES and can be seen in figure B.8. The regressions depend on the temperature and the SC ratio of the fuel. As the SC ratio is constant it can be displayed as a function of temperature.

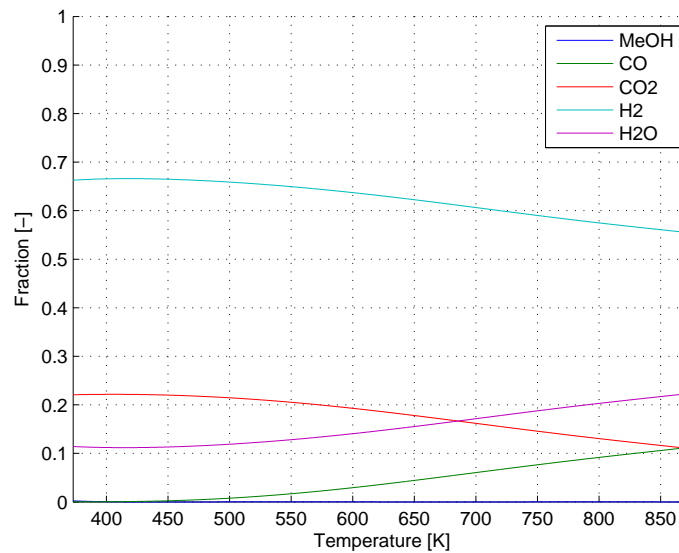


Figure B.8: Gas fractions at a SC ratio of 1.5

The calculation of the gas fractions can be seen in Gas_fractions_plot.m on the CD.

The model calculates both the molar fractions and the dry molar fractions, and this can be seen in figure B.9(a) and figure B.9(b).

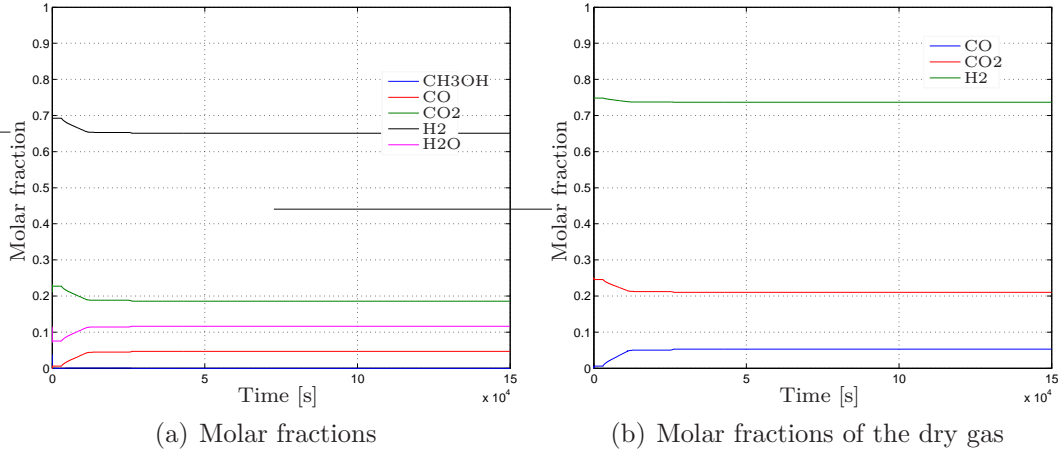


Figure B.9: Molar fractions from model

B.3.2 Calculation of reformer temperature

Contributions

- Heat is added by burning hydrogen
- WGS heat contributions are neglected ($\text{CO} + \text{H}_2\text{O} \rightarrow \text{CO}_2 + \text{H}_2$)

Losses

- Steam-reforming ($\text{CH}_3\text{OH} + \text{H}_2\text{O} \rightarrow \text{H}_2 + \text{CO} + \text{CO}_2$)
- Heat loss from conduction

The power balance is calculated from the total amount of power that is in the reformer.

Temperature change based on \dot{Q}

$$T = \frac{1}{m \cdot c} \int \dot{Q} dt \quad (\text{B.1})$$

Conduction

$$\dot{Q} = k \cdot A \cdot (T_{\text{surface}} - T_{\text{amb}}) \quad (\text{B.2})$$

Convection

$$\dot{Q} = \dot{n}(H_{\text{out}} - H_{\text{in}}) \quad (\text{B.3})$$

Assumptions:

The weight of the reformer is assumed to be about 1.5kg aluminum and the specific heat transfer is based on this. It is assumed that the temperature throughout the reformer is the same. The temperature at startup is set to 180 [°C] to avoid the fuel cell will take any damage. The molar fractions is only dependent on the reformer temperature because of the SC-ratio is constant.

B.3.3 Calculation of the molar flow out of reformer

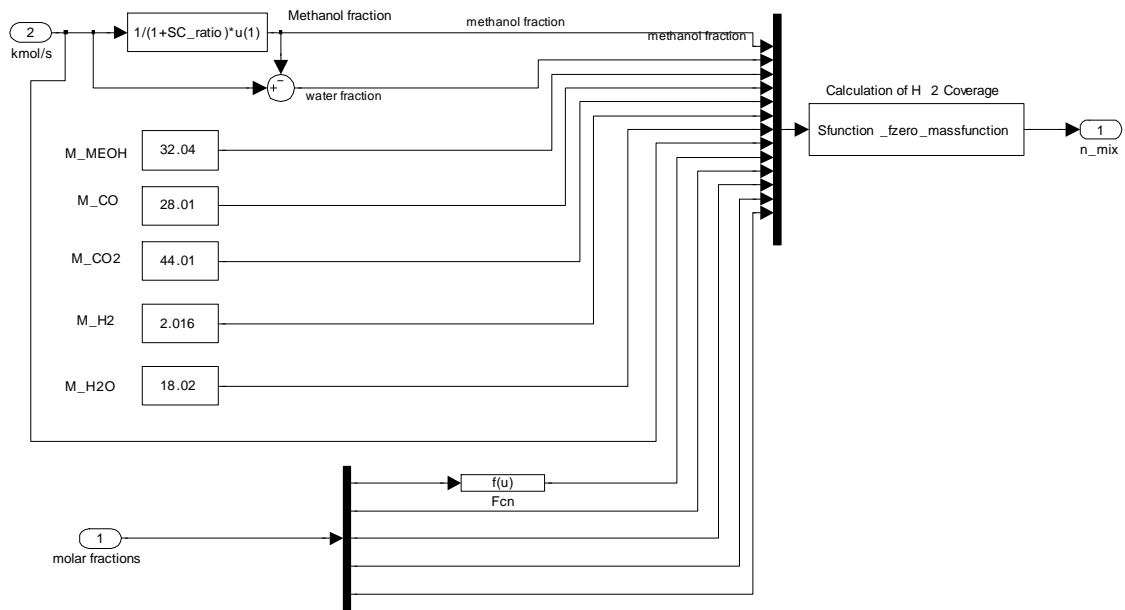


Figure B.10: Calculation of molar flow before and after reformation

Because the reformation reaction processes methanol, the molar flow is different. The rate of which the output flow is calculated by applying the rules of conservation of mass. This equation is the central equation in the Sfunction_fzero_massfunction block seen in figure B.11.

$$\begin{aligned}
 \dot{n}_{MeOH} \cdot M_{MeOH} + \dot{n}_{H_2O} \cdot M_{H_2O} &= x_{MeOH} \cdot M_{Meoh} \cdot \dot{n}_{gas} \\
 &+ x_{CO} \cdot M_{CO} \cdot \dot{n}_{gas} + x_{CO_2} \cdot M_{CO_2} \cdot \dot{n}_{gas} + \\
 &x_{H_2} \cdot M_{H_2} \cdot \dot{n}_{gas} + x_{H_2O} \cdot M_{H_2O} \cdot \dot{n}_{gas}
 \end{aligned} \tag{B.4}$$

The input for (B.4) is the molar flows of methanol and water. This is equal to the sum of all molar flows of the reformatted gas. The plot shown in figure B.11 is a calculation from the model that shows the ratio of the output flow compared to the input flow. This ratio is used in the estimator.

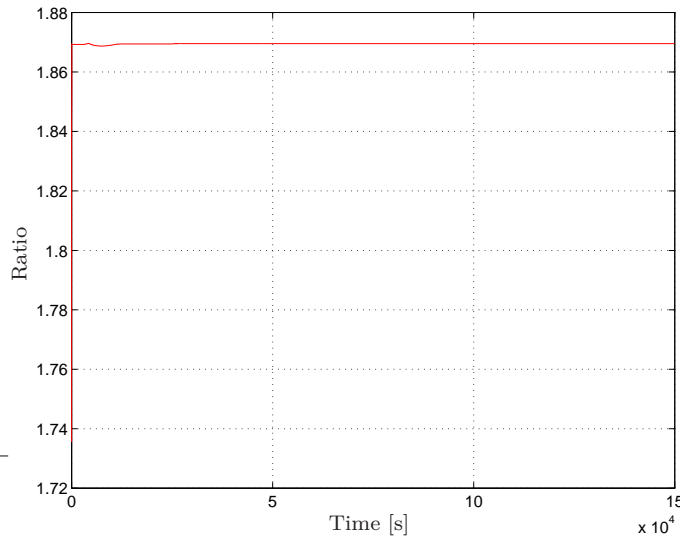


Figure B.11: *Reformer flow rate compared before and after reformation*

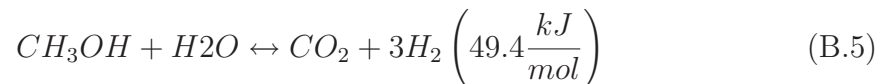
B.3.4 Reformer temperature

The model shown in figure B.13 describes the different heating contributions to the reformer. It involves four different heating models; Burning hydrogen, steam-reforming, convection and conduction.

Burning gas in the reformer is shown in figure B.14. It depends on the mode of the system, which selects if the gas is methanol or hydrogen. The “heat of combustion” (kJ/mol) is selected for both gases and is multiplied with the flow (mol/s).

The convection in the reformer is shown in figure B.15. The convection is calculated by the difference in enthalpy multiplied with the molar flow of the air. The enthalpy is calculated from the air at ambient temperature and from the temperature of the reformer.

The steam reforming process is calculated by the enthalpy of the reaction multiplied with the molar flow (mol/s)



The conduction is calculated by a heat transfer coefficient multiplied with the total areal of the reformer. This heat transfer coefficient was calculated from the fact that there is a 1cm rockwool, though later experiments show that the coefficient was about 6.5 times higher. All this is multiplied with the temperature difference from ambient temperature to the reformer temperature, and this gives the heat transfer from convection. This model is based on the fact that there is no forced convection,

though the reformer was placed in a very ventilated room, so the coefficient needs to be verified again when the system is taken in use. The model also assumes that the reformer is totally isolated, though the area of the fittings and tubes are not, so the estimated conduction is expected to be lower than the real conduction.

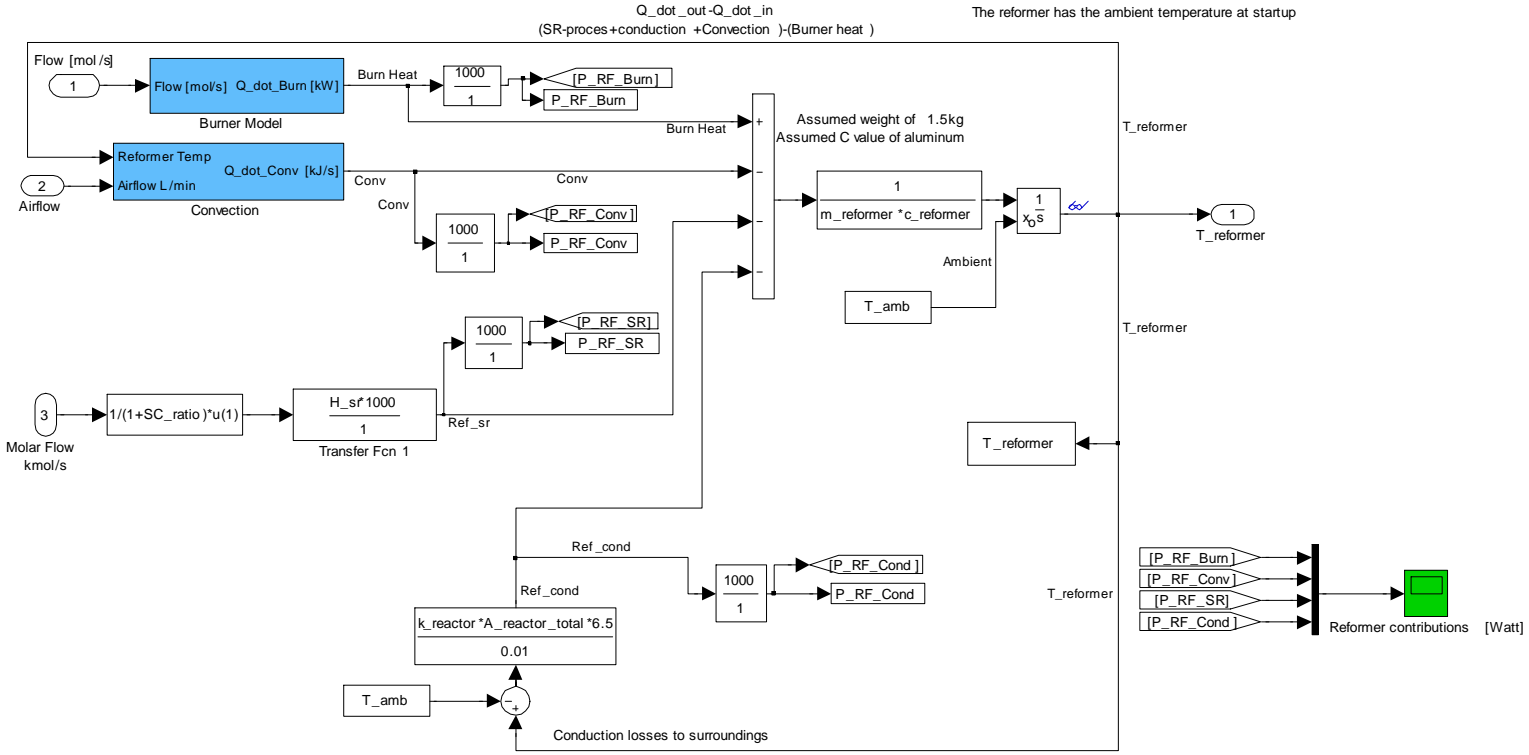


Figure B.12: Reformer temperature model

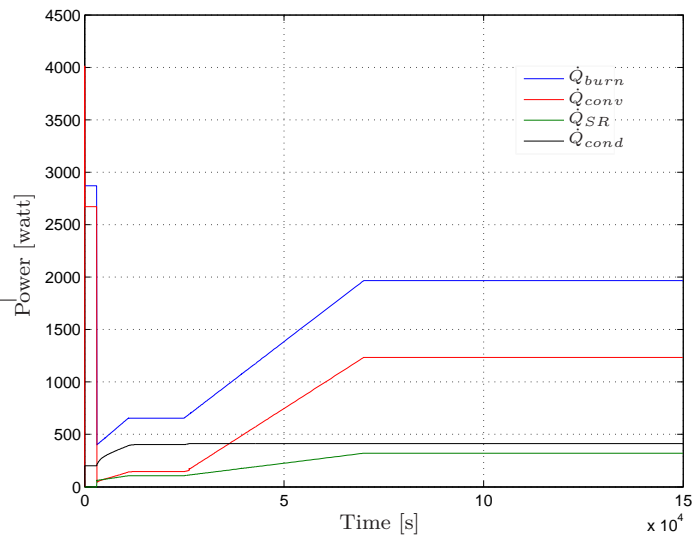


Figure B.13: Different heating contributions to reformer temperature [watt]

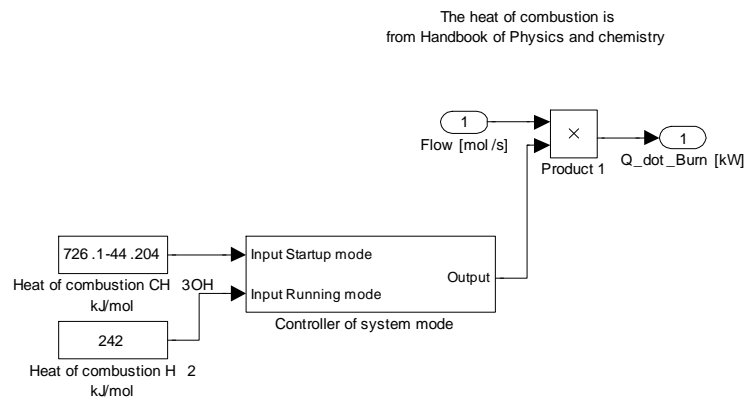


Figure B.14: Burning gas in reformer

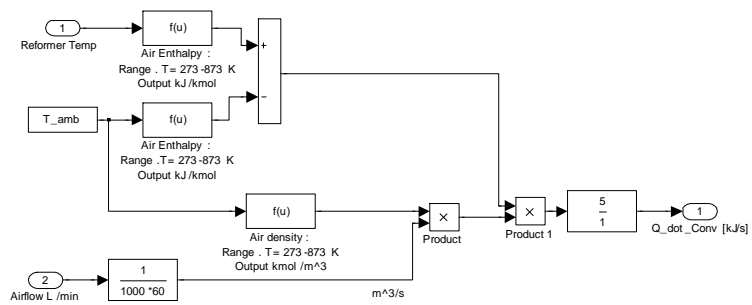


Figure B.15: Reformer temperature calculation - Convection

B.4 Fuel Cell

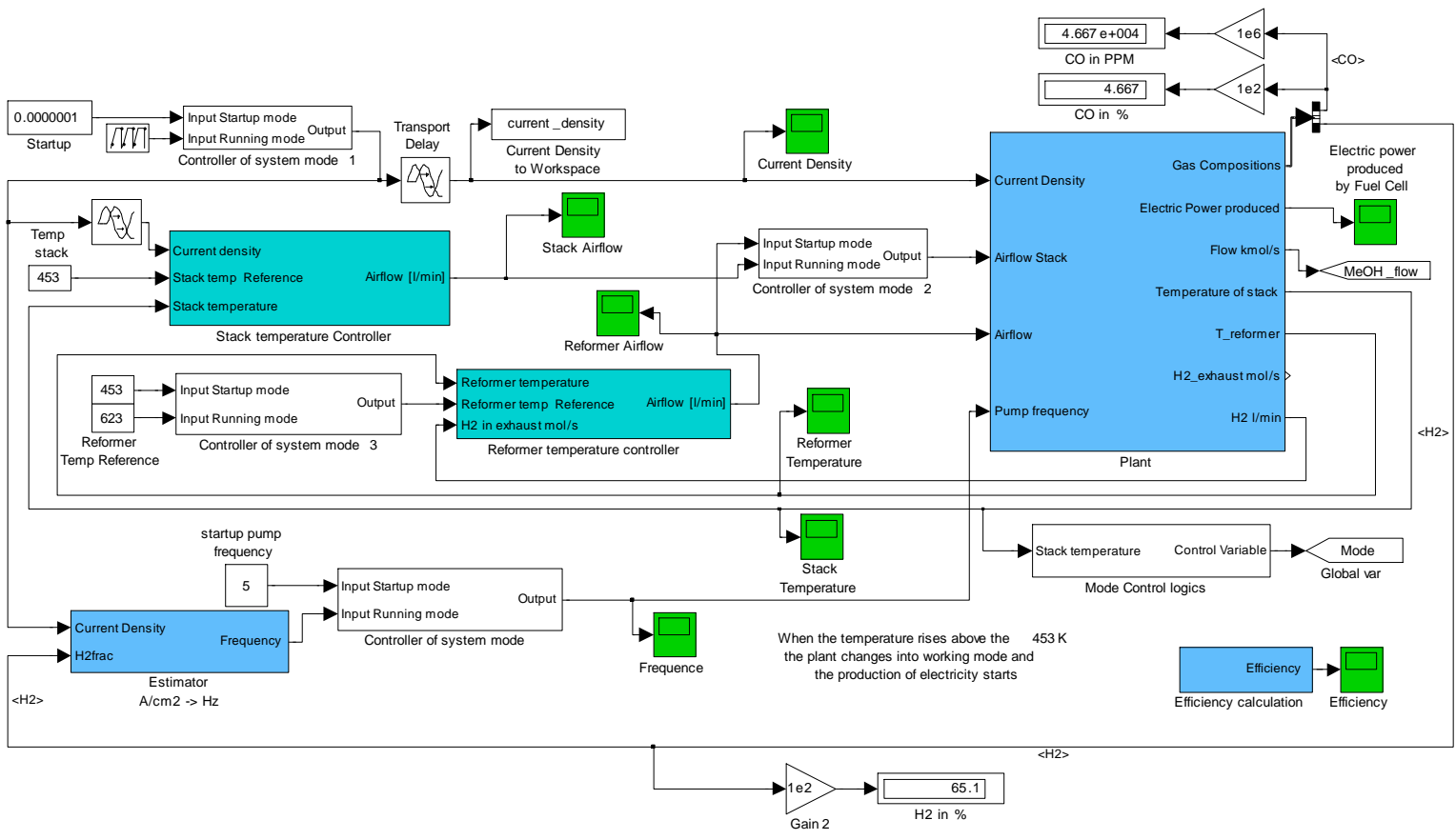


Figure B.16: Fuel Cell Stack Model

There is 3 major parts of the fuel cell stack as shown in figure B.16.

- Calculation of the stack temperature
- Calculation of the stack voltage
- Calculation of the stack hydrogen usage

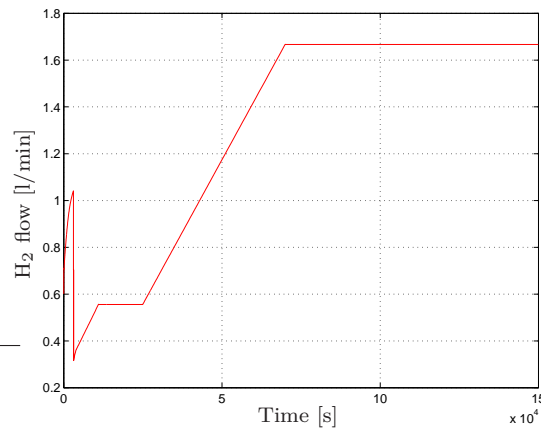


Figure B.17: Hydrogen in exhaust gas [l/min]

The hydrogen in the exhaust gas can be seen from figure B.17 and is calculated in figure B.20

Hydrogen usage in cell

The calculation on the hydrogen usage is based on

$$H2_{usage} = \frac{(cells \times cell\ area) \cdot i}{2F} \quad (B.6)$$

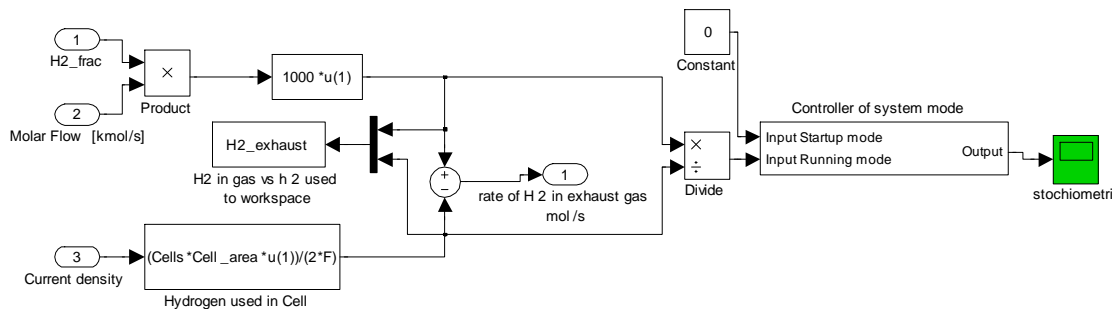


Figure B.18: Fuel Cell Stack - Calculation of Hydrogen usage

The output of figure B.18 is the rate of H_2 in exhaust gas. The flow of syngas from the reformer is multiplied with the fraction of hydrogen, and the fuel cell usage of hydrogen is subtracted. The amount of hydrogen in the syngas compared to the usage in the fuel cell is shown in figure B.19. This constant is and should be equal to the stoichiometry chosen in Appendix B.1.

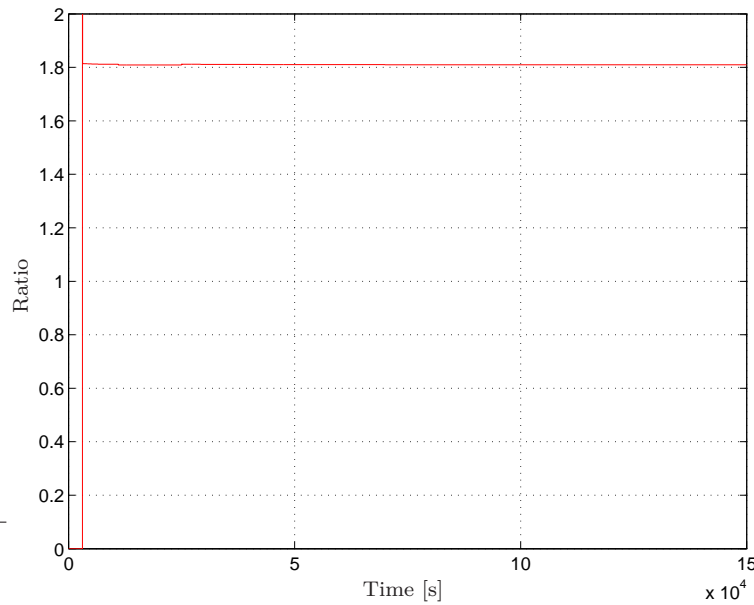


Figure B.19: Ratio of hydrogen used vs hydrogen present in fuel cell

To compare the molar flow of the gas in an experiment, the hydrogen exhaust gas is calculated by figure B.20. The hydrogen in the exhaust gas is divided by the density of the gas. The density of the gas is calculated from the temperature of the gas at atmospheric pressure by an regression made in EES.

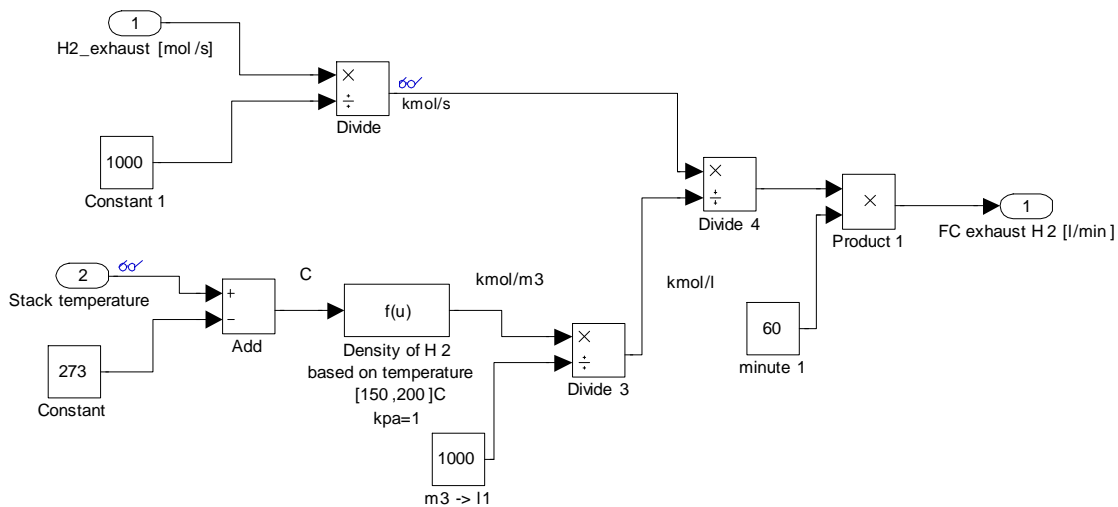


Figure B.20: Fuel Cell Stack - Calculation of hydrogen in exhaust gas [l/min]

Current model

The total electric power that can be drawn from the fuel cell is calculated by (B.7)

$$P = U \cdot I = (\text{cell voltage} \times \text{cells}) \cdot (\text{cell area} \times \text{current density}) \quad (\text{B.7})$$

This equation is displayed in figure B.21

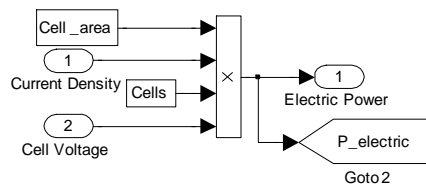


Figure B.21: *Fuel Cell Stack - Current Model*

B.4.1 Stack temperature

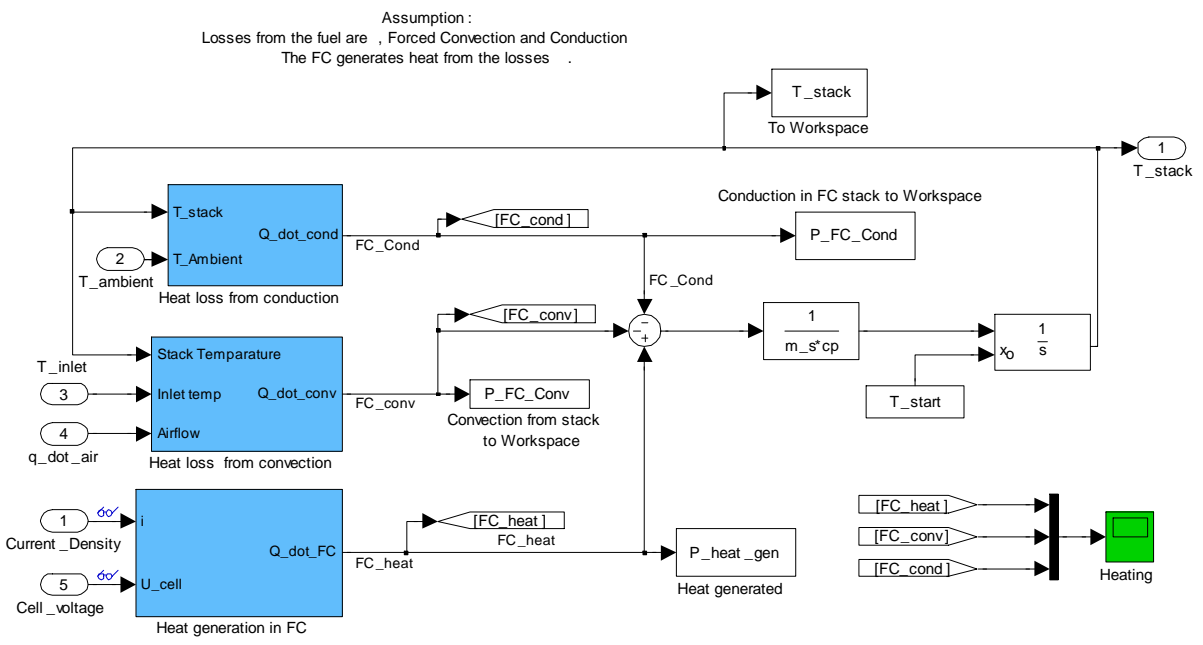


Figure B.22: Fuel Cell Stack - Temperature

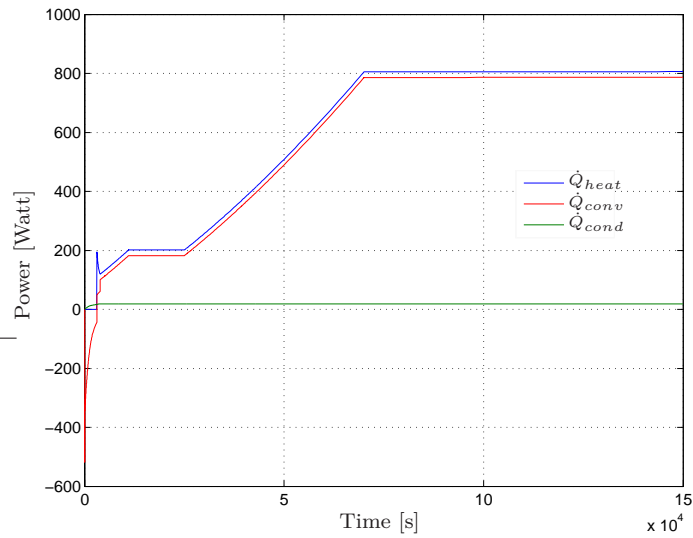


Figure B.23: Heating contributions for the fuel cell stack

There are 3 parts of the temperature calculation of the fuel cell stack. Heat generated in fuel cell, convection and conduction. The tree calculated contributions can be seen in figure B.23. The convection in this figure is a lot higher compared to the conduction, and this is because of the high airflow in the fuel cell, see figure B.3(a).

The total wattage from the heat generated minus convection and conduction is multiplied with the mass and the specific heat transfer coefficient. This gives a temperature difference pr second and this is calculated from the starting temperature T_{start}.

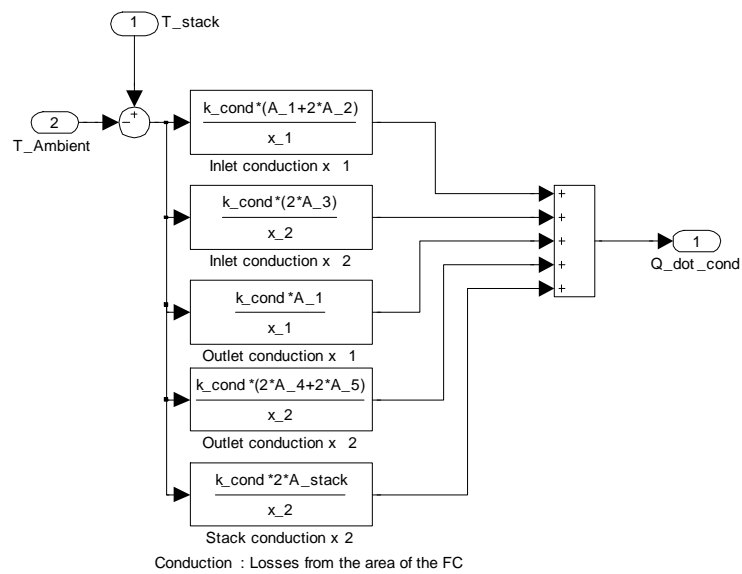


Figure B.24: Fuel Cell Stack Model - Temperature - Conduction

The conduction of the stack is shown in figure B.24 and is based on [3]. The different areas of the fuel cell is multiplied with the difference in temperature from the ambient and the stack temperature.

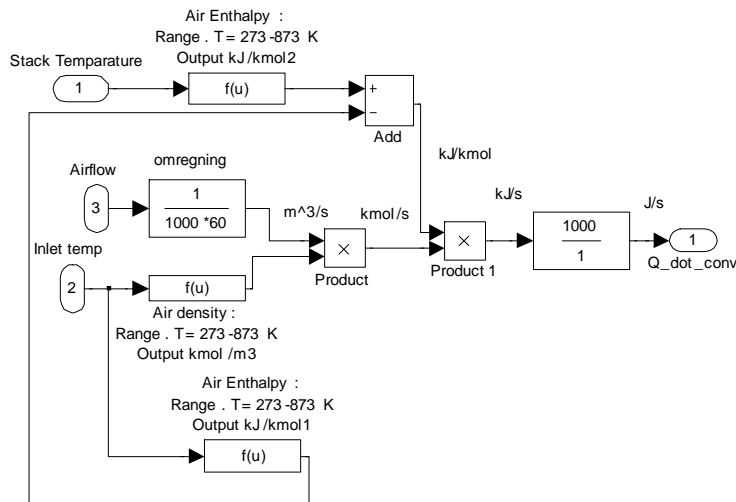


Figure B.25: Fuel Cell Stack - Temperature - Convection

Convection in the stack is calculated as shown in figure B.25. The difference in enthalpy is calculated from the stack temperature and the inlet air temperature. This is multiplied with the airflow in kmol/s and this gives a rate of heat (J/s).

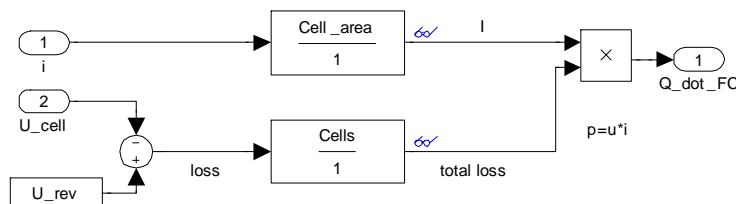


Figure B.26: Fuel Cell Stack - Temperature - Heat generation in fuel cell

The heat generated in the fuel cell is calculated as shown in figure B.26. The total loss is calculated and multiplied with the total current drawn from the stack. This current is calculated by multiplying the cell area with the current density. The total voltage loss in the fuel cell is calculated by taking the reversible voltage u_{rev} minus the actual cell voltage. This voltage loss is multiplied with the number of cells.

B.4.2 Stack voltage

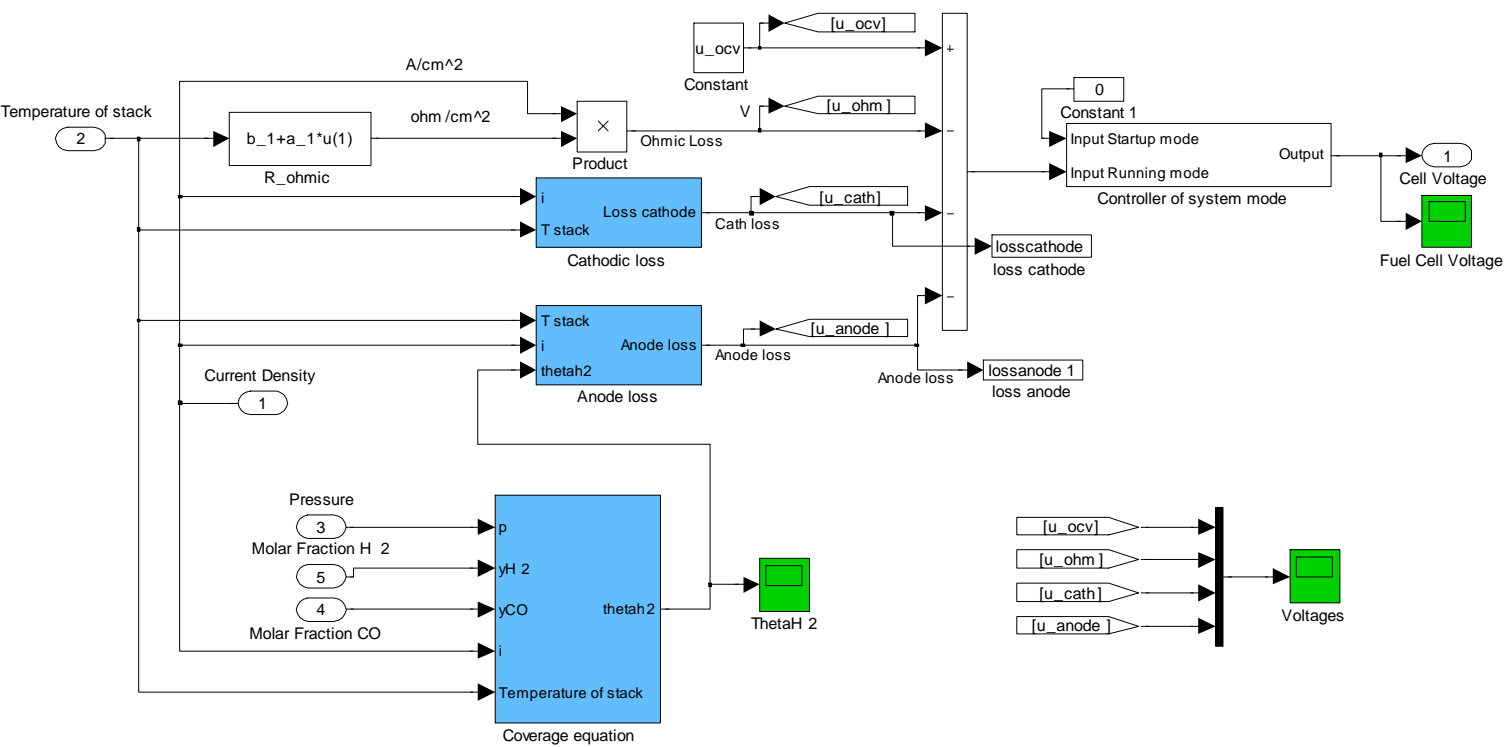


Figure B.27: Fuel Cell Stack - Voltage

The stack voltage in the fuel cell is dependent on the “open circuit voltage”, “ohmic losses”, cathode losses and anode losses. The open circuit voltage is constant and calculated from [6]. The different losses and the open circuit voltage can be seen in figure B.28(a). The fuel cell voltage can be seen in figure B.28(b)

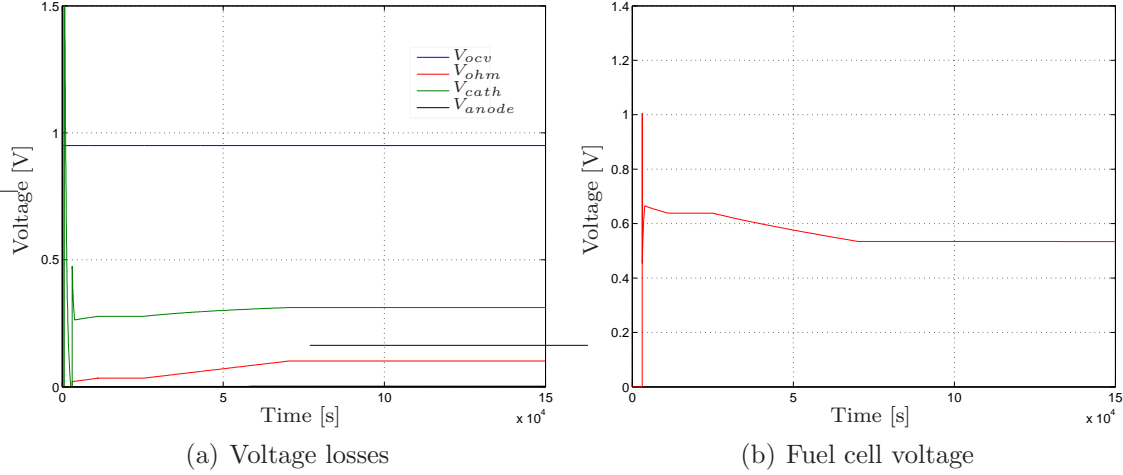


Figure B.28: Fuel Cell stack voltages

Coverage of the Cell

In the calculation of the anode voltage loss the coverage of the cell is needed. The equations for the coverage of the cell is (B.8) and (B.9) respectively. These are based on an equilibrium and this results in both equations are equal to zero.

$$\rho \frac{d\Theta_{H_2}}{dt} = k_{fh} \cdot x_{H_2} \cdot p \cdot (1 - \Theta_{H_2} - \Theta_{CO})^n - b_{fh} \cdot k_{fh} \cdot \Theta_{H_2}^n - i = 0 \quad (\text{B.8})$$

$$\rho \frac{d\Theta_{CO}}{dt} = k_{fc} \cdot x_{CO} \cdot p(1 - \Theta_{H_2} - \Theta_{CO}) - b_{fc} \cdot k_{fc} \cdot \Theta_{CO} - \frac{i \cdot k_{ec} \cdot \Theta_{CO}}{2 \cdot k_{eh} \cdot \Theta_{H_2}} = 0 \quad (\text{B.9})$$

Since both (B.8) and (B.9) are equal to zero and assuming that the H_2 -coverage is a second order reaction where n equals 2, it is possible to calculate a value of the H_2 -coverage that satisfies the equations. The pressure p is represented and molar fraction of the respective gasses is denoted with x_k . The coefficients (k_{ij} and b_{ij}), in both the equations, are based on the temperature of the cell. These coefficients are modeled with Arrhenius expressions, see (B.10)

$$k_{ij} = k_{ij0} \cdot e^{\left(\frac{-\text{ActivationEnergy}}{R \cdot T_s}\right)} \quad (\text{B.10})$$

The constant k_{ij0} used in figure B.10 is equal to k_{ij} when the temperature is infinite and this constant called the pre-exponential factor. R_u is the gas constant and T_s is the stack temperature.

The calculation of the hydrogen coverage is based on solving (B.9) with respect to Θ_{CO} and inserting the expression in (B.8) results in an implicit equation that equal to zero. Solving (B.9) with respect to Θ_{CO} can be seen from (B.11)

$$\Theta_{CO} = \frac{k_{fc} \cdot x_{CO} \cdot p (1 - \Theta_{H_2})}{k_{fc} \cdot x_{CO} \cdot p + b_{fc} \cdot k_{fc} + \frac{i \cdot k_{ec}}{2 \cdot k_{eh} \cdot \Theta_{H_2}}} \quad (\text{B.11})$$

Inserting (B.11) in (B.8) can be seen from (B.12)

$$k_{eh} \cdot x_{H_2} \cdot p \cdot \left(1 - \Theta_{H_2} - \frac{k_{fc} \cdot x_{CO} \cdot p (1 - \Theta_{H_2})}{k_{fc} \cdot x_{CO} \cdot p + b_{fc} \cdot k_{fc} + \frac{i \cdot k_{ec}}{2 \cdot k_{eh} \cdot \Theta_{H_2}}} \right)^2 - b_{fh} \cdot k_{fh} \cdot \Theta_{H_2}^2 - i = 0 \quad (\text{B.12})$$

(B.12) can be solved numerically in MATLAB using the "fzero"-function and a script for the model has been written as an Sfunction. The inputs for the fzero function is shown in figure B.29 and the

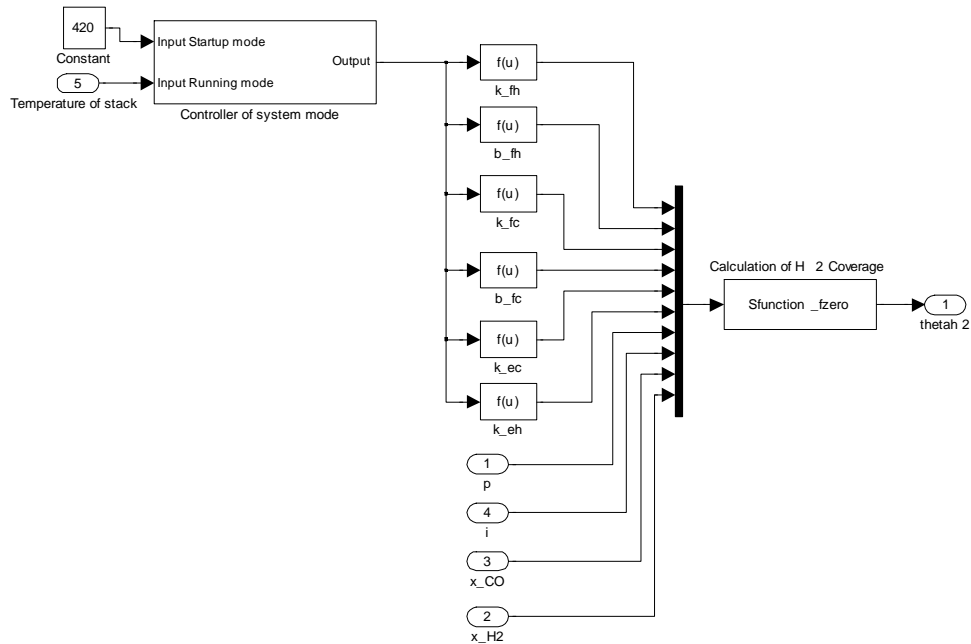
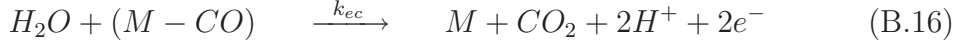
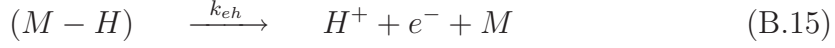
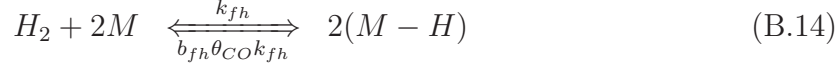
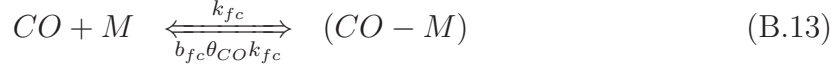


Figure B.29: Fuel Cell Stack - Voltage - Coverage Equation

Anode loss

The reactions that take place at the anode when CO is present



The double arrows used in (B.13) and (B.14) where the top is the reaction rate to the right. Reaction (B.13) and (B.14) defines the absorption process of CO and H₂, where reaction (B.15) and (B.16) describes the electro oxidation of CO and H₂.

<i>Pre-exponential factors</i>		
CO desorption rate, b_{fc0}	8.817e12	bar
H2 desorption rate, b_{fh0}	2.038e6	bar
CO electrooxidation rate, k_{ec0}	3.267e18	A/cm^2
H2 electrooxidation rate, k_{eh0}	25607	A/cm^2
CO adsorption rate, k_{fc0}	94.08	$A/(cm^2 \cdot bar)$
H2 adsorption rate, k_{fh0}	2.743e24	$A/(cm^2 \cdot bar)$
<i>Activation energy values</i>		
CO desorption rate, E_{bfc}	127513	$kJ/kmol$
H2 desorption rate, E_{bfh}	47904	$kJ/kmol$
CO electrooxidation rate, $E_{k_{ec}}$	196829	$kJ/kmol$
H2 electrooxidation rate, $E_{k_{eh}}$	34777	$kJ/kmol$
CO adsorption rate, $E_{k_{fc}}$	19045	$kJ/kmol$
H2 adsorption rate, $E_{k_{fh}}$	1899e5	$kJ/kmol$

Table B.1: Values used in Anode loss equation

The anode loss is calculated in (B.17) where the anode overpotential is related to the current density and the surface coverage of.

$$V_{anode}(T_s, i) = \frac{R \cdot T_s}{\alpha_a \cdot F} \cdot \sinh^{-1} \left(\frac{i}{2 \cdot k_{eh}(T_s) \cdot \Theta_{H_2}(T_s, i)} \right) \quad (B.17)$$

This is modeled as shown in figure B.30.

θ_{H_2} is calculated from the coverage equations, see figure B.29.

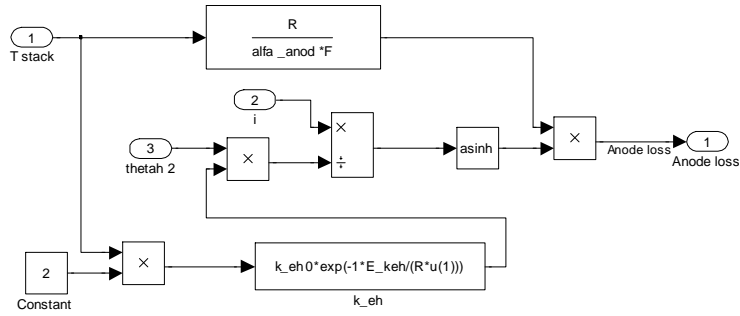


Figure B.30: Fuel Cell Stack - Voltage - Anode Loss

Cathode loss

Cathode constants		
Ohmic loss constant, a_1	-0.000166667	[-]
Ohmic loss constant, b_1	0.228858333	[-]
Exchange current density constant, a_2	4.641e-2	[-]
Exchange current density constant, b_2	6.143e3	[-]
Empirical constant, a_3	0.000820312455	[-]
Empirical constant, b_3	0.430604326	[-]

Table B.2: Values used in Cathode loss equation

The cathode loss can be seen in figure B.31. The calculation is based on (B.18) and the empirical value can be seen in figure B.32. This equation is based on the work done in [15].

$$V_{cathode}(T_s, i) = \frac{R \cdot T_s}{4 \cdot \alpha(T_s) \cdot F} \cdot \ln\left(\frac{i}{i_0}\right) + EMP \quad (B.18)$$

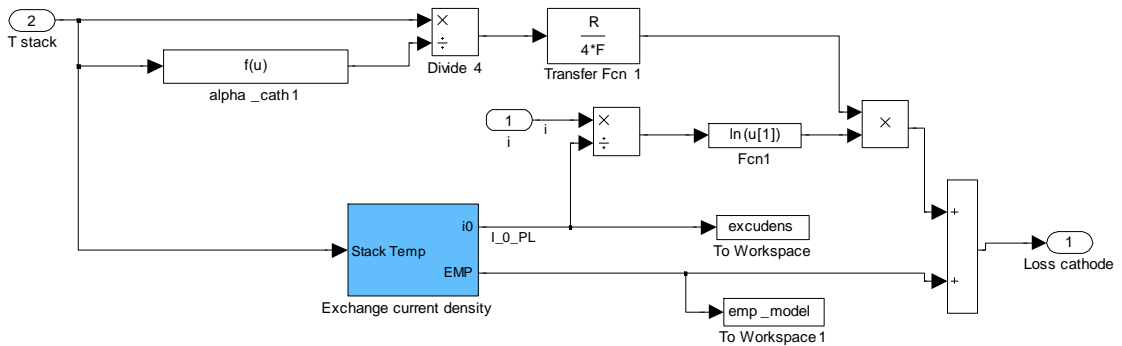


Figure B.31: Fuel Cell Stack - Voltage - Cathode loss

As alpha is dependent on the fuel cell temperature, the function can be seen in (B.19). This regression is based on [9]

$$\alpha_{cath1} : (-1.89064783 + 5.52249057E - 3 * u(1)) * 0.5 \quad (B.19)$$

The current density and the empirical value of the cathode loss is shown in figure B.32. The constants used in this model can be seen in (B.1). T_{limit} is 433K(160°C) which is the lower limit of the HTPEM's temperature operating range.

$$i_0(T_s) = a_2 \cdot e^{-b_2 \left(\frac{1}{T_s} - \frac{1}{T_{limit}} \right)} \quad (B.20)$$

The empirical value can be seen in (B.21) and is graphed in figure B.33

$$EMP(T_s) = a_{30} \cdot e^{-b_{30}(T_s - T_{limit})} \quad (B.21)$$

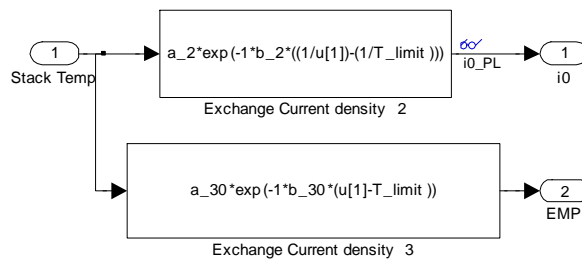
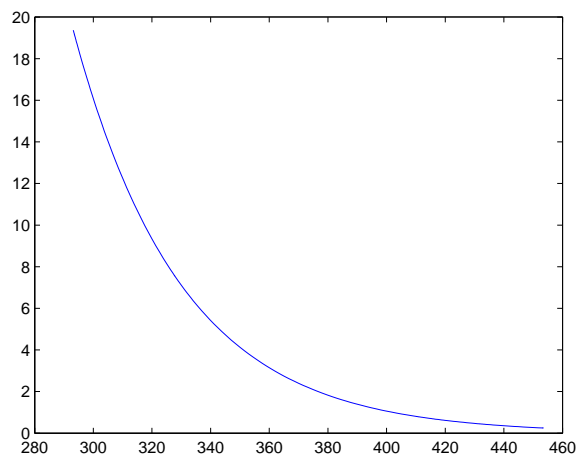


Figure B.32: Fuel Cell Stack - Voltage - Cathode loss - Exchange Current Density



FiXme ! Figure B.33: The Empirical change of the Cathodic loss compared to temperature

1

¹FiXme: enheder på figur

B.5 Evaporator

The evaporator is a 1kg heat exchanger made of aluminum. The evaporator is fitted with 200 watt electric heaters, and this can be seen from the red wires in figure B.34. The inlet of the methanol mixture has its inlet from the front side of the evaporator, and the outlet is shown in the left of the picture. As the evaporator is installed on the system, the evaporator is covered with a layer of Rockwool on the top side.

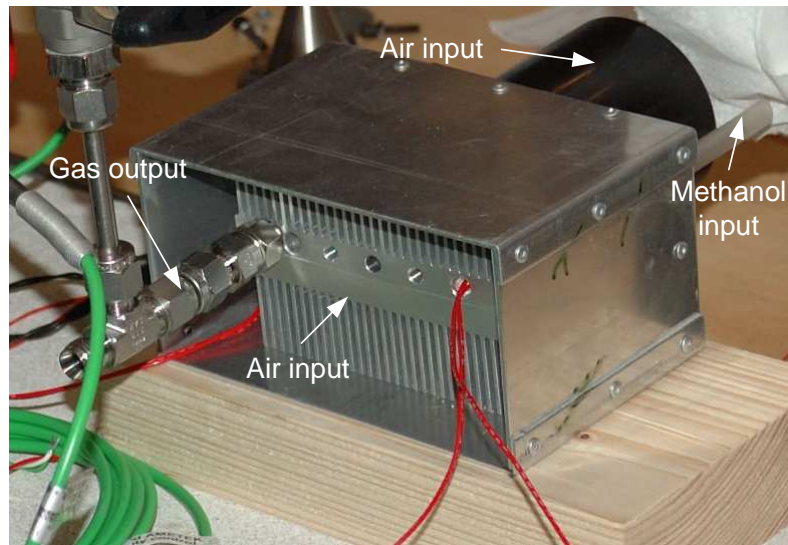


Figure B.34: Evaporator seen from the air outlet side

The model got 3 inputs, and 2 outputs. The first output is the temperature of the evaporator and the second is the flow of methanol. The flow of methanol is used in calculation of the temperature, where the airflow from the fuel cell and the temperature of the air is input as well.

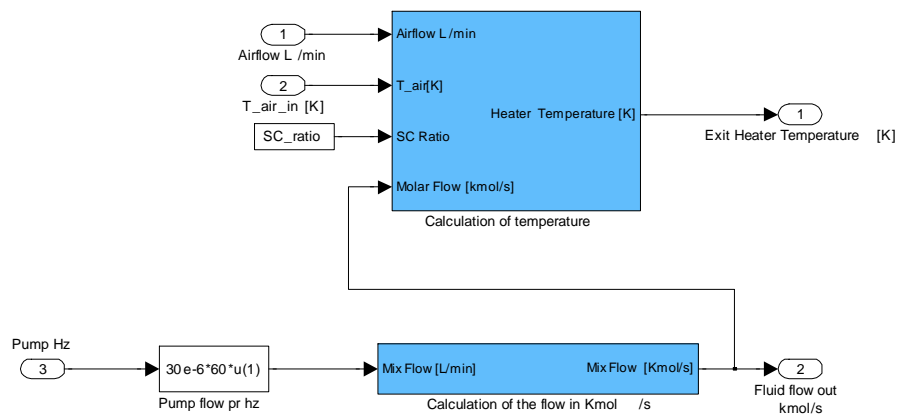


Figure B.35: Evaporator Model

The density of the mixture is based on

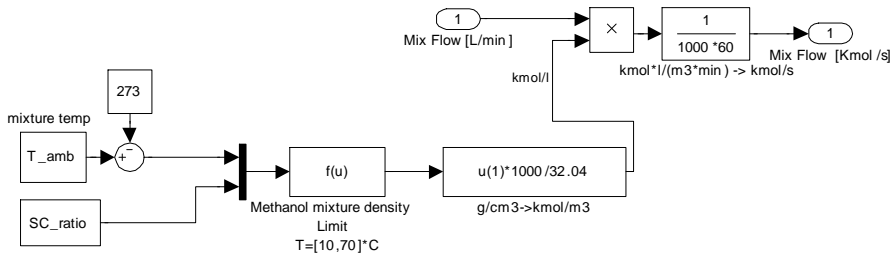


Figure B.36: Evaporator - Calculation of flow in kmol/s

$$\rho_{MeOH} = 1/(9,72192540E - 01 + 8,24527833E - 04 * T + 2,00480577E - 06 * T^2 + 2,77045714E - 01 * x_{MeOH} + 8,91428571E - 03 * x_{MeOH}^2)$$

where x_{MeOH} is the MeOH fraction of the mixture, and is calculated by $1/(1 + SC)$. The density of the methanol is multiplied with the molar mass and multiplied with the flow. The flow is converted to a molar flow and is set as output.

B.5.1 Temperature of evaporator

The temperature is calculated from four contributions and solves the total amount of power added or subtracted from the evaporator block. The different powers can be seen in figure B.38, and can be seen in figure B.39

The air from the fuel cell and the electric heaters all contribute power to the evaporator, and the vaporization of methanol and water is subtracted. The temperature is initially 20 [°C].

B Description of model

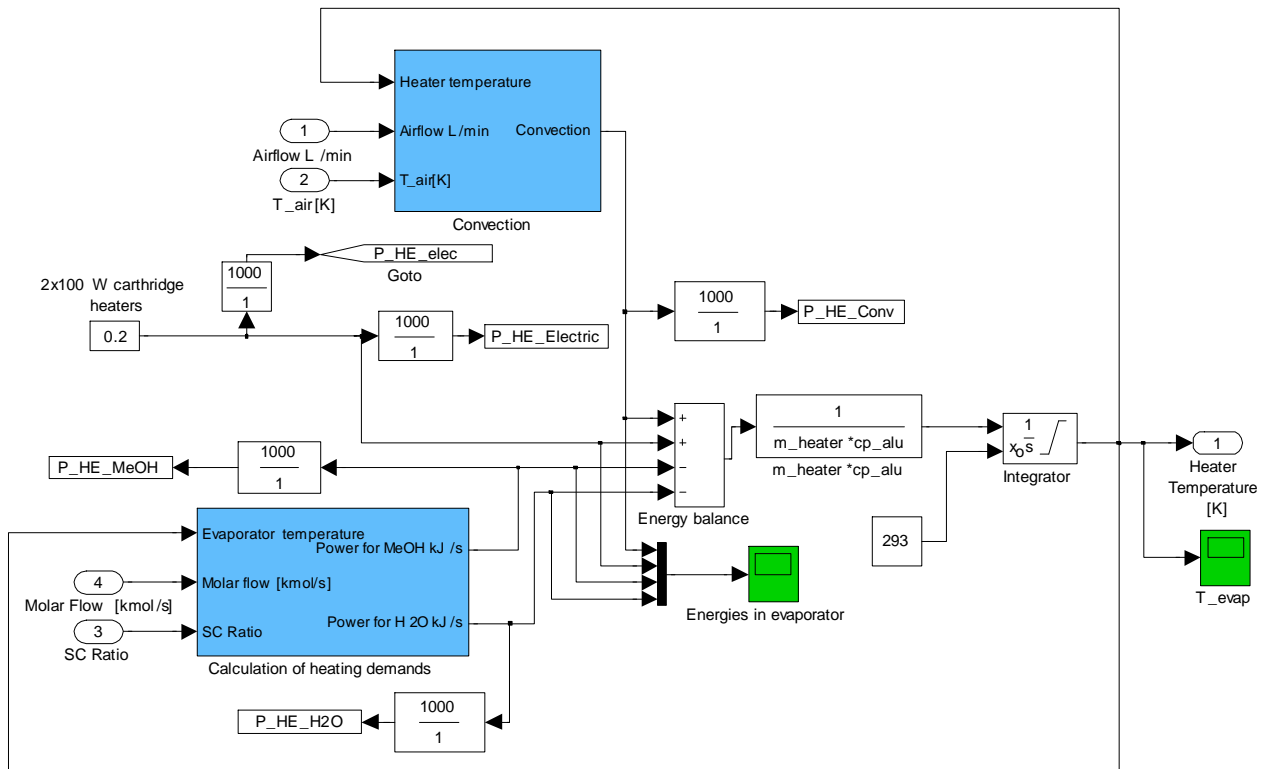


Figure B.37: *Evaporator - Temperature*

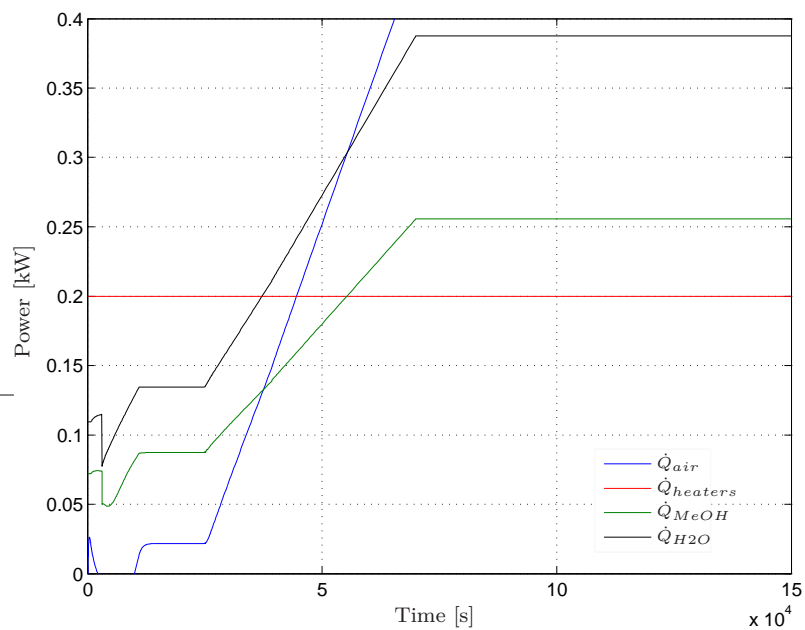


Figure B.38: *Comparison of difference energies in the evaporator*

The total power is divided by the mass of the heater and the specific heat capacity and is integrated to output the temperature over time.

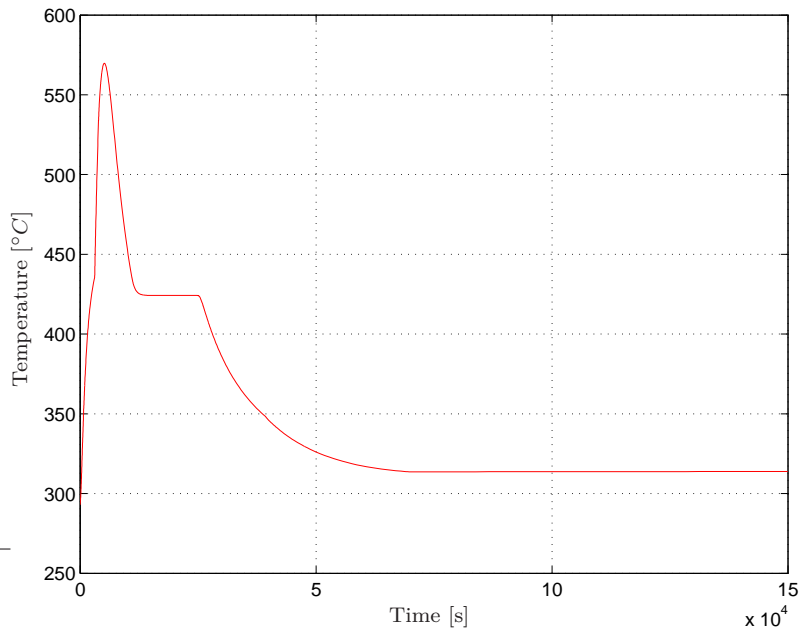


Figure B.39: Temperature of evaporator

The air from the fuel cell will in the startup phase cool the evaporator down until it reaches a higher temperature compared to the evaporator. This heat is calculated by figure B.40.

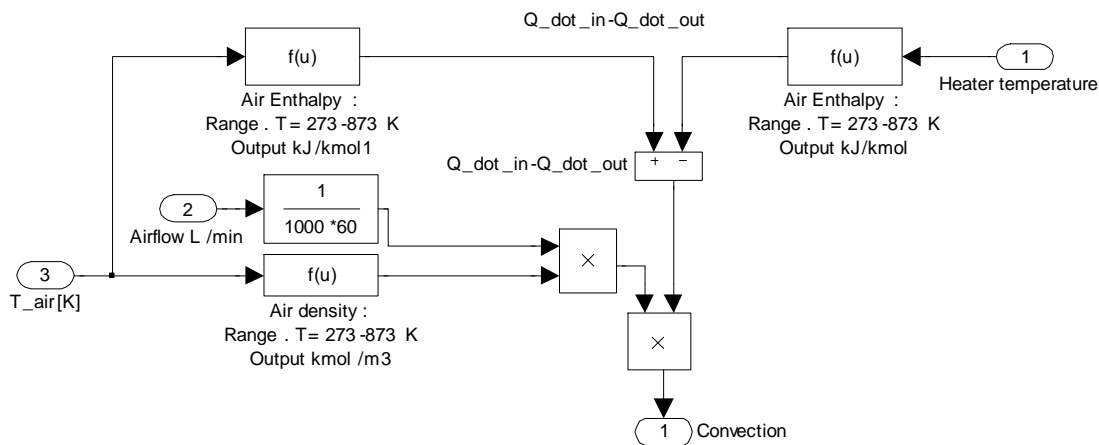


Figure B.40: Evaporator - Temperature - Conduction

The heat transfer from the fuel cell air exhaust is assumed to reduce its temperature to the evaporator when it is blown through the heat exchanger. From this temperature the enthalpy is calculated and it is subtracted from the enthalpy of the fuel cell air exhaust air. The airflow in m^3/s is multiplied with the density of the exhaust air and this molar flow is multiplied with the difference in enthalpy, as shown in (B.3).

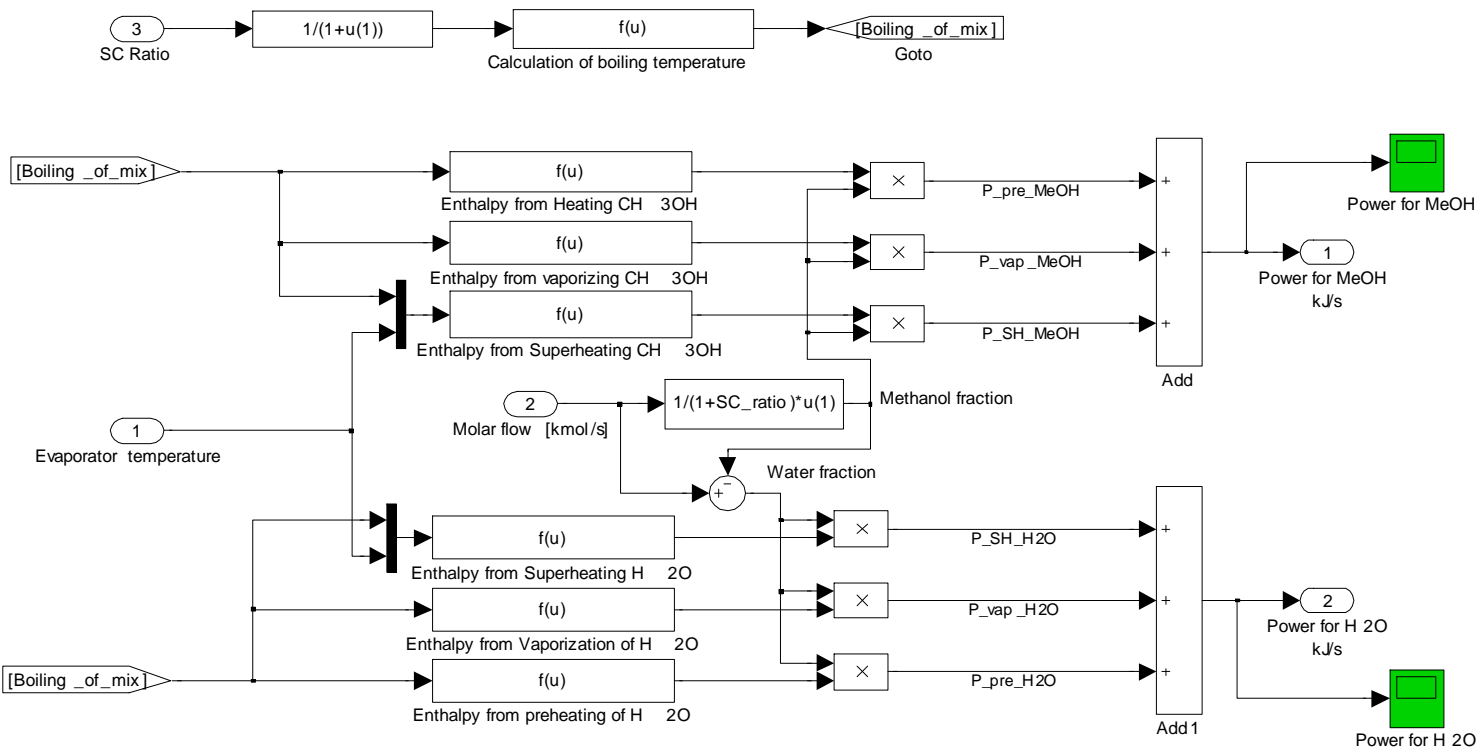


Figure B.41: Evaporator - Temperature - Heating demands

The heating demands of the methanol and water mixture is calculated by figure B.41. The model assumes that the heating, evaporation, and super heating happens instantly. The inputs are the SC ratio, evaporator temperature and the molar flow

of the mixture, and the outputs are the power needed to superheat a mix of CH₃OH and H₂O.

The boiling temperature of the mix are calculated by [12]

$$T_{boiling} = (99.6186125 - 148.761078 * vapor_frac + 432.651496 * vapor_frac^2 - 734.917965 * vapor_frac^3 + 616.827122 * vapor_frac^4 - 200.586579 * vapor_frac^5) + 273$$

where $vapor_frac$ is $1/(1 + SC)$. The boiling point of the mix is used in the calculation of the enthalpy for the different stages of the superheating. These regressions are made with EES and can be seen from Model_heat_vapo.EES on the CD. The evaporator temperature is used in the superheating of both CH₃OH and H₂O because, because of a check if the temperature of the heater is below the boiling point. This does only apply when the system is starting up because the temperature of the evaporator always is above the boiling point of the mixture. The enthalpy is multiplied with the molar flow of either the CH₃OH fraction or the H₂O fraction, and this gives the power needed to preheat, vaporize, and super heat to a temperature of about 120 [°C].

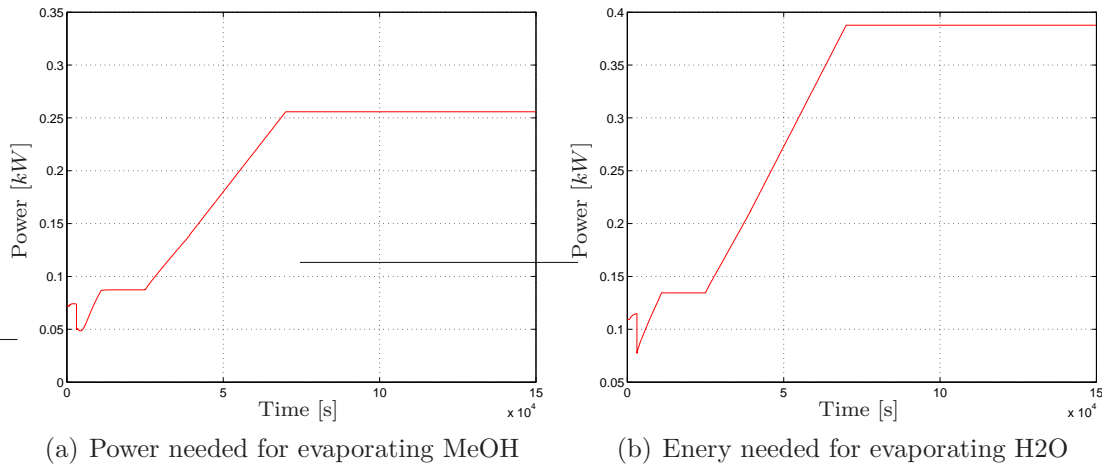


Figure B.42: Power needed for evaporating input fuel

The power needed to preheat, vaporize and superheat can be seen from figure B.42(a) and figure B.42(b), both for CH₃OH and H₂O.

B.5.2 Fuel pump estimator

The fuel cell pump frequency estimator is based on an assumption that it needs to be implemented on a real controlling system. This means that the conversion factor on the flow in the reformer is inserted directly into the model. This can be seen in

figure B.43, and is a constant of about 1.86. This requires the molar mass of the methanol and this is calculated by dividing with the methanol density. Fuel required is based on the fuel cell hydrogen consumption and this amount is multiplied with the excess value used for the burner. The excess hydrogen, λ_{h_2} is set to 1.5, which means 50% more hydrogen compared to the fuel cell consumption.

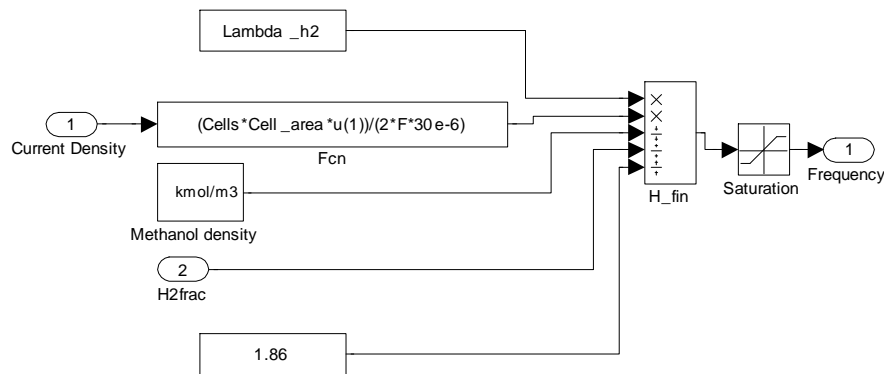


Figure B.43: Estimator of frequency

B.5.3 Electric efficiency

The efficiency is calculated by comparing the electric output to the heating value of the methanol flow. This can be seen in figure B.44. The electric power from the electric heaters and the blower in the fuel cell, is subtracted from the electric power of the fuel cell. This gives a total electric power output from the system.

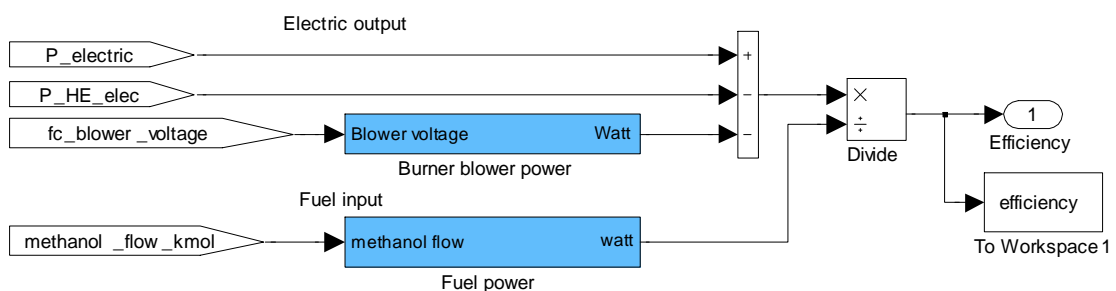


Figure B.44: Electric efficiency

The blower power usage is calculated in figure B.45.

The power for the blower is calculated by $P = U \cdot I$, where the current is calculated from the used blower voltage.

$$f(u) = 0.003081 * u(1)^2 + 0.01201 * u(1) \tag{B.22}$$

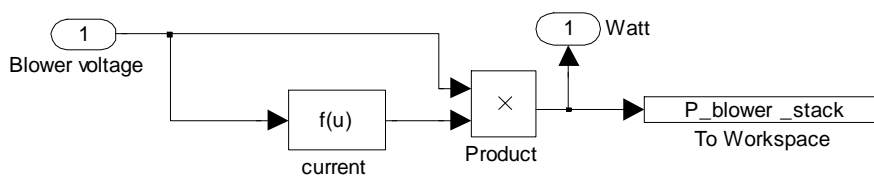


Figure B.45: *Electric efficiency - FC blower power*

The methanol fuel power is calculated by figure B.46

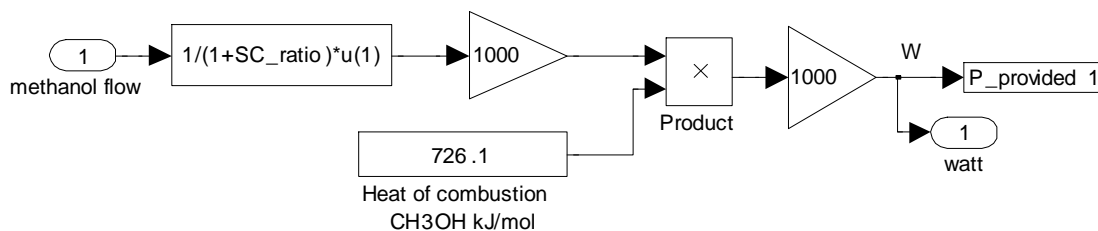


Figure B.46: *Electric efficiency - Energy from methanol fuel based on HHV*

The water is subtracted from the methanol fuel mix and is converted to mol/s . This is multiplied with the higher heating value of methanol and the output is kJ/s . This is multiplied with 1000 and the output is watt. The higher heating value is used because the input fuel is in a liquid phase.

Linearisation

The linearisation of the stack temperature model is needed in order to apply linear control algorithms and the linearisation can be found in this appendix. The first part of this appendix is the linearisation of the convective part and the second part is the linearisation of the stack voltage.

C.1 Convective loss

The convective losses depend on the temperature of the stack and the air blown into the stack. Assuming that the density of the air is constant within the temperature range of the model is a valid assumption. The convective losses can be seen from (3.4) which is repeated here.

$$\dot{Q}_{conv}(T_s, \dot{n}) = \dot{n} \cdot (H(T_s) - H(T_a))$$

Since the molar flow of air is represented in (3.4) by \dot{n} but this is a nonintuitive variable, and rewriting the equation to depend of the flow of air \dot{q} and multiplying the flow with a constant results in (C.1). Assuming that the enthalpy of the air can be modeled by a first order regression of temperature is applied.

$$\dot{Q}_{conv}(T_s, \dot{q}) = \dot{q} \cdot K_{rho} \cdot ((K_{H1} + K_{H2} \cdot T_s) - (K_{H1} + K_{H2} \cdot T_a)) \quad (C.1)$$

Equation (C.1) can be differentiated with respect to the airflow see (C.2)

$$\frac{\partial \dot{Q}_{conv}}{\partial \dot{q}} = K_{rho} \cdot ((K_{H1} + K_{H2} \cdot T_s) - (K_{H1} + K_{H2} \cdot T_a)) \quad (C.2)$$

Taking the partial derivative of (C.1) with respect to temperature results in (C.3)

$$\frac{\partial \dot{Q}_{conv}}{\partial T_s} = \dot{q} \cdot K_{rho} \cdot K_{H2} \quad (C.3)$$

Linearizing the convective part of the nonlinear model is done by evaluating (C.1) at the working point and add the linear changes from the working point.

$$\dot{Q}_{conv,lin} = \dot{Q}_{conv}(\bar{T}_s, \bar{q}) + \left. \frac{\partial \dot{Q}_{conv}}{\partial \dot{q}} \right|_{\bar{T}_s, \bar{q}} \cdot (\dot{q} - \bar{q}) + \left. \frac{\partial \dot{Q}_{conv}}{\partial T_s} \right|_{\bar{T}_s, \bar{q}} \cdot (T_s - \bar{T}_s) \quad (C.4)$$

Since the derivatives are evaluated at the working point parameters these are constant for the given working point and applying this to (3.5) results in

$$\dot{Q}_{conv,lin} = \dot{Q}_{conv}(\bar{T}_s, \bar{q}) + K_{conv_q} \cdot (\dot{q} - \bar{q}) + K_{conv_{T_s}} \cdot (T_s - \bar{T}_s)$$

C.2 Cell voltage

The cell voltage is dependent on the temperature of the stack and the current density, and in order to apply the voltage to the calculation of the current the voltage must be linearized with respect to the stack temperature and current density. The cell voltage can be seen from (C.5) and this represents the nonlinear cell voltage.

$$V_{cell}(T_s, i) = U_{ocv} - \eta_{ohmic}(T_s, i) - \eta_{cathodic}(T_s, i) - \eta_{anodic}(T_s, i) \quad (C.5)$$

The three negative parts of the equation is highly nonlinear and needs to be linearized in order to determine the change in voltage from the working point based on a change in either current density or stack temperature. The parts will be linearized in the order they appear in (C.5). The working point for the system is defined by the temperature of the stack in the working point \bar{T}_s and the current density in the working point \bar{i} . The MATLAB script `Temperature_linear.m` on the CD in the MATLAB folder contains the calculation of the gradients and the working points.

C.3 Nonlinear voltage parts

The calculation of the linear approximations of the nonlinear equations based on a Taylor series expansion of the equations. By neglecting the higher order terms above the first order, a linear equation can be produced from the derivatives by both the temperature and the current density.

C.3.1 The Ohmic Losses

The model applies the calculation of the Ohmic voltage losses based on a linear regression for the ohmic resistance inside the fuel cell, see (C.6)

$$\eta_{ohmic}(T_s, i) = (b_1 + a_1 * T_s) \cdot i \quad (C.6)$$

When a Taylor series is applied the ohmic losses can be divided into parts containing only current density and temperature respectively.

$$\eta_{ohmic}(\bar{T}_s, \bar{i}) = (b_1 + a_1 \cdot \bar{T}_s) \cdot \bar{i} \quad (C.7)$$

$$\frac{\partial \eta_{ohmic}}{\partial T_s} = a_1 \cdot i \quad (C.8)$$

$$\frac{\partial \eta_{ohmic}}{\partial i} = b_1 + a_1 \cdot T_s \quad (C.9)$$

$$\eta_{o,lin}(T_s, i) = \eta_{ohmic}(\bar{T}_s, \bar{i}) + \left. \frac{\partial \eta_{ohmic}}{\partial i} \right|_{\bar{T}_s} \cdot (i - \bar{i}) + \left. \frac{\partial \eta_{ohmic}}{\partial T_s} \right|_{\bar{i}} \cdot (T_s - \bar{T}_s) \quad (C.10)$$

In (C.10) the expressions for the ohmic losses changes with respect to the current density, see (C.9), and stack temperature, see (C.8). These have been multiplied with the change of the given variables from the working point and they are valid for small changes in the signals.

C.4 Cathode loss

The Cathodic losses are based on highly nonlinear factors and subfunctions based on the stack temperature and can be seen from (C.11)

$$\eta_{cathodic}(T_s, i) = \frac{R \cdot T_s}{\alpha(T_s) \cdot 4 \cdot F} \cdot \ln \left(\frac{i}{i_0(T_s)} \right) + EMP(T_s) \quad (C.11)$$

The factor $\alpha(T_s)$, see (C.12), the exchange current density $i_0(T_s)$, see (C.13) and the empirical part, see (C.14) is based on the stack temperature and they need to be linearized in order to obtain a cathodic loss based on the input of the temperature and the current density.

$$\alpha(T_s) = (k_1 + k_2 \cdot T_s) k_3 \quad (\text{C.12})$$

$$i_0(T_s) = a_2 \cdot e^{-b_2 \left(\frac{1}{T_s} - \frac{1}{T_1} \right)} \quad (\text{C.13})$$

$$EMP(T_s) = a_{30} \cdot e^{-b_{30}(T_s - T_1)} \quad (\text{C.14})$$

Taking the partial derivative of the cathodic loss, see (C.11), with respect to the current density is calculated and evaluated, see (C.15). The equations of (C.12), (C.13) and (C.14) are observed as constants since the equations only depend on the temperature.

$$\frac{\partial \eta_{cathodic}}{\partial i} = \frac{R \cdot T_s}{\alpha(T_s) \cdot 4 \cdot F} \cdot \frac{1}{i} \quad (\text{C.15})$$

The partial derivative of the cathodic losses, see (C.11), with respect to temperature is also calculated in order to obtain the linearized expression of the cathodic losses, see (C.16). The equations of (C.12), (C.13) and (C.14) are observed as functions that also needs to be derived. The derivation of the cathode loss is performed with Symbolic Toolbox in Matlab.

$$\frac{\partial \eta_{cathodic}}{\partial T_s} = \frac{R \cdot T_s}{4 \cdot F \cdot \alpha(T_s)} \cdot \left(\ln \left(\frac{i}{i_0} \right) - \frac{k_2}{\alpha(T_s)} \cdot \ln \left(\frac{i}{\alpha(T_s)} \right) - \frac{b_2}{T_s} \right) - a_{30} \cdot b_{30} \cdot e^{-b_{30}(T_s - T_1)} \quad (\text{C.16})$$

The calculation of the linear contribution from the cathodic losses is based on (C.11) evaluated at the working point temperature and current density. The deviations in the current density multiplied with (C.15), evaluated at the working point temperature and current density, is added to the linear expression. The deviation of the temperature multiplied with (C.16), evaluated at the working point temperature and current density, is added to the linearized expression, see (C.17)

$$\begin{aligned} \eta_{c,lin}(T_s, i) = & \eta_{cathodic}(\bar{T}_s, \bar{i}) + \left. \frac{\partial \eta_{cathodic}}{\partial i} \right|_{\bar{T}_s, \bar{i}} (i - \bar{i}) \\ & + \left. \frac{\partial \eta_{cathodic}}{\partial T_s} \right|_{\bar{T}_s, \bar{i}} (T_s - \bar{T}_s) \end{aligned} \quad (\text{C.17})$$

The linearized cathodic losses are applied into the linearisation of the cell voltage.

C.5 Anodic loss

The anodic losses are based on equations that both use the stack temperature and the current density and in order to obtain the linear approximation of the voltage the anodic losses need to be differentiated with respect to both variables, see (C.18)

$$\eta_{anodic}(T_s, i) = \frac{R \cdot T_s}{\alpha \cdot F} \cdot asinh \left(\frac{i}{2 \cdot k_{eh}(T_s) \cdot \Theta(T_s, i)} \right) \quad (C.18)$$

The coverage of the cell Θ_{H_2} is a 3rd order regression based on the coverage equations from the model of the system, see (C.19). This regression is also based on the molar fractions of the reformat gas stream and these are assumed constant based on a reformer temperature of 500 K (227°C) and a SC-ratio of 1.3. If the reformer or the SC-ratio is changed the coefficients must be recalculated in EES.

$$\begin{aligned} \Theta_{H_2}(T_s, i) = & A0 + A1 \cdot T_s + A2 \cdot T_s^2 + A3 \cdot T_s^3 + B1 \cdot i + B2 \cdot i^2 + B3 \cdot i^3 \\ & + C1 \cdot T_s \cdot i + C2 \cdot T_s \cdot i^2 + C3 \cdot T_s^2 \cdot i + C4 \cdot T_s^2 \cdot i^2 \end{aligned} \quad (C.19)$$

The coverage regression, from (C.19), is derived with respect to the current in order to calculate the change of the coverage, see (C.20)

$$\begin{aligned} \frac{\partial \Theta_{H_2}}{\partial i} = & B1 + 2 \cdot B2 \cdot i + 3 \cdot B3 \cdot i^2 + C1 \cdot T_s \\ & + 2 \cdot C2 \cdot T_s \cdot i + C3 \cdot T_s^2 + 2 \cdot C4 \cdot T_s^2 \cdot i \end{aligned} \quad (C.20)$$

The coverage regression of the cell, from (C.19), is derived with respect to the temperature of the stack, see (C.21)

$$\begin{aligned} \frac{\partial \Theta_{H_2}}{\partial T_s} = & A1 + 2 \cdot A2 \cdot T_s + 3 \cdot A3 \cdot T_s^2 + C1 \cdot i \\ & + C2 \cdot i^2 + 2C3 \cdot T_s \cdot i + 2 \cdot C4 \cdot T_s \cdot i^2 \end{aligned} \quad (C.21)$$

The change of the variable k_{eh} is dependent of the temperature and is described by an Arrhenius-like equation, see (C.22)

$$k_{eh}(T_s) = k_{eh} \cdot e^{\frac{-E_{keh}}{R \cdot T_s}} \quad (C.22)$$

The derivative of k_{eh} with respect is calculated, see (C.23)

$$\frac{\partial k_{eh}}{\partial T_s} = \frac{k_{eh} \cdot E_{keh}}{R \cdot T_s^2} \cdot e^{\frac{-E_{keh}}{R \cdot T_s}} \quad (C.23)$$

when the derivatives have been calculated for the variables the derivative for the anodic loss can be calculated. The derivative with respect to current density, see (C.24). This equation refers to the derivative of the cell coverage with respect to the current density, see (C.20)

$$\begin{aligned} \frac{\partial \eta_{anodic}}{\partial i} &= \frac{R}{\alpha \cdot F} \cdot \frac{T_s}{\sqrt{\left(\frac{i}{2 \cdot k_{eh}(T_s) \cdot \Theta_{H_2}}\right)^2 + 1}} \cdot \\ &\frac{2 \cdot k_{eh}(T_s) \cdot \Theta_{H_2} - i \cdot 2 \cdot k_{eh}(T_s) \cdot \frac{\partial \Theta_{H_2}}{\partial i}}{(2 \cdot k_{eh}(T_s) \cdot \Theta_{H_2})^2} \end{aligned} \quad (C.24)$$

Linearisation of the anodic loss with respect to the temperature is calculated, see (C.25). The equation refers to the partial derivative of both the coverage equations and variable k_{eh} with respect to temperature, see (C.21) and (C.23) respectively.

$$\begin{aligned} \frac{\partial \eta_{anodic}}{\partial T_s} &= \frac{R}{\alpha \cdot F} a \sinh \left(\frac{i}{2 \cdot k_{eh}(T_s) \cdot \Theta_{H_2}} \right) \\ &+ \frac{R}{\alpha \cdot F} \frac{T_s}{\sqrt{\left(\frac{i}{2 \cdot k_{eh}(T_s) \cdot \Theta_{H_2}}\right)^2 + 1}} \cdot \frac{-i \cdot 2 \cdot \frac{\partial k_{eh}}{\partial T_s} \cdot \Theta_{H_2}}{(2 \cdot k_{eh}(T_s) \cdot \Theta_{H_2})^2} \\ &+ \frac{R}{\alpha \cdot F} \frac{k_{eh}(T_s) \cdot \frac{\partial \Theta_{H_2}}{\partial T_s}}{(2 \cdot k_{eh}(T_s) \cdot \Theta_{H_2})^2} \end{aligned} \quad (C.25)$$

Both (C.24) and (C.25) contains the functions of (C.19) and (C.22) and these equation are evaluated in the same point as the derivatives. The anodic loss can linearized around the working point based on the value of the anodic losses, see (C.18), evaluated in the working point of the model. Applying the deviations from the working point of the anodic loss, with respect to the given variables i and T_s multiplied with their respective derivatives of the anodic losses, see (C.24) and (C.25) respectively, results in the linear approximation of the anodic loss, see (C.26)

$$\begin{aligned} \eta_{a,lin}(T_s, i) &= \eta_{anodic}(\bar{T}_s, \bar{i}) + \left. \frac{\partial \eta_{anodic}}{\partial i} \right|_{\bar{T}_s, \bar{i}} \cdot (i - \bar{i}) \\ &\quad + \left. \frac{\partial \eta_{anodic}}{\partial T_s} \right|_{\bar{T}_s, \bar{i}} \cdot (T_s - \bar{T}_s) \end{aligned} \quad (C.26)$$

C.6 Linear voltage approximation

When inserting the linearized expressions for the different nonlinear parts into (C.5), an expression for the linearized voltage can be solved.

$$V_{cell,lin} = u_{ocv} - \eta_{o,lin}(T_s, i) - \eta_{c,lin}(T_s, i) - \eta_{a,lin}(T_s, i) \quad (C.27)$$

Summing up the constants of the linearized expressions, from (C.10), (C.17) and (C.26) resulting in the working point of the voltage. This can be expressed

$$v_{cell_{wp}} = u_{ocv} - \eta_{ohmic}(\bar{T}_s, \bar{i}) - \eta_{cathodic}(\bar{T}_s, \bar{i}) - \eta_{anodic}(\bar{T}_s, \bar{i}) \quad (C.28)$$

The voltage changes in a general direction based on the working point parameters of stack temperature and current density. This direction is based on the derivatives of the nonlinear parts of the voltage. The Taylor series applies only to small changes in the variables and the difference in the current density results in a change of the voltage.

$$\begin{aligned} V_{change_i}(i) &= -\left. \frac{\partial \eta_{ohmic}}{\partial i} \right|_{\bar{T}_s, \bar{i}} \cdot (i - \bar{i}) - \left. \frac{\partial \eta_{cathodic}}{\partial i} \right|_{\bar{T}_s, \bar{i}} \cdot (i - \bar{i}) - \left. \frac{\partial \eta_{anodic}}{\partial i} \right|_{\bar{T}_s, \bar{i}} \cdot (i - \bar{i}) \\ &= -\underbrace{\left(\left. \frac{\partial \eta_{ohmic}}{\partial i} \right|_{\bar{T}_s, \bar{i}} + \left. \frac{\partial \eta_{cathodic}}{\partial i} \right|_{\bar{T}_s, \bar{i}} + \left. \frac{\partial \eta_{anodic}}{\partial i} \right|_{\bar{T}_s, \bar{i}} \right)}_{K_{Voltage_{di}}} \cdot (i - \bar{i}) \end{aligned} \quad (C.29)$$

$$\begin{aligned} V_{change_{T_s}}(T_s) &= -\left. \frac{\partial \eta_{ohmic}}{\partial T_s} \right|_{\bar{T}_s, \bar{i}} \cdot (T_s - \bar{T}_s) - \left. \frac{\partial \eta_{cathodic}}{\partial T_s} \right|_{\bar{T}_s, \bar{i}} \cdot (T_s - \bar{T}_s) - \left. \frac{\partial \eta_{anodic}}{\partial T_s} \right|_{\bar{T}_s, \bar{i}} \cdot (T_s - \bar{T}_s) \\ &= -\underbrace{\left(\left. \frac{\partial \eta_{ohmic}}{\partial T_s} \right|_{\bar{T}_s, \bar{i}} + \left. \frac{\partial \eta_{cathodic}}{\partial T_s} \right|_{\bar{T}_s, \bar{i}} + \left. \frac{\partial \eta_{anodic}}{\partial T_s} \right|_{\bar{T}_s, \bar{i}} \right)}_{K_{Voltage_{dT_s}}} \cdot (T_s - \bar{T}_s) \end{aligned} \quad (C.30)$$

Expanding equation (C.27) with the constants from (C.29) and (C.30) and separating the variables

$$V_{cell,linear} = v_{cell_wp} + K_{Voltage_{di}} \cdot (i - \bar{i}) + K_{Voltage_{dT_s}} (T_s - \bar{T}_s) \quad (C.31)$$

C.7 Heat generated

In order to calculate the heat generated by the fuel cell (C.32) is used.

$$\dot{Q}_{heat} = (v_{rev} - v_{cell}(T_s, i)) \cdot i \cdot n_{cell} \cdot A_{cell} \quad (C.32)$$

By inserting (C.31) in (C.32) and replacing V_{cell} with the expression of (C.31) results in (C.33).

$$\dot{Q}_{heat} = \left(v_{rev} - \left(v_{cell_wp} + V_{change_i}(i) + V_{change_{T_s}}(T_s) \right) \right) \cdot i \cdot n_{cell} \cdot A_{cell} \quad (C.33)$$

the expression of the heat can be expanded by inserting the expressions of (C.29) and (C.30), results in (C.34)

$$\begin{aligned} \dot{Q}_{heat} &= \left(v_{rev} - \left(v_{cell_wp} + K_{Voltage_{di}} \cdot (i - \bar{i}) + K_{Voltage_{dT_s}} \cdot (T_s - \bar{T}_s) \right) \right) \\ &\cdot i \cdot n_{cell} \cdot A_{cell} \end{aligned} \quad (C.34)$$

The expanded expression can be differentiated with respect to the current density results in (C.35)

$$\begin{aligned} \frac{\partial \dot{Q}_{heat}}{\partial i} &= \left(v_{rev} - v_{cell_wp} - 2 \cdot K_{Voltage_{di}} \cdot i + K_{Voltage_{di}} \cdot \bar{i} - K_{Voltage_{dT_s}} \cdot (T_s - \bar{T}_s) \right) \\ &\cdot n_{cell} \cdot A_{cell} \end{aligned} \quad (C.35)$$

Differentiating (C.34) with respect to the temperature results in (C.36)

$$\frac{\partial \dot{Q}_{heat}}{\partial T_s} = -K_{Voltage_{dT_s}} \cdot i \cdot n_{cell} \cdot A_{cell} \quad (C.36)$$

Linearizing (C.34) with a first order Taylor Series results in (3.8)

$$\dot{Q}_{heat,linear} = \dot{Q}_{heat}(\bar{T}_s, \bar{i}) + \left. \frac{\partial \dot{Q}_{heat}}{\partial i} \right|_{\bar{T}_s, \bar{i}} \cdot (i - \bar{i}) + \left. \frac{\partial \dot{Q}_{heat}}{\partial T_s} \right|_{\bar{T}_s, \bar{i}} \cdot (T_s - \bar{T}_s)$$

C.7.1 Linearisation of the reformer temperature

In order to control the temperature of the reformer the temperature calculation must be linearized. The temperature is calculated from an power balance, see (3.14). The convective part has been linearized in (3.6). The excess hydrogen from the fuel cell heats up the reformer and this can be related to the current density.

Labview program

D

The system is controlled by a Texas Instruments cRIO 9012. This cRIO has a Real-Time(RT) module and a Field-Programmable Gate Array(FPGA) module. The FPGA modules controls the input and output from the module bay, where a various set of plugin modules are installed.

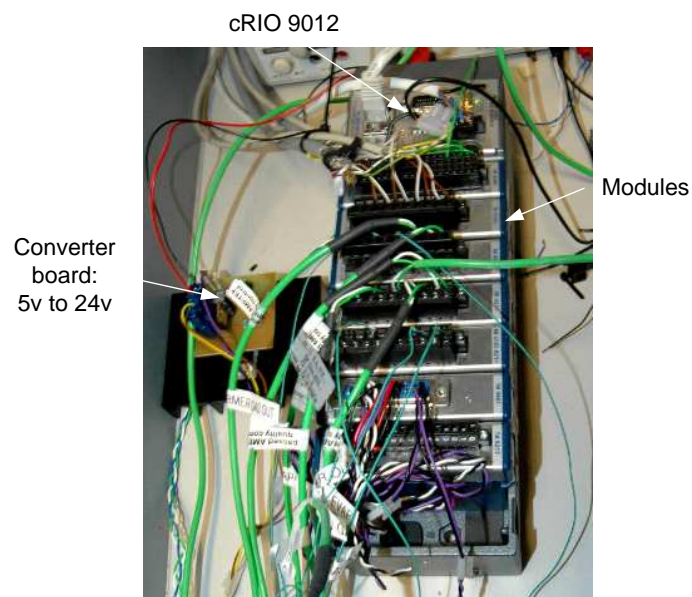


Figure D.1: *cRIO 9012 and modules*

The controlling system consists of 3 programs combined in a project. A FPGA program, RT program and a host program. The FPGA module communicates with the RT module and the RT module communicates with the HOST, see figure D.2



Figure D.2: *Communication between HOST, RT module, and FPGA*

The communication between the host program and RT module is with shared network variables and a list of variables can be seen in table D.1.

Variable name	Description
Variables from HOST(Boolean)	Boolean values from the controlling host interface
Variables from HOST(Double)	Double values from the controlling HOST interface
Variables from RT(Boolean)	Boolean values from the RT module
Variables from RT(Double)	Double values from the RT module
Timing constants from HOST(Double)	Timing constants for controllers
Datalog (String)	Measured data logged to file
Current log file (String)	Name of current logging file
Usernotes (String)	User notes describing the logged experiment
End notes to log file (String)	User notes added to the end of a logging session
Destination (String)	The destination of the file (RT module storage or USB flash drive)

Table D.1: *Shared network variables*

D.1 FPGA Program

The FPGA program is designed to read the data from the module bay and output to a variable the RT module can read. A list of modules can be seen in table D.2

Placement	Module	Description
Slot 1	AI (NI 9205)	Analog input module(32-Ch 16bit +/- 10V)
Slot 2	AO (NI 9263)	Analog Output module(4-Ch 16bit +/- 10V)
Slot 3	TC1 (NI9211)	Thermocouple input(4-Ch 24bit)
Slot 4	TC2 (NI9211)	Thermocouple input(4-Ch 24bit)
Slot 5	TC3 (NI9211)	Thermocouple input(4-Ch 24bit)
Slot 6	DIO (NI9401)	Digital Input/Output(8-Ch Highspeed TTL)
Slot 7	RTD (NI9217)	RTD module(4-Ch 24-bit Analog input)

Table D.2: *Plugin modules*

As for the Analog input(AI) and Analog output(AO) the program checks if the input refresh rate is too fast for the FPGA. This is done by comparing the difference in the tick counter, which should be the same as the user input tick count. This tick count can be changed from the host program, and if the loop finishes late, it is notified in the “AI AO Late Counter”. This part of the program can be seen in figure D.7.

The same check is made with the temperature modules (TC1, TC2, TC3). The default refresh tick rate is 2 for both the AI/AO modules and the TC modules.

The fuel pump is driven by a digital output of 24 Volt. This is made by a PWM module, where the duty cycle is 50%. The frequency of the PWM signal determines the frequency of the pump. The maximum frequency of the pump is 20 Hz, and this limit is set in the HOST program. Since the pump runs on 24 V, and the digital output is 5V, there is a converter board between the DIO module and the pump. This converter consists of a MOSFET and an Optocoupler, to prevent the board to damage the DIO module. The program consist of two pwm output in case of a seperate water and methanol pump, and PWM for the control of the electric heaters in the evaporator. The DIO part of the FPGA program can be seen from figure D.3.

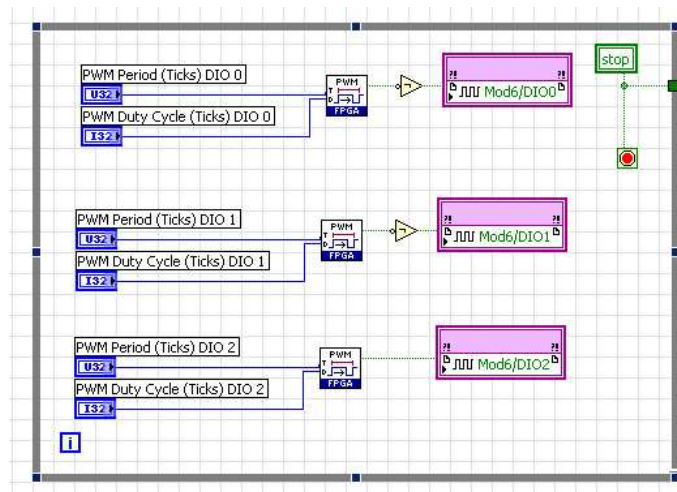


Figure D.3: PWM output in FPGA

D.2 RT program

The RT module consist of a 400Mhz CPU, and this module handles all of the calculations done in the program. This includes controllers, data logging, temperature handling and input/output for the FPGA. The read/write control can be seen from figure D.4, where the inputs are accessed from the left and output is accessed from the right. All of the thermo couplers used in this project is of the K type. The reference signal from the MFC's is read and the NI/volt

The inputs AO0-3 are all setpoints for the MFC's, where AO0-2 are controlling the air and AO3 are for the hydrogen. The thermo couplers(TC) are read from a cluster where all information is evaluated and extracted. The reference signals from the MFC's are read and added to the AI array. The 4 signals from the MFC's are individually read and the signal is multiplied with the specific "NI/min". The largest MFC is a 1300 NI/min MFC and got an input range of 10V, and this is why the reference value is multiplied with 130. The FPGA returns checks for stopped loops and the "tick late count".

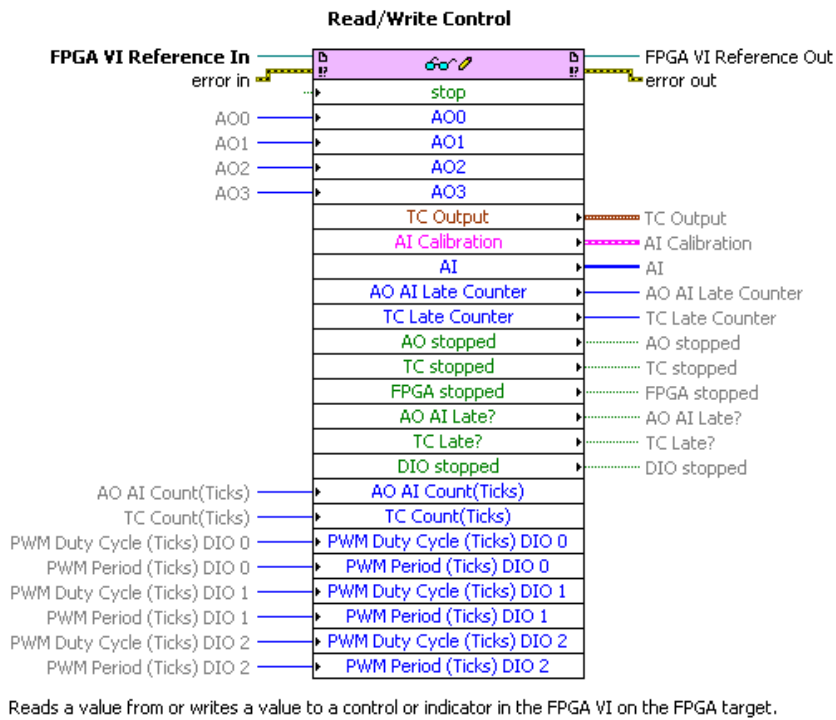


Figure D.4: FPGA Read/Write control

These checks are saved into the shared variable “Variables from RT(Boolean)”. The variable also contains the “datalogging enabled” boolean. The inputs for the Tick count in AO/AI and TC are set from the HOST program and passed on to the FPGA, while the inputs for the PWM is calculated by figure D.5.

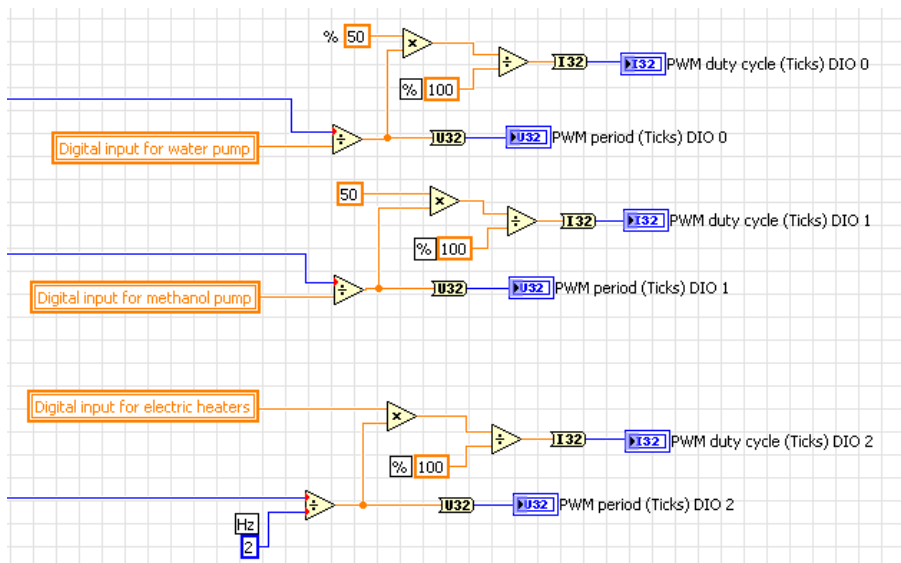


Figure D.5: PWM calculation for pump 1+2 and electric heaters

The input for the PWM blocks are the duty cycle and the duty period. As for the frequency to change, the period must be changed accordingly. The input frequency is divided into the tick count for 1 second. This count is 40.000.000 because the FPGA runs at 40 Mhz. If the frequency input from the user interface is 0, the output will be left in an enabled state. Because the pump should be left in an disabled state, the signal is inverted in the FPGA code. The duty cycle for the pump are set to 50%.

For the electric heaters there is installed a switch to allow the 5V signal to pass 240V to the heaters. The heaters are each 100 watt and the period is set to 2Hz. This is set low because of the net frequency of 50Hz. The input for the heaters is set to a value between 0 and 100%.

The regulating PID regulator can be enabled and disabled from the user interface. By disabling the PID regulator, a manual slider can control the air flow for the hydrogen. This manual slider is default set to a high value (50l/min), so in case of an emergency, the default value would be a high flow of air compared to the hydrogen added. The setpoint is also set from the user interface and is default set to 350 [°C]. The refresh speed and PI parameters is also available from the user interface.

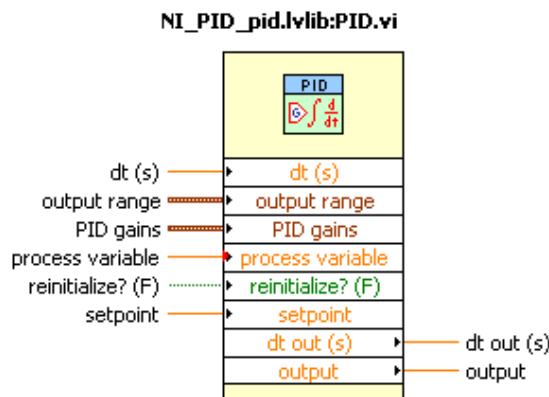


Figure D.6: *PID controller*

The measured temperature are read and the regulator is set to an output range of 0 to -20. This value is set because of the negative influence the blower has on the temperature of the controlled system. The measured temperature is compared to the setpoint and an regulated signal is outputted. This signal is inverted and the feed forward gain is applied. This feed forward gain is multiplied with the reference flow of the hydrogen, which gives an minimum airflow for the reaction. This feed forward signal is added to the regulated output from the PID regulator, and the new signal is converted to a 16 bit value and send to the AO. The PID input and output can be seen in figure D.6, and the program can be seen in figure D.8

The network shared variable “Variables from RT(Double)” contains the following

Nr.	Variable
00	Datalog time
01	Evaporator gas outlet Temperature
02	Reformer gas outlet Temperature
03	Burner Temperature 1
04	Burner Temperature 2
05	WGS Temperature
06	Burner gas outlet temperature
07	Fuel cell gas outlet temperature
08	Burner gas inlet temperature
09	Fuel cell gas inlet temperature
10	Evaporator air input temperature
11	Evaporator temperature
12	Evaporator air output temperature
13	MFC 1 (Cooler)
14	MFC 2 (Burner)
15	MFC 3 (Evaporator)
16	MFC 4 (H2)
17	Pressure feedback
18	AO AI Late Counter
19	TC Late Counter
20	Digital input for methanol pump (Hz)
21	Digital input for Water pump (Hz)
22	Digital input for electric heaters (watt)
23	Feedback from PI regulator (Burner)

Table D.3: *Variables from RT(Double)*

D.3 Host program

The host program handles the input and output for the user interface. The user interface consists of input for the PI controller, Mass Flow Controllers(MFC), Hydrogen usage, electric heaters and datalog information. The output from the RT consists of logged data i.e. temperatures, air-/h2-flow and pressure.

D.4 Figures

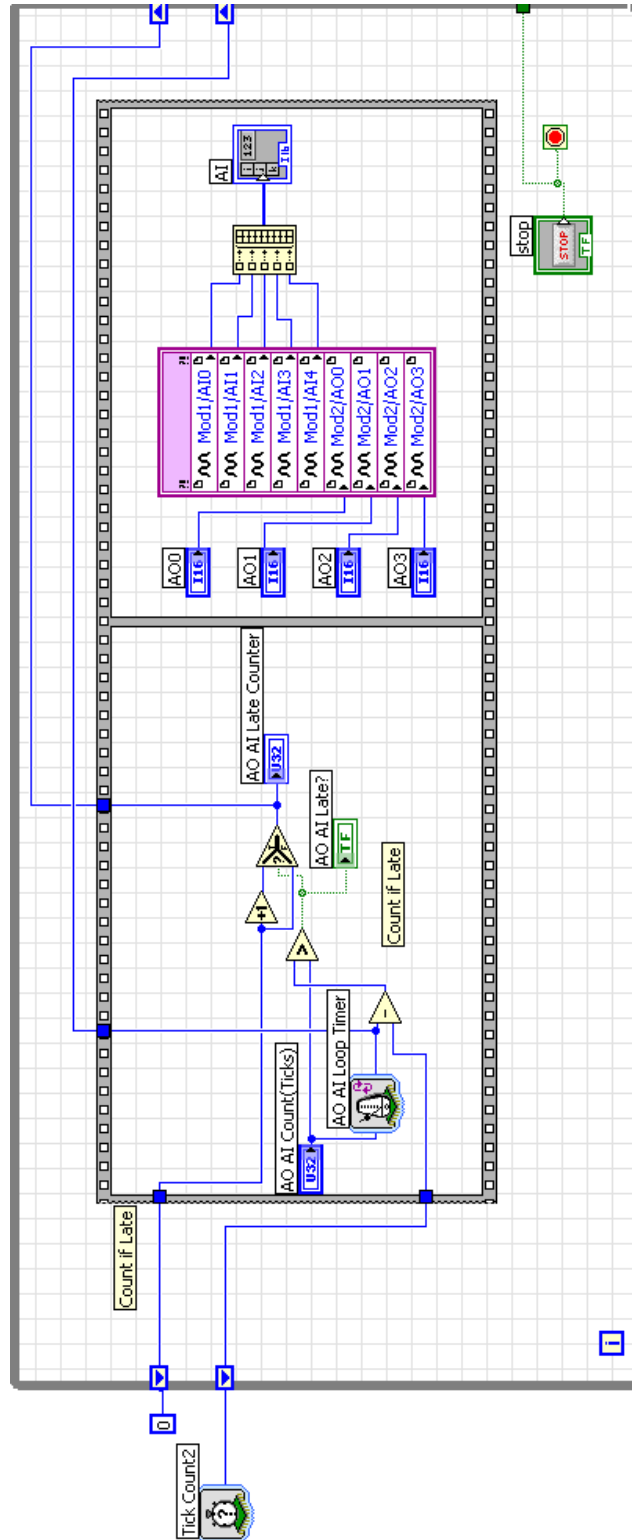


Figure D.7: AI and AO in FPGA

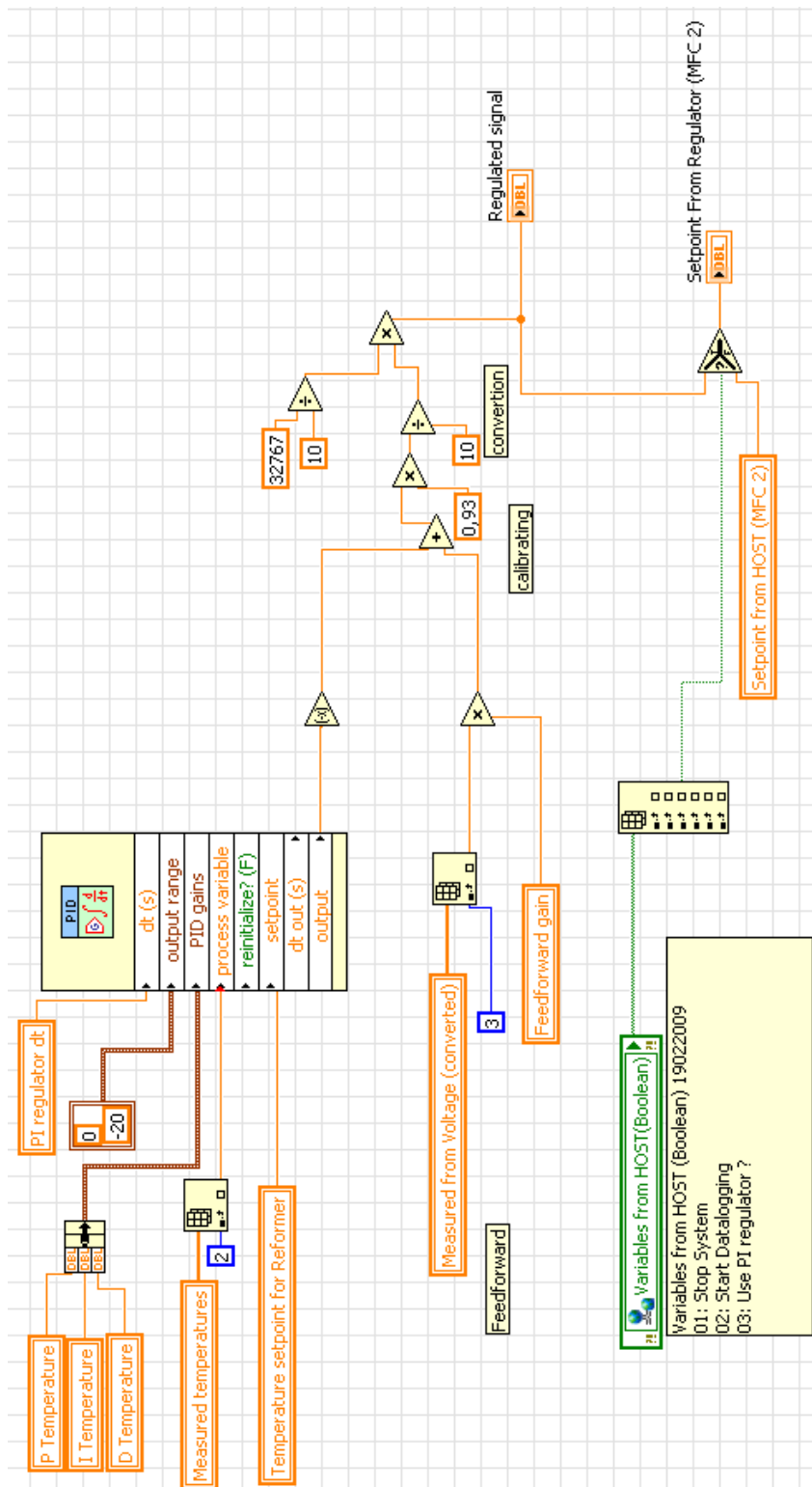


Figure D.8: PID control with feed forward

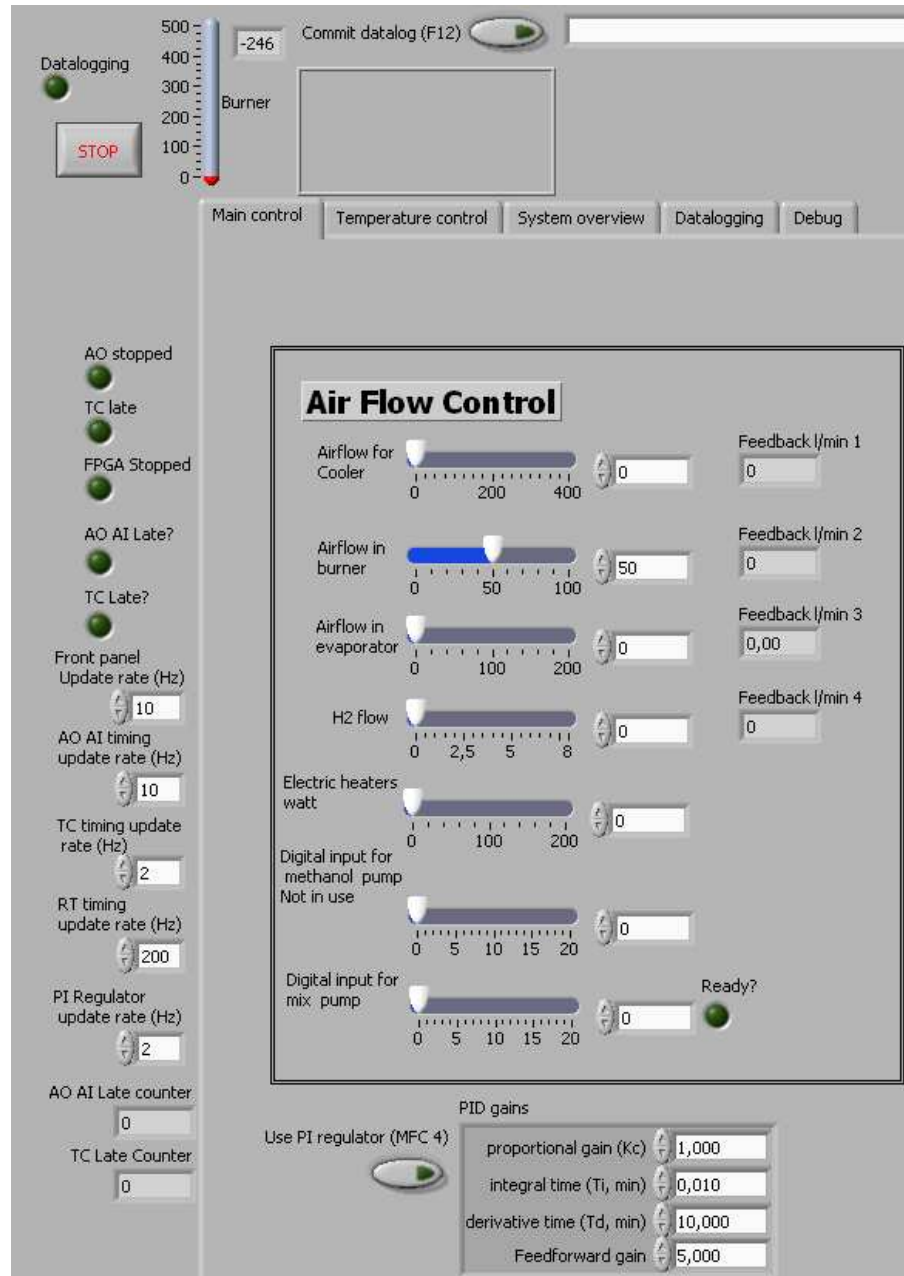


Figure D.9: Main control

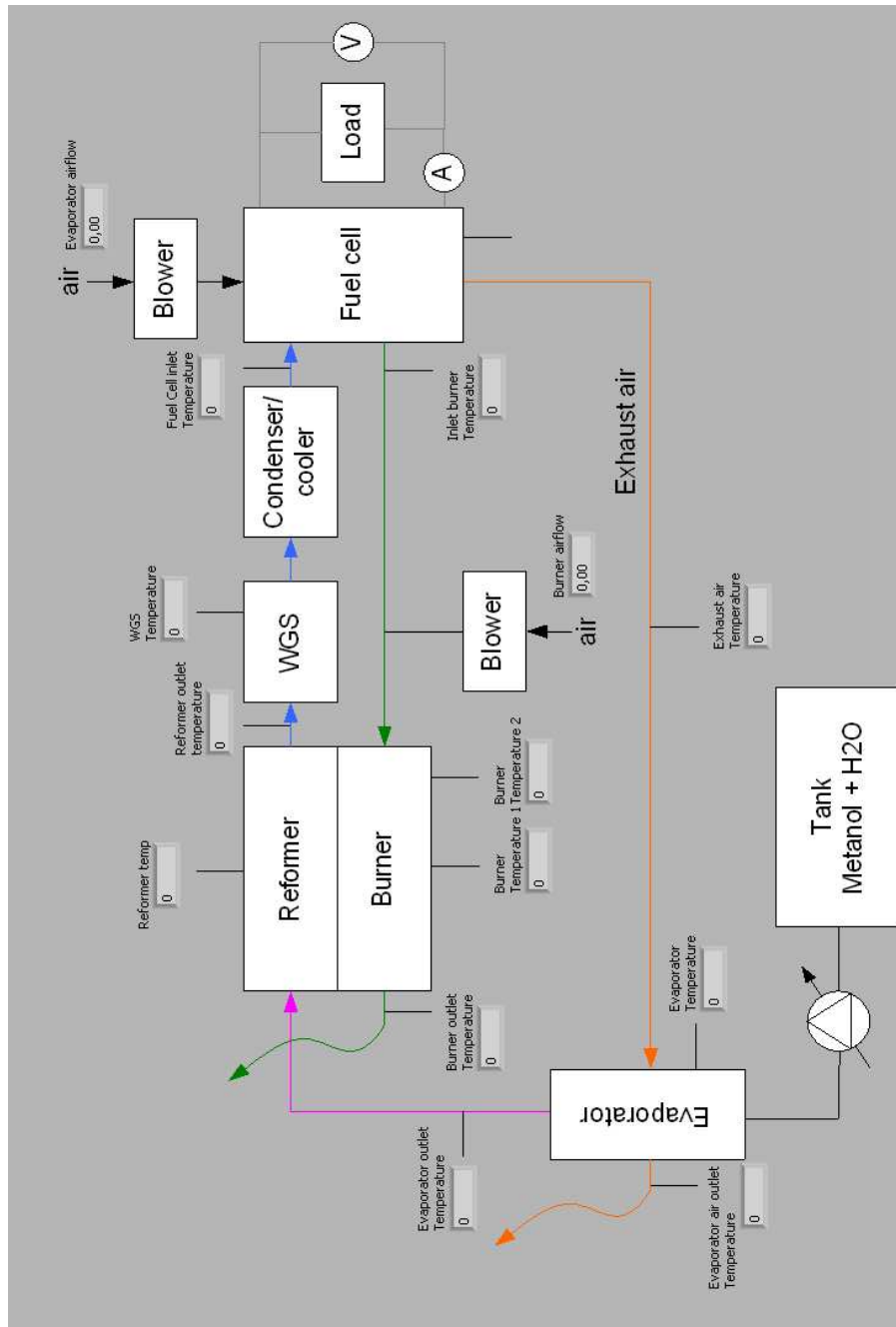


Figure D.10: System temperature overview

Matlab scripts



E.1 Fzero coverage

```
1 %%%%%%%%%%%%%%%%%%%%%%%%%%%%%%%%%%%%%%%%%%%%%%%%%%%%%%%%%%%%%%%%%%%%%%%%%%
2 %
3 %           Redigeret til udregning af H2 coverage ligninger af           %
4 %           Jesper Kjær Sørensen og Simon Sahlin                         %
5 %
6 %           Originalt designet af Søren Juhl Andreasen og Thomas Bagger Madsen %
7 %
8 %           EMSD9, November 2004                                         %
9 %           Modellen har taget udgangspunkt i varmevekslermodel af       %
10 %           Mads Pagh Nielsen                                           %
11 %%%%%%%%%%%%%%%%%%%%%%%%%%%%%%%%%%%%%%%%%%%%%%%%%%%%%%%%%%%%%%%%%%%%%%%%%%
12 %
13 %
14 %%%%%%%%%%%%%%%%%%%%%%%%%%%%%%%%%%%%%%%%%%%%%%%%%%%%%%%%%%%%%%%%%%%%%%%%%%
15 function [sys,x0,str,ts] = Sfunction_fzero(t,x,u,flag)
16
17 switch flag,
18
19 %%%%%%%%%%%%%%%%%%%%%%%%%%%%%%%%%%%%%%%%%%%%%%%%%%%%%%%%%%%%%%%%%%%%%%%%%%
20 % Initialisering %
21 %%%%%%%%%%%%%%%%%%%%%%%%%%%%%%%%%%%%%%%%%%%%%%%%%%%%%%%%%%%%%%%%%%%%%%%%%%
22 case 0,
23     [sys,x0,str,ts]=mdlInitializeSizes();
24
25 %%%%%%%%%%%%%%%%%%%%%%%%%%%%%%%%%%%%%%%%%%%%%%%%%%%%%%%%%%%%%%%%%%%%%%%%%%
26 % Output %
27 %%%%%%%%%%%%%%%%%%%%%%%%%%%%%%%%%%%%%%%%%%%%%%%%%%%%%%%%%%%%%%%%%%%%%%%%%%
28 case 1,
29     [sys]=mdlDerivatives(t,x,u);
30
31 %%%%%%%%%%%%%%%%%%%%%%%%%%%%%%%%%%%%%%%%%%%%%%%%%%%%%%%%%%%%%%%%%%%%%%%%%%
32 % Output %
33 %%%%%%%%%%%%%%%%%%%%%%%%%%%%%%%%%%%%%%%%%%%%%%%%%%%%%%%%%%%%%%%%%%%%%%%%%%
34 case 3,
35     sys=mdlOutputs(t,x,u);
36
37 %%%%%%%%%%%%%%%%%%%%%%%%%%%%%%%%%%%%%%%%%%%%%%%%%%%%%%%%%%%%%%%%%%%%%%%%%%
38 % Ikke benyttede flags %
39 %%%%%%%%%%%%%%%%%%%%%%%%%%%%%%%%%%%%%%%%%%%%%%%%%%%%%%%%%%%%%%%%%%%%%%%%%%
40 case {1,2, 4, 9 },
41     sys = [];
42
43 %%%%%%%%%%%%%%%%%%%%%%%%%%%%%%%%%%%%%%%%%%%%%%%%%%%%%%%%%%%%%%%%%%%%%%%%%%
44 % Uventede flags %
45 %%%%%%%%%%%%%%%%%%%%%%%%%%%%%%%%%%%%%%%%%%%%%%%%%%%%%%%%%%%%%%%%%%%%%%%%%%
46 otherwise
47     error(['Unhandled flag =',num2str(flag)]);
48
49 end
50 % end switch-funktion
51
52 %=====
53 % mdlInitializeSizes
54 % Funktionen returnerer the vektorstørrelser , start betingelser , og
55 % sample-tider for S-funktionen .
56 %=====
57
58
59 function [sys,x0,str,ts]=mdlInitializeSizes()
60
61                                     % Interne grid points
62     sizes = simsizes;
63     sizes.NumContStates = 1;          % Antallet af tilstande
64     sizes.NumDiscStates = 0;
65     sizes.NumOutputs = 1;            % Antal output
66     sizes.NumInputs = 10;           % Antal Input
67     sizes.DirFeedthrough = 1;
68     sizes.NumSampleTimes = 1;
69
70 us=0;
71
72
73 sys = simsizes(sizes);
```

```

75     x0=0;                                     % Begyndelsesvektor
77     str = [];
78     ts = [0 0];
79     =====
80     % mdlDerivatives
81     % Funktionen returnerer de afledte tilstande
82     % =====
83     function [sys]=mdlDerivatives(t,x,u);
84
85
86
87     sys = [0];                                % Resultat returneres til integrator
88
89     % =====
90     % mdlOutputs
91     % Returnerer output af Simulink-blok.
92     % =====
93     function sys=mdlOutputs(t,x,u)
94
95     k_fh=u(1);
96     b_fh=u(2);
97     k_fc=u(3);
98     b_fc=u(4);
99     k_ec=u(5);
100    k_eh=u(6);
101    p=u(7);
102    i=u(8);
103    x_co=u(9);
104    x_h2=u(10);
105    if x_co>0
106        y=fzero(@(TH2) k_fh*x_h2*p*(1-TH2)-(k_fc*x_co*p*(1-TH2)/(k_fc*x_co+b_fc+(i*k_ec/(2*k_eh*TH2))))
107            ^2-b_fh*k_fh*TH2^2-i,0.2);
108    else
109        y=0;
110    end
111    sys=y;

```

E.2 Fzero conservation of mass

```

%%%%%%%%%%%%%%%%%%%%%%%%%%%%%%%%%%%%%%%%%%%%%%%%%%%%%%%%%%%%%%%%%%%%%%%%
2 %
3 %           Redigeret til udregning af massebevarelse i reformering           %
4 %           Jesper Kjær Sørensen og Simon Sahlin                             %
5 %
6 %           Original design by Søren Juhl Andreasen og Thomas Bagger Madsen   %
7 %
8 %           EMSD9, November 2004                                             %
9 %           Modellen har taget udgangspunkt i varmevekslermodel af          %
10 %           Mads Pagh Nielsen                                               %
%%%%%%%%%%%%%%%%%%%%%%%%%%%%%%%%%%%%%%%%%%%%%%%%%%%%%%%%%%%%%%%%%%%%%%%%

function [sys,x0,str,ts] = Sfunction_fzero(t,x,u,flag);

switch flag,

16 %%%%%%%%%%%%%%%%%%%%%%%%%%%%%%%%%%%%%%%%%%%%%%%%%%%%%%%%%%%%%%%%%%%%%%%%%
18 % Initialisering %
19 %%%%%%%%%%%%%%%%%%%%%%%%%%%%%%%%%%%%%%%%%%%%%%%%%%%%%%%%%%%%%%%%%%%%%%%%%
20 case 0,
21     [sys,x0,str,ts]=mdlInitializeSizes();
22
23 %%%%%%%%%%%%%%%%%%%%%%%%%%%%%%%%%%%%%%%%%%%%%%%%%%%%%%%%%%%%%%%%%%%%%%%%%
24 % Afledte %
25 %%%%%%%%%%%%%%%%%%%%%%%%%%%%%%%%%%%%%%%%%%%%%%%%%%%%%%%%%%%%%%%%%%%%%%%%%
26 case 1,
27     [sys]=mdlDerivatives(t,x,u);
28
29 %%%%%%%%%%%%%%%%%%%%%%%%%%%%%%%%%%%%%%%%%%%%%%%%%%%%%%%%%%%%%%%%%%%%%%%%%
30 % Output %
31 %%%%%%%%%%%%%%%%%%%%%%%%%%%%%%%%%%%%%%%%%%%%%%%%%%%%%%%%%%%%%%%%%%%%%%%%%
32 case 3,
33     sys=mdlOutputs(t,x,u);
34
35 %%%%%%%%%%%%%%%%%%%%%%%%%%%%%%%%%%%%%%%%%%%%%%%%%%%%%%%%%%%%%%%%%%%%%%%%%
36 % Ikke benyttede flags %
37 %%%%%%%%%%%%%%%%%%%%%%%%%%%%%%%%%%%%%%%%%%%%%%%%%%%%%%%%%%%%%%%%%%%%%%%%%
38 case {1 2, 4, 9 },
39     sys = [];
40
41 %%%%%%%%%%%%%%%%%%%%%%%%%%%%%%%%%%%%%%%%%%%%%%%%%%%%%%%%%%%%%%%%%%%%%%%%%
42 % Uventede flags %
43 %%%%%%%%%%%%%%%%%%%%%%%%%%%%%%%%%%%%%%%%%%%%%%%%%%%%%%%%%%%%%%%%%%%%%%%%%
44 otherwise
45     error(['Unhandled flag=',num2str(flag)]);
46
47 end
48 % end switch-funktion

=====
50 % mdlInitializeSizes
52 % Funktionen returnerer the vektorstørrelser , start betingelser ,
53 % og sample-tider for S-funktionen .
54 %=====

55 function [sys,x0,str,ts]=mdlInitializeSizes();
56
57                                     % Interne grid points
58     sizes = simsizes;
59
60 sizes.NumContStates = 1;           % Antallet af tilstande
61 sizes.NumDiscStates = 0;
62 sizes.NumOutputs = 1;             % Antal output
63 sizes.NumInputs = 13;            % Antal Input
64 sizes.DirFeedthrough = 1;
65 sizes.NumSampleTimes = 1;
66
67 us=0;
68
69 sys = simsizes(sizes);
70
71     x0=0;                           % Begyndelsesvektor
72
73 str = [];
74 ts = [0 0];

=====
76 % mdlDerivatives
78 % Funktionen returnerer de afledte tilstande
79 %=====

80     function [sys]=mdlDerivatives(t,x,u);
81
82     sys = [0];           % Resultat returneres til integrator

=====
86 % mdlOutputs
87 % Returnerer output af Simulink-blok .
88 %=====

```

```
90 function sys=mdlOutputs(t,x,u);
91   n_meoh=u(1);
92   n_h2o=u(2);
93   m_meoh=u(3);
94   m_co=u(4);
95   m_co2=u(5);
96   m_h2=u(6);
97   m_h2o=u(7);
98   n_mix_in=u(8);
99   x_meoh=u(9);
100  x_co=u(10);
101  x_co2=u(11);
102  x_h2=u(12);
103  x_h2o=u(13);
104  if n_mix_in>0
105    y=fzero(@(nmixout) n_h2o*m_h2o+n_meoh*m_meoh-(x_meoh*m_meoh*nmixout+x_co*m_co*nmixout+x_co2*
106              m_co2*nmixout+x_h2*m_h2*nmixout+x_h2o*m_h2o*nmixout),0.01);
107  else
108    y=0;
109  end
110  sys=y;
```

E.3 Repeating simulation optimizer

```

%%%%%%%%%%%%%%%%%%%%%%%%%%%%%%%%%%%%%%%%%%%%%%%%%%%%%%%%%%%%%%%%%%%%%%%%
2 %
%           Repeating the simulation to find a more precise value of
4 %           a_30 and b_30
%
6 %           Jesper Kjær Sørensen og Simon Sahlin
%           EMSD10, Maj 2009
8 %%%%%%%%%%%%%%%%%%%%%%%%%%%%%%%%%%%%%%%%%%%%%%%%%%%%%%%%%%%%%%%%%%%%%%%%%

10 %% Constants
clear all
12 tic
%clf
14 sampledata.time=0;
%Lambda_air=2.5
16 i_start=0.01;
i_max=0.66;
18 T_test=180+273.15;
CO_ppm=1000;
20

22 repeat=10;
% a_1_start=-0.0001
% a_1_slut=-0.0002
% a_1_slut=-5
26 % a_1_delta=(a_1_slut-a_1_start)/repeat
opts = simset('debug', 'off');
28 n = 1:repeat^2;
score_sample(n,1)=0;
30

32 a_30_start=3e-1;
a_30_end=6e-1;
34 a_30_delta=(a_30_end-a_30_start)/repeat;

36 b_30_start=2.8e-2;
b_30_end=2.6e-2;
38 b_30_delta=(b_30_end-b_30_start)/repeat;

40 %% Model run
for a = 1:repeat
42     a_30=a_30_start+a_30_delta*(a-1);
    for b = 1:repeat
44         b_30=b_30_start+b_30_delta*(b-1);
        score_sample((b+(repeat*(a-1))),2)=a_30;
46         score_sample((b+(repeat*(a-1))),3)=b_30;

48

50
52         %run model
        sim('fuelcell_model_repeating_fc_voltage.mdl',100,opts);
54

56 % Check if we got the larges value of time intervals and save the largest
%(for plotting purpose)
58     if (size(simout.signals.values,1) > size(sampledata.time,1))
        sampledata.time=simout.time(:,1);
60     end

62     (b+(repeat*(a-1)));

64     for m=1:size(simout.signals.values,1)
        % save data from model
66         sampledata.values(m,(b+(repeat*(a-1))))=simout.signals.values(m,1);
        sampledata.simulated(m,(b+(repeat*(a-1))))=measout.signals.values(m,1);
68         sampledata.currentdensity(m,(b+(repeat*(a-1))))=current_density.signals.values(m,1);
        % Calculate the difference between model and measured data
70         sampledata.diff(m,(b+(repeat*(a-1))))=simout.signals.values(m,1)-measout.signals.
            values(m,1);

72         % Calculate the rms value of the difference
        scoreadd_rms = sqrt(sampledata.diff(m,(b+(repeat*(a-1))))^2);
74

        % Add the
76         score_sample((b+(repeat*(a-1))),1) = score_sample((b+(repeat*(a-1))),1)+scoreadd_rms
            ;
    end
78 end
end
80
82 %time measured between tic and toc
toc
%% Aftermath
84
% Find lowest score and the index
86 [min_score_value,min_score_index] = min(score_sample(:,1));

```

```

88 %% Figures
89 close all
90 %% Figure 1
91 % Plot the difference every <repeat> number of samples
92 z1 = '../eps/plot_repeated_compared_difference.eps';
93 figure1 = figure('PaperSize',[20.98 29.68]);
94
95 X1=sampledata.currentdensity(:,min_score_index);
96 YMatrix1=sampledata.diff(:,min_score_index);
97
98 fig1_tick_y1=max(max(YMatrix1))+max(max(YMatrix1))/10;
99 fig1_max_y1=max(max(YMatrix1))+0.02;
100 fig1_min_y1=min(min(YMatrix1))-0.02;
101 % Create axes
102 axes1 = axes('Parent',figure1,...
103             'YGrid','on',...
104             'XGrid','on',...
105             'LineWidth',1);
106 % Uncomment the following line to preserve the X-limits of the axes
107 % xlim([0 1317]);
108 % Uncomment the following line to preserve the Y-limits of the axes
109 ylim([fig1_min_y1 fig1_max_y1]);
110 box('on');
111 hold('all');
112 % Create multiple lines using matrix input to plot
113 plot1 = plot(X1,YMatrix1,'Parent',axes1);
114 set(plot1(1),'DisplayName','Voltage_difference');
115
116 % Create ylabel
117 ylabel('RMS_voltage_difference','FontSize',10);
118
119 % Create xlabel
120 xlabel('Current_density','FontSize',10);
121
122 % Create legend
123 legend1 = legend(axes1,'show');
124 set(legend1,'Edgecolor',[1 1 1],'Location','Northeast');
125
126 print(gcf,'-depsc2','-r600', z1)
127 disp(z1)
128
129 %% Figure 2
130 %plot(score_sample(:,1))
131 z2 = '../eps/plot_repeated_compared_scores.eps';
132 figure2 = figure('PaperSize',[20.98 29.68]);
133 YMatrix1 = score_sample(:,1);
134
135 fig2_tick_y1=max(max(YMatrix1))+max(max(YMatrix1))/10;
136 fig2_max_y1=max(max(YMatrix1))+max(max(YMatrix1))*0.1;
137
138 % Create axes
139 axes1 = axes('Parent',figure2,'YTick',(0:1:fig2_max_y1),...
140             'YGrid','on',...
141             'XGrid','on',...
142             'LineWidth',1);
143 % Uncomment the following line to preserve the X-limits of the axes
144 % xlim([0 1317]);
145 % Uncomment the following line to preserve the Y-limits of the axes
146 ylim([0 fig2_max_y1]);
147 box('on');
148 hold('all');
149 % Create multiple lines using matrix input to plot
150 plot2 = plot(YMatrix1,'Parent',axes1);
151 set(plot2(1),'DisplayName','Voltage_score');
152
153 % Create ylabel
154 ylabel('RMS_voltage_difference','FontSize',10);
155
156 % Create xlabel
157 xlabel('Run_session','FontSize',10);
158
159 % Create legend
160 legend1 = legend(axes1,'show');
161 set(legend1,'Edgecolor',[1 1 1],'Location','Northeast');
162
163 print(gcf,'-depsc','-r600', z2)
164 disp(z2)
165
166 %% Figure 3
167 z3 = '../eps/plot_repeated_polarisation_curves_1.eps';
168 X1=sampledata.currentdensity(:,min_score_index);
169
170 figure3 = figure('PaperSize',[20.98 29.68]);
171 YMatrix1 = [sampledata.values(:,min_score_index),sampledata.simulated(:,min_score_index)];
172
173 fig3_tick_y1=max(max(YMatrix1))+max(max(YMatrix1))/10;
174 fig3_max_y1=max(max(YMatrix1))+max(max(YMatrix1))*0.1;
175
176 % Create axes
177 axes1 = axes('Parent',figure3,'YTick',(0:0.1:fig3_max_y1),...
178             'YGrid','on',...

```

```
180     'XGrid','on',...
      'LineWidth',1);
182 % Uncomment the following line to preserve the X-limits of the axes
      % xlim([0 1317]);
184 % Uncomment the following line to preserve the Y-limits of the axes
      ylim([0 fig3_max_y1]);
186 box('on');
      hold('all');
188 % Create multiple lines using matrix input to plot
      plot3 = plot(X1,YMatrix1,'Parent',axes1);
      set(plot3(1),'DisplayName','Experimental');
190 set(plot3(2),'DisplayName','Simulated');

192 % Create ylabel
      ylabel('Voltage','FontSize',10);
194
196 % Create xlabel
      xlabel('Current density','FontSize',10);

198 % Create legend
      legend1 = legend(axes1,'show');
200 set(legend1,'Edgecolor',[1 1 1],'Location','Northeast');

202 print(gcf,'-depsc','-r600',z3)
      disp(z3)
```

E.4 Controller parameter search

```

%%%%%%%%%%%%%%%%%%%%%%%%%%%%%%%%%%%%%%%%%%%%%%%%%%%%%%%%%%%%%%%%%%%%%%%%
2 %           Script for searching for controller parameters for           %
%           a PI-controller for the reformer.                             %
4 %           Created by: Simon Sahlin and Jesper Kjær Sørensen           %
%%%%%%%%%%%%%%%%%%%%%%%%%%%%%%%%%%%%%%%%%%%%%%%%%%%%%%%%%%%%%%%%%%%%%%%%
6 t=0:0.01:100; %Time vector for the stepfunction
K_V=37; %Voltage constant for the controller
8 k=0; %Counting variable for the table
%Clear the variables for the script
10 clear table
clear sortedrows
12 %set the timestamp for the calculations beginning
tic
14 for i=1:125; %Integration constant Loop for changing the placement of the zero on the negative
axis
T_i(i)=2+0.1*i; %Reciprocal value of the zero
16 for j=1:125; %Loop for the gain of the closed loop function.
K_P(j)=2*j; %Gain value
18 %numerator of the transferfunction
num_parameter=[K_P(j)*K_V*K_conv_ref_dq 1/T_i(i)*K_P(j).*K_V*K_conv_ref_dq];
20 %denominator of the transfer function
den_parameter=[m_ref*c_ref (K_conv_ref_dTr+K_cond_ref+K_P(j).*K_V*K_conv_ref_dq) 1/T_i(i)
).*K_P(j).*K_V*K_conv_ref_dq];
22 %Creating the transfer function
G_closed=tf(num_parameter,den_parameter);
24 %Apply the step function to obtain the response, using the time
%vector t
26 y=step(G_closed,t);
%Calculate the overshoot for the stepfunction
28 n=max(y);
%Calculate the settling time with 2% deviance from the input of the
30 %step. s is the fixed number of samples
s=10001;while y(s)<1.02 & y(s)>0.98;s=s-1;end;
32 %Convert from samples to time in s multiply with the time step
setlingtime=(s-1)*0.1;
34 %Sort the step responses and save the ones that fits inside the
%parameters of the demands from the report and <10 second setling
36 %time
if m<1.10 && m>1.01 && setlingtime<10
38 k=k+1; %Count up the variable for table.
table(k,1)=K_P(j); %Save the gain in 1st column
40 table(k,2)=T_i(i); %Save the integral constant in 2nd column
table(k,3)=n; %Save the maximum overshoot in 3rd column
42 table(k,4)=setlingtime; %Save the setling time in the 4th column
end
44 end
end
46 %stop the time calculation and plot it in the command window
toc
48 %sort the table from the simulations with solumn 3 in ascending order
sortedrows=sortrows(table,3);
50 K_P=sortedrows(:,1);
T_i=sortedrows(:,2);
52 f=0;
for j=1:1:3;
54 num_parameter=[K_P(j)*K_V*K_conv_ref_dq 1/T_i(j)*K_P(j).*K_V*K_conv_ref_dq];
den_parameter=[m_ref*c_ref (K_conv_ref_dTr+K_cond_ref+K_P(j).*K_V*K_conv_ref_dq) 1/T_i(j)*
K_P(j).*K_V*K_conv_ref_dq];
56 G_closed=tf(num_parameter,den_parameter);
f=f+1;
58 y(:,f)=step(G_closed,t);
end;
60 %Create the labels for the figure legends
label1=['K_P=' num2str(K_P(1)) ' and T_i=' num2str(T_i(1))];
62 label2=['K_P=' num2str(K_P(2)) ' and T_i=' num2str(T_i(2))];
label3=['K_P=' num2str(K_P(3)) ' and T_i=' num2str(T_i(3))];
64 %plot the stepresponse for the reference controller
figure(1)
66 plot(t,y(:,1),t,y(:,2),t,y(:,3))
axis([0 1 0.5 1.02])
68 legend(label1,label2,label3,'Location','SouthEast')
%Plotting the stepresponse for the current density closed loop transfer
70 %function.
f=0;
72 for j=1:1:3;
closedloop_num=conv([-1 1/60]*(K_H2BURN-K_SR-K_ref_ff*37*K_conv_ref_dq),[1 0]);
74 closedloop_den=conv([1 1/60],[m_ref*c_ref (K_cond_ref+K_conv_ref_dTr+K_V*K_P(j)*
K_conv_ref_dq) 1/T_i(j)*K_V*K_P(j)*K_conv_ref_dq]);
G_closed_i=tf(closedloop_num,closedloop_den);
76 f=f+1;
y_disturbance(:,f)=step(G_closed_i,t);
78 end;
80 figure(2)
plot(t,y_disturbance(:,1),t,y_disturbance(:,2),t,y_disturbance(:,3))
82 legend(label1,label2,label3,'Location','SouthEast')

```